Terms and Conditions of Use of Digitised Theses from Trinity College Library Dublin

Copyright statement

All material supplied by Trinity College Library is protected by copyright (under the Copyright and Related Rights Act, 2000 as amended) and other relevant Intellectual Property Rights. By accessing and using a Digitised Thesis from Trinity College Library you acknowledge that all Intellectual Property Rights in any Works supplied are the sole and exclusive property of the copyright and/or other IPR holder. Specific copyright holders may not be explicitly identified. Use of materials from other sources within a thesis should not be construed as a claim over them.

A non-exclusive, non-transferable licence is hereby granted to those using or reproducing, in whole or in part, the material for valid purposes, providing the copyright owners are acknowledged using the normal conventions. Where specific permission to use material is required, this is identified and such permission must be sought from the copyright holder or agency cited.

Liability statement

By using a Digitised Thesis, I accept that Trinity College Dublin bears no legal responsibility for the accuracy, legality or comprehensiveness of materials contained within the thesis, and that Trinity College Dublin accepts no liability for indirect, consequential, or incidental, damages or losses arising from use of the thesis for whatever reason. Information located in a thesis may be subject to specific use constraints, details of which may not be explicitly described. It is the responsibility of potential and actual users to be aware of such constraints and to abide by them. By making use of material from a digitised thesis, you accept these copyright and disclaimer provisions. Where it is brought to the attention of Trinity College Library that there may be a breach of copyright or other restraint, it is the policy to withdraw or take down access to a thesis while the issue is being resolved.

Access Agreement

By using a Digitised Thesis from Trinity College Library you are bound by the following Terms & Conditions. Please read them carefully.

I have read and I understand the following statement: All material supplied via a Digitised Thesis from Trinity College Library is protected by copyright and other intellectual property rights, and duplication or sale of all or part of any of a thesis is not permitted, except that material may be duplicated by you for your research use or for educational purposes in electronic or print form providing the copyright owners are acknowledged using the normal conventions. You must obtain permission for any other use. Electronic or print copies may not be offered, whether for sale or otherwise to anyone. This copy has been supplied on the understanding that it is copyright material and that no quotation from the thesis may be published without proper acknowledgement.

A Biochemical Oscillator: Experimental and Theoretical Studies of the Peroxidase-Oxidase Reaction

BY

Andrew McDonald

A dissertation submitted to the University of Dublin in candidature for the degree of Doctor of Philosophy.

Department of Biochemistry
Trinity College
Dublin

August 1999

DECLARATION

I certify that none of the work presented in this thesis has been submitted for any degree, at this, or any other University. I declare that this thesis is entirely my own work.

Andrew McDonald

Andrew McDonald

From: Andrew G. McDonald, Ph.D.
To: The Library, Trinity College Dublin
Re: Permission for copying and lending Ph.D. thesis

To whom it may concern,
I hereby give permission to the Library of Trinity College Dublin to copy and lend my Ph.D. thesis.

Andrew G. McDonald

Contents

List of Figures

List of Tables

Acknowledgments

I would like to thank Professor Keith Tipton, of this department, for his help and guidance through the duration of this project, and for his enthusiasm for the subject matter. I owe a debt of gratitude to Dr. Dean Olson, of the University of Illinois at Urbana-Champaigne, for the invaluable information that he gave during our correspondence by electronic mail during the early stages of this work, and the time and effort that he invested in aiding my first steps towards achieving sustained oscillations in the peroxidase-oxidase reaction.

The workshop technicians in this department, Noel Breslin and Martin Grady, deserve special recognition for their work in helping with the assembly and, on occasion, repair of the laboratory apparatus. Noel Breslin engineered the aluminium plates that were used to cover the spectrophotometer.

This document was typeset in LaTeX on Apple Macintosh computers, using OzTeX, a computer program written by Andrew Trevorrow. The colour plates in Appendix D were printed on a colour laser printer that was kindly provided by Aonghus de Barra. A word of thanks is due Dr. Toni Kazic, of the Washington University at St. Louis, who brought the book *The LaTeX Graphics Companion* to my attention, the information in which was used to generate Figures 1.1 and 7.16. My thanks also go to Dave Delaney for many interesting discussions.

This work was supported by grants from Forbairt and Bioresearch Ireland.

Summary

The peroxidase-oxidase (PO) reaction is the haem-peroxidase catalysed reaction of molecular oxygen with NADH, and has been shown previously to behave in an oscillatory fashion. It has been used here as a useful laboratory model of the types of complex biochemical kinetics that are evinced by cellular systems.

A laboratory apparatus for the study of this oscillator under conditions of steady-state substrate influx was designed and characterised. A standard set of experimental conditions was defined and a number of dynamical behaviours were observed using horseradish peroxidase; these included switching between coexistent steady-states (bistability), damped and sustained oscillations in the measurable components of the reaction when using NADH as the reducing agent. Special attention was paid to the methods of measurement of the mass-transfer of oxygen across the gas-liquid interface, and the determination of the rate constants of two models of the process. The reproducibility of the rate of oxygen mass-transport under standard conditions was also examined.

A study of the physical and chemical parameters affecting the reaction was carried out. Through a series of experiments at different pH values and using two different buffers, it was found that the PO reaction has a pH optimum at approximately 5.0. Two pH indicators were tested for use with the oscillator: chlorophenol red (3',3"-dichlorophenolsulphonphthalein) and methyl red (4-dimethylaminobenzene-2'-carboxylic acid), and both were found to inhibit NADH oxidation. The effect of ionic strength was examined, and it was found that low ionic strengths favour oscillatory kinetics.

The role of free radicals in the mechanism of the oscillator was probed by the use of perturbants such as superoxide dismutase and ascorbic acid, both of which were found to inhibit nonlinear oxidation of NADH. Tyramine (4-[2-aminoethyl]phenol), 4-aminophenol and 2,6-dichlorophenol were each tested for use in the PO reaction as in place of 2,4-dichlorophenol, the most commonly used promoter of oscillations. Tyramine was found to weakly stabilise oscillations, and its conversion to dityramine, a reaction shown to be catalysed by horseradish peroxidase, was taken to be indirect

evidence for the formation of a phenolic free radical. 2,6-dichlorophenol was shown to be capable of generating sustained, and 4-aminophenol to completely inhibit, oscillations.

Three mathematical models of the peroxidase-oxidase reaction were developed. Starting with a realistic model based on published and experimentally-verified rate constants which gave rise to similar oscillations to those observed in laboratory experiments, two successive reductions in the number of variables were made, generating two further models that like the first showed oscillations when integrated numerically on a computer. The simplest model, in two variables, views the basis of the peroxidase-oxidase reaction as being the interconversion of two forms of an enzyme acting upon a substrate intermediate, the assumed autocatalytic nature of the reaction providing the nonlinearity required for oscillations. A stability analysis of the model was carried out, revealing the presence of a Hopf bifurcation, a fact that was verified in computer simulations.

Chapter 1

Introduction

Dynamic phenomena are ubiquitous in the natural sciences, and no study of the chemical branches of these sciences would be complete without knowledge of the kinetic behaviour of chemical reactions. The study of the chemistry of living systems — biochemistry — is no different, and it is the object of this present work to further our knowledge of one little-known reaction catalysed by haem-containing peroxidases, the peroxidase-oxidase reaction; this is, at the time of writing, one of only a few known single-enzyme systems which is capable of displaying oscillatory kinetics. That oscillatory behaviour is possible in a chemical reaction has previously been the subject of some debate in the scientific community, and prior to the work of Ilya Prigogine on non-equilibrium thermodynamics [2] it was held that any set of reactants would approach chemical equilibrium monotonically. This was refuted by the theoretical work of Prigogine, in which he showed that classical thermodynamics could not restrict the time-dependant behaviour of 'far from equilibrium' systems, nor preclude fluctuations in reactant concentrations about the equilibrium position. The theory gives credence to several experimentally-known chemical oscillators, among which are the Bray reaction [3], which is the decomposition of hydrogen peroxide in the presence of the catalyst iodide, the Belousov-Zhabotinsky (BZ) reaction, in which an organic species, typically malonic acid, is oxidised by acid bromate ion [4, 5], and the chlorite-iodide reaction, first discovered in 1982 [6].

It is hardly surprising that with the growing number of chemical oscillators that similar discoveries have been made in the field of biological chemistry. Several examples of biological phenomena with the potential for non-simple dynamics can be given. Possibly the best known biochemical oscillator is that of gylcolysis. Glycolytic oscillations in yeast were first observed by Duysens and Amesz in 1957 [7], and further studied by Chance and others [8, 9, 10, 11]. Although the functional significance of

time-periodic behaviour in the glycolytic pathway remains a matter for debate, this is certainly not the case for another well-known biochemical oscillator, the cAMP signalling mechanism of cellular slime moulds such as *Dictyostelium discoideum*, in which cellular aggregation occurs in response to pulsatile secretion of cyclic AMP and the outcome of which is the formation of the spore stage in the life cycle of these species. Another area of biochemistry which has received much attention is that of oscillations in intracellular calcium [12, 13, 14, 15]. Cytosolic calcium levels have been observed to oscillate through the mobilisation of intracellular calcium stores by hormone-induced inositol triphosphate (IP_3) synthesis, which is itself activated by calcium in the calcium-induced calcium release (CICR) model.

Common to all of these oscillators, chemical and biochemical, is the property of feedback. The response to a small change in the concentration of one chemical species may induce a much greater change in that of another if it is a promoter or inhibitor in steps leading to the generation or removal of another species. For example, in the glycolytic pathway the allosteric enzyme phosphofructokinase is modulated by ATP and AMP, which alter its kinetic properties and binding affinity for the substrate fructose-6-phosphate. Since ATP is a product of glycolysis, this may be viewed as a form of negative feedback. Another property of some oscillators is autocatalysis, whereby a reactant molecule increases the rate of its own formation, examples of which would be feed-forward or feedback activations resulting in self-amplification of signal molecules. As we shall see in future chapters, these concepts are relevant in the mechanism of the peroxidase-oxidase oscillator, which is the subject of this work.

1.1 Theoretical concepts

Before turning to an historical account of the peroxidase-oxidase reaction, it will be helpful to a better understanding of the subject matter if a brief introduction to theory of dynamical systems is first given, as this will accustom the reader to some of the terminologies used later. The kinetics of chemical reaction or group of reactions are generally modelled by continuous-time differential equations, where the variables $x_1(t), x_2(t), \ldots, x_n(t)$ of the mathematical model represent the concentrations of n reacting species at time t. The collection of such variables describes a point in *phase space*, and a study of the rates at which the variables change can be thought of as the time-evolution of the point in such a space. The rate laws of chemical reactions are dependent on parameters such as rate constants, and so we assume that in a system of n reactants, there will be m elementary reactions with rate constants $k_1, k_2, \ldots, k_m$. The simplest type of reaction scheme is linear, for which it is the case that $m = n - 1$.

In mathematical notation, a model of the rate of change of the set of concentrations may be written in vector form as

$$d\mathbf{x}(t)/dt = \mathbf{f}(\mathbf{x};\mu) \tag{1.1}$$

which is an m-dimensional system of (ordinary) differential equations, and $\mathbf{x}$ and μ are n- and m-dimensional vectors of reactant concentrations and parameters, respectively. We shall assume that for some μ, time $t = t_0$ and initial conditions $\mathbf{x}(t_0) \equiv \mathbf{x}_0$ a solution to Equation 1.1 exists, which we denote $\phi_t(t_0, \mathbf{x}_0)$, or simply ϕ_t. ϕ_t is called a *flow*, and for any given set of initial conditions the solution defines a set of points in n-dimensional space which is called a *trajectory*. We note that for a chemical system, or any model thereof, the values of concentrations will always be positive, although the theory discussed here is of general application. A point $\mathbf{y}$ is said to be an *ω-limit* point of $\mathbf{x}$ if ϕ_t repeatedly enters some neighbourhood N of $\mathbf{y}$ as $t \to \infty$. The set $\mathcal{L}(\mathbf{x})$ of all such points of $\mathbf{x}$ is called the ω-limit set of $\mathbf{x}$. A key property of a limit set is that of its *stability*. A set $\mathcal{L}(\mathbf{x})$ is said to be *stable* if all nearby trajectories remain nearby under the action of the flow ϕ_t, and *unstable* if nearby trajectories (not on $\mathcal{L}(\mathbf{x})$) move away from $\mathcal{L}(\mathbf{x})$. The set $\mathcal{L}(\mathbf{x})$ is *asymptotically stable* if all $\mathbf{x}$ nearby $\mathcal{L}(\mathbf{x})$ approach $\mathcal{L}(\mathbf{x})$ as $t \to \infty$. This stable, attracting ω-limit set is called an *attractor*.

The equilibrium points of (1.1) are the solutions to $\mathbf{x}^* = \mathbf{f}(\mathbf{x}^*)$, and their stability may be considered in the same terms as the foregoing. The stability of the equilibrium, or *steady state* points can depend on the position of the system in the space of parameters μ. A change in the pattern of stability can occur as μ is varied, causing one limit set to become unstable and a new, attracting limit set to become stable. A qualitative change in the nature of the limit sets is called a *bifurcation*. We now make the claim that for some systems there are attracting limit sets which are not fixed, or stationary, states, but are periodic orbits. The purely general treatment of stable limit sets does not preclude a closed loop in the n-dimensional phase space of the phase space, and there exists one class of bifurcation called the Hopf bifurcation, which describes how under the variation of a parameter an equilibrium point of the system can lose stability as μ passes through some critical parameter value, μ_c, and a *limit cycle* becomes stable about the (now unstable) stationary state. A *supercritical* Hopf bifurcation occurs when a stable limit cycle emerges as μ increases through μ_c, and *subcritical* when it appears for $\mu < \mu_c$[1]. This is illustrated in Figure 1.1, which shows the emergence and growth of a stable limit cycle in 2-dimensional phase space

[1] Alternative definitions of the terms supercritical and subcritical exist. See, for example, reference [16].

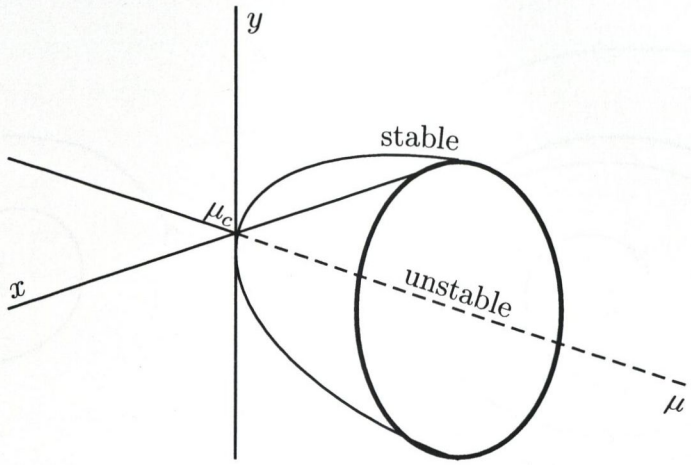

Figure 1.1: Hopf bifurcation to a limit cycle in x-y phase space. The fixed point is the origin in the (x, y) plane, drawn as a solid line along the parameter axis for $\mu < \mu_c$. As the parameter μ is increased through a critical value μ_c, the stationary state becomes unstable (dashed line) and a stable limit cycle grows around it (heavy line).

as a parameter is varied. Figure 1.2 illustrates the behaviour of trajectories in a two-dimensional phase space, first for the case $\mu < \mu_c$, in which trajectories spiral away from the (unstable) limit cycle B′ and towards the (stable) stationary state A′. For $\mu > \mu_c$, the limit cycle B is stable and fixed point A is unstable, with trajectories moving towards B and away from A.

The appearance of limit-cycle behaviour in a chemical or biochemical reaction is revealed by sustained oscillations in the observable components. The number of oscillations per cycle denotes the period order. A single oscillation in one cycle is called a period-1 oscillation, and higher periods are possible in systems of dimension greater than 2. Bifurcations of period-1 oscillations to period-2, -4, -8,. . . ,2^k are called *period doubling* bifurcations. More complex patterns of behaviour are also possible.

As an illustration of the simplest, period-1 oscillations, we consider the following abstract chemical reaction scheme due to Lotka [17]

$$\mathrm{A} + \mathrm{X} \xrightarrow{k_a} 2\mathrm{X}$$

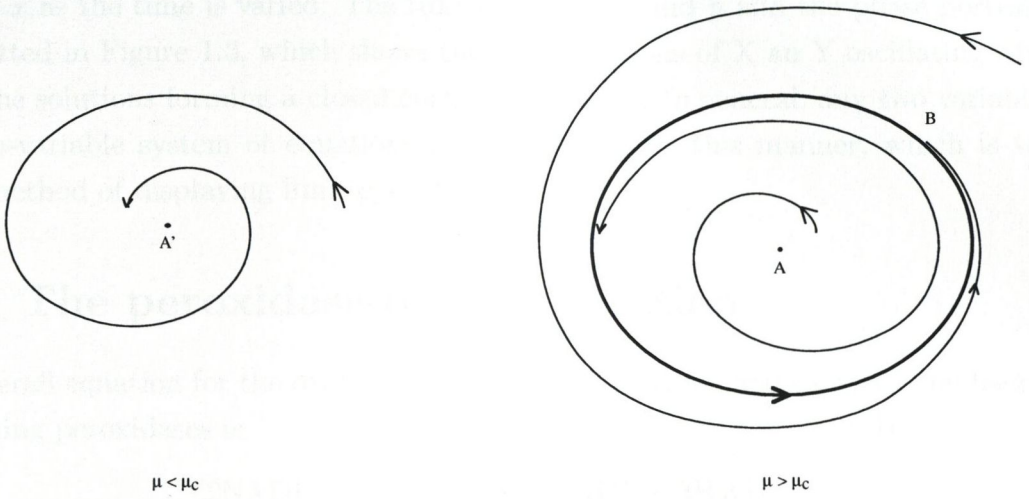

Figure 1.2: Birth of a stable limit cycle as a bifurcation parameter μ passes through a critical value μ_c. The left figure shows a stable stationary state (A′); on the right, the stationary state (A) is unstable, whereas the limit cycle (B) is stable, and is the attracting limit set for trajectories of points starting both from the inside and outside the area that it encloses.

$$\begin{aligned} \mathrm{X} + \mathrm{Y} &\xrightarrow{k_b} 2\mathrm{Y} \\ \mathrm{Y} &\xrightarrow{k_c} \mathrm{B} \end{aligned}$$

where X and Y are molecules in a homogeneous solution and A, B, and C are abundant molecules (whose concentrations may be considered as constant). If we let x and y represent the concentrations of X and Y at time t then the following rate equations may be used to model the scheme:

$$\begin{aligned} \frac{dx}{dt} &= x(k_a - k_b)y \\ \frac{dy}{dt} &= (k_b x - k_c)y \end{aligned}$$

. These equations were used independently by Lotka and Volterra[2] in modelling the above chemical reaction scheme and the dynamics of predator-prey interactions, respectively, and consequently are usually referred to as the Lotka-Volterra equations.

[2]Volterra, V. (1926) Vatiazioni e fluttuazioni del numero d'individui in specie animali conviventi. *Mem. Accad. Naz. Lincei* **2**, 31–113. English translation in Chapman, R. N. (1931) *Animal Ecology*, pp. 409–448, McGraw-Hill, New York.

A *phase portrait* is a useful graphical method of displaying the solutions to a set of differential equations. The phase portrait of the Lotka-Volterra system is a plot of y against x as the time is varied. The time courses of x and y and the phase portrait, are plotted in Figure 1.3, which shows the concentrations of X an Y oscillating with time, the solutions forming a closed curve in x-y space. In general, any two variables of an n-variable system of equations may be plotted in this manner, which is the usual method of displaying limit cycle behaviour.

1.2 The peroxidase-oxidase reaction

The overall equation for the oxidation of NADH by dioxygen and catalysed by haem-containing peroxidases is

$$2\mathrm{NADH} + \mathrm{O_2} + 2\mathrm{H^+} \rightarrow 2\mathrm{NAD^+} + 2\mathrm{H_2O} \tag{1.2}$$

and is called the peroxidase-oxidase (PO) [19] or peroxidase-NADH [20] reaction. In the case of horseradish peroxidase, observations of its NADH-oxidation abilities *in vivo* have been made [21].

Oscillatory kinetics of this reaction were first reported in 1965 by Yamazaki, Yokota and Nakajima [22], who monitored NADPH and oxygen levels in a system comprising horseradish peroxidase, glucose-6-phosphate dehydrogenase, glucose-6-phosphate and $\mathrm{NADP^+}$. The experimental system was held open through the continuous introduction of oxygen, and damped oscillations were observed in the concentrations of the substrates and of oxidation states of the enzyme. They observed that the reaction was favoured by acidic pH, and noted in the same article that NADH was the only known substrate that could be oxidised in an oscillatory manner, examples of other substrates being indole acetic acid and dihydroxyfumarate. Since that time, however, oscillations have been observed using indole-3-acetic acid in place of NADH [23].

In a subsequent paper, Yamazaki and Yokota reported [24] that the rate of oscillatory NADH oxidation was also a function of NADH concentration and oxygen influx rate. Degn [25] stated that a key feature of the kinetic mechanism might be substrate inhibition by oxygen, since Yamazaki and Yokota had noticed that at high oxygen concentrations the peroxidase was converted to a catalytically inactive form that they identified as Compound III, a complex of superoxide anion and the native enzyme (see Table 1.1). Degn proposed that the enzyme rate law could be expressed as:

$$v_0 = -d\mathrm{O_2}/dt = \frac{V_m \mathrm{O_2}}{K_m + \mathrm{O_2} + \mathrm{O_2^2}/K_s} \tag{1.3}$$

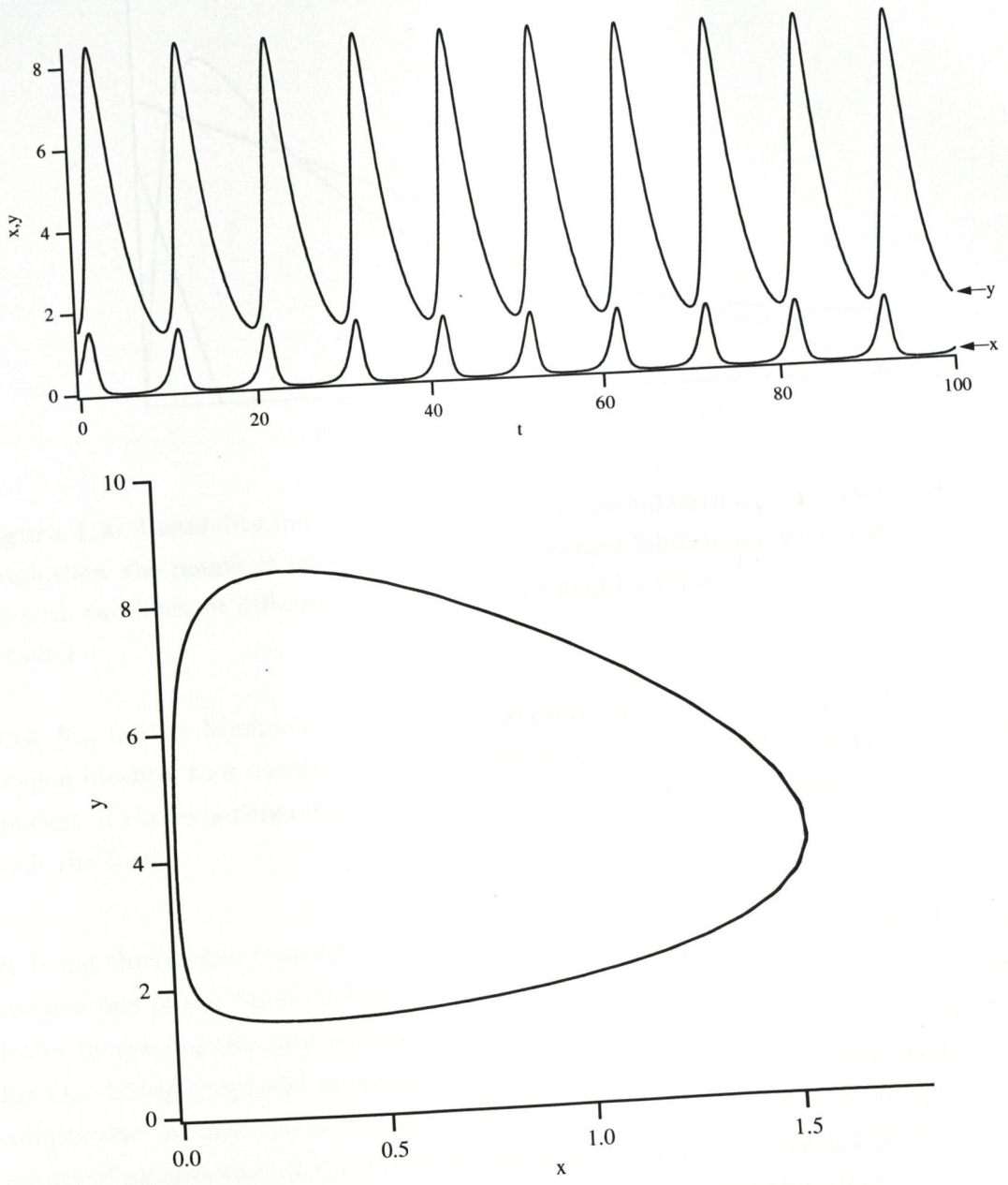

Figure 1.3: Example of a phase portrait. The Lotka-Volterra equations were integrated numerically using a Runge-Kutta algorithm (see Press *et al.* [18]). The upper graph shows oscillations in x and y, the lower graph shows the phase portrait.

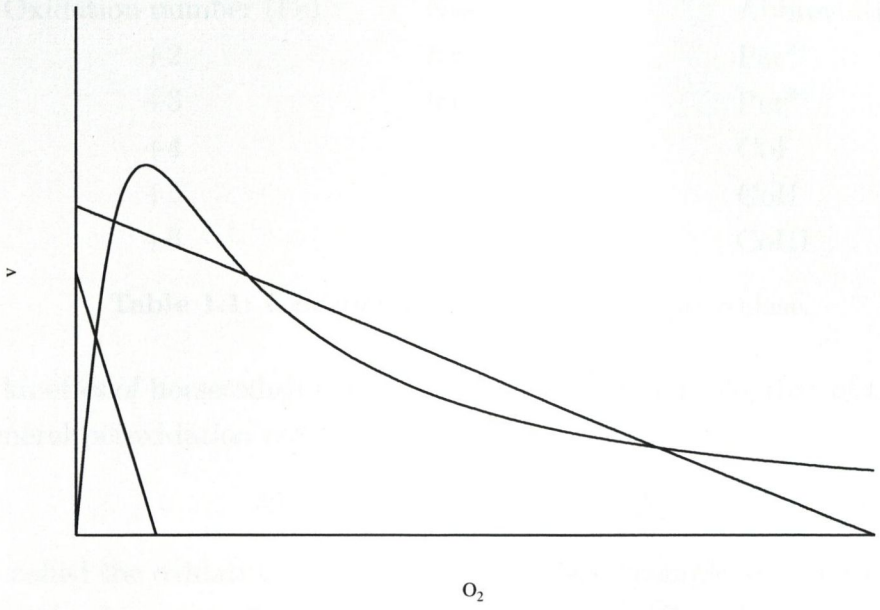

Figure 1.4: Bistability introduced through substrate inhibition in an open system. The graph show the points of intersection of the substrate inhibition curve given by Equation 1.3 with two lines, at different values of K, described by Equation 1.4. See text for further details.)

with K_m as the Michaelis constant for oxygen and K_s the equilibrium constant of oxygen binding to a catalytically active enzyme-oxygen complex, forming an inactive species. If the experimental system was held open and if the oxygen transfer function took the form

$$dO_2/dt = K(O_{2(g)} - O_2), \tag{1.4}$$

K being the oxygen transfer constant and $O_{2(g)}$ the (fixed) concentration of oxygen in the gaseous phase, then multiple steady states would be possible, predictable theoretically by setting the rate equations (1.3) and (1.4) equal to one another and solving for O_2. Using graphical methods (see Figure 1.4), Degn showed that such a system admits one or three steady state values depending on the value of K, given by the points of intersection of the substrate inhibition and linear oxygen transfer functions. With three steady states, the middle point is unstable and the other two are stable, hence the coexistence of two stable steady state points (bistability), which Degn went on to demonstrate experimentally in a study of the peroxidase-oxidase reaction in an open system.

The oxidation states of horseradish peroxidase and their nomenclature are summarised in Table 1.1. The history of the compounds referred to in the table can be traced back to the seminal work of Chance [26], who studied the properties and

Oxidation number (Fe)	Name	Abbreviation
+2	ferroperoxidase	Per^{2+}
+3	ferriperoxidase	Per^{3+}
+4	Compound I	CoI
+5	Compound II	CoII
+6	Compound III	CoIII

Table 1.1: Oxidation states of horseradish peroxidase.

reaction kinetics of horseradish peroxidase in its more usual rôle, that of the catalysis of the general peroxidation reaction

$$AH_2 + HOOR \rightarrow ROH + A, \tag{1.5}$$

and who called the oxidation states of the peroxidase "complexes". Throughout this document, the "compound" terminology is used since "Complex I", "Complex II", etc., are more usually associated with the respiratory complexes of the mitochondrial electron transport chain. A rapid-flow kinetics study [26] revealed that Compound II is the Michaelis-Menten, enzyme-substrate, complex of the peroxidative reaction, which proceeds according to the following elementary steps; first, a reaction occurs between native peroxidase (peroxidase-hydroxide, or Per-OH) and the peroxide, to form Compound I:

$$Per - OH + HOOR \rightarrow Per - OOH - I + H_2O, \tag{1.6}$$

where the Per-OOH-I is Chance's notation for Compound I in Table 1.1. This complex undergoes a transition to a second compound, Per-OOH-II,

$$Per - OOH - I \rightarrow Per - OOH - II, \tag{1.7}$$

which reacts with an electron acceptor AH_2 to reform the native peroxidase,

$$AH_2 + Per - OOH - I \rightarrow Per - OH + A. \tag{1.8}$$

These oxidation states of the peroxidase, along with the Compound III referred to above, are all involved in the oxidation reaction of NADH.

In 1969, Nakamura *et al.* published the first recorded example of sustained oscillations in the peroxidase-oxidase system [27]. The enzyme was in this case lactoperoxidase purified from bovine milk, and the reaction was coupled to an NADPH-regenerating reaction catalysed by glucose-6-phosphate dehydrogenase. The oscillations were observed at neutral pH, in order to maximise the efficiency of the recycling enzyme [24]. Nakamura and coworkers observed that, unlike peroxidase from

horseradish, the Compound III form of the enzyme did not readily break down to (native) ferriperoxidase when oxygen levels declined sufficiently. They found that methylene blue (MB) was a good promoter of Compound III decomposition and that 2,4-dichlorophenol (2,4-DCP) was very effective at stabilising oscillations, particularly at neutral pH. These additional compounds have seen widespread use in studies of the oscillators since this work was published. Nakamura *et al.* [27] used a pulse of methylene blue to start oscillations.

A study of the NADH-oxidation catalysed by horseradish peroxidase in a closed system was carried out by Yokota and Yamazaki [28], who examined the effect of initial NADH concentration on the reaction dynamics, and found that elevated levels of initial NADH increased the rate of production of peroxidase Compound III. Adding trace amounts of H_2O_2 gave rise to an initial burst in Compound III formation, about 2 mol of which were formed per mol of the peroxide. This study also revealed that the absorbance at 418 nm that is typically used to follow the Compound III form of the enzyme may in fact be a combination of Compounds II and III, since its value was found to be approximately the sum of the individual species followed at 463 and 452 nm, respectively.

Yokota and Yamazaki concluded their study with a computer simulation of a nine-variable model of the peroxidase-oxidase reaction in a closed system that was capable of reproducing the induction, steady state (during which oxygen is consumed and H_2O_2 produced) and termination phases of a single oscillation.

Olsen and Degn [19] discovered that in the presence of 2,4-dichlorophenol and methylene blue the phenomenon of bistability due to substrate inhibition of horseradish peroxidase by oxygen was no longer apparent, and also that 2,4-dichlorophenol was necessary to observe sustained oscillations in an open reaction system. Their experimental apparatus comprised an infusion pump to maintain the average NADH concentration in the reaction and oxygen was introduced by blowing a regulated oxygen/nitrogen mixture over the surface of the solution. In this and a companion paper [29], it was proposed that the basic mechanism involved a free radical branched chain reaction in which Compounds I and II were implicated in reactions determining critical concentrations of NADH and O_2 that defined the switch to an oscillatory mode. The theoretical model proposed was based on a model of the Bray reaction due to Lindblad and Degn [30], since there were similarities between the waveforms of NADH and diiodine in the two oscillators.

The peroxidase-oxidase reaction is recognised as the first enzyme reaction capable of exhibiting chaotic behaviour, as was first discovered by Olsen and Degn [31] in 1977. A conjecture was made that a next-amplitude plot of oxygen maxima A_{n+1} versus

A_n could be modelled by a discrete function (recursion relation) that would admit period-3 oscillations, and therefore chaotic behaviour, by invoking a mathematical theorem of Li and Yorke [32].

The bistability aspects of the PO reaction and its role in producing feedback (specifically, feed-forward inhibition) were modelled by Degn, Olsen and Perram [33], and a modified version of their model was used by Olsen to show the formation of a strange attractor, a term first coined by Ruelle and Takens [34] in relation to models of fluid turbulence.

Olsen [35] has extended the Degn-Olsen-Perram model [33] to include more exotic behaviours than simple sustained oscillations. Certain patterns of oscillations observed in experimental studies are successfully reproduced in the Olsen model. A strange attractor was shown to exist for some combinations of the model parameters using the next-amplitude plotting method described above, and this appeared to take the form of a two-dimensional fractal.

Experiments by Lazar and Ross [36] showed that perturbation of the reaction via oscillatory oxygen input to the PO reaction caused a shift in the average concentrations of oscillating species such as NADH. The frequency of the oscillating input was an integral factor of the natural frequency of the oscillator prior to perturbation. They also observed a phase shift between the reactant/product oscillations and oscillations in free energy output (ΔG) which they likened to regulation of energy transduction processes through modulation of reactant inputs.

Aguda *et al.* [37] have shown that a stable stationary state and oscillations may be coexistent in the PO reaction, evidence for which became evident through perturbation of the oxygen supply. Cutting off the oxygen supply caused oscillations to emerge from a stable steady state, which was reversible through the administration of a pulse of hydrogen peroxide.

Geest *et al.* [38] reported that the concentration of 2,4-dichlorophenol can be used as a bifurcation parameter, showing that both intra- and inter-experimental variation of [2,4-DCP] gave rise to period-doubling bifurcations and chaos. Evidence for the chaotic nature of the seemingly aperiodic trajectories was provided through the discovery of a positive Lyapunov exponent, indicating sensitive dependence on initial conditions.

Rys and Wang [39] attempted to show that deuterated NADH (NADD) increases the amplitudes and periods of oscillations with the hope that isotope effects might be useful in mechanistic studies of the reaction, however, as Olson [40] has pointed out, reproducibility of this effect was not established, which limits the usefulness of their study.

Hauck and Schneider [41] created a continuous-flow well-stirred tank reactor[3] for their study of this oscillator, and with it were able to observe mixed-mode and quasiperiodic oscillations[4]. This behaviour was the first such that was experimentally observed in the PO reaction; similar types of complex behaviour had been predicted previously in a model by Larter *et al.* [42, 43].

Recent work on this oscillator has frequently focused on the roles of the auxiliary reagents methylene blue and 2,4-dichlorophenol. Low-level chemiluminescence studies by Watanabe and Inaba [44] revealed fluctuations in chemiluminescence intensity throughout the reaction; the type of oscillations included damped, sustained and bursting types as the concentration of 2,4-DCP was varied. The reaction mechanism that they described assigned to 2,4-DCP (referred to below as DCP) a role in catalysing the production of $NAD^{\bullet}$, the free radical form of NAD, through the agency of superoxide anion, as follows:

$$DCP + O_2^- \rightarrow DCP^{\bullet} + O_2 \tag{1.9}$$

$$DCP^{\bullet} + NADH \rightarrow DCP + NAD^{\bullet} \tag{1.10}$$

Since it has elsewhere been claimed that DCP promotes the decomposition of CoIII [19], Hung *et al.* [45] have proposed direct involvement of DCP with that species,

$$DCP + CoIII \rightarrow DCP^{\bullet} + Per^{2+} + NAD^{\bullet} \tag{1.11}$$

with DCP regenerated through 1.10.

The existence of $NAD^{\bullet}$ in the PO reaction comes from absorbance spectra taken after pulse radiolysis of NADH, in experiments performed by Land and Swallow [46], who also noted the production of an inert NAD dimer, which we denote here NAD_2. The possible formation of NAD dimer as an end product of the PO reaction means that the overall equation 1.2 may well be a simplification, a matter which will be further examined in the mathematical models proposed in Chapter 7.

A role for methylene blue in the PO reaction has been suggested by Olson *et al.*, whereby this species cycles between oxidised (MB^+) and reduced (MBH) forms in catalysing the reaction between NADH and O_2. Hence the following reaction

$$NADH + O_2 + H^+ \rightarrow NAD^+ + H_2O_2 \tag{1.12}$$

[3]CSTR

[4]Mixed-mode oscillations are discussed in Ch.7.

may be viewed as the sum of two steps involving methylene blue:

$$MBH + O_2 + H^+ \rightarrow MB^+ + H_2O_2 \quad (1.13)$$

$$MB^+ + NADH \rightarrow MBH + NAD^+ \quad (1.14)$$

Hauser and Olsen [1] have studied the effects of naturally occurring phenols on the PO reaction dynamics, including vanillin, *o*-coumaric acid, and various chlorophenols. They concluded that the readiness of such phenols to form a phenoxyl radical (as measured by the reduction potential) determined the type of behaviour: inhibition, steady-state, damped, sustained or complex oscillations.

Kummer *et al.* [47] have demonstrated that structurally distinct peroxidases can also catalyse the oxidation of NADH, and were able to observe oscillations with soybean peroxidase, chloroperoxidase and microperoxidase, amongst others. Valeur and Olsen [48] also published the first example of sustained oscillations using dihydroxyfumaric acid in place of NADH.

1.2.1 Experimental techniques

The methods of study of this oscillator in the laboratory have differed in the detail. However, the majority of studies are conducted using a semi-batch apparatus, in which one or both substrates (NADH and O_2) were continuously infused into a stirred reactor, and the products allowed to accumulate. Although such products as NAD^+ are assumed to be inert, in the previously noted study by Hauck and Schneider (p.12) the solution volume was maintained allowing excess volumes to drain out of the reactor. In addition to the removal of products, the CSTR approach makes it necessary to replenish the reactants lost by this method, including the enzyme and other catalysts, which makes it a more costly option.

With respect to methods of NADH supply there are two that have been used, direct infusion and coupled reactions, the latter of which has generally been a recycling mechanism that uses glucose-6-phosphate dehydrogenase, with glucose-6-phosphate and $NAD(P)^+$ in excess or continuously supplied. The direct infusion method has typically featured a motor-driven infusion pump, however, Olson and Scheeline eschewed this method in favour of a pulseless delivery of NADH, since pulsatile infusion might be contributor to the dynamics of the reaction. Their method [49] consisted of pressurising a vial containing concentrated NADH with nitrogen gas, and regulating the flow of NADH into the reactor by varying the applied pressure.

Oxygen delivery was usually performed using specialised apparatus. Olsen [29] used a digital gas mixer to combine air and nitrogen using a custom-built apparatus

originally described by Lundsgaard and Degn [50], that was also used in subsequent work [33, 37]. More recent work has employed commercially available mass flow controllers for the purpose of regulating gas flow, as exemplified by Hung and Ross [51] and Olson and Scheeline [49], with one controller assigned to oxygen and another to its diluent.

Reaction progress was measured directly by means of a spectrophotometer and dioxygen probe. Absorbances of NADH and the peroxidase enzyme in its various oxidation states can be monitored as well as the dissolved oxygen. Reactors have frequently been quartz cuvettes, although the dimensions of these vary considerably between research groups. Custom cuvettes were not unusual. Degn *et al.* [33] have used hexagonal 5 ml cuvettes, and Olson [40] has used cost- efficient cylindrical quartz vessels, taking into account the adjustments that must be made due to their atypical optics. The CSTR cuvette of Hauck and Schneider used a Plexiglas reactor with quartz faces for passage of the light beam of the spectrophotometer. One Plexiglas side was used to house the oxygen electrode, a practice which is in common with other experimenters [33, 38].

Olson [40, 49] has made a rigorous examination of the experimental apparatus and methodologies used to study the peroxidase-oxidase reaction and paid careful attention to the details of oxygen and NADH delivery, the stirring apparatus, both with regard to efficacy of mixing and its effect on oxygen transport constants, and also the influence of wavelengths of light (for example, through continuous illumination of a sample in a spectrophotometer) on the type and duration of oscillations. Olson has demonstrated that oxygen transfer into semi-batch and continuous-flow reactor systems is a mass transport phenomenon [52], and not diffusion-controlled. Due to concerns with the use of stainless steel and its possible effect on the PO reaction by acting as a catalyst of free radical production, Olson has used Teflon impellers exclusively and conducted a study which showed that a stainless-steel coil inserted into the reaction mixture can increase the lifetime of oscillations [40].

1.3 Aims

The aims of this work were: (i) to design and characterise an experimental apparatus for the study of the PO reaction, (ii) to study the effects of pH and ionic strength, and investigate the possibility of using indicators to follow pH changes in a weakly-buffered reaction, (iii) to study the effects of (a) phenols other than 2,4-DCP and (b) free radical scavengers on the appearance and sustenance of oscillations, and (iv) to develop new mathematical models of the PO oscillator and to develop the simplest

possible model that would sensibly describe the behaviour of the system.

Chapter 2 deals with the apparatus used in experimental work, and describes the procedures used. Chapter 3 describes physical experiments that were used to test the apparatus, and determine the control parameters. The general behaviours that were observed in this study of the PO reaction are to be found in Chapter 4. An account of the use of pH indicators, the variation of pH and ionic strength is to be found in Chapter 5, as are the results obtained from studies where lactoperoxidase replaced horseradish peroxidase. Chapter 7 describes three new models of the oscillator, using as a basis a subset of the elementary chemical steps for which rate constants are known [53], and relates where possible the simulation results of these models to the laboratory data. Concluding remarks and a prospectus for future avenues of enquiry are given in Chapter 8.

Chapter 2

Materials and Methods

2.1 Reagents

Horseradish peroxidase (immunoassay purity) was obtained from Sigma (St. Louis, MO, Cat. No. P-8375, 288 U/mg) as a salt-free, lyophilised powder and stored at -20°C, desiccated. β-NADH was purchased from Sigma as the disodium salt (Cat. No. N-8129, 98% purity) and stored at 4°C. Methylene blue and 2,4-dichlorophenol were obtained from Sigma (Cat. Nos. MB-1 and D-6023). Acetic acid and anhydrous sodium acetate were obtained from BDH Limited (Poole, England, Cat. Nos. 3014 and 27013). For the assay of horseradish peroxidase, pyrogallol and hydrogen peroxide were obtained from Sigma. Potassium dihydrogen orthophosphate and dipotassium hydrogen orthophosphate were obtained from BDH. Distilled, deionised water from a Millipore Milli-U10 water purification system was used in all experiments, unless stated otherwise. 5% oxygen in nitrogen and 100% nitrogen gases were purchased from Air Products Ltd, Dublin.

2.2 Apparatus

2.2.1 Overview

The reaction described by Equation 1.2 was studied in a thermodynamically open system, where reduced nicotinamide adenine dinucleotide and gaseous dioxygen were supplied steadily and continuously into a thermostated, homogeneous solution of peroxidase, buffered with 0.1 M sodium acetate/acetic acid and containing the auxiliary reagents methylene blue (MB^+) and 2,4-dichlorophenol (2,4-DCP). An overview of the components of the apparatus used is shown in Figure 2.1, which describes the

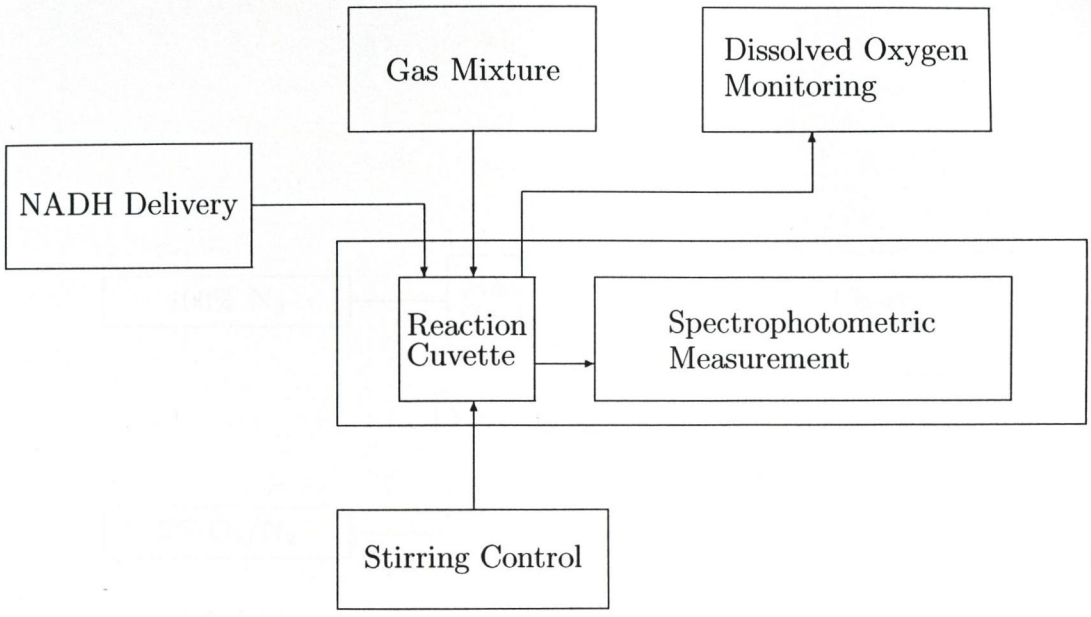

Figure 2.1: Overview of the experimental apparatus.

reagent inputs and data outputs. A more detailed picture is given in Figure 2.2.

2.2.2 Reaction vessel

The reaction vessel used in this study of the peroxidase-oxidase reaction was a quartz $1 \times 1 \times 4.2$ cm cuvette fitted with a Teflon lid in which holes were drilled for the NADH and O_2/N_2 mixture gas input capillaries, gas outlet, and oxygen electrode. The solution volume was 2 ml, and was stirred from beneath by a magnetic stirrer (Rank Bros., U.K., Model 200). The stirring bar, of dimensions $2 \times 2 \times 7$ mm was Teflon-coated. Figure 2.3 (see p. 19) shows the arrangement of the inlet and outlet lines, oxygen electrode and stirring mechanism with respect to the cuvette.

The stirring control box featured a power switch and a single rotating knob which lacked a graduated scale. A graduated overlay was constructed manually for the knob which allowed the region between the minimum and maximum positions to be subdivided on a scale of 0 to 100%, accurate to within $\pm$ 5%. The manufacturer's specifications gave a minimum speed of 120 rpm and maximum of 1500 rpm for the stirrer, both figures approximate. Assuming that these figures are those obtained at the extrema of the speed settings and that a linear relationship exists between knob

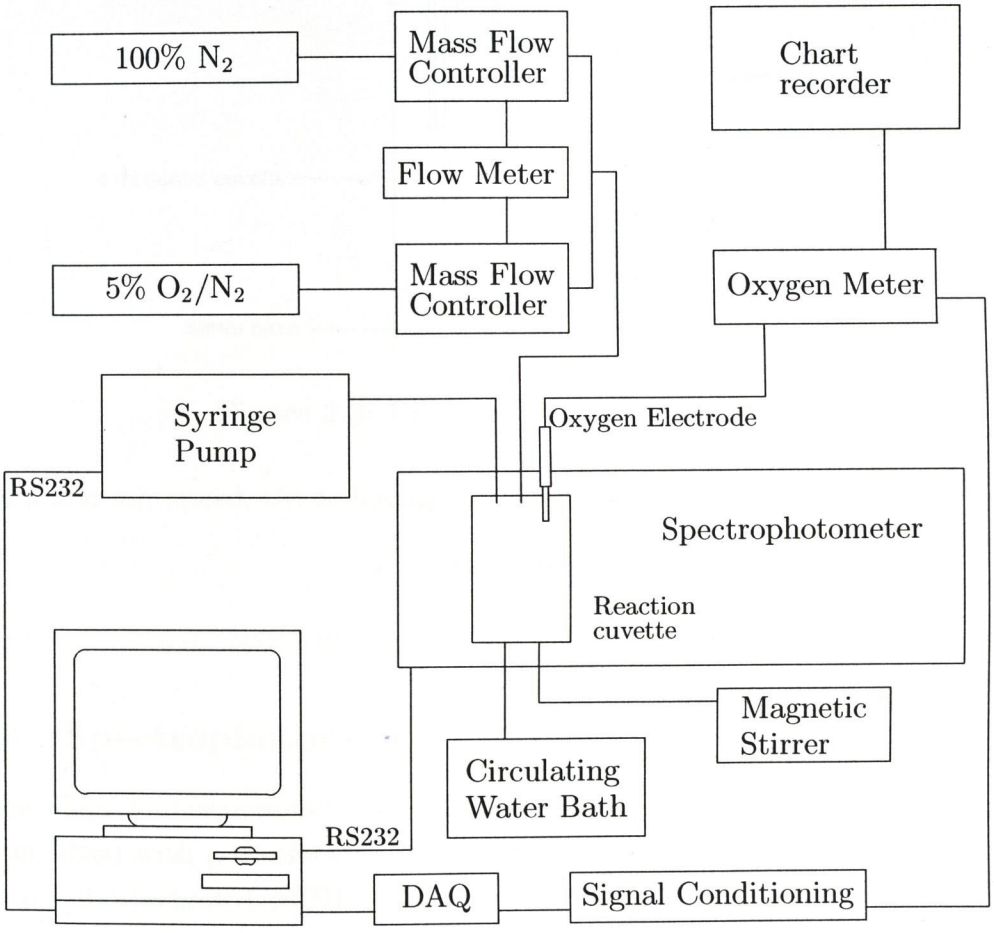

Figure 2.2: Detailed diagram of the apparatus. NADH is contained in a syringe on the syringe pump. Both the pump and the spectrophotometer are under computer control, via a serial RS232 interface. Further details are given in the text. See the Glossary on p. 189 for definitions of abbreviations used.

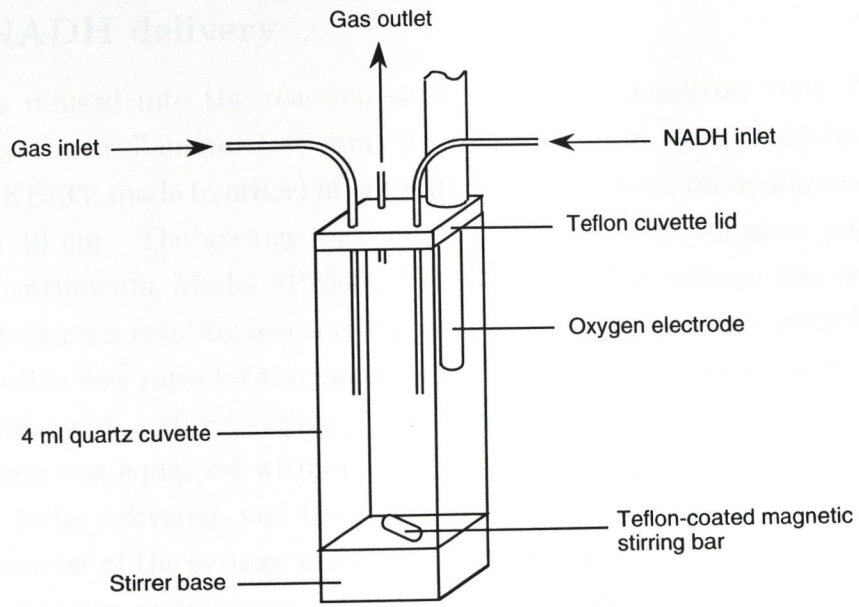

Figure 2.3: Diagram of the reaction cuvette.

position and stir speed, the following formula may be used:

$$s = 120 + 1380p/100 \tag{2.1}$$

where s is the stirrer speed in rpm and p is the setting on the controller in percent.

2.2.3 Spectrophotometry

All absorbance measurements were made with a Kontron Uvikon 931 spectrophotometer fitted with a thermostated cell holder connected to a circulating water bath (Julabo Labortechnik GMBH, Germany; Model U3). The instrument was a split-beam type, and contained a reference cell position which could be used to subtract a continually changing reference sample; in practice this was used to hold a buffer blank. The spectrophotometer was controlled by an internal IBM PC-AT compatible computer. Absorbance readings were usually taken every 6 seconds. Three wavelengths were used to follow the course of the peroxidase-oxidase reaction over time, 360 nm, 402 nm and 418 nm, which are usually taken as markers for NADH and two oxidation states of the enzyme's haem group. The software driving the instrument was capable of remote control by a second external computer, a feature which was used to advantage (see Section 2.2.7).

The cuvette was seated on top of the stirrer base in the cell holder. Aluminium covers were constructed in-house to allow the passage of the dioxygen probe and capillary tubing into the spectrophotometer whilst minimising the effect of stray light.

2.2.4 NADH delivery

NADH was infused into the reaction solution from a Hamilton 1710 TLL 100 μl glass syringe (inner diameter 1.46 mm) through a stainless steel, blunt-tipped needle (Hamilton KF733; made to order) of outer diameter 0.21 mm, inner diameter 0.11 mm and length 40 cm. The syringe was mounted on a syringe infusion pump (World Precision Instruments, Model SP250i). The plunger of the syringe was depressed by a pusher block on a rotating leadscrew driven by a microprocessor-controlled stepper motor. Possible flow rates for the pump ranged from 0.01 μl/h (using a 10 ml syringe) to 71 ml/min (with a 60 ml syringe).

The pump was equipped with an alphanumeric display and keypad. The volume of solution to be delivered, and the required flow rate were entered before use. The internal diameter of the syringe was entered directly or from a table of known syringe types stored in the pump's non-volatile memory. With this information all further calibration and calculations were performed automatically by the pump. More frequently, the included serial interface was used to control the pump from a remote computer, which made changes to parameters faster and more convenient.

At the start of an experiment, the syringe was filled with NADH solution and locked into place on the pump. The tip of the needle was then inserted into the cuvette through a supporting sheath in the cuvette top, and the needle tip placed approximately 2 mm beneath the surface of the liquid.

NADH influx rate can be expressed in units of either volume or concentration per unit time (usually μl/h and mM/h, respectively). If the volume change is small, so that the reaction volume in the cuvette remains approximately constant, then the following equation may be used to convert between volume and concentration units of flow rate:

$$r = \frac{c_s v_i}{V_T}, \tag{2.2}$$

where

r = NADH concentration-influx rate (mM/h)
c_s = concentration of NADH in syringe (mM)
V_T = reaction mixture volume (μl)
v_i = NADH volume-influx rate (μl/h)

An heuristic derivation of the above equation may be constructed as follows. If there are n mol in volume v, the concentration is given by $c = n/v$. We wish to find the rate of change of c, dc/dt, after making a small volume addition dv of substance at a concentration c_s in time dt. If the instantaneous concentration is $c = n/v$, then after

an arbitrarily small time increment dt,

$$c + dc = \frac{n + dn}{v + dv}.$$

Therefore

$$dc = \frac{n + dn}{v + dv} - \frac{n}{v}$$
$$= \frac{vdn - ndv}{v^2 + vdv}.$$

Since $dv \ll v$ this reduces to simply $dc \approx dn/v$. An expression for the concentration change over time is

$$\frac{dc}{dt} = \frac{1}{V_T}\frac{dn}{dt},$$

where the V_T is the (constant) volume. The concentration of the added substance is constant, so that the number of mol added will be $dn = c_s dv$, so that $dn/dt = c_s dv/dt$.

Finally, if we let $r = dc/dt$ and $v_i = dv/dt$ we obtain Equation 2.2 as an expression for the concentration-influx rate r.

2.2.5 Oxygen delivery

Two gas cylinders, one containing 5% oxygen in nitrogen, the other pure nitrogen, were each connected to a mass flow controller (Sierra Instruments, Inc., Model 840) calibrated to 0–100 ml min^{-1} (O_2/N_2) and 0–200 ml min^{-1} (N_2), and accurate to within ± 1% of full scale. Repeatability was ± 0.2% of full scale (manufacturer's specifications). The mass flow controllers (MFCs) were connected to a dual-channel control unit (Sierra Model 902c) which was used to set the gas flow rates. The gas lines were joined downstream of the mass flow controllers to form a single stream with oxygen composition variable between 0 and 5% and flow rate between 0 and 300 ml min^{-1}.

On entering the cuvette, the oxygen stream can either be blown across the surface of the solution, maintaining a specified oxygen composition in the gas headspace above the liquid, or bubbled (at flow rates typically less than 50 ml min^{-1}) into the liquid by placing the end of the gas line about 2 mm below the surface. Rys and Wang [39], and was the predominant method in the experiments to be described here. In order to maximise their effective accuracy at these lower flow rates, the MFCs were recalibrated by the manufacturer to 0–20 ml min^{-1} (O_2/N_2) and 0–40 ml min^{-1} (N_2), giving a total possible gas flow rate of 60 ml min^{-1}.

Gas composition was determined from the equation

$$c_{O_2} = \frac{v_{O_2}}{v_{O_2} + v_{N_2}} P \tag{2.3}$$

where c_{O_2} is the final composition of oxygen downstream of the joined gas lines, P is the percentage of oxygen present in the oxygen gas tank, and v_{O_2} and v_{N_2} are the individual flow rates of oxygen/nitrogen and pure nitrogen gases. As an example of the use of this equation consider the case where $P = 5\%$, $v_{O_2} = 7.4$ ml/min and $v_{N_2} = 12.6$ ml/min, from which one can predict that the final composition of the gas will be 1.85% in oxygen.

Relying on the manufacturer's quoted accuracy for these devices, the improvement in error associated with their recalibration may estimated as follows; if a gas composition of 2% in oxygen at a flow rate of 20 ml/min was desired, the fraction of the maximum possible oxygen composition would be given by

$$\frac{8 \pm 1\%}{20 \pm 3\%},$$

which would equal 2/5. The error associated with the final composition of the gas can be calculated from Equation (B.1) as 0.4% in oxygen. The corresponding value for the mass flow controllers after recalibration to lower flow ranges would be less than 0.1%, which is a significant improvement in accuracy.

2.2.6 Dissolved oxygen monitoring

A Clark-type electrode (Microelectrodes, Inc., Model MI-730) was used to measure dissolved oxygen. The electrode was shielded by an acrylic housing 3 mm in diameter containing electrolyte solution and with a Teflon membrane at its tip. The response range of the electrode is 0–100% oxygen and sensitivity is 1700 pA in air at 25°C. An oxygen meter (Microelectrodes, Inc., Model OM-4) performed the conversion of current to voltage, and which could display oxygen readings as a percentage or in millivolts. A chart recorder (Philips, Model PM 8252A) was used to monitor dissolved oxygen data and record any changes made to gas flow rate or composition.

2.2.7 Data acquisition and instrument control

Voltage output from the oxygen meter was connected to a PCI-1200 (National Instruments, TX, USA) data acquisition card installed in an Apple Power Macintosh desktop computer (Model 7200 fitted with 32 Mb RAM). The voltage signal was conditioned prior to sampling using a 5B-30 signal-conditioning module (National Instruments) to remove 50-60 Hz electronic noise. The millivolt signal from the oxygen meter was simultaneously converted from a 0-50 mV range to 0-5 V, which allowed acquired data to be directly compared to percentage oxygen (0-5%).

The data acquisition driver software was NI-DAQ (National Instruments) and both the oxygen data sampling and control of the spectrophotometer and syringe pump were coordinated by a LabVIEW (National Instruments Inc., USA) program, `PO_Control.vi`, written by the author, the source code for which is given in Appendix A.7. The user interface of this program is displayed in Figure 2.4. Oxygen data were acquired and displayed continuously. In addition to the signal conditioning, software averaging was employed to further smooth the sampled signal. The spectrophotometer was programmed to take absorbance readings at user-defined regular intervals and the pump parameters were read and set when desired. Three files were created automatically at the start of execution of `PO_Control.vi`: a pump log file, an oxygen data file and a file containing any absorbance measurements. The pump log file recorded the date and time of day, and thereafter any commands sent to the syringe pump during the course of the experiment, along with the elapsed time in seconds. The oxygen data file contained ASCII data in two columns: elapsed time in seconds and oxygen reading in volts. The absorbance data file comprised three columns, the first the time at which the absorbance measurement was taken (elapsed time), the wavelength in nanometers, and the absorbance reading.

2.3 Methods

2.3.1 Peroxidase assay

The quantitative measure of peroxidase used in experiments was the pyrogallol unit of enzymatic activity, defined as the amount of enzyme that will catalyse the formation of 1.0 mg purpurogallin from pyrogallol in 20 s at pH 6.0 at 20°C. The activity unit is desirable since it is independent of the degree of purity of the enzyme preparation. Other enzyme measures are less direct, for example, the R.Z. (Reinheitszahl: the ratio A_{403}/A_{280}) is a measure of haemin content and not catalytic activity [54]. Similarly, concentration is dependent on the value of the molecular weight, inherently a less precise measure since carbohydrate content must be taken into account.

The assay used was that of Sigma [55]. A 3 ml, 1 cm path-length cuvette containing 2.10 ml water, 0.32 ml of 0.1 M potassium phosphate buffer at pH 6.0, 0.16 ml of 0.147 M hydrogen peroxide solution (1.67 ml of a 30% solution diluted to 100 ml with water), and 0.32 ml of 5% (w/v) pyrogallol solution was equilibrated to 20°C in a thermostated spectrophotometer. To this were added 0.10 ml of a solution containing 0.4–0.7 units of HRP per ml of 0.1 M phosphate buffer at pH 6.0, which was then mixed by inversion and the absorbance at 420 nm monitored for up to 2 minutes.

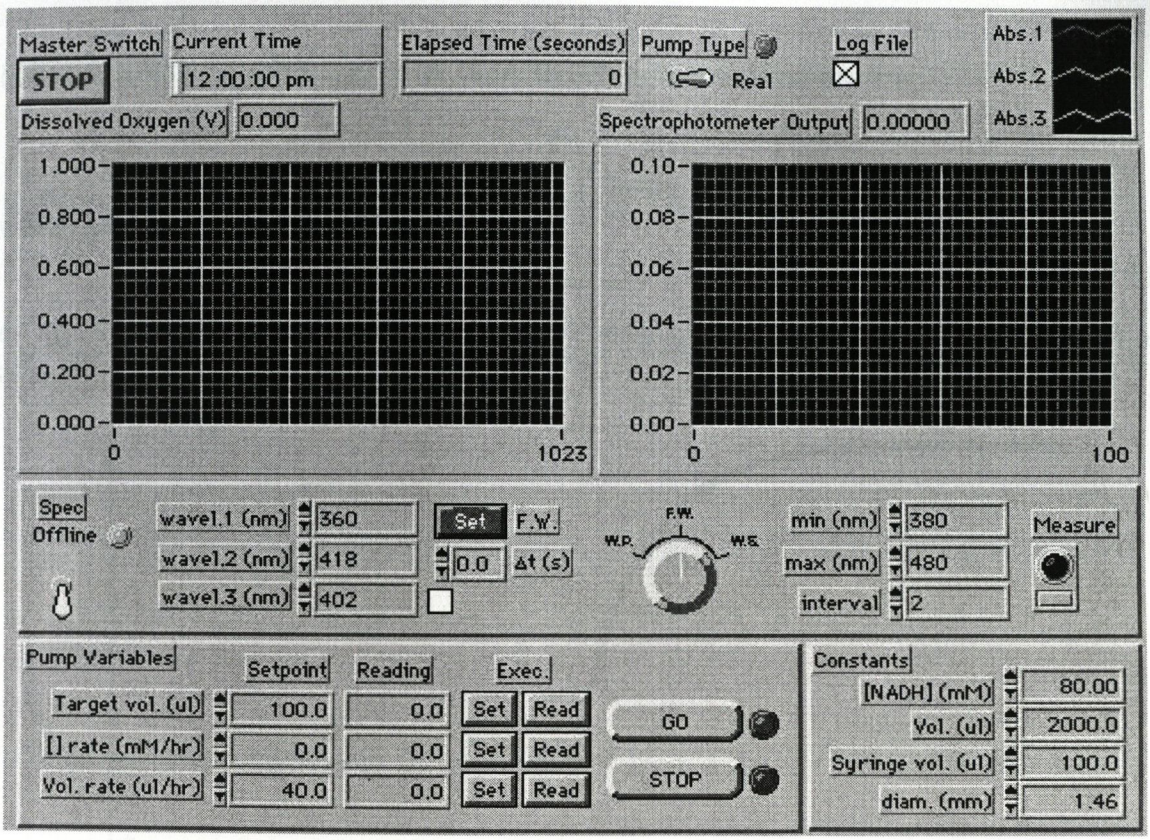

Figure 2.4: User interface of the LabVIEW program `PO_Control.vi`.

The maximal change in absorbance at 420 nm over a 20 s interval was noted and the activity was calculated from the equation

$$\text{Units/mg} = \frac{\max_{\Delta t=20s} \Delta A_{420}}{12 \times (\text{mg enzyme as solid/ml reaction mix})}$$

where the factor 12 is the absorbance coefficient (determined by Sigma).

2.3.2 Oxygen mass-transport constant

The equilibrium between the gas (g) and liquid (aq) phases of the reaction vessel may be expressed as:

$$O_{2(g)} \underset{k_{-t}}{\overset{k_t}{\rightleftharpoons}} O_{2(aq)}. \tag{2.4}$$

The differential equation describing the rate of change of oxygen concentration in the aqueous phase is

$$\frac{d[O_{2(aq)}]}{dt} = k_t[O_{2(g)}] - k_{-t}[O_{2(aq)}]. \tag{2.5}$$

The term $k_t[O_{2(g)}]$ may be replaced with $[O_{2(aq)}]_{eq}$ by employing the equilibrium relationship $[O_{2(aq)}]_{eq}/[O_{2(g)}]_{eq} = k_t/k_{-t}$. Rearranging and integrating,

$$\int_0^{[O_{2(aq)}]} \frac{d[O_{2(aq)}]}{[O_{2(aq)}]_{eq} - [O_{2(aq)}]} = k_{-t} \int_0^t dt,$$

which yields

$$[O_{2(aq)}] = [O_{2(aq)}]_{eq}(1 - e^{-k_{-t}t}) \tag{2.6}$$

as an expression for the dissolved oxygen concentration at time t. In this model k_{-t} is the mass transport constant of oxygen.

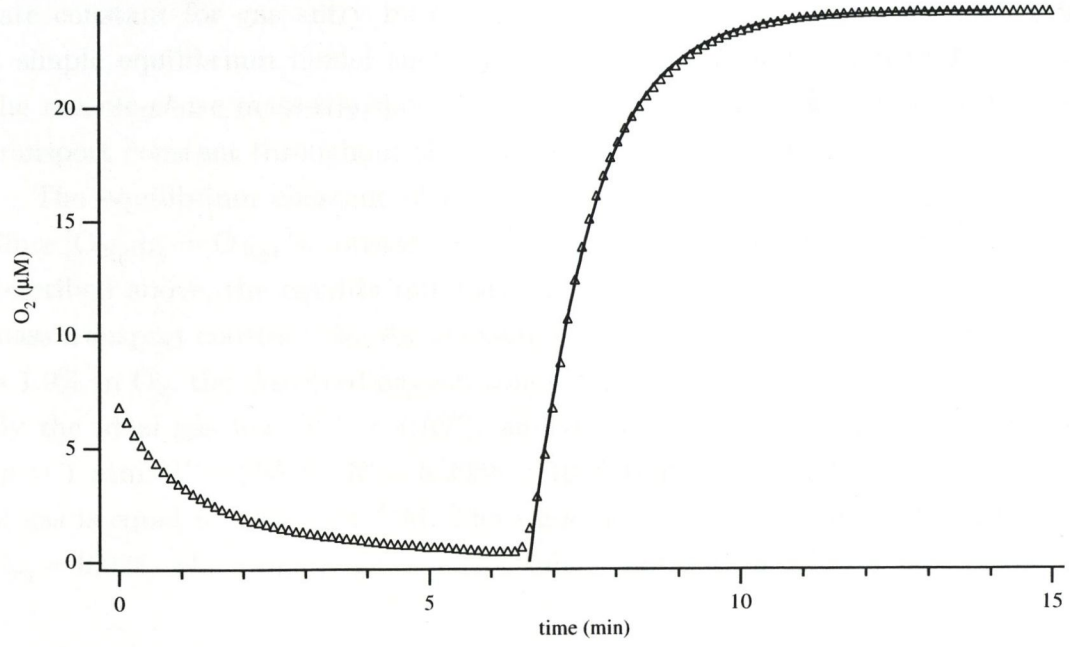

Figure 2.5: Determination of k_{-t} from dissolved oxygen data. Equation 2.6 was fitted by nonlinear regression to acquired oxygen data. The sampling frequency was 0.133 Hz. The value of k_{-t} obtained in this case was 0.99 $\pm$ 0.01 min^{-1}.

The mass-transport constant was determined by first purging the contents of the cuvette with nitrogen to achieve a baseline zero-oxygen concentration. Oxygen was then reintroduced and the time course of aqueous oxygen recorded, which could be modelled by the first-order growth process (2.6). This procedure was followed prior to oscillatory experiments. The equation may be linearised by rearranging and taking the logarithm of both sides to give

$$\log([O_{2(aq)}]_{eq} - [O_{2(aq)}]) = \log[O_{2(aq)}]_{eq} - k_{-t}t. \tag{2.7}$$

The constants $[O_{2(aq)}]_{eq}$ and k_{-t} can be obtained from a plot of $\log([O_{2(aq)}]_{eq} - [O_{2(aq)}])$ against t and further optimised by a method of iterative linear regression, a method

developed by Olson [40]. Details of such a method and the source code of a computer program written for its implementation are to be found in Appendix A.1. Nonlinear curve fitting was the preferred method of determination of k_{-t}, however, and was performed using Igor Pro graphing software (Wavemetrics, Inc., USA) by the Levenberg-Marquhardt nonlinear least-squared algorithm. An example of dissolved oxygen data is shown in Fig. 2.5 along with a curve defined by Eq. 2.6 fitted to the re-equilibration portion.

Since the methodology describes a process whereby dissolved oxygen concentration rises from zero to the equilibrium position, it may seem intuitively obvious that the rate constant for gas entry into solution is that obtained from the application of a simple equilibrium model such as (2.4). The measured quantity k_{-t} is strictly the *reverse-phase* mass-transport constant, but for convenience is termed the mass-transport constant throughout this volume.

The equilibrium constant of the process is $K_{eq} = [O_{2(aq)}]_{eq}/[O_{2(g)}]_{eq} = k_t/k_{-t}$. Since $[O_{2(g)}]_{eq} = O_{2(g)} =$ constant and $[O_{2(aq)}]_{eq}$ and k_{-t} are obtainable by the methods described above, the equilibrium constant can be calculated, and thereby the 'true' mass transport constant, k_t. As an example, consider the case in which the gas stream is 1.9% in O_2, the dissolved oxygen concentration is 21.6 μM and $k_{-t} = 0.55$ min^{-1}. By the ideal gas law ($pV = nRT$), and assuming standard conditions for the gas ($p = 1$ atm; $T = 298$ K; $R = 8.2058 \times 10^{-2}$ L atm K^{-1} mol^{-1}), the concentration of gas is equal to 4.09×10^{-2} M. The value of $[O_{2(g)}]$ is therefore 7.8×10^{-4} M, and $K_{eq} = 0.028$, which finally gives 0.0154 min^{-1} as the value of k_t in this case.

2.3.3 Experimental procedure

It was considered desirable to select a set of standard experimental conditions as a reference point which would describe a region of parameter space where oscillations were most likely to appear and against which the results of other conditions could be compared. The set so chosen is shown in Table 2.1. What follows is an account of a typical oscillatory run under such standard conditions.

Into a clean 1 cm quartz cuvette were pipetted 1824.8 μl of a 0.1 M sodium acetate/acetic acid buffer at pH 5.1, 50 μl of 8 μM methylene blue, 50 μl of 0.8 mM 2,4-dichlorophenol and 18.8 μM horseradish peroxidase, all dissolved in 0.1 M sodium acetate buffer. The stirring bar was added to the cuvette, which was then placed in the thermostated cell holder in the spectrophotometer (set to maintain 25 °C), the cuvette lid affixed and the join sealed using a strip of Parafilm. The stirrer control box was switched on and set to a speed of 1155 ± 66 rpm. A 100 μl Hamilton syringe

Variable	Value
Buffer	0.1 M sodium acetate, pH 5.10 0.01 M sodium acetate, pH 7.00
Enzyme	horseradish peroxidase, 40 U/ml
NADH	0.08 M, in pH 7.0 buffer Initial flow rate: 40 μl/h (1.6 mM/h) Final flow rate: 30 μl/h (1.2 mM/h)
methylene blue	0.2 μM
2,4-dichlorophenol	20 μM
Gas	Flow rate: 8 ml/min (O_2), 12 ml/min (N_2), bubbled Composition: 2.0% in O_2
Stir speed	1155 rpm
Temperature	25°C

Table 2.1: Standard experimental conditions used in the peroxidase-oxidase reaction. The solution volume was 2 ml for all experiments.

was fitted with the 40 cm syringe needle, filled with a solution of 80 mM NADH dissolved in 0.01 M buffer at pH 7.0, taking care that bubbles were excluded, placed on the syringe pump and locked into place. The tip of the gas line was inserted just beneath the surface of the liquid in the cuvette as described in Section 2.2.5. A pure nitrogen stream was bubbled gently into the solution to purge the contents of oxygen, at a flow rate in the region 30–35 ml/min. During this period the LabVIEW program `PO_Control.vi` was started and dissolved oxygen monitoring was commenced (see Section 2.2.7) with a sampling frequency of 1 Hz. The start of oxygen data acquisition was chosen as a convenient mark of zero time. When dissolved oxygen had reached a resting level, the mass flow controllers were set to deliver 8 ml/min of 5% O_2 and 12 ml/min N_2, giving a total gas flow rate of 20 ml/min and composition of 2% oxygen. The chart recorder was used to record changes in gas flow rate or composition. After dissolved oxygen had re-equilibrated with the gaseous phase, the syringe needle was inserted into its supporting sheath in the cuvette lid, and the tip placed beneath the liquid meniscus. Neither the needle, stirring bar nor the oxygen stream entered the light path of the spectrophotometer.

A wavelength scan over the range 340–700 nm was recorded and saved to the hard disk of the spectrophotometer's internal computer (see Figure 2.7). The pump parameters were set using the remote LabVIEW program, absorbance data acquisition at 360 nm was commenced at a sampling rate of between 10 and 20 data points per minute, and NADH delivery was started at 40 μl/h (1.6 mM/h). Within a period of 5–10 minutes, dissolved oxygen began to decline. The rate of decline accelerated until most of the oxygen in the cuvette had been consumed. NADH levels, which by this time had risen from zero to about 0.1 mM, decreased also. Oxygen and NADH increased again, and continued to oscillate regularly thereafter for more than an hour. After the first two full oscillations had appeared the NADH influx rate was dropped to a value of around 30 μl/h, which was chosen to balance the net rate of consumption of NADH with its supply. A graph depicting aqueous oxygen and NADH time traces is shown in Figure 2.6. At the end of the experiment, usually when the NADH supply was depleted, the pump was stopped, a final absorbance scan was made, and the execution of program `PO_Control.vi` terminated. Figure 2.7 shows the wavelength scans obtained before and after the experiment.

The experimental conditions were recorded in a database[1] after each experiment, which allowed for ready comparison of settings used on different occasions. An example of one record taken from this database is given in Figure 2.8.

[1]FileMaker Pro 4.0, FileMaker Inc.

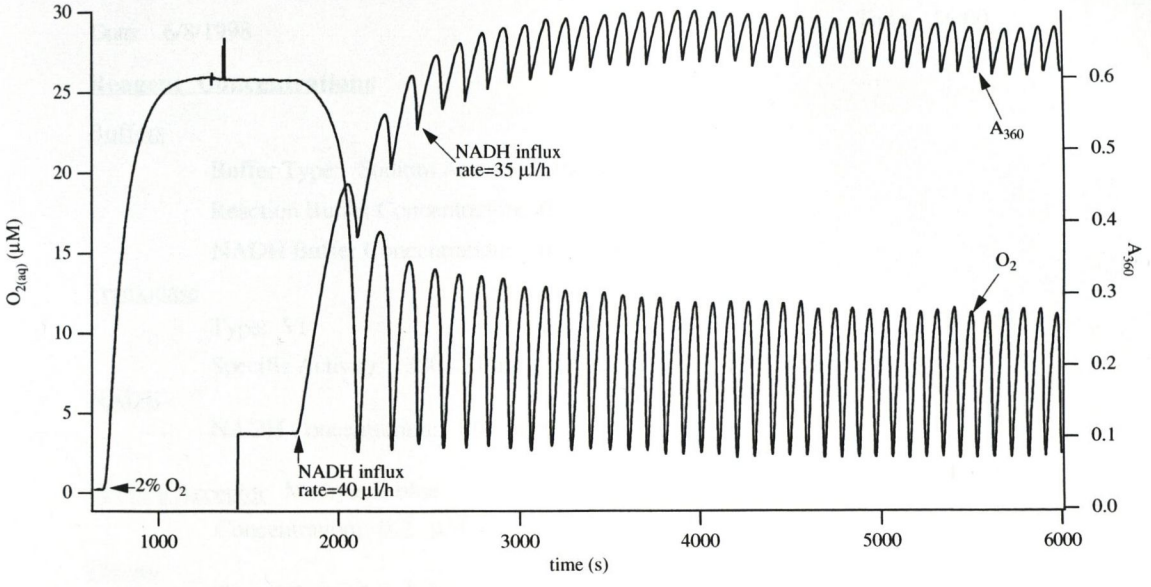

Figure 2.6: Oscillations in dissolved oxygen and NADH. Experimental parameters were as Table 2.1, with the exception of NADH volume-influx rate, which was 35 μl/h.

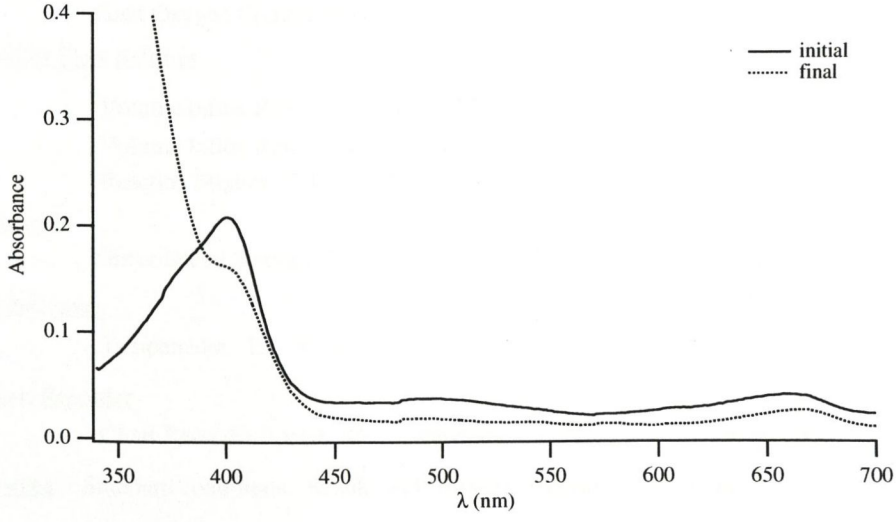

Figure 2.7: Wavelength scans of a solution containing, initially, 40 U/ml horseradish peroxidase, 0.2 μM methylene blue and 20 μM 2,4-dichlorophenol. Peaks on the first curve are evident at 402 nm and 664 nm, which correspond to the haem moiety of the peroxidase and the absorbance maximum of the electron acceptor, methylene blue. The second trace shows the increase in absorbances below 400 nm after an oscillatory experiment, which is due to the presence of NADH.

PO Oscillator Experimental Parameters Acc. No.: 23

Date: 6/8/1998 Time: 16:00

Reagent Concentrations

Buffers

Buffer Type: Sodium Acetate/Acetic Acid
Reaction Buffer Concentration: 0.1 M pH: 5.1
NADH Buffer Concentration: 0 M pH: 7

Peroxidase

Type: VI from horseradish
Specific Activity: 380 U/mg Final Activity: 40 U/ml

NADH

NADH Concentration: 80 mM

Electron Acceptor Methylene blue
Concentration: 0.2 μM

Phenol

Phenol Type: 2,4-dichlorophenol Phenol Concentration: 20 μM

Physical Parameters

Gas Flow Settings

Oxygen Composition: 5 % Gas Delivery Method: Bubbled
Oxygen Flow Rate: 8 ml/min Nitrogen Flow Rate: 12 ml/min
Final Oxygen Composition: 2 %

NADH Flow Settings

Volume Influx Rate, initial 40 μl/hr Influx Rate, initial 1.6 mM/hr
Volume Influx Rate, final 35 μl/hr Influx Rate, final 1.4 mM/hr
Reaction Mixture Volume 2000 μl

Stirring

Stirrer Speed Setting: 75 % Stirring Speed: 1155 rpm

Temperature

Temperature: 25 ℃

Chart Recorder

Chart Recorder Speed 10 mm/min Chart Recorder Range 50 mV

Notes Standard conditions. Result: well-formed, sustained oscillations.

Ref.

Figure 2.8: Sample record from a FileMaker Pro database that was used to store the experimental parameters from each oscillator run.

Chapter 3

Validation

3.1 Introduction

Certain physical properties of the apparatus described in Chapter 2 were investigated in order to validate the results obtained in experiments, a imperative task given the inherently nonlinear nature of the system. Among the most important of these properties was considered to be the phenomenon of mixing: a well-stirred mixture was essential in order to prevent the formation of travelling waves in solution, a common property of excitable media (for a discussion from a theoretical standpoint see [56]). A well-known chemical example is the Belousov-Zhabotinsky reaction, which generates spiral waves in an unstirred medium. The effect of stir speed on reaction dynamics has been examined in some studies (see, for example, [57]). Although stable spatial structures have elsewhere been predicted to be impossible in a thermodynamically open system such as this [33], solution homogeneity was nevertheless considered to be an important objective in order to eliminate concentration gradients resulting from reagent infusion.

Evaporation rates were investigated since any change in volume induced by passing a gas stream into or over the surface of the solution would affect the concentrations of all reactants.

3.2 Stirrer calibration

A basic measure of stirring ability of the system is the mixing time. In order to observe the effect of stirring speed on mixing time, 10 μl of a solution of 0.2 mM methylene blue were injected quickly by micropipette into 2 ml water in a cuvette, and the absorbance at 664 nm was monitored until equilibrium was attained, for

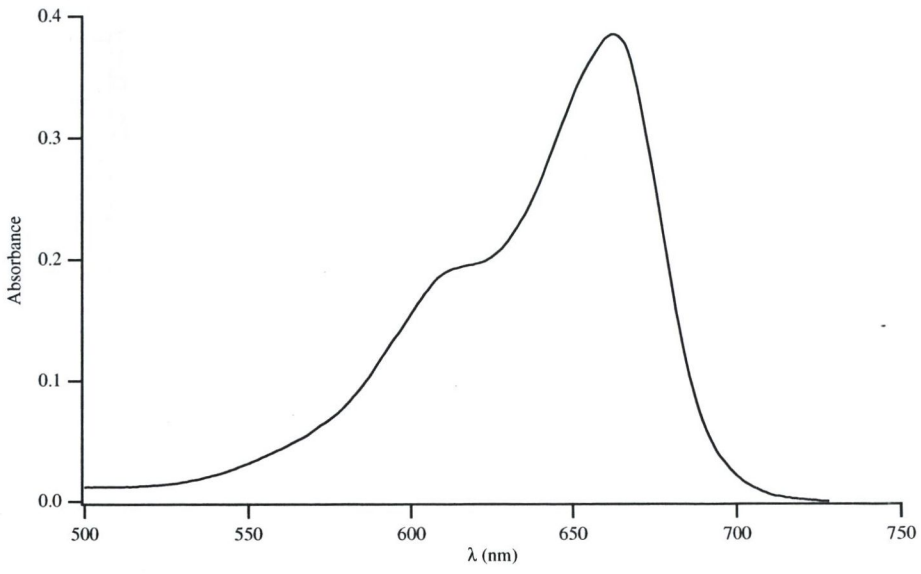

Figure 3.1: Absorbance spectrum of a 3 μM solution of methylene blue. λ_{max} for this compound is 664 nm.

stirring speeds in the range 400-1500 rpm. Methylene blue was chosen since it has a high molar extinction coefficient at this wavelength (see Figure 3.1). The sampling interval was 0.1 seconds. All measurements were performed in triplicate.

A computer program was written in Microsoft QuickBasic™ to compute the mixing time, which was defined as the time taken for the absorbance to rise from its baseline to within 5% of the equilibrium position[1]. The source code of the program, `MIXTIMES.BAS`, is reproduced in Appendix A.3. The time courses generally reached a maximum within a few milliseconds of the addition of dye and thereafter approached equilibrium monotonically from above (see Figure A.2 on page 173). The region of the graph after the maximum is smoothed by the computer program before the mixing time is measured. A graph of mixing time, τ, as a function of stir speed is shown in Figure 3.2. The fitted function suggests that a natural linearisation of the graph is to take the reciprocal of τ and plot with the same abscissa. The result is displayed in the inset to Figure 3.2. A derivation of the equation for the error involved in the variable $1/\tau$ is given in appendix B. Mixing time is under 2 seconds for stir speeds above 1000 rpm, which is comparable with values from other sources [49, 51], and was achieved at settings above 65% of full scale on the stirrer control box (see Equation 2.1 in Section 2.2.2).

[1]Or more precisely, 5% of the value of $A_{664}(equilibrium) - A_{664}(baseline)$

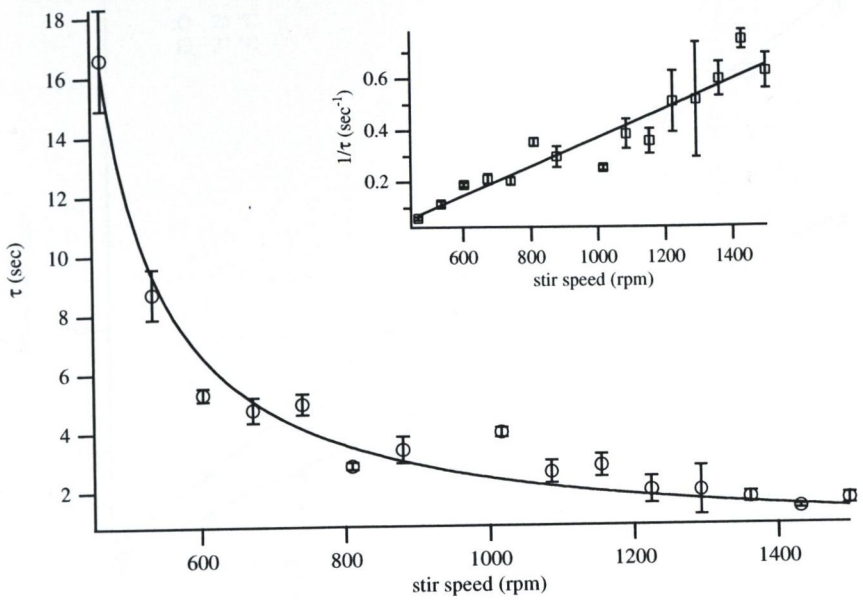

Figure 3.2: Calculated mixing time as a function of stirring speed. Optimal mixing times are less than 2 seconds. The fitted curve is purely empirical in nature and is described by the function $F(x) = a/(x + b)$. Inset: Transformed plot of $1/\tau$ against stir speed. See text for further details.

3.3 Physical properties

3.3.1 Evaporation rate

A natural consequence of the continuous oxygen supply was an increase in evaporation rate of water from the reaction solution. Experiments were carried out to determine the amount of evaporation at varying gas flow rates. In the first such experiment the mass flow controllers were calibrated from 0–100 ml/min oxygen and 0–200 ml/min pure nitrogen, respectively. The cuvette, gas input lines and stirring apparatus were arranged as shown in Figure 2.3. A 2 ml volume of water was pipetted into the cuvette and the mass of cuvette and its contents was noted. A stir speed of 948 ± 69 rpm was used, and a nitrogen gas stream was passed into the headspace above the liquid, which was thermostated, for a period of 45 minutes, after which time the cuvette and its contents were re-weighed and the change in mass recorded. This procedure was conducted in duplicate for gas flow rates in the range 0–200 ml/min and at temperatures of 25 and 37 °C. The results are shown in Figure 3.3. From this graph we may define the evaporation coefficient, $e(F;T)$, as the slope of the regression line, where F is flow rate (ml/min) and T is temperature (°C). The value of $e(F;25)$

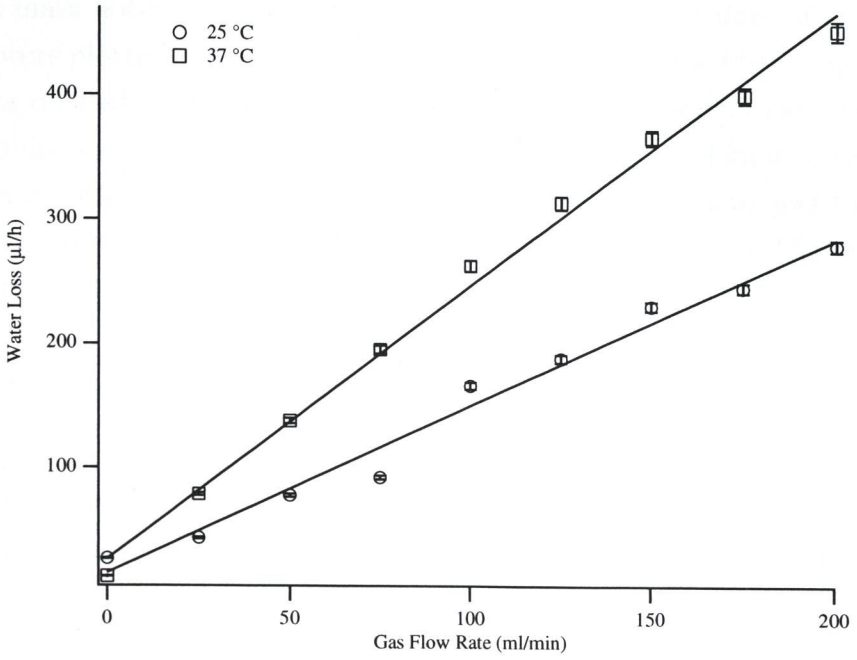

Figure 3.3: Evaporation rates as a function of gas flow rate. A nitrogen stream was passed over the surface of a 2 ml volume of water in a cuvette for 45 minutes, and the decrease in mass recorded. The stir speed was 948 ± 69 rpm. Lines are fitted by linear regression. See text or further details.

in Figure 3.3 is 2.3×10^{-5} and $e(F;37)$ is 3.7×10^{-5}. The case of zero gas flow gives evaporation rates of 0.249 μl/min and 0.435 μl/min at 25 and 37 °C respectively.

In oscillatory reaction runs in which the gas blowing method was used, the evaporation rate was balanced by the NADH influx rate [49], using the calibration data of Figure 3.3 as a guide. Another method of overcoming the evaporation effect is that of humidification of the gas stream, as employed by Hung and Ross [51]. Initial studies with humidification using an apparatus constructed in-house gave rise to artefactual dissolved oxygen behaviour, possibly due to back pressure, and the claim has been made that humidification can yield noisy oxygen data[2].

With the nitrogen MFC calibrated to a 0–40 ml/min range a similar experiment was performed, this time under gas bubbling conditions. A Dreschel bottle, purchased from Philip Harris Ltd[3], was used to humidify both gas lines; Figure 3.4 shows a diagram of this item and its location relative to the other gas control instruments. As before, 2 ml of water, equilibrated to 25 °C in a cuvette, were subjected to a bubbled nitrogen stream over the range 10–40 ml/min for a period of 45 minutes, and the

[2]D.L. Olson, Chemistry Department, University of Illinois, personal communication.

[3]Philip Harris Ltd, Staffordshire, UK.

change in mass noted. Evaporation rates were expressed in units of microlitres per hour and were plotted as a function of gas flow rate (see Figure 3.5). The evaporation coefficients defined above can also be applied to this method of gas delivery. From the humidified gas series, the slope of the regression line was found to be 1.49. After conversion of ordinate and abscissa to the same units of volume and time (dividing the slope by 60,000) this gives a value for $e(F;25)$ of 2.5×10^{-5}. The corresponding value for the case of bubbling dry gases is $e(F;25) = 4.4 \times 10^{-5}$.

3.3.2 Methods of mass-transport constant determination

In Chapter 2 a model of oxygen equilibration between gas and liquid phases of the experimental system was presented and a first-order equation describing the process was derived (Equation 2.6). In this section the methods of determination of the mass-transport constant will be elaborated upon, and certain practical issues arising therefrom will be discussed. The first such is the nature of the equilibration curve, an illustration of which is to be seen in Figure 2.5. Close examination of the data reveals a slight lag-time in the rising portion of the dissolved oxygen data. This was mostly evident in cases where gas bubbling was employed. The lower oxygen and nitrogen gas flow rates that were required for this delivery method may have been responsible for slower response times in the gas control apparatus, which were the effect of slower gas mixing. Therefore, a study of the methods used to determine k_{-t} was deemed necessary.

An approximation to k_{-t} may be obtained by the half-life, which in this instance is defined as the time taken for the dissolved oxygen concentration to rise from its basal value to half of the observed maximum. It is an approximation since (a) the observed maximum will not reach the equilibrium position in finite time and (b) the presence of a lag time will make the starting position less easy to determine. From Equation 2.6, if $t = t_{1/2}$, then $[O_{2(aq)}] = [O_{2(aq)}]_{eq}/2$, and k_{-t} may be isolated from the resulting expression to give

$$k_{-t} = \frac{\ln 2}{t_{1/2}}. \tag{3.1}$$

To calculate the half-life, the minimum and maximum oxygen values were chosen, and the starting position of the oxygen re-equilibration curve determined as the time at which oxygen concentration reached a desired fraction f of the total change in oxygen observed ($O_2(max) - O_2(min)$, or simply ΔO_2). The half-life was defined as the time taken for oxygen concentration to rise to within $f.\Delta O_2$ concentration units of $\Delta O_2/2$.

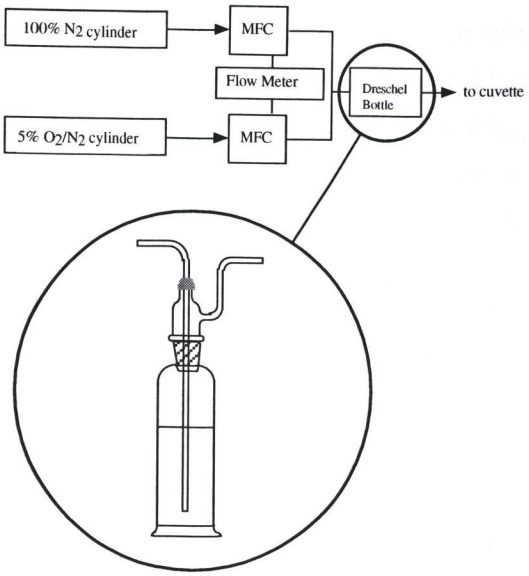

Figure 3.4: Diagram of a Dreschel bottle used in experiments determining the effect of gas humidification on evaporation rate. A section of Figure 2.2 is reproduced which shows the bottle as being placed downstream of the merged gas lines.

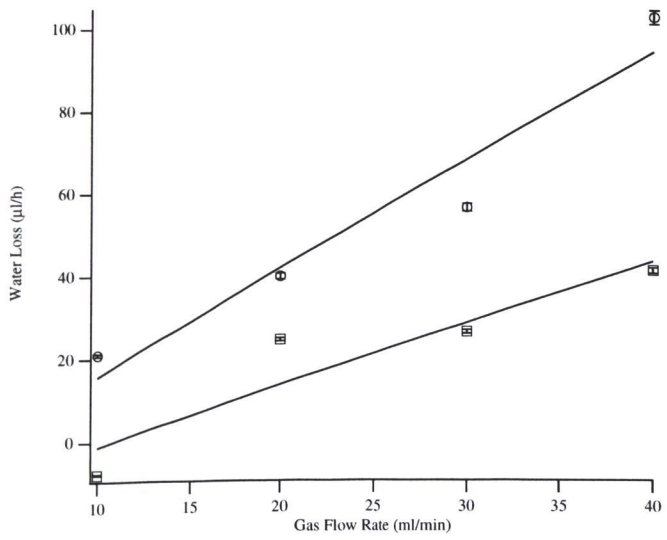

Figure 3.5: Evaporation rates under gas bubbling conditions as a function of gas flow rate, with and without humidification of the gas stream. A nitrogen stream was bubbled into a 2 ml volume of water in a cuvette for 45 minutes and the change in mass recorded. The stir speed was 1155 rpm and the temperature was held constant at 25 °C. Points are averages of duplicate readings and the lines are fitted by linear regression. See text for further details.

As stated in Chapter 2, the method of determination of k_{-t} most frequently employed was that of nonlinear least-squares fitting of Equation 2.6 to oxygen data, which was performed by a Marquhardt-Levenberg algorithm with Igor Pro graphing software. For this purpose a segment of data enclosing the region of dissolved oxygen data to be analysed was chosen between time points t_{min} and t_{max}. The value of t_{max} was held constant and the lower bound gradually increased by a distance δ from t_{min} through the lag portion of the data, fitting the model to the data at each step. The values of k_{-t} and the goodness of fit parameter χ^2 were recorded at each iteration of the procedure. It is important to note that the data were rescaled to time zero during curve fitting, which meant that points before $t_{min} + \delta$ were ignored. It was observed that a plot of χ^2 versus δ formed a parabolic arc, displayed a local minimum. The value of k_{-t} at the minimum was taken to be the mass-transport constant for that data set. Figure 3.6 illustrates the method and shows a graph of both k_{-t} and χ^2 plotted against δ. The Igor Pro built-in programming language was used to construct a routine that would automate the steps of the procedure, and its source code is given in Appendix A.4.

Values for the mass-transport constant were found to vary markedly depending on the method used, the optimised curve fitting method just described tending to generate higher values than the half-life method. For example, the data shown in Figure 3.6 (a) yielded values of 0.32 min^{-1} from the half-life (with $f = 0.01$) and 0.69 min^{-1} by nonlinear regression. The lag time made log-linear analysis of the oxygen data more difficult[4], in that the transformed data departed from linearity at low and high time values, and occasionally did not display any linearity, which made convergence to a stable value unlikely (see Equation 2.7 and Appendix A.1). Data obtained using the gas blowing approach were more amenable to treatment by log-linear analysis, but since such experiments were in the minority they will not be discussed further here.

Although the lag time was in many cases only a small portion of the complete time series data that were used to determine k_{-t}, and its effect minimised using the procedure outlined above, it will be interesting to see how a theoretical model might be able to account for the observation. The response time of the gas apparatus combined with the bulk volume of gas contained in the tubing leading to the cuvette, and also the efficiency of gas mixing, may contribute to the lag. A point of note is that the response time of the electrode is lower than the lag, so is unlikely to making a significant contribution. An extension to the Olson model of oxygen mass transport (Section 2.3.2) can be made by proposing that the oxygen gas passes through an

[4]See Equation 2.7 and Appendix A.1

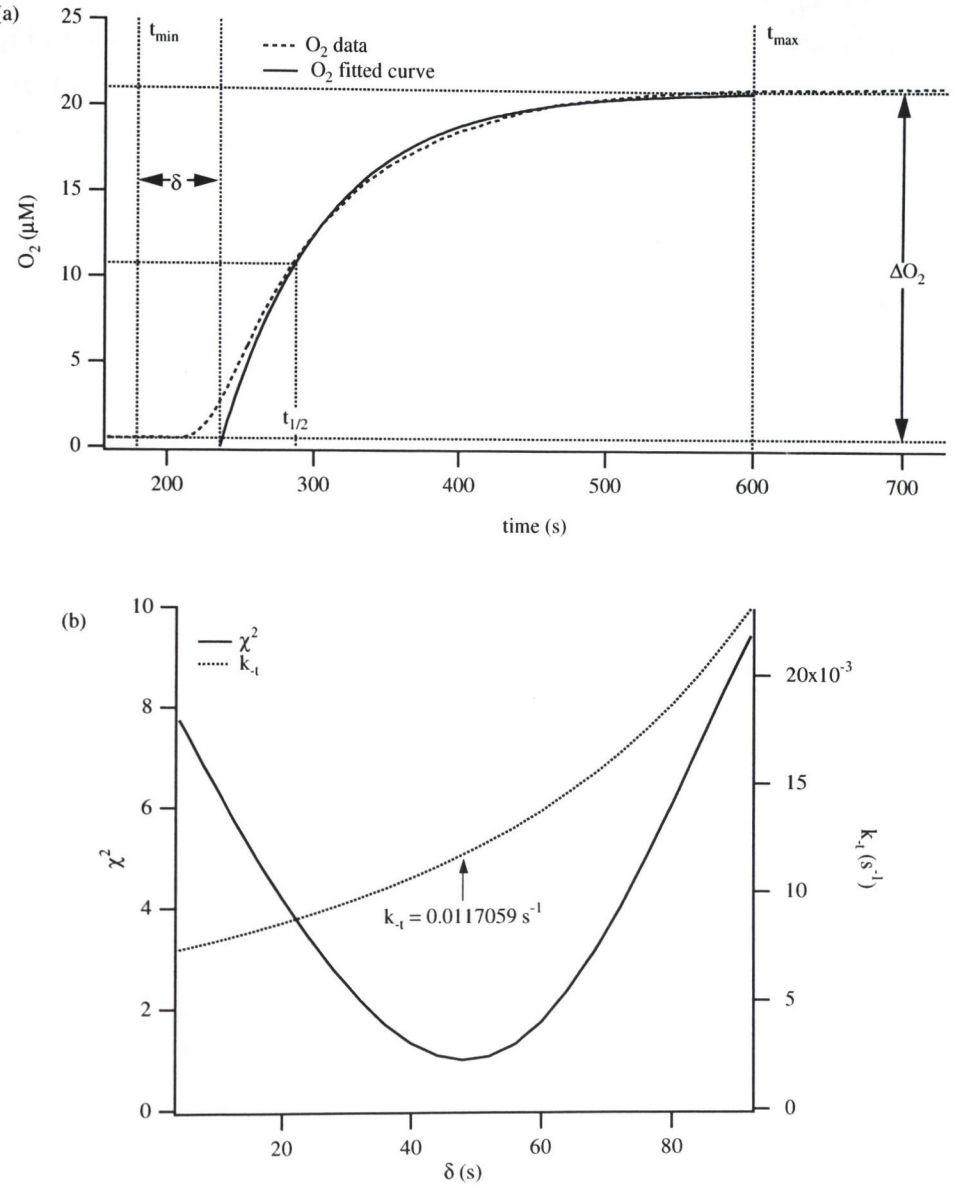

Figure 3.6: Best-fit value of the mass-transport constant. Graph (a) shows sample oxygen data which indicate the boundary times (t_{min} and t_{max}) used to delimit the region used for curve fitting, and the time increment δ that was an offset to the minimum. The data in this region were rescaled to zero time before applying Equation 2.6 in a nonlinear least-squares regression analysis. In (b) the values of the k_{-t} and goodness of fit parameter χ^2 are plotted against the variable δ.

intermediate step, which can be interpreted as the delivery through the gas tubing from the mass flow controllers. Denoting the concentration of oxygen at the point of mixing by A, its concentration in the gas tubing and in the gas headspace above the liquid (relevant in the technique of gas blowing) by x_1 and the dissolved oxygen concentration by x_2, it is proposed that the measured oxygen concentration is the product of two equilibria:

$$\mathrm{A} \underset{k_{-1}}{\overset{k_1}{\rightleftharpoons}} \mathrm{B} \underset{k_{-2}}{\overset{k_2}{\rightleftharpoons}} \mathrm{C}. \tag{3.2}$$

where B and C represent the oxygen in transit and in solution, respectively. Similar to the theoretical treatment of the model given in Section 2.3.2, the assumption is made that the oxygen gas concentration at the source (A) is a constant, which gives us a linear system of ordinary differential equations in two variables

$$\frac{\mathrm{d}x_1}{\mathrm{d}t} = k_{-1}A - (k_{-1} + k_2)x_1 + k_{-2}x_2 \tag{3.3}$$

$$\frac{\mathrm{d}x_2}{\mathrm{d}t} = k_2 x_1 - k_{-2}x_2 \tag{3.4}$$

in which x_1 and x_2 represent the concentrations of B and C, subject to the initial conditions $x_1 = x_2 = 0$. Solutions can be obtained by using Laplace transforms [58] to translate from time t to a new independent variable s. The new dependent variables, $X_1(s)$ and $X_2(s)$ are, respectively, the Laplace transforms of $x_1(t)$ and $x_2(t)$, and the differential equation system above becomes

$$\begin{aligned} sX_1 - x_1(0) &= \frac{k_{-1}A}{s} - (k_{-1} + k_2)X_1 + k_{-2}X_2 \\ sX_2 - x_2(0) &= k_2 X_1 - k_{-2}X_2 \end{aligned}$$

Substituting the initial conditions and solving for X_1 and X_2 gives

$$\begin{aligned} X_1 &= \frac{k_1 A(s + k_{-2})}{s(s^2 + (k_{-1} + k_{-2} + k_2)s + k_{-1}k_{-2})} \\ X_2 &= \frac{k_{-1}k_2 A}{s(s^2 + (k_{-1} + k_{-2} + k_2)s + k_{-1}k_{-2})} \end{aligned}$$

An expression for $x_2(t)$ is all that is required, which is obtained by taking the inverse Laplace transform of the second of these two expressions. Before doing so, we observe that the quadratic in the denominator of the expression for X_2 will have two roots, which we call a_1 and a_2, thus

$$a_{1,2} = \tfrac{1}{2}[-(k_{-1} + k_{-2} + k_2) \pm \Gamma] \tag{3.5}$$

where

$$\Gamma = \sqrt{(k_{-1} + k_{-2} + k_2)^2 - 4k_{-1}k_{-2}} \tag{3.6}$$

This simplifies the expression for X_2, making it easy to convert Equation 3.5 to partial fraction form,

$$Y(s) = \frac{k_{-1}k_2A}{a_1a_2}\frac{1}{s} + \frac{k_{-1}k_2A}{a_1(a_1 - a_2)}\frac{1}{s - a_1} + \frac{k_{-1}k_2A}{a_2(a_1 - a_2)}\frac{1}{s - a_2}$$

before taking the inverse Laplace transforms of each term, to yield

$$x_2(t) = \frac{k_{-1}k_2A}{a_1a_2} + \frac{k_{-1}k_2A}{a_2(a_1 - a_2)}e^{a_1t} + \frac{k_{-1}k_2A}{a_1(a_1 - a_2)}e^{a_2t} \tag{3.7}$$

Upon observing that $a_1a_2 = k_{-1}k_{-2}$ and $a_1 - a_2 = \Gamma$, this simplifies to

$$x_2(t) = \frac{k_2A}{k_{-2}}\left(1 + \frac{a_2}{\Gamma}e^{a_1t} - \frac{a_1}{\Gamma}e^{a_2t}\right) \tag{3.8}$$

Figure 3.7 shows an example curve generated using Equation 3.8 that is overlayed by some real dissolved oxygen data in which a lag was apparent, and from this it is evident that the model is capable of reproducing the lag phenomenon. Nonlinear regression analysis was not able to find a good fit to the data using the Igor Pro graphing software, and trial and error was used to obtain the results illustrated. It would appear that the complexity of the model solution makes it unsuitable for application to laboratory data, and so the single equilibrium model has been used for all analyses.

3.3.3 Effect of gas flow rate on k_{-t}

In studies on chemical oscillators the rate at which reagents enter or leave a thermodynamically open system has been shown to have an important influence on the resulting dynamical behaviour. Since one of the substrates of the peroxidase-oxidase reaction is oxygen, it was necessary to study the physical parameters controlling its rate of transport across the gas-liquid interface. The mass-transport constant is the natural measure of the latter, and its dependence on the total gas flow rate was examined.

The standard reaction cuvette used in the study of the peroxidase-oxidase reaction, containing 2 ml of distilled water, was placed in a thermostated cuvette holder and after equilibration to 25 °C a pure nitrogen stream bubbled into the liquid at a flow rate of 30 ml/min. The stirring speed was set to 1155 rpm. When dissolved oxygen had reached a constant minimum the gas composition was changed to 2%

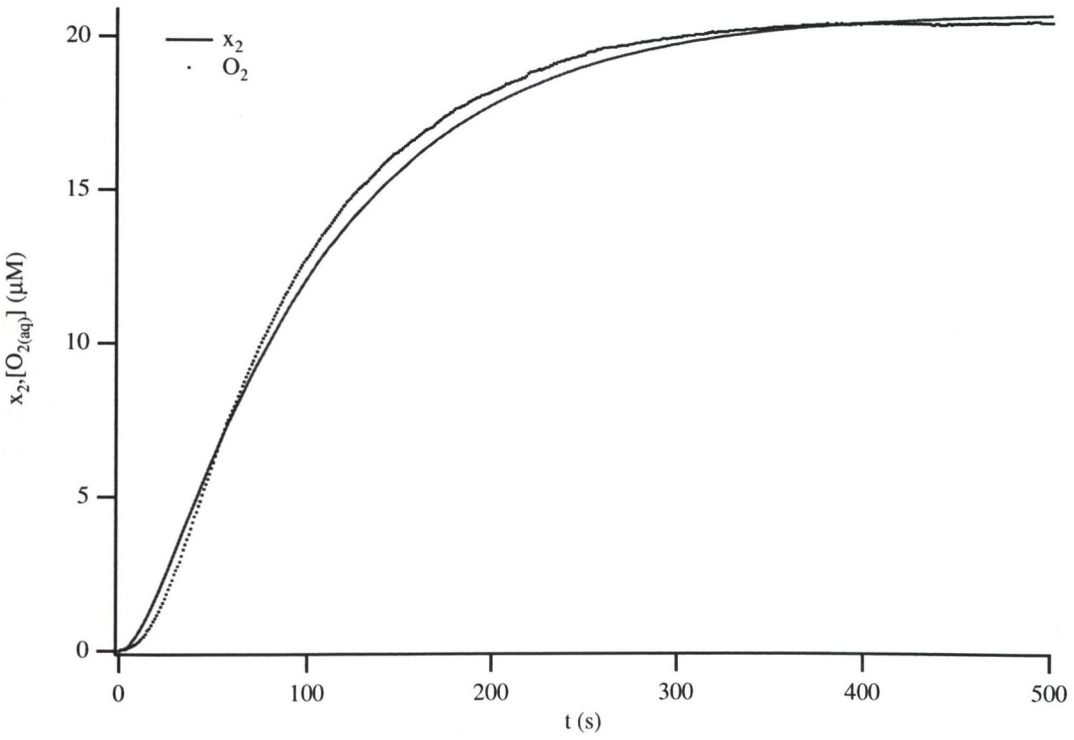

Figure 3.7: Example curve of the bi-equilibrium model of oxygen delivery. The values of the parameters were: $k_{-1} = 0.32\ s^{-1}$, $k_2 = 0.1\ s^{-1}$, $k_{-2} = 0.095\ s^{-1}$ and $A = 20\ \mu M$. Also shown (dotted curve) are oxygen data obtained in the laboratory for which a lag period was evident. The chosen values of the parameters of the model were those which gave the best fit to the data.

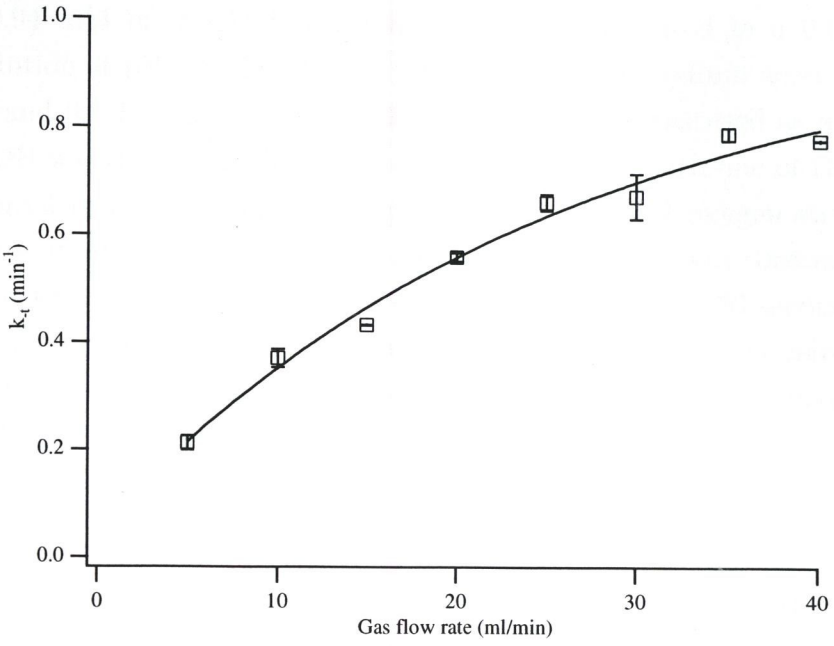

Figure 3.8: Mass-transport constant versus gas flow rate. The stir speed was 1155 rpm and the temperature was held constant at 25 °C. Points are averages of duplicate readings and the fitted curve is an exponential function used to illustrate the apparent trend. See text for details.

in oxygen, with a total gas flow rate of 20 ml/min, and the system was allowed to re-equilibrate. The oxygen data were collected for analysis using the data acquisition system described in Section 2.2.7, and the mass-transport constant was determined by the nonlinear regression method of Section 2.3.2. This procedure was repeated for total gas flow rates in the range 5–40 ml/min incremented in steps of 5 ml/min; duplicate readings were obtained at each gas flow rate. mass-transport constants are plotted against gas flow rate in Figure 3.8.

3.4 Chemical properties

Some properties pertaining to the chemical components of the reaction system under study are described in this section.

3.4.1 NADH stability

Since the peroxidase-oxidase reaction is studied at acidic pH values, where NADH is known to be unstable, it was deemed appropriate to measure the rate of degradation of this reagent in the buffer used for a typical oscillatory run. To this end, a stock

solution 0.94 mM of β-NADH (disodium salt) was prepared in a 0.01 M sodium acetate solution at pH 7.4. Two buffers were made: 0.1 M sodium acetate/acetic acid at pH 5.1 and 0.1 M Tris-HCl[5] (pH 7.4 at 25 °C), which was used as a control. The stock NADH was diluted in a quartz cuvette to 0.08 mM with one of the two buffers to give a total volume of 2 ml, then equilibrated with a 2% oxygen stream and to a temperature of 29 °C in a spectrophotometer. The mixture was continuously stirred at a rate of 1086 rpm. Absorbance readings were taken every 30 seconds at 340 nm for a 10 minute duration. The procedure was repeated in triplicate using the sodium acetate buffer at acidic pH and the data averaged. The results were fitted by a linear model and the values of the slopes thus obtained were converted to concentration units. The data are summarised in Table 3.1.

	Standard	Control
Buffer	0.1 M NaAc	0.1 M Tris-HCl
Degradation Rate (μM/h)	13.9 ± 0.2	0.0 ± 0.1

Table 3.1: Rates of degradation of NADH at pH 5.1 and 7.4, in 0.1 M sodium acetate/acetic acid (NaAc) buffer and 0.1 M Tris-HCl, respectively.

3.4.2 Enzyme stability

The stability of a stock solution of horseradish peroxidase in 0.1 M acetate buffer at pH 5.1 was examined. Horseradish peroxidase (Type II) was purchased from Sigma as a lyophilised powder. On a 4-digit mass balance, 4.0 ± 0.1 milligrams of the enzyme were weighed and dissolved in 1 ml of 0.1 M sodium acetate/acetic acid buffer at pH 5.1 and stored at 0–4 °C. The stock preparation was assayed for peroxidative activity by the Sigma method (Section 2.3.1) on several occasions over the course of a week. A graph of activity against time is shown in Figure 3.9.

3.5 Discussion

The results of Section 3.2 have shown that mixing times of approximately 2 seconds or less could be expected from the stirring apparatus used in this work at stirring speeds over 1000 rpm. Other factors affecting mixing efficiency were not investigated, among them the position and shape of the impeller. Treybal [52] states that stirring

[5]The pH 7.4 Tris-HCl buffer was made as follows: 50 ml of 0.1 M Tris(hydroxymethyl)aminomethane, 42 ml 0.1 M HCl, both at 25 °C, were mixed and diluted to 100 ml with H_2O.

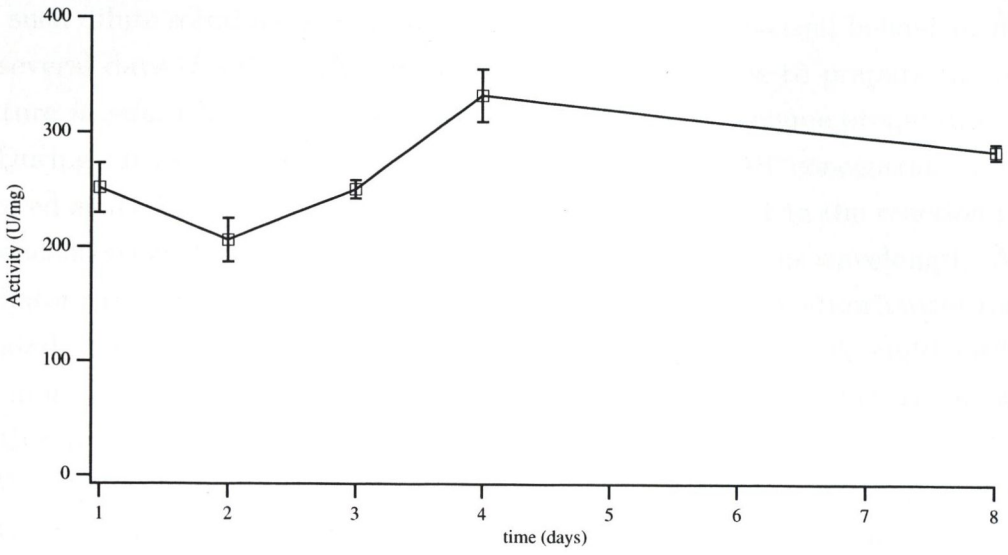

Figure 3.9: Stability of horseradish peroxidase. The activity of a stock solution of Sigma Type II horseradish peroxidase in 0.1 M acetate buffer at pH 5.1, final concentration 4.0 mg/ml and stored at 0–4 °C, was measured regularly over the course of a week using the pyrogallol assay method described elsewhere (Section 2.3.1).

from the middle of the liquid allows convection currents to form above and below the stirring position, optimising mixing efficiency. Olson [40] took this approach, using a cylindrical 7 ml quartz cuvette, stirring from above and radially off centre, with the dioxygen probe acting as a baffle. However, the smaller solution volume used in the present work helped to make such considerations unnecessary.

Water loss by evaporation was balanced by the infusion of NADH stock solution into the reaction mixture. A more dilute stock NADH solution was used when higher volume-influx rates were required, in particular for the method of blowing gas into the headspace situated above the liquid surface. The evaporation coefficients (page 33 *et seq.*) obtained under gas bubbling conditions are higher than those corresponding to gas blowing due to the increased surface area implicated in the former case. This explanation may also account for the 3- or 4-fold difference in mass-transport constants observed using these two gas delivery methods under otherwise similar experimental conditions.

The stability of HRP in concentrated stock solution has been demonstrated (see Figure 3.9). In practice enzyme was weighed approximately once a week and stored as a 16 mg/ml solution in 0.1 M Na acetate buffer at 0–4 °C until required. Appropriate dilutions were made into a 10 ml volumetric flask, 2 ml portions of which were used for a single experiment. Since much of this stock was unused at the end of each day,

and such dilute solutions would eventually give rise to artefactual behaviour if stored for several days (Section 4.2.6) it became common practice to prepare the reaction mixture *in situ*, which was a more economical use of the enzyme preparation.

During an oscillatory run the time-evolution of NADH concentration was not followed at its λ_{max} of 340 nm because it was usually present in the reaction mixture at concentrations too high to be measured with accuracy at this wavelength. After an oscillatory run, wavelength scans below 340 nm revealed that absorbances remained elevated, indicating that the ascending shoulder of the NADH peak could not be used any more reliably than at the NADH λ_{max}. This was probably due to the presence of other products of the reaction, most probably NAD^+.

With the preceding experiments the apparatus described in Chapter 2 for the study of the peroxidase-oxidase reaction has been effectively characterised and the methodology validated.

Chapter 4

Dynamical Behaviour

4.1 Introduction

This chapter commences with a description of the various modes of kinetic behaviour observed with this oscillator, beginning with the most simple dynamics and advancing through to examples of irregular and artefactual behaviour. System response to physical and chemical perturbations will be discussed in following sections, which conclude with a discussion of the important topic of reproducibility and its relation to comparisons with published work from other laboratories. Materials and methods used were those of Chapter 2, unless otherwise indicated.

4.2 Oscillations

4.2.1 Single

The first experiments made with the oscillator yielded nonlinear behaviour in the form of a single 'oscillation', or spike, in the absorbance of the peroxidase at 418 nm (λ_{max} of peroxidase compound III, which is possibly a ferriperoxidase-O_2^- complex), an example of which is shown in Figure 4.1. The experimental parameters contain points of similarity to those quoted in both Rys and Wang [39] and Olson and Scheeline [49]. Higher NADH infusion rates resulted in a sharper peak in A_{418}, qualitatively similar to the data of Rys and Wang, but no further oscillations were observed at longer times.

A second example is shown in Figure 4.2, which shows a sharp nonlinear change in both the dissolved oxygen and A_{418} traces after a perturbation. The reaction commenced with the start of NADH infusion, and as the dissolved oxygen approached

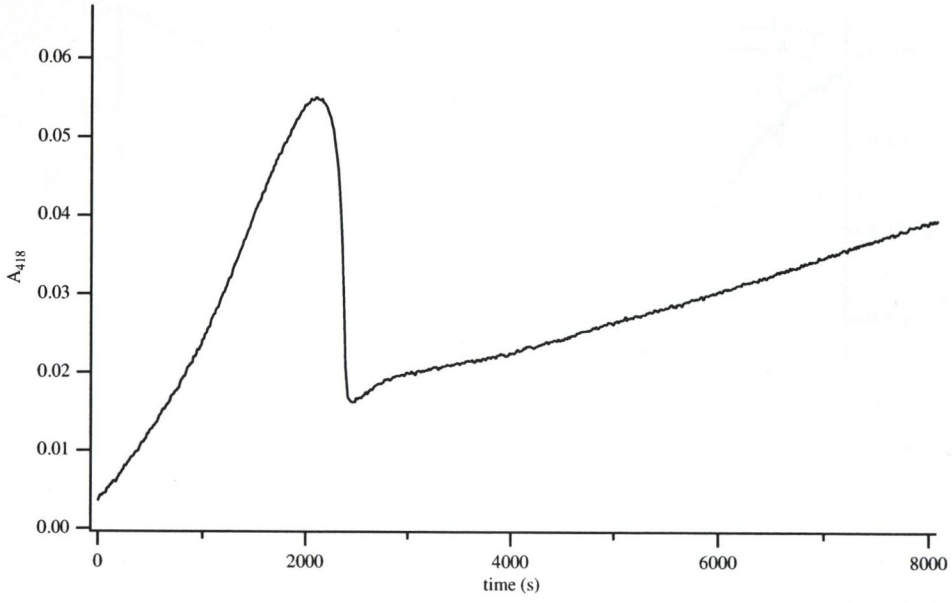

Figure 4.1: Single oscillation in the absorbance of peroxidase compound III. Composition of the reaction mixture was as follows: 107 U/ml HRP, 0.2 μM methylene blue, 20 μM 2,4-dichlorophenol, dissolved in 0.1 M sodium acetate at pH 5.2. A solution of 57.6 mM NADH in 0.01 M sodium acetate (pH = 7.2) was infused at a rate of 150 μl/h, a 1 ml plastic syringe being used place of the 100 μl Hamilton type (see section 2.2.4. The oxygen composition was 2% O_2, blown into the gas headspace above the solution at a rate of 100 ml/min. The temperature was maintained at 25°C. Stir speed was 1017 $\pm$ 69 rpm.

a steady value, the oxygen supply was cut off for approximately 5 minutes. Upon the reintroduction of gas the dissolved oxygen concentration in the reaction mixture rose quickly. Instead of levelling in the region of the first steady state, the direction reversed spontaneously and the oxygen level fell to a lower steady state value. This can be interpreted as a demonstration of bistability in the PO reaction, that is to say, the coexistence of two stable steady states. Further changes in gas flow rate, specifically, increases in gas flow rate and composition, did not induce similar switching behaviour after the occurrence described. The fact that the procedure was not repeatable within the same experiment might contradict the interpretation being made here, since it contrasts with results from an earlier report by Degn *et. al.* [33]. However, the switching behaviour is still a valid example of the nonlinear character of the system, and reveals the potential for more complex behaviour.

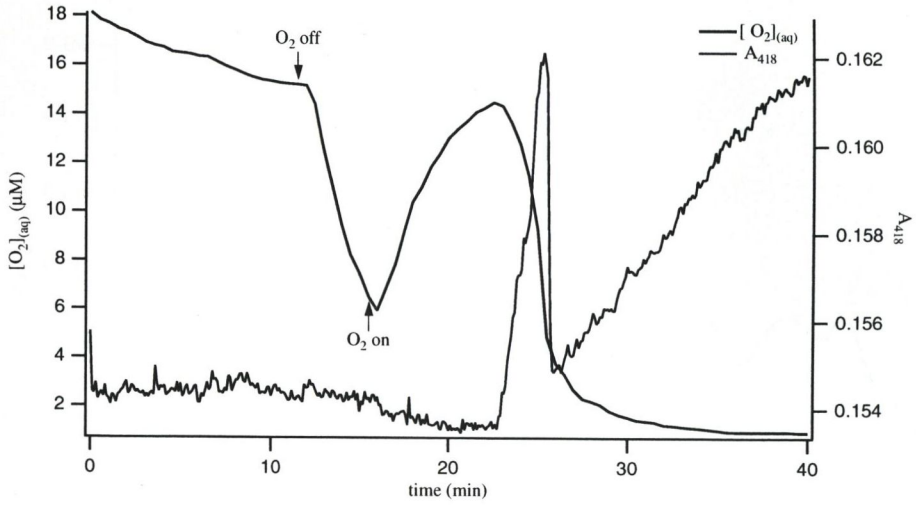

Figure 4.2: Putative bistability in the peroxidase-oxidase reaction. Shown are dissolved oxygen concentration and compound III absorbance, with arrows indicating where oxygen supply was cut off and reintroduced. The reaction mixture contained 35 U/ml HRP (approx. 2.6 μM), 0.2 μM methylene blue, 20 μM 2,4-dichlorophenol, dissolved in 0.1 M sodium acetate at pH 5.2. The NADH concentration was 200 mM in 0.01 M acetate, infused at a rate of 1.6 mM/h from a 1 ml syringe. The oxygen composition was 1.9%, bubbled into the solution at a rate of 10.2 ml/min. The temperature was 29°C, and stir speed was 1017 ± 69 rpm.

4.2.2 Damped

Damped oscillations were observed with this reaction on a number of occasions; the data from selected experiments will be used here. Oscillations in CoIII are shown in Figure 4.3, and combined dissolved oxygen and NADH time series data are shown in Figure 4.4. The method of initiation of oscillations is that of Section 2.3.3, where NADH was infused into a solution of horseradish peroxidase in equilibrium with an oxygen/nitrogen gas mixture. The linear upward trend seen towards the end of the NADH time series in Figure 4.4 indicates that there is a residual rate of NADH influx in excess of its mean rate of oxidation. Given from a separate experiment that the molar extinction coefficient of NADH at 360 nm, $\epsilon_{360}^{\mathrm{NADH}}$, is 3950 mM^{-1} cm^{-1}, some simple calculations can be performed. The slope of the data in the range 20.5–25 minutes is $3.89 \times 10^{-3} \pm 8 \times 10^{-5}$ mM/min; the average rate of change of NADH concentration in the reaction is therefore 0.234 ± 0.005 mM/h. Since it is being infused at a rate of 2.25 mM/h (computable from the details in the legend to Figure 4.4 and Equation 2.2) this gives a mean oxidation rate of approximately 2 mM/h under these conditions.

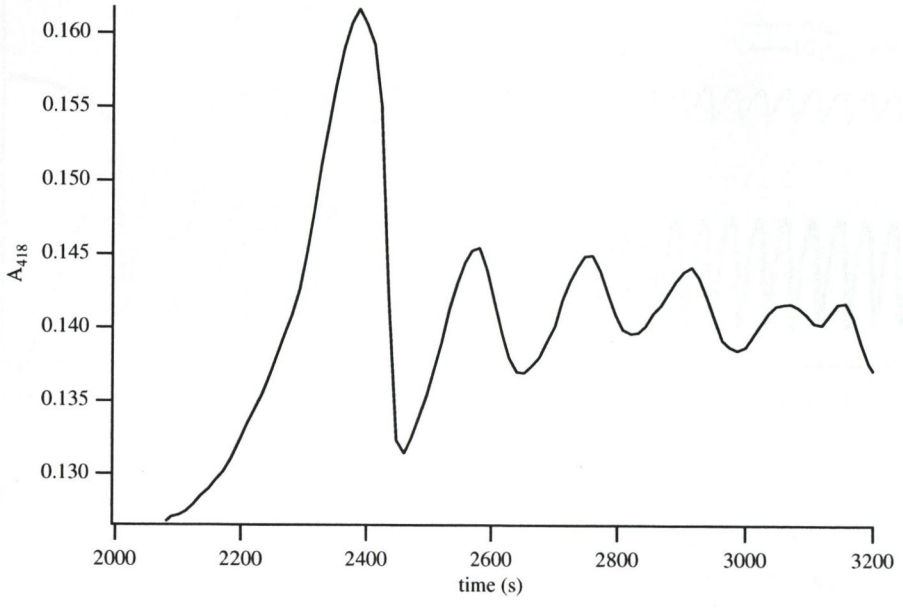

Figure 4.3: Damped oscillations in CoIII. Experimental conditions were: 23.4 U/ml HRP, 0.2 μM MB, 20 μM DCP, in 0.1 M sodium acetate buffer at pH 5.1. The reservoir NADH concentration was 203 mM, infused at 1.6 mM/h, 1.9% oxygen was bubbled at 10 ml/min; the temperature was 29°C, and stirring speed was 1155 rpm.

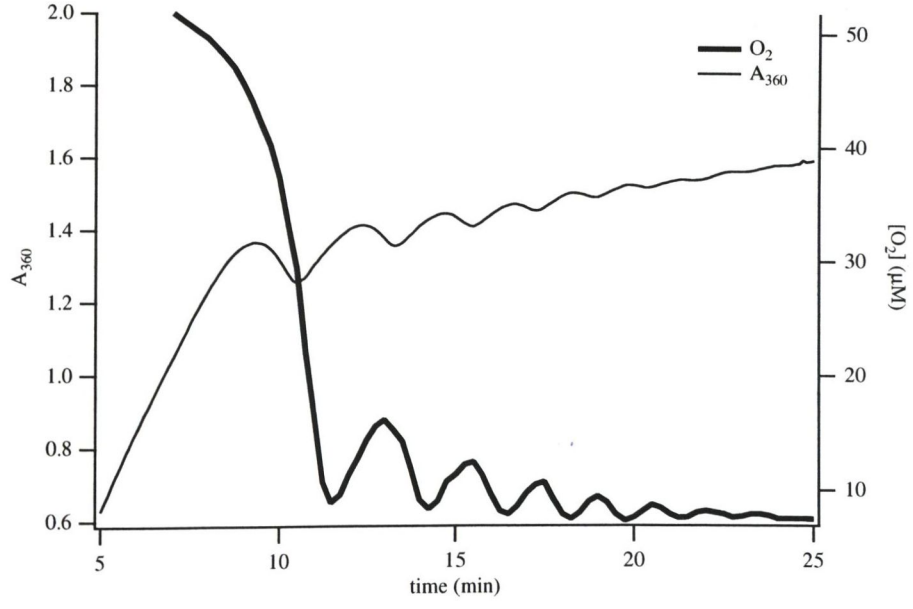

Figure 4.4: Damped oscillations in the peroxidase-oxidase reaction. Experimental conditions were: 23.4 U/ml HRP, 0.2 μM MB, 20 μM DCP, in 0.1 M sodium acetate buffer at pH 5.1. Initial NADH concentration was 150 mM, infused at 1.2 mM/h into a solution volume of 2 ml; 1.9% oxygen was bubbled at 10 ml/min, the temperature was 29°C, and the stir speed was 1155 rpm.

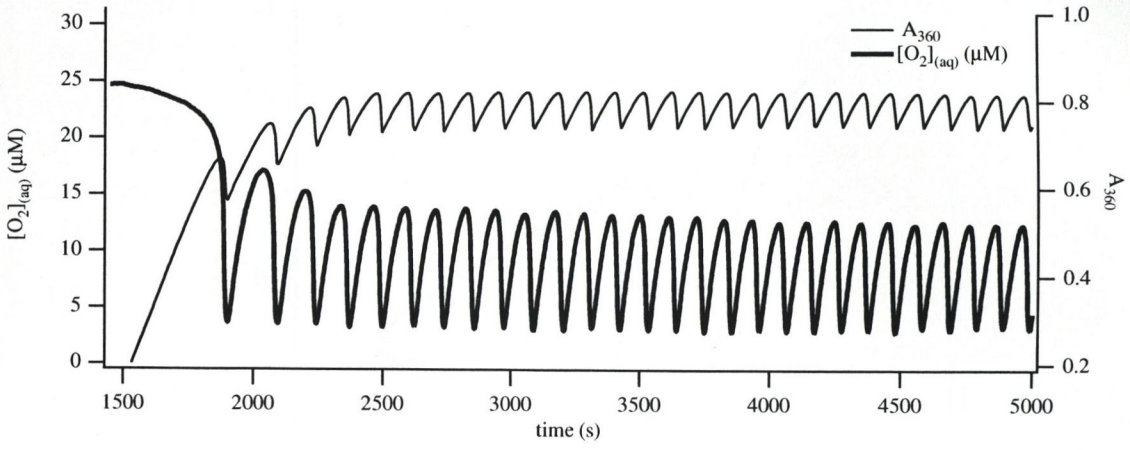

Figure 4.5: Sustained oscillations in the peroxidase-oxidase reaction. Shown are time series data of dissolved oxygen and NADH, the former drawn using a heavier line style. Experimental conditions were: 40 U/ml HRP, 0.2 μM MB, 20 μM DCP, in 0.1 M sodium acetate buffer at pH 5.1. NADH stock concentration was 80 mM, infused at 35 μl/h (1.4 mM/h) into a solution of volume 2 ml; 2.0% oxygen was bubbled at 20 ml/min, the temperature was 25°C, and the stir speed was 1155 rpm.

4.2.3 Sustained

Sustained oscillations in all of the observable components of the reaction were obtained in various experiments. The standard experimental conditions shown in Table 2.1 describe a region of parameter space where sustained oscillations were frequently observed. As will be described in later sections, minor deviations from the exact conditions did not inhibit the dynamics *per se*, but did in some cases alter the shape of the waveform of oscillations. An example of sustained behaviour is given in Figure 4.5, which shows the time courses of dissolved oxygen and NADH concentrations in the reaction mixture, for experimental conditions close to those of the standard set. Sampling frequencies were 1 Hz for the oxygen trace and 0.166 Hz for the absorbance of NADH at 360 nm.

The semi-batch nature of the experimental system has the disadvantage that products are allowed to accumulate in the reaction vessel, possibly altering the conditions of the reaction throughout an oscillatory run, which contrasts with the continuously stirred tank reactor (CSTR) approach of Hauck and Schneider [41], where reactant influx is balanced by removal of excess liquid volumes. The present method was capable of maintaining oscillations for several hours, sufficient to observe the dynamics and acquire data for later analysis.

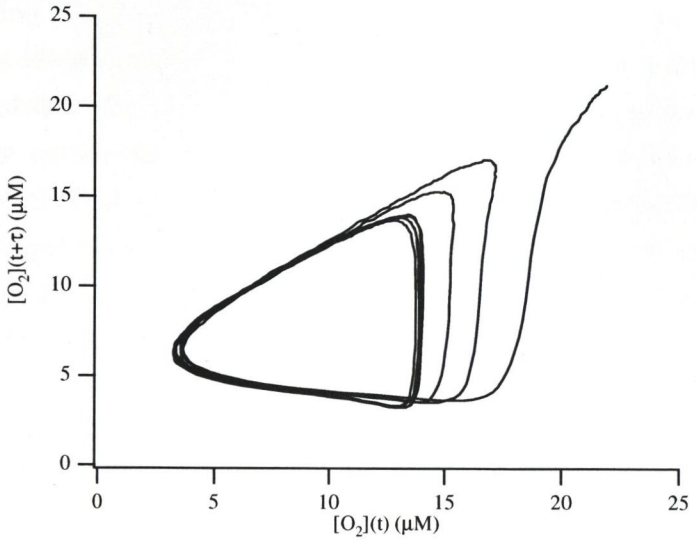

Figure 4.6: Reconstruction of the attractor using the oxygen data of Figure 4.5, which shows the system settling down to a regime of stable period-1 oscillations. One thousand and twenty-four data values are plotted, commencing at 1700 seconds. The sampling frequency of the oxygen data was 1 Hz. The value of T is 20 s. Other details are given in the text.

4.2.4 Attractor visualisation

The dynamical behaviour in the results obtained with this experimental system were in general relatively simple, consisting of period-1 oscillations[1] in each of the measurable components of the reaction. We can predict that the geometry of the attractor underlying the flow will be a simple closed curve in phase space. One method of visualising this attractor is to plot the value of one time-dependent variable against the other, for example, [NADH] against $[O_2]$. In some cases this was not possible when the sampling rates of oxygen and species measurable with the spectrophotometer were a non-integer ratio. A method exists for attractor reconstruction from a single time series, the mathematical basis for which is attributable to Takens [59], and has been described for the case of so-called chaotic attractors by Packard *et al.* [60]. In essence, an N-dimensional attractor is reconstructed by sampling one variable $x(t)$ and then plotting a graph of $[\,x(t) \quad x(t+T) \quad x(t+2T) \quad \cdots \quad x(t+(N-1)T)\,]^{\mathrm{T}}$, or if $N > 3$, some combination of these coordinates. The value of T is chosen by eye as that which gives the most easily discernible figure. The method has been used previously by Geest *et al.* [38] in the visualisation of the dynamics of the peroxidase-oxidase reaction.

Figure 4.6 illustrates the technique with a plot of oxygen concentration in two

[1]The term 'period-1' means that the pattern of oscillations repeats after one period.

dimensions, using $[O_2](t)$ as abscissa and $[O_2](t+T)$ as ordinate. The data set used in this graph is identical to that of Figure 4.5, and provides a demonstration of the formation of a stable limit cycle from the starting conditions, in a region of parameter space where the non-oscillatory steady-state position has become unstable.

The effect of varying T is presented in Figure 4.7. This shows how the 'delay time' can affect the appearance of the attractor, which in the present case can be thought of as a two-dimensional projection of an object existing in an 'embedding space' of dimension greater than two.

4.2.5 Absorbance spectra versus time

The spectrophotometer used in this apparatus (Section 2.2.3) was unable to record more than 1001 data points at a single wavelength in one continuous time series, a figure which declined appreciably as the number of wavelengths per sample was increased. This problem could be partially alleviated by the use of the LabVIEW program used to drive the spectrophotometer, in which single readings were taken at regular intervals and sent to the remote computer. On one occasion the spectrophotometer was operated manually to record absorbance spectra over the wavelength range 380–480 nm, of a peroxidase-oxidase reaction running under standard conditions[2]. The wavelength interval was 2 nm and 271 scans were recorded at 15-second intervals. Figure 4.8 shows a sample of sustained oscillations taken from a subset of the acquired absorbance data. From the same experimental data it is possible to extract time series data at various wavelengths, examples of which are plotted in Figure 4.9, for the wavelengths 380, 402, 406, 418, 450 and 480 nm. An isosbestic point occurs at 406 nm, at which point no oscillations are observed. Immediately above and below 406 nm two enzyme species appear to interconvert: peroxidase compound III and the native form, which has an absorbance maximum at 402 nm. The oscillations at 402 nm appears to be mirrored at 418 nm through the absorbance at 406 nm. A second isosbestic point occurs at 462 nm, the character of oscillations below this wavelength matching that of compound III absorbance, and immediately above to that of the native enzyme. These observations are summarised in Figure 4.10, where two successive spectra are plotted, which were taken at the times indicated therein.

Also of note from Figure 4.9 is that the absorbance trace at 380 nm bears the character of the native peroxidase and not the sawtooth appearance of NADH oscillations, since the latter compound does not absorb strongly at this wavelength. The volume-influx rate was reduced to 30 μl/h at $t = 4191$ s, evidence for which is given

[2]See Table 2.1.

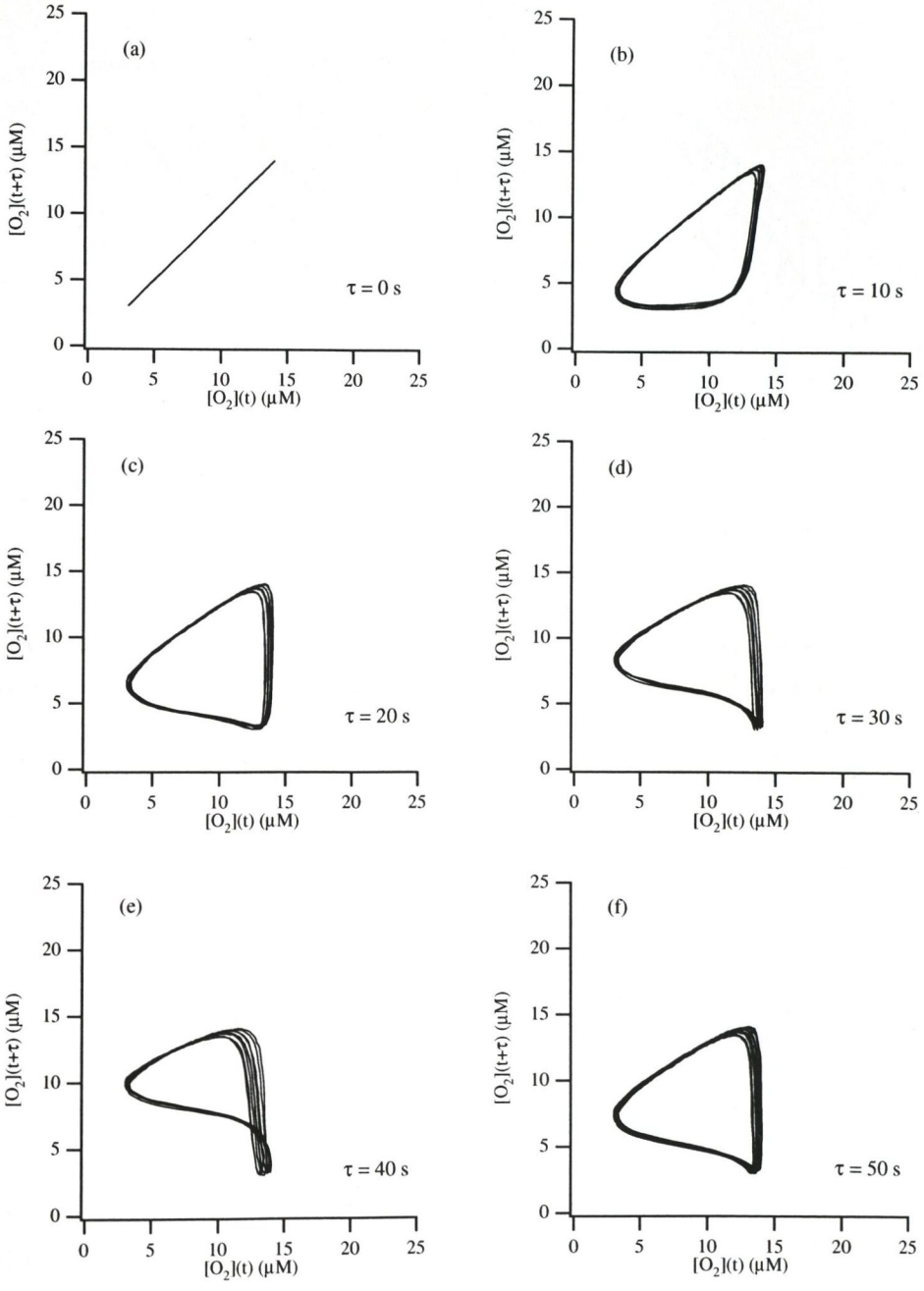

Figure 4.7: Effect of delay time on reconstructed attractors. Graphs (a)–(f) display the effect of increasing T, in the range 0–50 time units (seconds). Data and sampling frequency are the same as Figure 4.6, each attractor comprises 1024 data points starting at 2240 seconds in order to bypass transient behaviour. The simplest figure that captures the essence of the dynamics occurs at $T = 20$ sec.

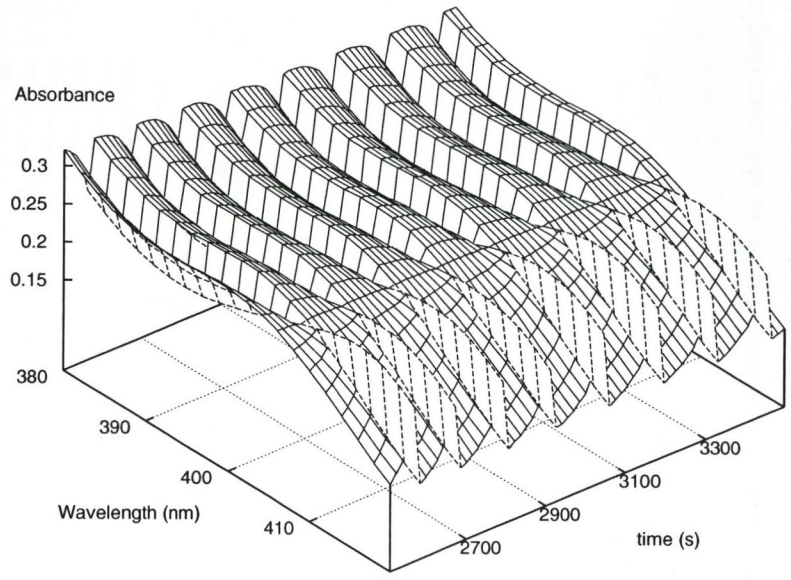

Figure 4.8: Absorbance spectra plotted against time, from an experiment performed with standard conditions. Times are relative to experimental time, and commence at 4800 s.

by the gradual decline in overall absorbance at 380 nm and concomitant increase in oscillation amplitude at all wavelengths (Section 4.3).

4.2.6 Irregular and artefactual behaviours

On certain occasions the pattern of oscillations obtained was irregular in all measured components, an example of which is to be seen in the NADH and oxygen data plotted in Figure 4.11, part (b) of which shows a reconstruction of the underlying attractor. Since no distinct pattern appears to be in evidence, a facile interpretation of the data is that the system has entered a 'chaotic' mode, a term which in its technical sense describes a system displaying apparently random behaviour arising from a wholly deterministic mechanism. Chaotic behaviour of the peroxidase-oxidase reaction was first described by Olsen and Degn [31]. Such an interpretation of these data cannot be made with confidence however, since a route to chaos [61] was never demonstrated in this laboratory. Evidence for a route to chaos via period-doubling has been provided by Geest *et al.* [38] using the concentration of 2,4-dichlorophenol as the bifurcation parameter, and via a quasi-periodic route by Hauck and Schneider [41], gaseous oxygen composition being the parameter in that instance.

On another occasion when unusual behaviour was observed with this system, the

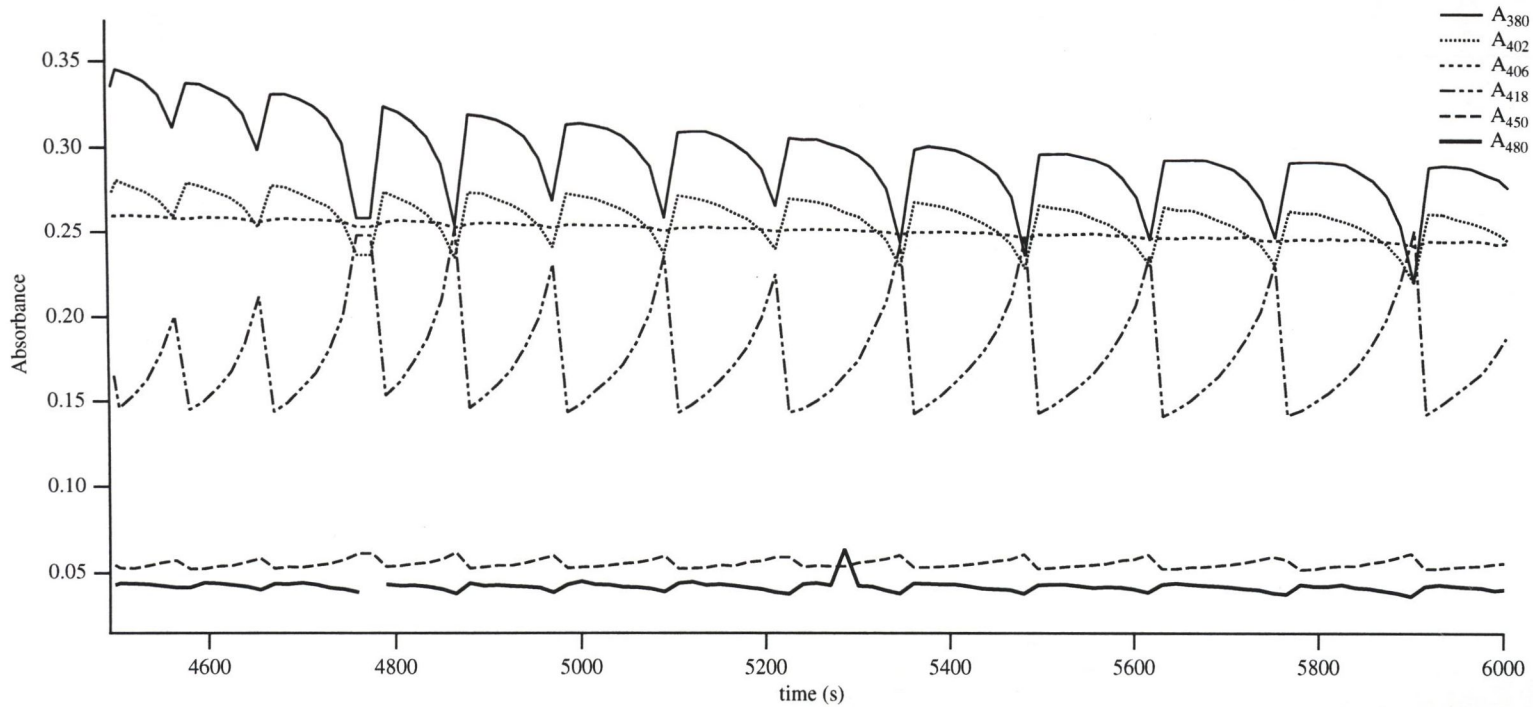

Figure 4.9: Absorbance data at selected wavelengths in the range 380–480 nm, in an alternative representation of the data displayed in Figure 4.8. An isosbestic point is apparent at 406 nm, below which the native form of horseradish peroxidase is prevalent. Above this value, to approximately 462 nm, the peroxidase compound III form predominates. See text for further details.

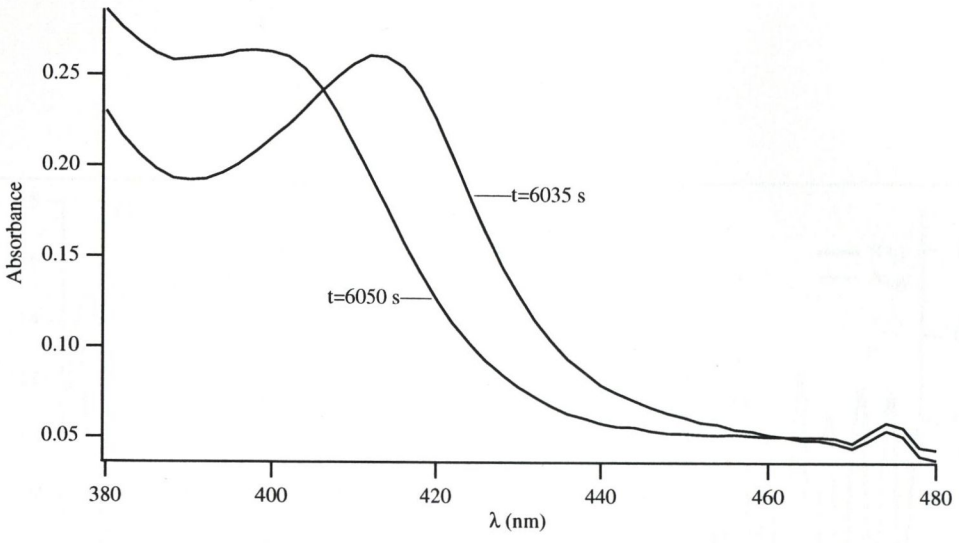

Figure 4.10: Isosbestic points in absorbance spectra taken during the experiment described in the text and illustrated in Figure 4.9.

oscillatory reaction was allowed to proceed for over 180 minutes until NADH supply was exhausted; the absorbance data for compound III are plotted in Figure 4.12. The reason for the overall decline in the baseline absorbance of compound III is unclear. After an initial damping period as transients decayed, the system settled to a steady state, the amplitude and period of the oscillations remaining approximately constant during the course of the reaction. To examine the phenomenon further, the full data set was subjected to several smoothing operations and the final running average sampled to reduce the number of points. A second-order decay process was found to adequately model the data.

Inactivation of the peroxidase, through free radical damage or some other mechanism, has previously been proposed by Olson and Scheeline [49] to explain the steady long-term damping consistently observed in their data. Since in the present case the dynamics themselves are stable the phenomenon is unlikely to be due to enzyme inactivation. Similarly, dilution effects due to an increase in solution volume would be small (<3%) and would not account for the fractional change in baseline observed. The phenomenon was most obvious in this experiment, though it might also account for the change in overall absorbances between spectra taken at start and end of other experiments, some indication of which is apparent in the data in Figure 2.7.

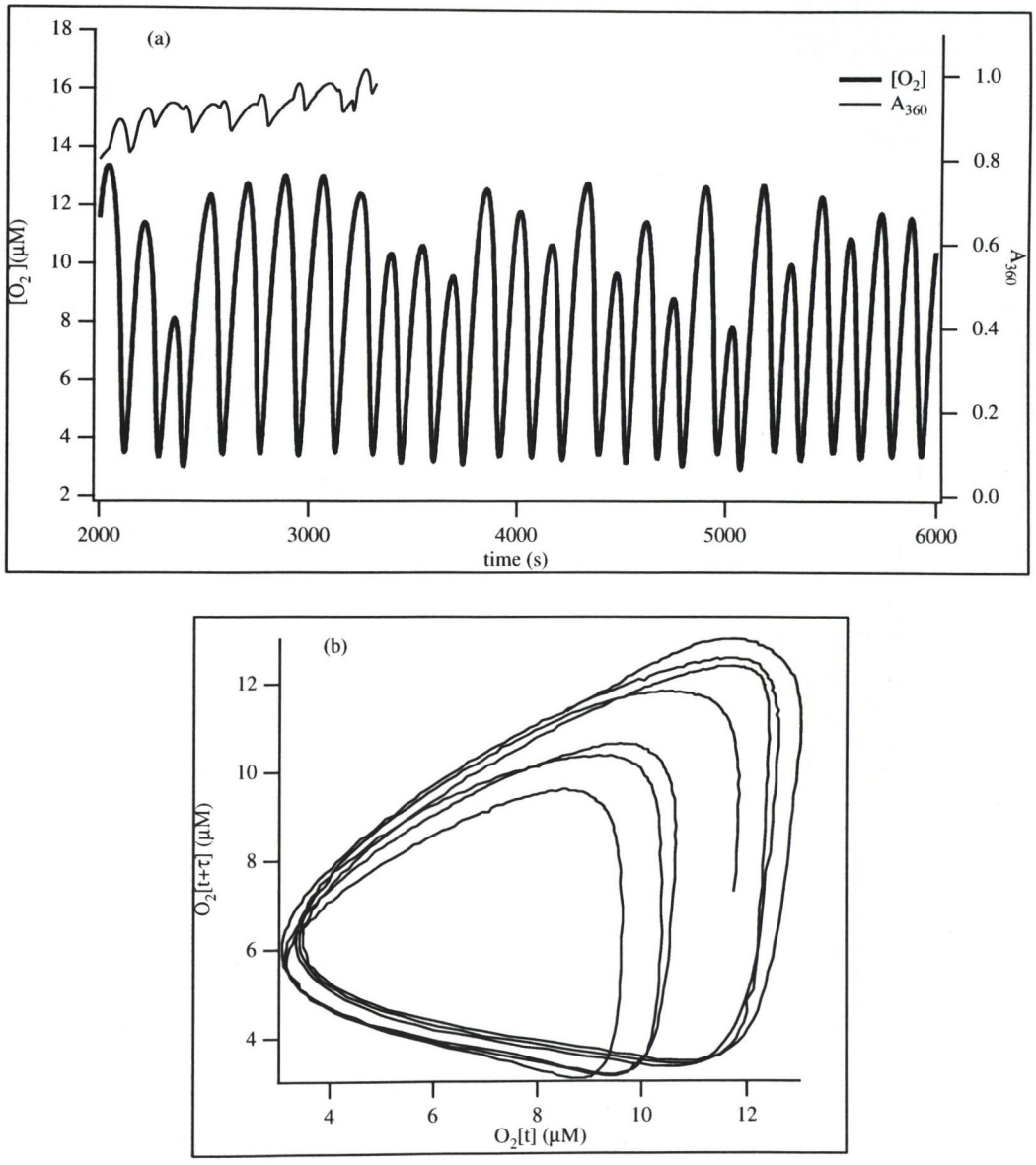

Figure 4.11: Irregular oscillations. Conditions were as Table 2.1 with the exception of horseradish peroxidase concentration, which was 46 U/ml. NADH oscillations are also irregular in character. (compare with Figure 4.5).

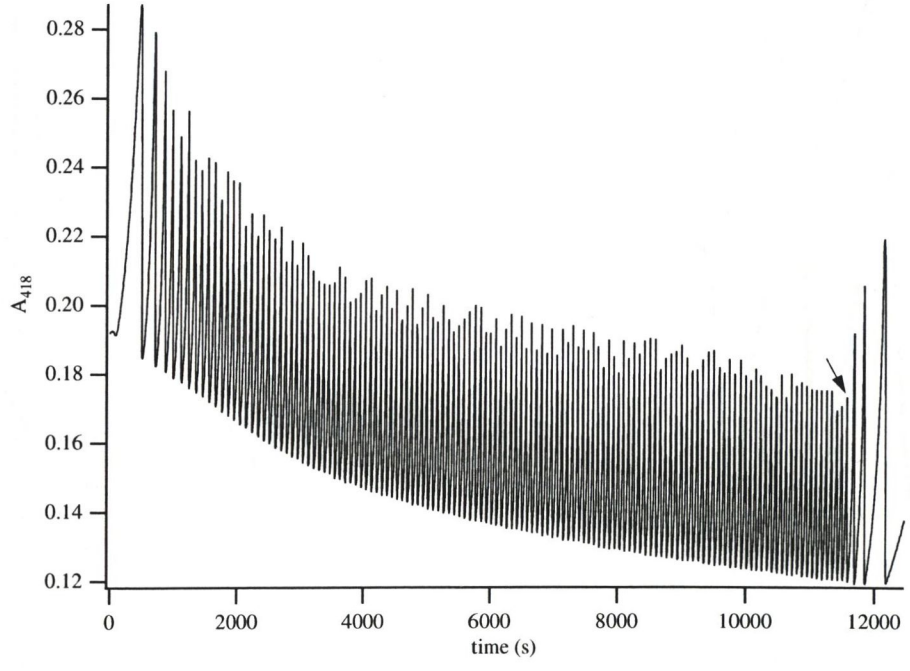

Figure 4.12: Decline in overall absorbance at absorbance at 418 nm. NADH was infused at 1.2 mM/h into a solution containing 50 U/ml horseradish peroxidase, 0.2 μM MB, 20 μM DCP in 0.1 M sodium acetate buffer at pH 5.1,in equilibrium with a 2% oxygen/nitrogen gas mixture bubbled at 20 ml/min. The temperature was 29°C, and the stir speed was 1155 rpm. NADH supply was stopped at the point indicated by the arrow.

4.3 Effect of NADH influx rate on oscillation amplitude and period

An oscillatory run was perturbed by a decrease in NADH volume-influx rate . The resulting change in $[O_2]$ and A_{418} is shown in Figure 4.13. Oscillations in dissolved

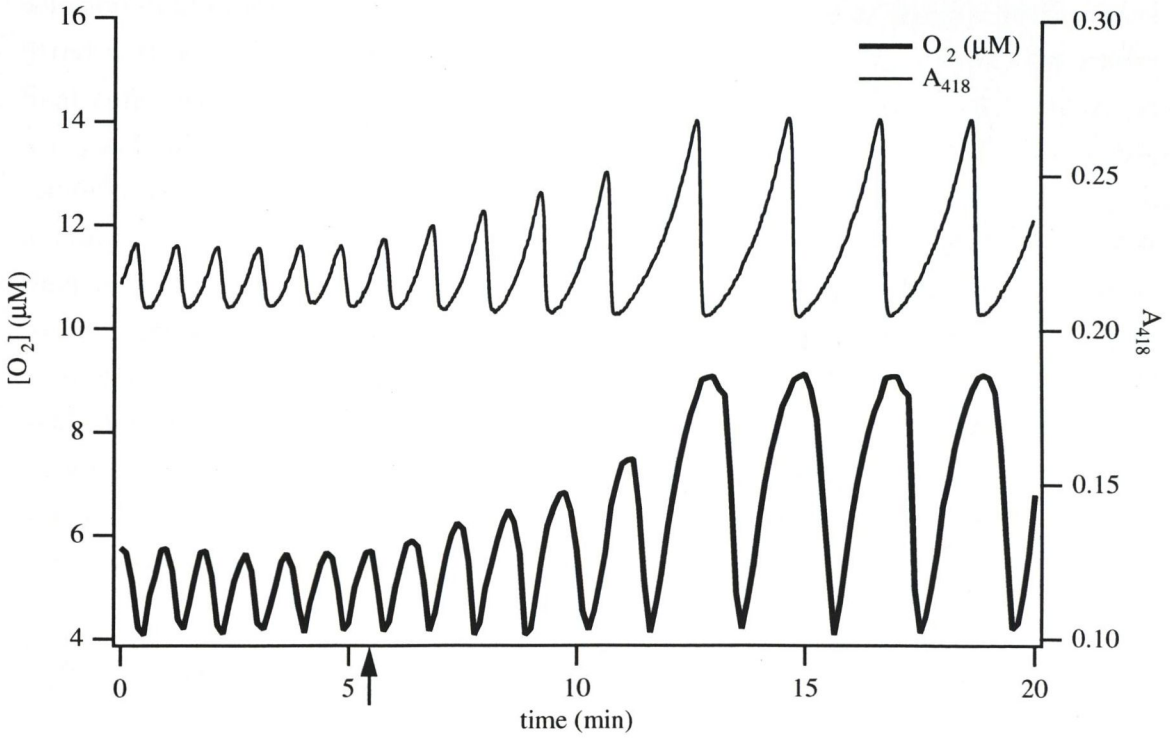

Figure 4.13: Effect of NADH influx rate on waveform amplitude. The arrow on the time axis indicates where the NADH influx rate was decreased from 1.2 mM/h to 1.0 mM/h. The oscillations increase in amplitude and period until a new stable limit cycle emerges. Other conditions were those of Figure 4.4.

oxygen were found to vary in size between experiments, and in many cases the variation can be attributed to the rate at which NADH was infused. In the present example the enzyme originated from a dilution of two-week old stock and the overall size of oscillations was smaller than on occasions in which a fresh preparation was used. In any experiment, when the supply of NADH was exhausted or infusion was suspended the oxygen amplitudes increased until all the remaining NADH in the reaction had been oxidised, the dissolved oxygen concentration returning to equilibrium with the gas phase. The fact that the conditions of Figure 4.13 are very similar to the damped oscillations experiment of Figure 4.4 would seem to indicate that high NADH influx rate was a contributing factor to the behaviour in that instance.

4.4 Variation of enzyme concentration

In this experiment, small volume additions of concentrated horseradish peroxidase stock were made to an oscillating peroxidase-oxidase reaction and the effects observed. The data are plotted in Figure 4.14. Initial conditions were those of the standard set (Table 2.1). At the times indicated in the figure approximately 9.5 μl of stock enzyme solution containing 4 mg/ml HRP were added to the solution using a micropipette fitted with a stainless steel needle, through the gas outlet in the cuvette lid, to give final concentrations of 50, 60, 70, 80 and 90 U/ml. The NADH volume-influx rate was gradually decreased from 1.2 mM/h after enzyme additions in order to balance its net rate of influx with the rate of its consumption. No qualitative change in the dynamics is observable in the plot of NADH and dissolved oxygen against time other than a slight increase in amplitude and period, although this might be explained by the compensatory changes made to NADH influx rate (see Section 4.3). That such changes were necessary[3] might be due to a slight decrease in the rate of NADH oxidation with increased enzyme concentration, contrary to the behaviour of most enzyme-catalysed reactions. The gradual increase in the level of absorbance at 360 nm may be accounted for by the fact that the native peroxidase contributes somewhat to the absorbance at this wavelength (see Figure 2.7).

4.5 Variation of gas composition

In this and the following section, two simple experiments will be described which were done in order to examine the effects of changing gas-control parameters on a working oscillator. In the first such experiment, the gas composition was varied within one oscillatory run, using a fixed flow rate of 10 ml/min. All other conditions were standard, as given in Table 2.1. The method of initiation of oscillations was as described in Chapter 2, Section 4.2 where NADH was introduced to a mixture of all other reagents at equilibrium with an oxygen/nitrogen gas mixture. Oxygen composition was 4% prior to NADH infusion, which at equilibrium gave a dissolved oxygen concentration of 47 μM. NADH influx rate was started at 1.6 mM/h, which gave rise to heavily damped oscillations about a steady state value of approximately 18 μM oxygen. The gas composition was then lowered to 2% in oxygen upon which oscillations commenced. The data are shown in Figure 4.15. The oscillations which reappeared after switching to a lower oxygen composition declined in amplitude initially, spon-

[3]In general, changes in NADH influx rate were made in order to maintain a constant NADH concentration in the reaction vessel. See Section 2.3.3 and Ref. [38].

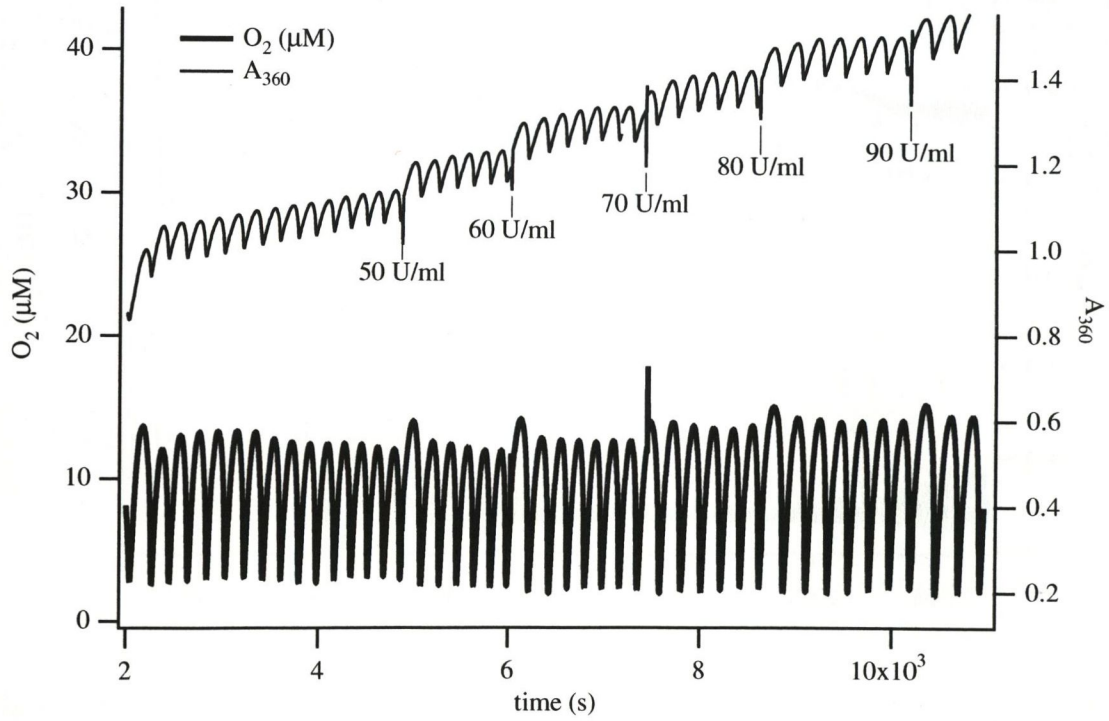

Figure 4.14: Effect of increasing enzyme concentration. Standard conditions prevailed at the outset of the reaction. Successive additions of HRP stock in 0.1 M acetate buffer were made at the times indicated, which also show the final concentration of enzyme in the reaction after delivery.

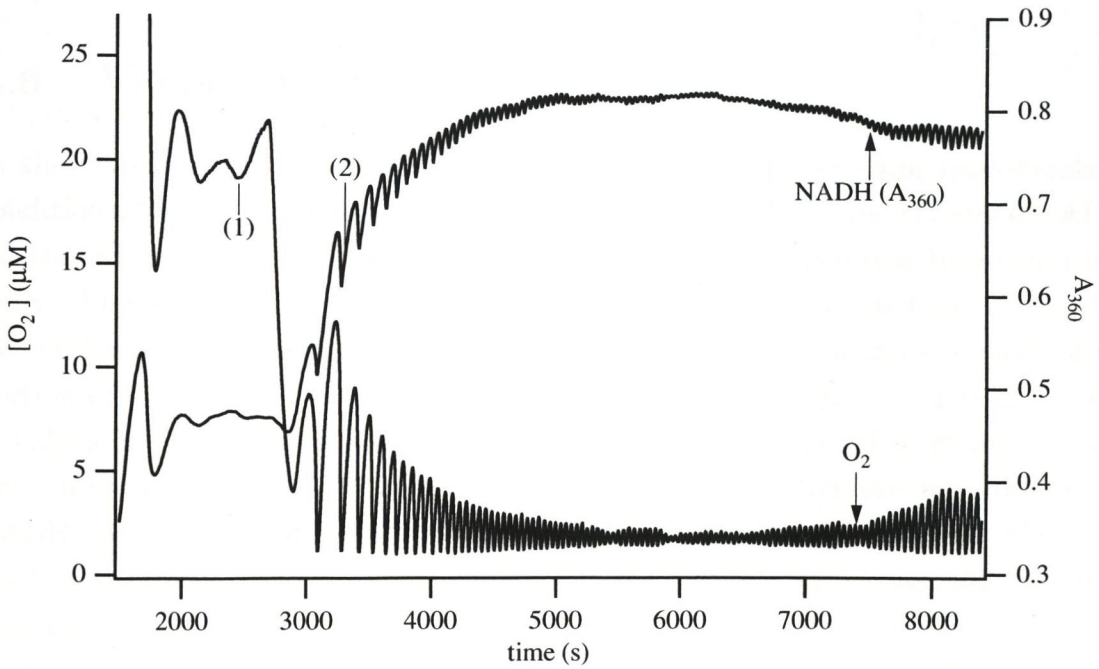

Figure 4.15: Variation of Gas Composition. A 2 ml solution containing 80 units of horseradish peroxidase, 20 μM 2,4-dichlorophenol and 0.2 μM methylene blue in 0.1 M sodium acetate buffer at pH 5.1 were in equilibrium with a 4% O_2/N_2 gas mixture, bubbled at 10 ml/min. NADH was introduced at an initial rate of 1.6 mM/h. At (1) the oxygen composition was reduced to 2% in oxygen, and the NADH influx rate was reduced to 1.2 mM/h at (2). The temperature was 25°C and the solution was stirred at 1155 $\pm$ 69 rpm.

taneously rising to a near-constant level two to three hours after the final NADH infusion rate was set, though it is not clear if this was the result of the gas change or inherent to the particular preparation of the reagents. Data will be presented in the next section which show that the variations in amplitude are not wholly the product of inaccurate gas delivery or control at lower flow rates. In summary, it would appear that high steady-state oxygen levels inhibit sustained oscillations but not the oxidation reaction itself, since NADH supply and net consumption were roughly equal prior to the change in oxygen composition.

4.6 Variation of gas flow rate

In this experiment, a peroxidase-oxidase reaction was set up using near-standard conditions, the only exceptions to the standard parameter set being the stock NADH solvent, which was distilled water, and the gas flow rate, which was 10 ml/min initially. Figure 4.16 plots dissolved oxygen concentration as a function of time for this system. The mass-transport constant was calculated from the re-equilibration portion of the oxygen data in the method described in Section 2.3.2, giving a value of 0.38 min^{-1}, which may be compared with the value predicted from the calibration curve in Figure 3.8. Stable oscillations commenced after the introduction of NADH into the reaction, and were seen to damp out almost immediately when the gas flow rate was changed to 5 ml/min. The flow rate was increased to 20 ml/min and oscillations restarted, with higher amplitude and period than before.

In a companion experiment (Figure 4.17) where the initial gas flow rate was 5 ml/min, bubbled, giving $k_{-t} = 0.21$ min^{-1}, damped oscillations were observed shortly after NADH infusion was started, which were not restarted switching to the initial gas flow rate of the previous experiment. Increasing the flow rate to 20 ml/min yielded well-formed, highly regular, period-1 sustained oscillations.

4.7 Methylene blue as effector

The electron acceptor methylene blue has for long been used as a promoter of sustained oscillations in the PO reaction. In one early study conducted by Nakamura, Yamazaki and Yokota [27], methylene blue was used to initiate sustained oscillations in a lactoperoxidase-catalysed system. More recently, Olson and Scheeline [62] looked at the role of methylene blue in the oscillator, using the more common horseradish peroxidase. One aspect of that work involved initially omitting MB from the reaction,

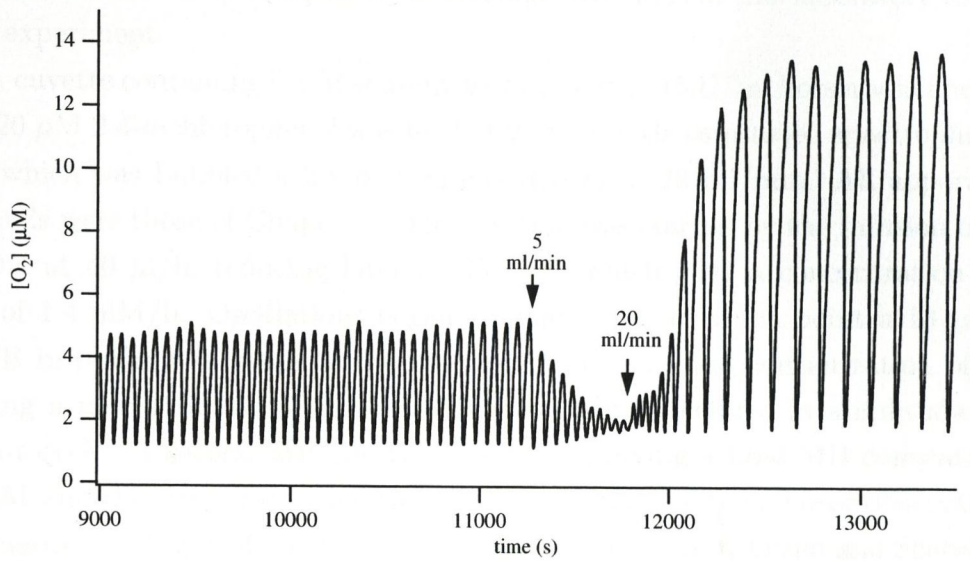

Figure 4.16: Variation of Gas Flow Rate – I. Intra-experimental variations of gas flow rate were made to a peroxidase-oxidase reaction proceeding under near-standard conditions; any deviations from the standard set are noted in the text. The flow rate, initially set to 10 ml/min, was changed at the points indicated, which altered the mass-transport constants of oxygen into and out of solution.

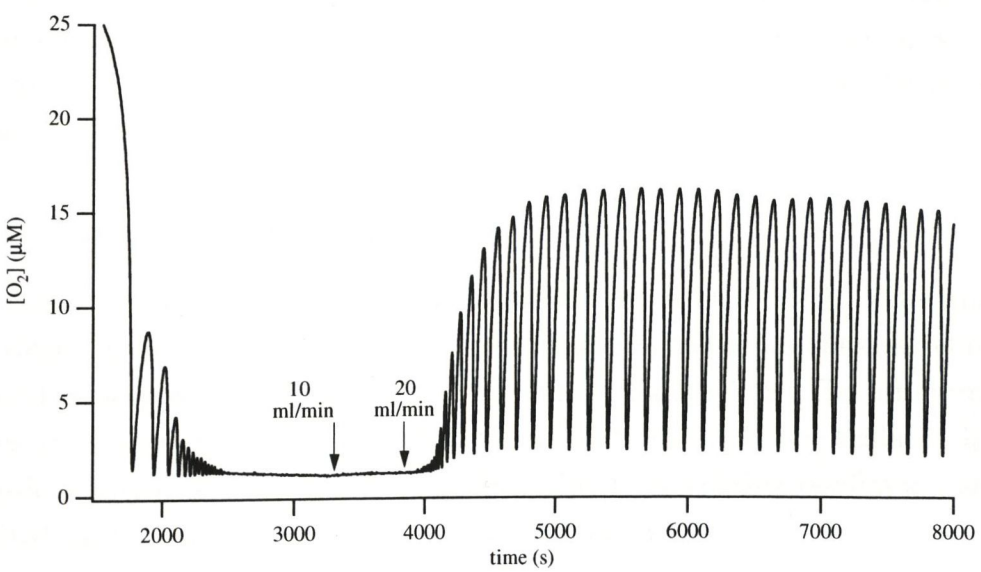

Figure 4.17: Variation of Gas Flow Rate – II. Intra-experimental variations of gas flow rate were made to a peroxidase-oxidase reaction proceeding under near-standard conditions; any deviations from the standard set are noted in the text. The gas flow rate was initially set at 5 ml/min and was varied thereafter as indicated by the arrows.

in order to add it later as a pulse. An attempt was made in this laboratory to emulate that experiment.

A cuvette containing 0.1 M sodium acetate buffer, 25 U/ml horseradish peroxidase and 20 μM 2,4-dichlorophenol was held at 28°C in a thermostated spectrophotometer into which was bubbled a 2% oxygen gas stream at 20 ml/min. All apparatus and methods were those of Chapter 2. The reaction was started by the infusion of 80 mM NADH at 40 μl/h, reducing later to 35 μl/h which gave a concentration infusion rate of 1.4 mM/h. Oscillations began to damp out, at which point a 13 μl aliquot of MB in buffer was made to the reaction, to give a final concentration of 0.1 μM causing a new train of oscillations to appear which declined in amplitude to form a limit cycle. A second MB addition was made, giving a final MB concentration of 0.2 μM and this gave rise to damped oscillations immediately. These observations are summarised by Figure 4.18. In the experiment performed by Olson and Scheeline [62], 2,4-dichlorophenol was excluded and methylene blue was added in a single pulse to a concentration of 0.2 μM, giving rise to oscillations markedly larger than any in the initial damping phase. The present data show oscillations reappearing at similar amplitudes to those at the start. Common to both experiments, however, is the stabilising influence of MB on oscillations. The second, damping episode was a surprising result, since sustained oscillations were observed with 0.2 μM methylene blue in separate experiments when all other parameters were similar, showing a certain degree of unpredictability inherent in the oscillator. Nevertheless, methylene blue has been shown to have the ability to initiate sustained oscillations in the peroxidase-oxidase reaction when in the presence of 2,4-dichlorophenol.

4.7.1 Brilliant cresyl blue

The possibility of the electron acceptor brilliant cresyl blue (BCB) substituting for methylene blue in the PO reaction was investigated in one series of experiments. The chemical structures of MB and BCB are shown in Figure 4.19. The structural similarities are not reflected in their diverse effects on the peroxidase oscillator, however. Pulsatile addition of 0.2 μM brilliant cresyl blue to a working oscillator completely inhibited oxidation, as shown by the data in Figure 4.20.

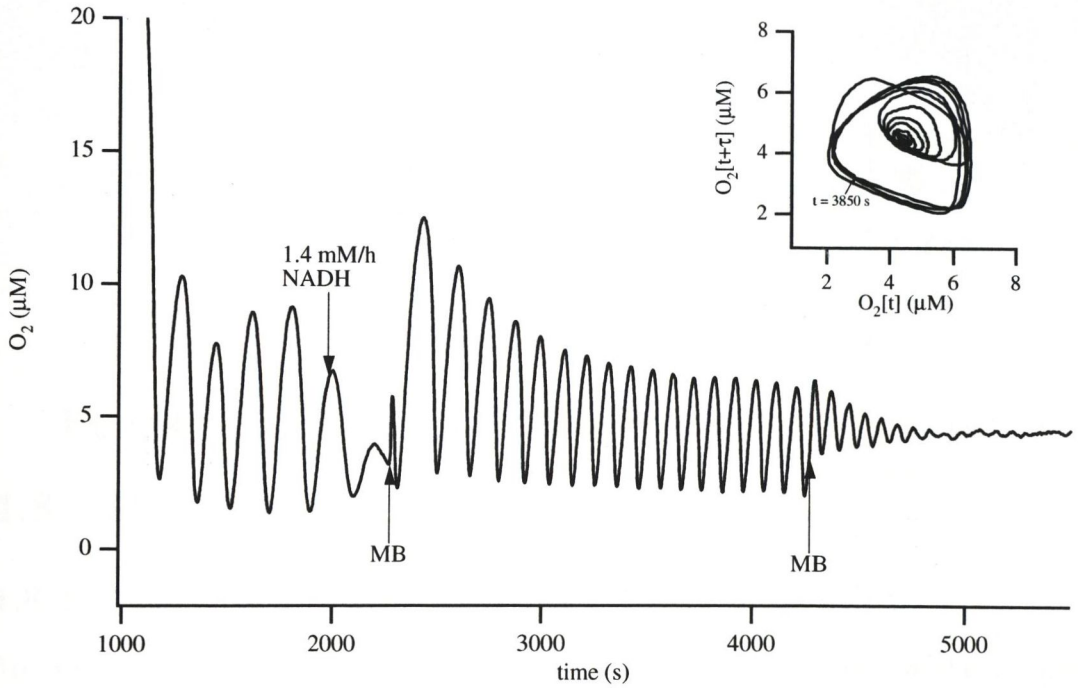

Figure 4.18: Methylene blue addition. Horseradish peroxidase was present at 25 U/ml in 0.1 M acetate buffer at pH 5.1, which also contained 20 μM 2,4-dichlorophenol, in a solution volume of 2 ml. 2% oxygen was bubbled at 20 ml/min. NADH influx rate was set to 1.4 mM/h at the time indicated. The stir speed was 1155 $\pm$ 69 rpm and the temperature was 28°C. Methylene blue was added as a pulse to give 0.1 μM concentration and sustained oscillations commenced. A second pulse caused oscillations to cease, at which point the effector concentration was 0.2 μM. Inset: reconstructed limit cycle attractor made from the oxygen data using a delay time of 25 s, showing the collapse of the stable limit cycle which followed the second methylene blue addition.

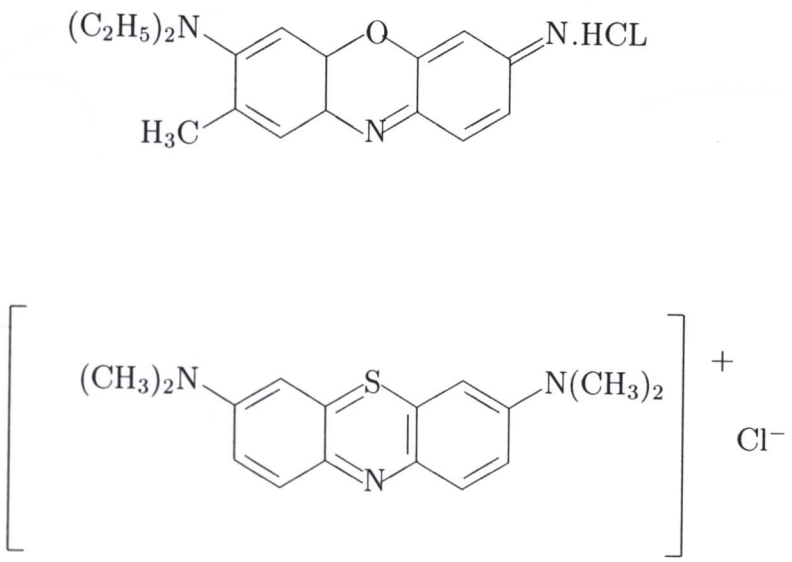

Figure 4.19: Chemical structures of methylene blue and brilliant cresyl blue.

4.8 Discussion

4.8.1 Studies and observations of reproducibility

An important consideration in the study of a nonlinear system such as the peroxidase-oxidase reaction is that of reproducibility of the observed behaviours, whether as relating to the type of dynamics or to effects on size or other aspects of the character of oscillations. The results obtained in this laboratory were for the most part reproducible, with certain exceptions. The standard experimental conditions introduced in Chapter 2 were, as stated previously, very likely to give rise to sustained oscillations, and departures from what became the expected behaviour were few. However, at certain times it became evident that accumulative contamination of the quartz cuvette (which was the reaction vessel used in all experiments) by metal ions or some other agent, came near to inhibiting the oxidation of NADH completely, and was only alleviated by cleaning the affected cuvette in a nitric acid bath. This is illustrated in Figure 4.21, showing portions of oxygen and absorbance data before and after cuvette cleaning. These data were obtained under standard conditions for the most part, except for the first data set, for which a potassium phosphate buffer of pH 4.8 was used, a fact which was not, however, responsible for the absence of oscillations; the effect of buffer and pH will be dealt with in a later chapter. The cuvette was usually cleaned

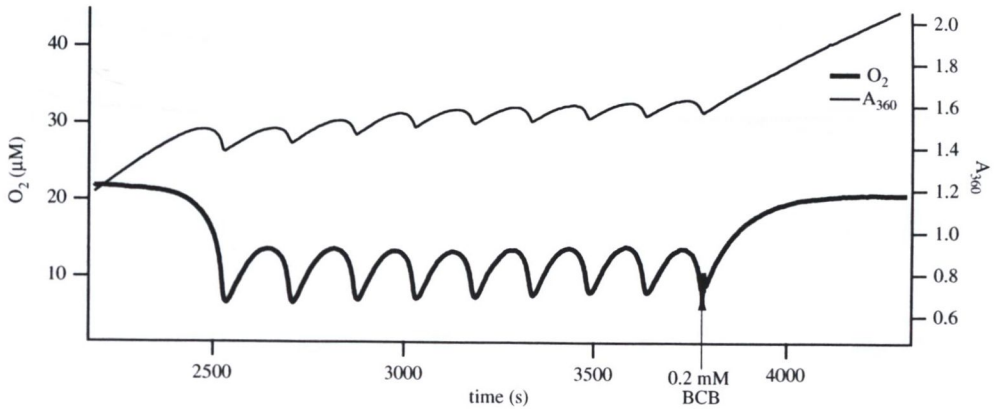

Figure 4.20: Brilliant cresyl blue addition. Initial conditions were standard (Table 2.1) with the exception of the buffer type, which was potassium phosphate. Addition of 0.2 μM BCB at the point indicated caused immediate cessation of the reaction.

by means of a detergent solution, and rinsed with distilled water.

The shape of individual oscillations was observed to change under diverse experimental conditions, although this was found to be reliant upon the particular preparation of the reagents used. Figure 4.22 shows some atypical appearance of oscillations that were generated under conditions close to the standard set. The enzyme, horseradish peroxidase, and auxiliary reagents methylene blue and 2,4-dichlorophenol were dissolved in 0.1 M acetate buffer at pH 5.1, and 2 ml of this solution assayed for oscillatory behaviour on two separate occasions by the usual procedure described in Section 2.3. A period of two days elapsed before the second experiment was carried out, during which time both the NADH stock and buffered HRP preparation were stored at 4-6°C.

The most notable feature of the data sets in Figure 4.22 are the sharp turning points of individual oscillations, and the closeness to bilateral symmetry about the vertical axis that is apparent in the absorbance peaks of CoIII. These can be contrasted with data presented earlier in Figures 4.5 and 4.9, in which the more rounded character of the oxygen peaks is evident, and also the asymmetric nature of individual CoIII oscillations. The shape of the waveform is largely unchanged between experiments; however, attempts to reproduce this behaviour with fresh reagent preparations were largely unsuccessful, and although sharp-pointed oxygen peaks were observed on a few other occasions, the data portrayed in this section were the most striking examples of their kind.

The results of Section 4.6 on the effect of gas flow rate on the viability of oscillations would seem to underline the importance of having reproducible mass-transport

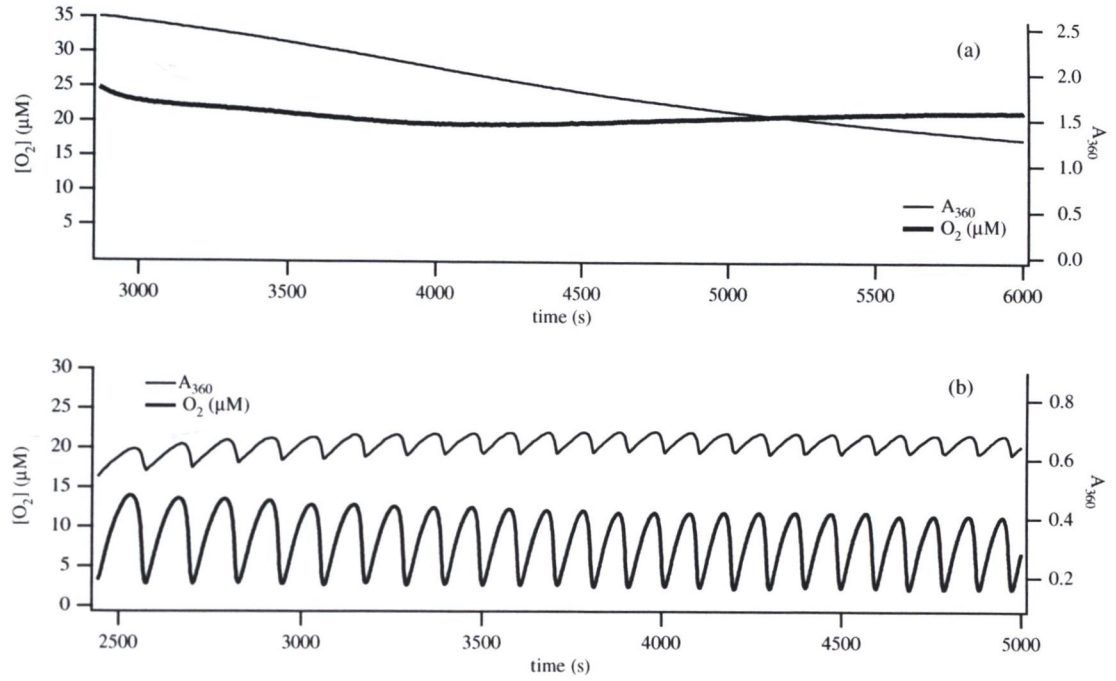

Figure 4.21: Data obtained before and after nitric acid wash of the cuvette. A phosphate buffer was used in the first experiment (a). All other conditions were standard. The cuvette was left in a nitric acid bath for twenty-four hours, which relieved the prevalent inhibition.

constant values. Since the majority of experiments were carried out under gas bubbling conditions at 20 ml/min and 2% oxygen composition, a statistical analysis was carried out on the values of k_{-t} obtained under these conditions and a frequency distribution calculated, which is shown in Figure 4.23 in which the k_{-t} axis is divided into 20 intervals of width 0.05 min^{-1}. The probabilities, or more properly the relative frequencies of occurrence, of k_{-t} in each interval are plotted on the ordinate of the graph. The Gaussian function

$$p(x) = a + \frac{1}{\sqrt{2\pi\sigma^2}} e^{-\frac{(x-u)^2}{2\sigma^2}}$$

with mean u and variance σ^2 (a is a constant) was fitted to the histogram data points to give a normal distribution $N(0.56, 0.05)$. This analysis shows that while the mass-transport constants ranged over the interval (0.2,1.0), slight variations between the values obtained in successive experiments did not greatly affect reproducibility, as is shown by the data in Figure 4.22.

A further objective of reproducibility must be the duplication and verification of results published in the literature, and this was one of the original objectives of this present study. Few, if any, of the experiments performed on this laboratory show

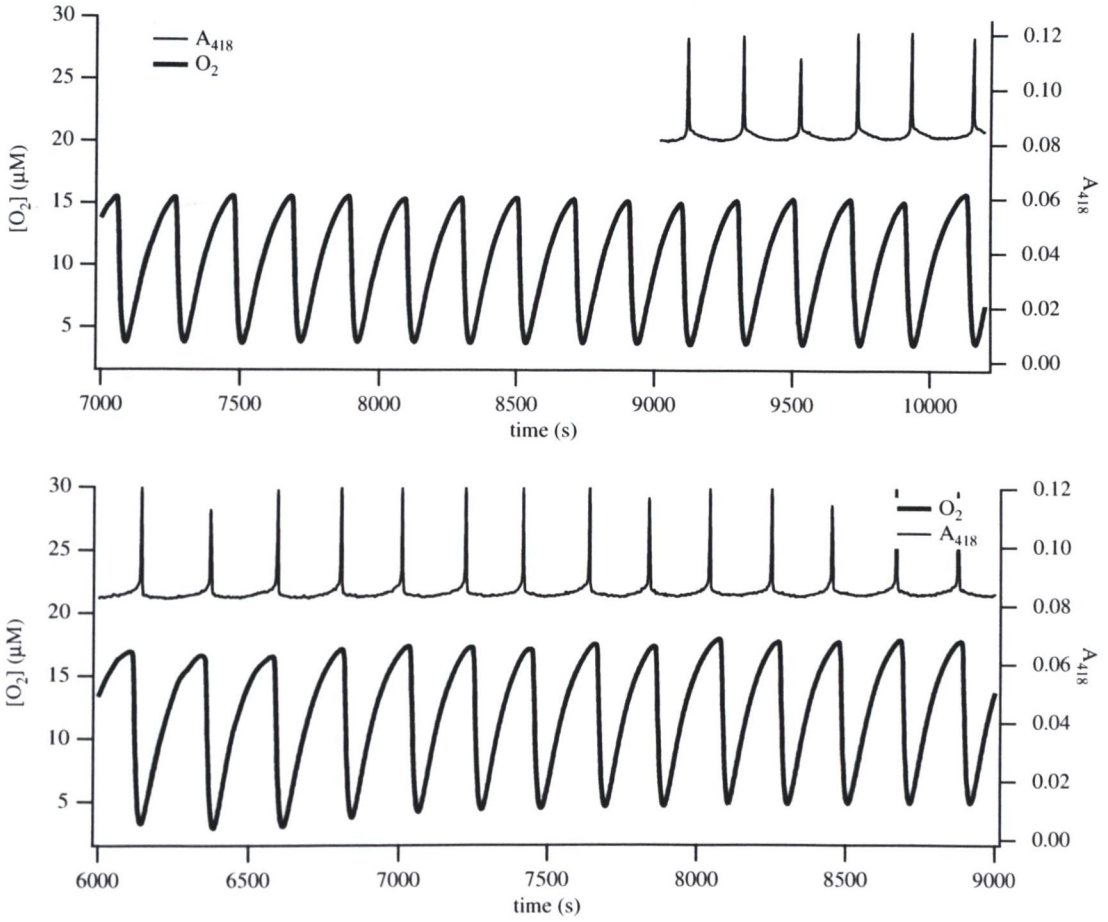

Figure 4.22: Reproducibility of oscillations. Conditions of the experiments were as follows: An oxygen/nitrogen gas stream of composition 2% in oxygen was bubbled at 20 ml/min into a 2 ml solution of horseradish peroxidase (50 U), 2,4-dichlorophenol (20 μM) and methylene blue (0.2 μM) in 0.1 M sodium acetate buffer at pH 5.1, stirred at 1155 $\pm$ 69 rpm. The temperature was 29°C. NADH (80 mM, dissolved in 0.01 M acetate buffer at pH 7.0) was infused at 0.8 mM/h. Calculated mass-transport constants (k_{-t}) were (*a*) 0.48 min^{-1} and (b) 0.55 min^{-1}.

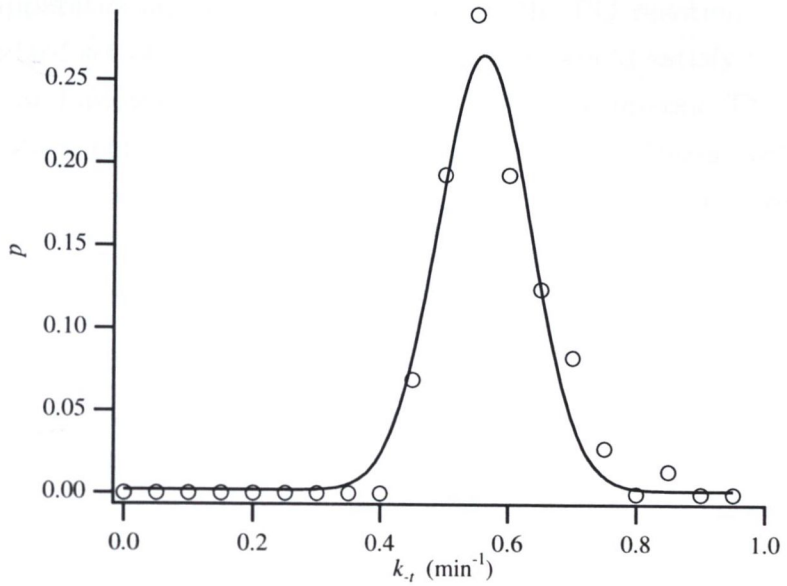

Figure 4.23: Frequency distribution of k_{-t} values. Mass-transport constants were calculated using the direct curve fitting method described in Sections 2.3.2 and 3.3.2 for dissolved oxygen data obtained at bubbled gas flow rates of 20 ml/min, 2% oxygen composition, temperature 25 °C and stir speed 1155 ± 69 rpm. The normalised frequency distribution of these data was calculated for a frequency interval of 0.05 min^{-1}. The fitted curve is a Gaussian function, the fitted parameters giving a normal distribution of mean 0.56 min^{-1} and variance 0.05. See text for further details.

results directly comparable with the data acquired by other laboratories; at best, a similar wave shape was obtained, and at worst, the experimental conditions were found not to favour oscillations. The latter was most evident where gas blowing methods were employed, the higher evaporation rates used being due in part to the higher flow rates necessary to achieve a particular mass-transport constant, and the higher NADH volume-influx flow rates (at reduced stock concentration) that were used to balance water loss did not provide conditions suitable for sustained oscillations, and the results showed only nonlinear behaviour in the absorbance of CoIII. Sustained oscillations were only obtained when the NADH stock concentration was raised, the gas bubbling method employed and the NADH volume influx rate reduced accordingly, but no experiment with other parameters adjusted to reproduce the conditions of an experiment published in the literature was successful in reproducing the reported behaviour. There are two possible reasons for this: (1) the actual apparatus used has a direct bearing on the results obtained, and (2) insufficient parameter data or information on methodology are included in the literature to be able to reproduce the experimental conditions. Olson [40] has performed a rigorous analysis of the ex-

perimental apparatus and reaction conditions of the PO reaction, in an attempt to create a standard set of materials and methods that would satisfy the criterion of reproducibility and allow direct comparison between experiments. The apparatus used in this laboratory contains several similarities to that of Olson, yet with sufficient differences, among them the NADH delivery apparatus, and also cuvette volume and stirring method, to make direct comparison difficult.

4.8.2 Comparisons with published work

In a development of the above argument, consider the information given in Table 4.1, which collates the parameters used by several groups and reflects the wide range of values and methods used by various workers over a period of nearly three decades. In the table there are a number of gaps where parameter values are either not available or are irrelevant. Olson *et al.* [49] provide the greatest quantity of experimental detail, and in the cited article recognise fifteen experimental control variables of the system. It is perhaps surprising that many experimenters do not quote values for gas diffusion parameters (the mass-transport constant), and those that do frequently omit the method of calculation, which, as has been shown in this and previous sections, can have a pronounced effect on the final value. Gas composition values vary considerably between experimenters. Hauck and Schneider [41] use this as a bifurcation parameter over the range 15-17%. Sustained oscillations were never observed in this laboratory with oxygen composition higher than 2%, with higher oxygen equilibrium concentration tending to be inhibitory, which confirms an observation by Hung and Ross [51]. In the Hauck and Schneider experiments, NADH was recycled from NAD^+ continuously using glucose-6-phosphate dehydrogenase in the presence of excess glucose-6-phosphate, a method that was attempted in this laboratory with the results to be discussed in Chapter 5.

Another apparent contradiction in literature values arises from the NADH concentration-influx rates quoted by Rys and Wang [39], which are over twice as high as those used in this laboratory, and, given their assertion that volume changes over the course of the reaction were less than 2%, would seem to indicate that their stock NADH was in excess of 250 mM (computable from the information in Table 4.1 and using Equation 2.2). This is surprising since although the other parameters are similar to the standard conditions used here, the higher influx rates would almost certainly lead to rapid damping to a low steady-state oxygen level and rapidly increasing NADH concentration (see Section 4.3).

Parameter	Standard	Ref. [38]	Ref. [39]	Ref. [27]	Ref. [49]	Ref. [44]	Ref. [41]	Ref. [1]	Ref. [51]	Ref. [47]
Gas Delivery										
Method	bubbled	blown	bubbled	bubbled	blown	blown	blown	blown	blown	blown
Flow Rate (ml/min)	20	-	10	4	190	-	-	-	120	-
O_2 composition (%)	2	1.42	1.9	5.5	1.5	2	15	1.05	1.0-2.4	1.05
k_{-t} (min^{-1})	0.5	0.224	-	-	0.15	-	0.066	0.36	-	0.288
Peroxidase										
Type	HRP	HRP	HRP	LP	HRP	HRP	HRP	HRP	HRP	Various
Conc. (μM)	3.2	0.7	1.86	27	ca. 7.9	-	-	1.2-1.5	0.65	2.0
Activity (U/ml)	40	-	-	-	100	1.66-8.33	75	-	-	-
NADH										
Conc. (mM)	80	80	-	2	6.37	0.4	-	100	150	130
Infusion rate (μl/h)	30-40	35-40	-	-	465,309	-	-	45-65	15-40	14-24
Infusion rate (mM/h)	1.2-1.6	0.4-0.46	4.08-5.16	-	0.59,0.39	0.2	-	-	-	-
Methylene Blue										
Conc. (μM)	0.2	0.1	0.2	1.0	0.2	-	1.0	0.1	0.1	0.0-1.0
2,4-dichlorophenol										
Conc. (μM)	20	20-35	20	20	10	9-25	50	25	10-25	30-287
Solvent	NaAc	EtOH	-	-	NaAc	EtOH	PO_4^{2-}	EtOH	EtOH	-
Buffer										
Type	NaAc	NaAc	NaAc	PO_4^{2-}	NaAc	NaAc	PO_4^{2-}	NaAc/PO_4^{2-}	NaAc	NaAc
Conc. (M)	0.1	-	-	-	0.1	-	0.1	0.1/0.1	0.1	0.1
pH	5.1	5.1	5.2	7.0	5.1	5.1	4.8	5.1/6.3	5.1	5.1
Solution Volume (ml)	2	7	2	6	5	12	4.3	10	7.0-7.5	7.0
Temperature (°C)	25	28	29	35	25	25	25	28	28	RT/28
Stir Speed (rpm)	1155	1420	1025	-	1300	-	750	1050	1000	850

Table 4.1: Comparison of experimental parameters. Peroxidase-oxidase oscillator experimental parameters from selected literature sources are compared with the standard values used in this present work. The abbreviations HRP and LP stand for horseradish peroxidase and lactoperoxidase, respectively, and RT denotes room temperature. Peroxidase concentrations quoted from reference [47] are for the case of horseradish peroxidase.

4.8.3 Conclusion

In summary, this study of the peroxidase-oxidase oscillator has yielded a variety of different behaviours depending on the parameters used, which include steady-state, bistability, damped, sustained and irregular patterns. Several methods have been used to display the time series data; limit cycle behaviour was evident in graphs of the reconstructed attractors in two dimensions. Analysis of absorbance spectra taken during an oscillatory run has revealed that each reaction cycle involves the interconversion of the native ferric enzyme (Per^{3+}) and oxyperoxidase (CoIII). The amplitude and period of oscillations were found to be affected by the rate of influx of NADH and oxygen into the reaction mixture. Intra-experimental increases in peroxidase enzyme concentration did not change the dynamics. The electron accepter methylene blue was found to sustain oscillations, but in contrast, a structurally similar compound, brilliant cresyl blue, inhibited all NADH-oxidation.

The reaction mixture was found to be stable for several days when stored at 4-6°C, with the pattern of oscillations being unchanged. Arising from the observation that oxygen flow rate affects oscillation amplitude and period, a statistical analysis of mass transport constants obtained under identical physico-chemical conditions was conducted and the data were found to follow a normal distribution. Under standard conditions the average mass-transport constant obtained was found to be $0.56 \pm 0.05\ \text{min}^{-1}$.

Chapter 5

Studies on pH and Ionic Strength

5.1 Preamble

The NADH-oxidase activity displayed by peroxidase enzymes is favoured by acidic conditions, and has been most often studied at pH 5.0–5.5. Table 4.1 gives some indication of the range of pH values employed in published data, in only one instance of which were experiments conducted at neutral pH, with lactoperoxidase in place of the more commonly used horseradish peroxidase [27]. If any systematic variation of pH has been performed in the time since the discovery of this biochemical oscillator, the results have not been published in the scientific literature. The experiments that are recorded in this chapter were performed in order to address the issue. Preliminary studies were performed on the the use of a pH indicator in a working oscillator, to monitor any changes that might occur during conditions of lowered buffer strength with constant ionic strength.

The method of regeneration of NADH by recycling from NAD^+ using a glucose-6-phosphate dehydrogenase mechanism will be discussed, since this has been used on a number of occasions, for example by Nakamura *et al.* and Hauck and Schneider [27, 41]. The effect on the peroxidase oscillator of any auxiliary reagents used in this method (for example, glucose-6-phosphate) has been claimed to be negligible by Hauck and Schneider, although without providing substantiating evidence. The effect of glucose-6-phosphate on a working oscillator will be considered in a later section. A series of experiments looking at the effect of varying ionic strength was performed as a logical adjunct to the aforementioned study, but the results will be presented before those obtained using a coupled enzyme system. This chapter concludes with a section on the use of lactoperoxidase in place of horseradish peroxidase under otherwise standard conditions.

5.2 Materials and methods

Chlorophenol red (3',3"-dichlorophenolsulphonphthalein) and methyl red (4-dimethylaminobenzene-2'-carboxylic acid) were purchased from Sigma (Sigma-Aldrich, Dublin, Ireland; Cat. Nos. 19,952-4 and M-7267). Glucose-6-phosphate (D-stereoisomer) was purchased from Sigma as the disodium salt (Cat. No. G-7250). Glucose-6-phosphate dehydrogenase was purchased from Sigma (Cat. No. 8404) as a suspension. $\beta-\mathrm{NAD}^+$ was purchased from Sigma (99%; Cat. No. N-1511). Lactoperoxidase from bovine milk was obtained from Sigma as a lyophilised powder (76 U/mg; Cat. No. L-2005).

All other reagents that were used are detailed in Section 2.1. pH measurements were made using a Corning Model 240 pH meter. Other apparatus was that described in Chapter 2.

5.3 pH studies

The investigation into the effects of pH on the PO reaction was carried out in two stages, in the first of which an attempt was made to find a suitable pH indicator for following pH changes of a weakly-buffered reaction medium containing additional salts to compensate for any change in ionic strength incurred by lowering the buffer concentration. The second approach was the systematic variation of buffer pH, in order to observe changes in the degree of oxidation of NADH and the character of oscillations.

5.3.1 pH indicators

A pH indicator was chosen for use with the PO oscillator if it satisfied two criteria: (*i*) its useful pH range lay between pH 4 and pH 7 and (*ii*) the absorbance spectrum of the compound was readily distinguishable from that of the peroxidase. Two potential candidates were chlorophenol red (CR) and methyl red (MR). The chemical structure of each indicator is shown in Figure 5.1. Chlorophenol red did not completely satisfy the criteria, since it was found at acidic pH to absorb most strongly at 432 nm, close to the HRP wavelength of maximum absorbance at 402 nm. A titration curve was constructed by taking absorbance spectra of a 50 μM solution of CR in 0.1 M buffer at pH values in the range 4.8–7.9. Sodium acetate/acetic acid buffer was used over the range 4.8–6.5 and sodium phosphate was used for 6.0–7.9. The resulting spectra are plotted in Figure 5.2, which shows that chlorophenol red has absorbance maxima

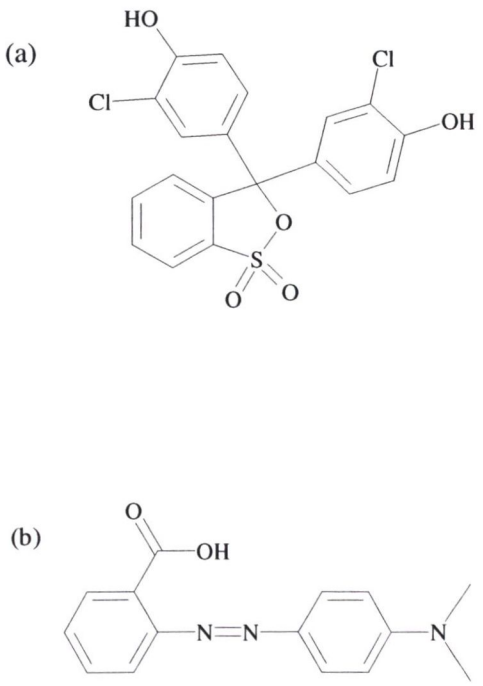

Figure 5.1: Structures of (a) chlorophenol red and (b) methyl red.

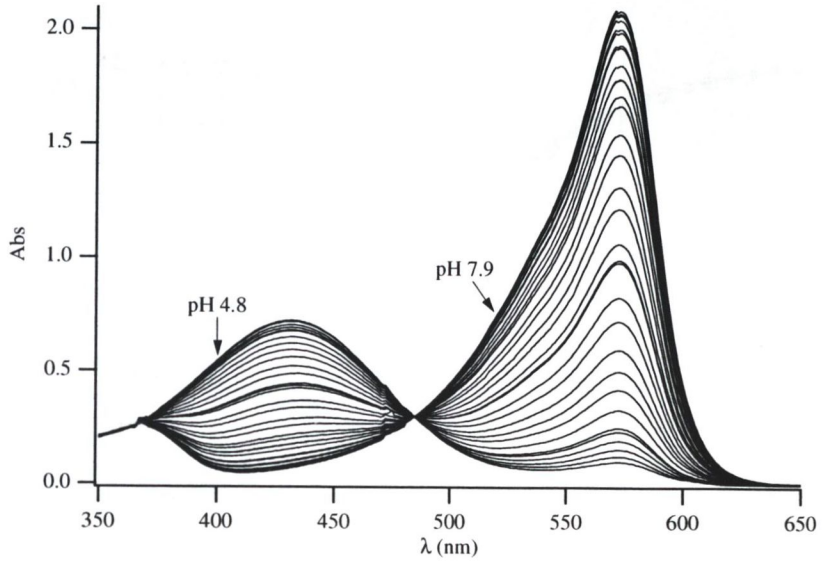

Figure 5.2: Absorbance Spectra of chlorophenol red at pH values in the range 4.8–7.9.

at 432 and 572 nm, and an isosbestic point at 485 nm. A plot of absorbance versus pH is shown in Figure 5.3.

The titration curves were fitted using the relationship

$$y = \frac{a + b \cdot 10^{pH-pK_a}}{10^{pH-pK_a} + 1}. \tag{5.1}$$

The dependent variable y is the concentration of the compound of interest, here interpreted as the absorbance, and a and b are its asymptotic minimum and maximum positions. The pK_a of chlorophenol red was determined to be 6.1. It was hoped that the indicator would prove useful in studying the PO reaction at pH 6.0, by following the absorbance at 572 nm, however, initial studies of its effect on a working oscillator were not favourable. Little oxidation of NADH was observed when 25 μM CR was present at the start of an oscillatory run, and a control experiment without CR but with identical PO conditions yielded damped oscillations using the same NADH influx rate (1.6 mM/h). Time-series data from both experiments are shown in Figure 5.4. Furthermore, a pulse of CR added during the course of a reaction caused oscillations to cease immediately, as evidenced by the data in Figure 5.5. Similar experiments to those just described were performed using Methyl Red. Figure 5.6 displays time courses of an oscillatory run to which an addition of 25 μM of this indicator was made, resulting in a return to oxygen equilibrium. Unlike the case of CR, oxygen depletion was no longer apparent after the addition (compare with Figure 5.5).

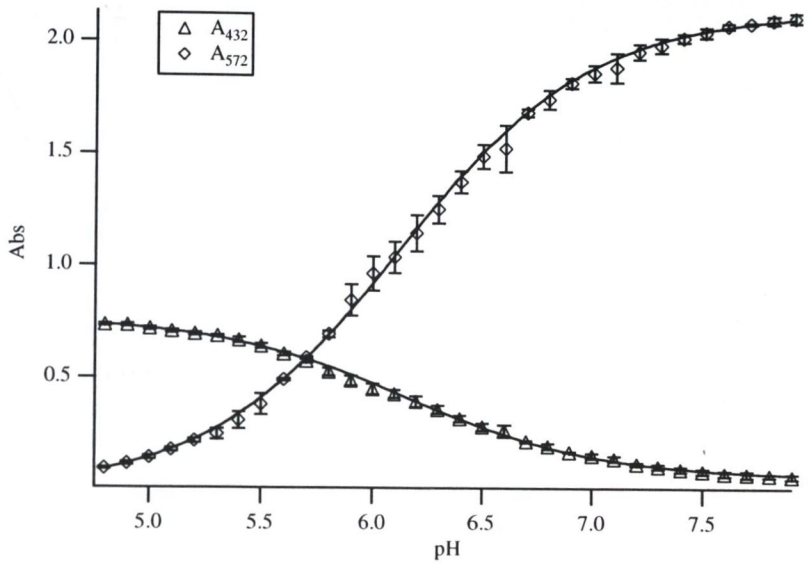

Figure 5.3: Titration curves of chlorophenol red.

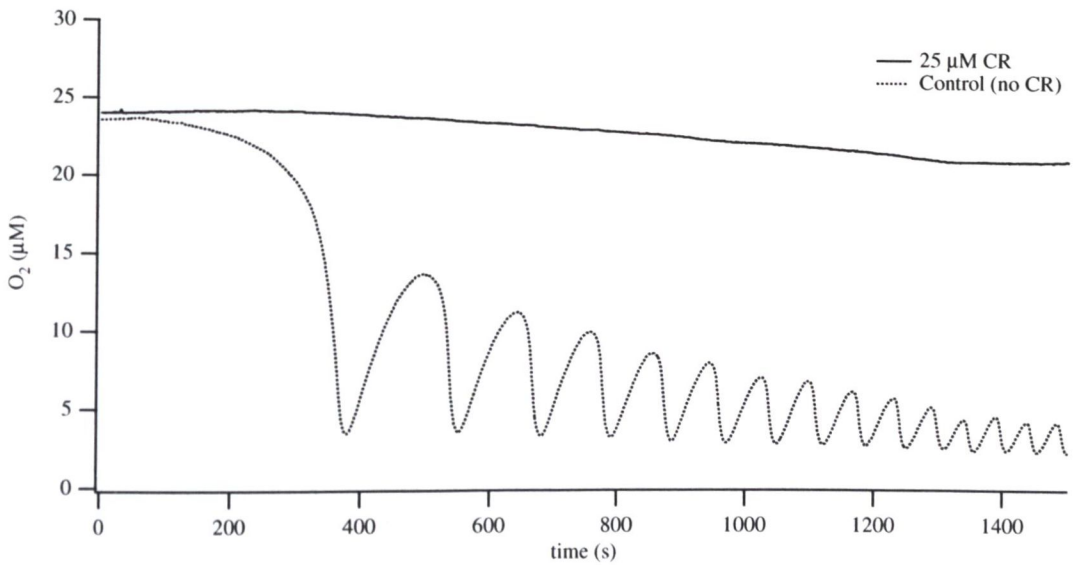

Figure 5.4: Effect of chlorophenol red on the PO reaction. Solid trace: horseradish peroxidase (35 U/ml), 0.2 μM methylene blue, 20 μM 2,4-dichlorophenol and 25 μM chlorophenol red were dissolved in 0.1 M sodium acetate buffer at pH 5.1 and 25 °C; 2% oxygen was bubbled at 20 ml/min and NADH (80 mM) was pumped at 1.6 mM/h. The solution volume was 2.0 ml. Dotted trace: control experiment, which used the same conditions but omitted CR.

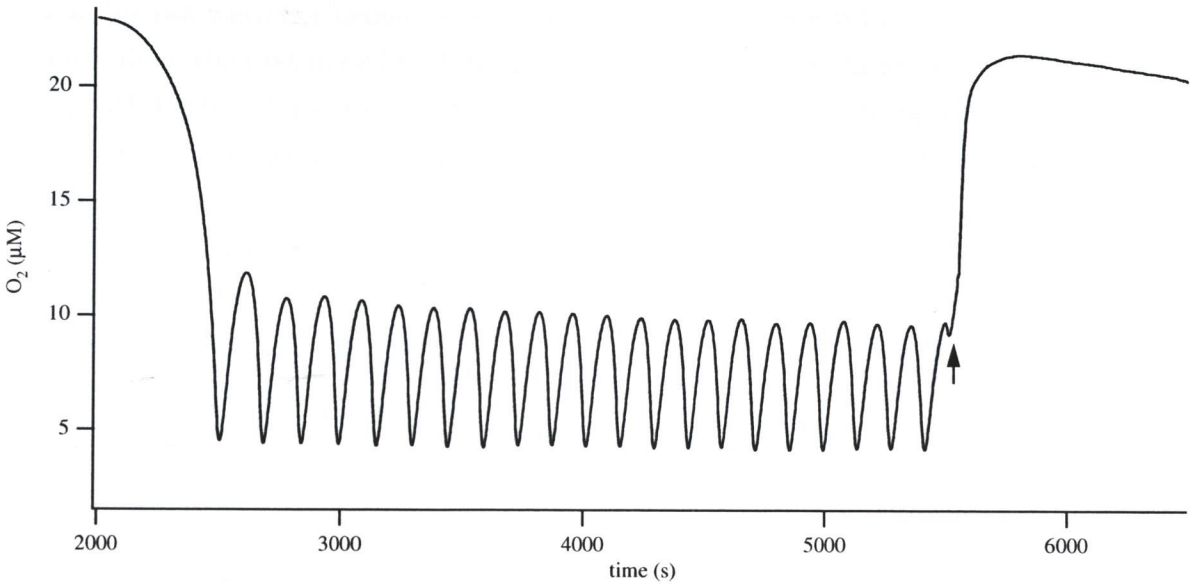

Figure 5.5: Effect of chlorophenol red pulse. 25 μM chlorophenol red were added as a pulse at the time indicated by the arrow to a working oscillator. All experimental conditions were those of Table 2.1, except for the temperature, which was 29°C.

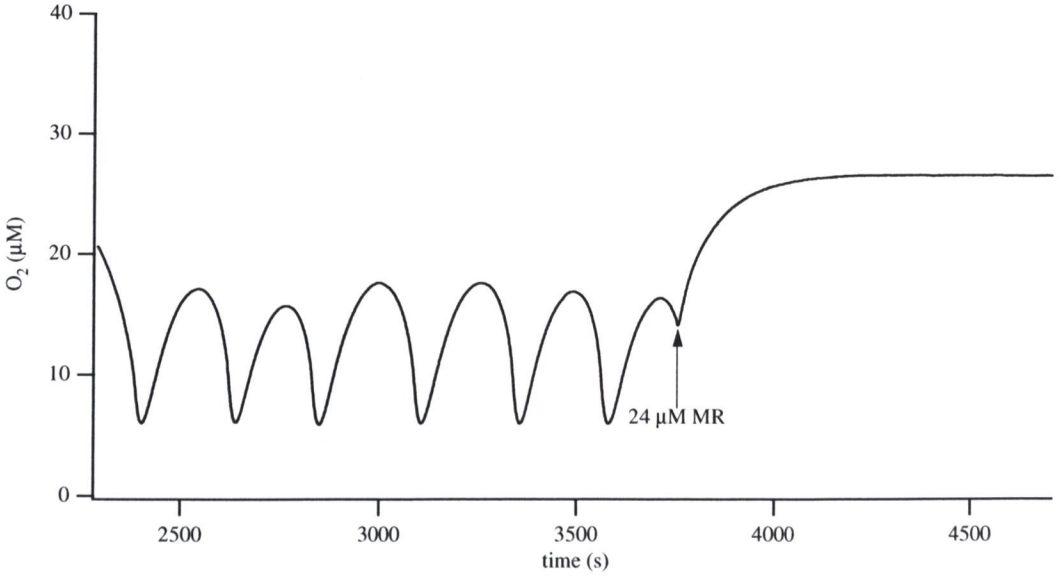

Figure 5.6: Effect of methyl red pulse. 24 μM methyl red were added to a working oscillator at the time indicated. Experimental conditions were those of the standard set.

5.3.2 Variation of pH

Experiments were performed at pH values ranging from 4.0 to 7.5. Two series were undertaken, the first in order of ascending pH using 0.1 M potassium phosphate buffer from pH 4.5 to 7.5 in steps of 0.5 pH units, and the second using 0.1 M sodium acetate buffer in descending order, from pH 6.0 to 4.0. The ordering was chosen so as to eliminate the effect of changes in the stock enzyme preparation that might have taken place during the course of each series. In each of the experiments of the first series, the following conditions applied: 40 U/ml of horseradish peroxidase, 20 μM 2,4-dichlorophenol, 0.2 μM methylene blue were dissolved in 0.1 M potassium phosphate buffer at the requisite pH. The solution volume was 2.0 ml. The concentration of NADH stock was 80 mM in 0.01 M phosphate at pH 7.0, initially infused into the reaction mixture at 1.6 mM/h. The temperature of the reaction medium was 25°C. A 2% oxygen/nitrogen gas mixture was bubbled into the enzyme solution at a flow rate of 20 ml/min. The second series was similar to the first, the only change being the buffer type. Figures 5.7 and 5.8 show the data that were obtained at each pH. The oscillations in dissolved oxygen at pH 5.0 in phosphate buffer are in appearance sharper than the data obtained at any other pH in that series. Above this value a more rounded character becomes increasingly prevalent, accompanied by an increase in period, though with little change in amplitude. Only a single oscillation was discernible at neutral pH, and no oscillations were obtained at pH 7.5. Where oscillations did appear they were found to be stable for over one hour in every case.

The series in which sodium acetate buffer was used is shown in Figure 5.8. In the case of pH 4.0, oscillations damped spontaneously after an hour to a steady-state oxygen concentration of 7.7 μM. The trend of the companion series is also in evidence, where the oscillation period increases with increasing pH, and the peaks become more rounded. Again, the dynamics are most stable at pH 5.0.

5.4 Ionic strength

The concentration of buffer was varied in order to test the PO reaction at different ionic strengths. The investigation was prompted in part by the possibility that the addition of compounds to a working oscillator might influence the dynamics by changing the ionic strength of the reaction medium, and also because the ionic strength varied throughout the pH studies. The chosen buffer was potassium phosphate, which has been used on a number of occasions in the study of the oscillator (see Table 4.1 for examples). Other than the buffer type and concentration, all other experimental

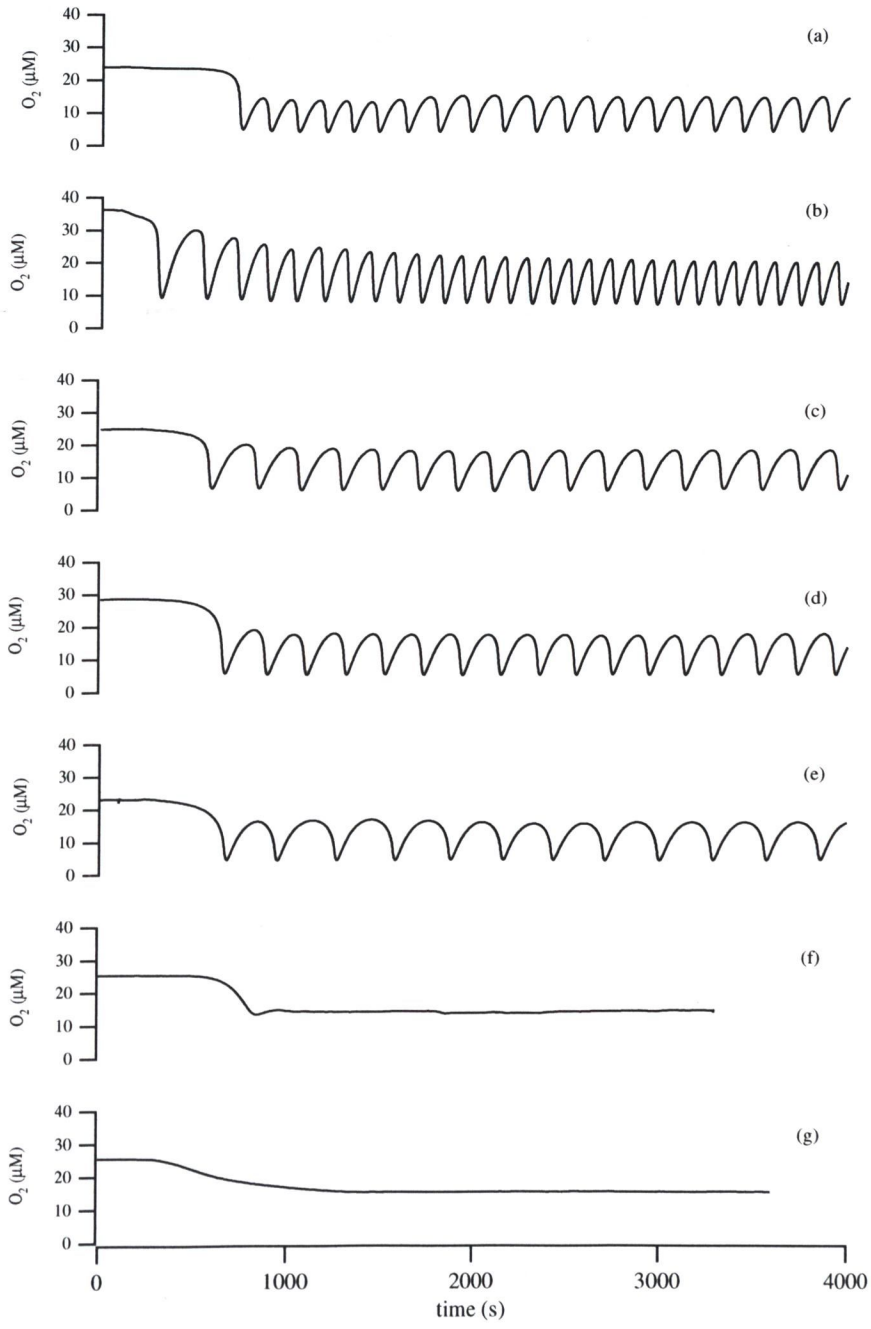

Figure 5.7: Variation of pH using potassium phosphate buffer. The pH of the buffers increased in steps of 0.5 pH units. (a)–(g): pH 4.5 - pH 7.5. Other parameters were those described in the text. Zero time has been chosen as the time at which NADH infusion commenced.

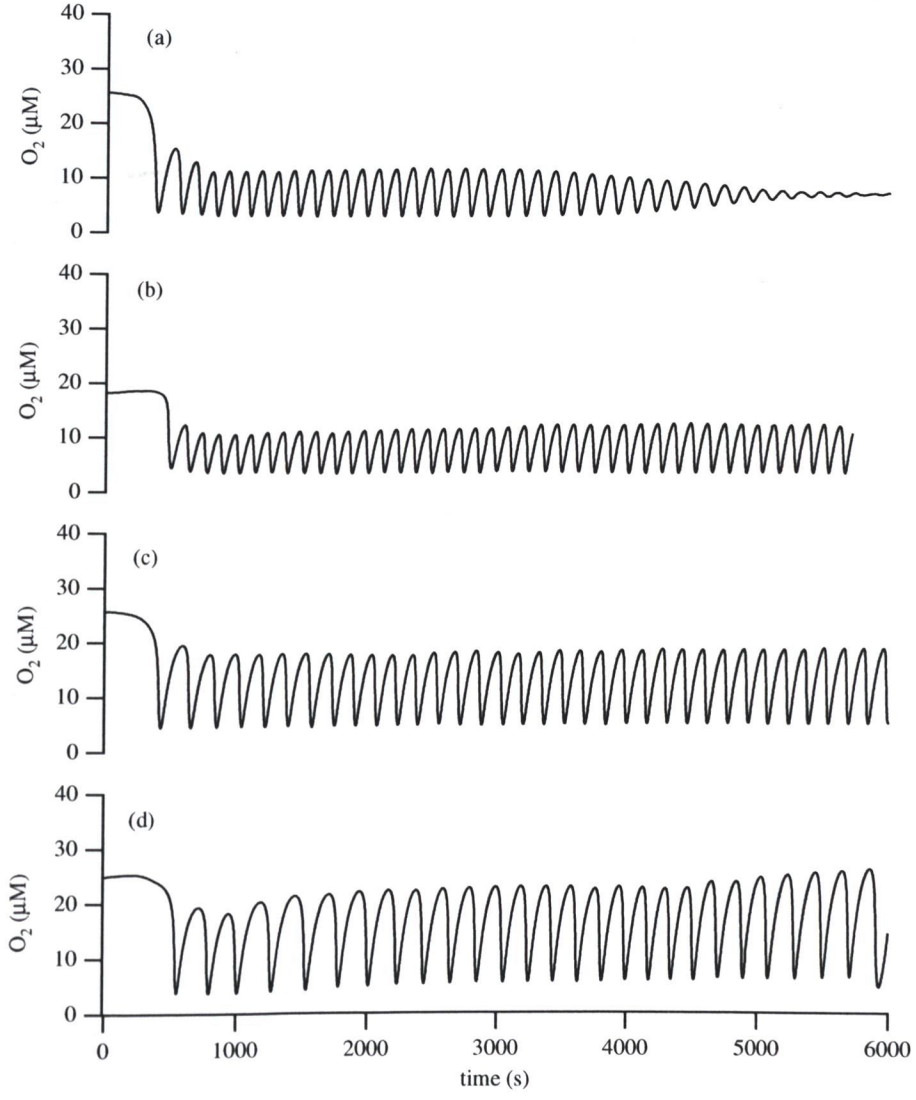

Figure 5.8: Variation of pH using sodium acetate buffer. The pH of the buffers were: (*a*) 4.0; (*b*) 4.5; (c) 5.0; (*d*) 5.5. Other parameters were those described in the text. Zero time has been chosen as the time at which NADH infusion commenced.

conditions were those of the standard set (Table 2.1).

The ionic strength of a solution may be calculated from the expression [63]:

$$I = \frac{1}{2}\sum_i z_i^2 c_i, \tag{5.2}$$

where I is the ionic strength (sometimes denoted $\Gamma/2$), z_i is the charge on ionic species i, and c_i is its concentration. A series of experiments were performed using potassium phosphate buffer at pH 5.1 at the concentrations 0.02, 0.08, 0.16 and 0.2 M; the results are collected in Figure 5.9. Since the concentrations of phosphate species greatly exceed that of any other component of the standard reagent profile, they will dominate the expression for the ionic strength. The acid and base forms of potassium phosphate are KH_2PO_4 and K_2HPO_4, and in the present case Equation 5.2 simplifies to

$$I = [KH_2PO_4] + 3[K_2HPO_4].$$

From the Henderson-Hasselbalch equation, $pH = pK_a + \log\frac{[base]}{[acid]}$, and taking the pK_a to be 6.82 [64], it can be seen that the ionic strengths are very close to the values of the buffer concentrations. The data show that the PO reaction is favoured by ionic strengths lower than 0.16 M, and this observation is borne out by the work performed in this laboratory, which was typically conducted using 0.1 M phosphate or acetate buffers. The degree of NADH-oxidation declines only very slightly as I increases from 0.16 to 0.2 M, as measured by the percentage decrease in dissolved oxygen concentration over a fixed time interval and with constant NADH influx rate. The time interval so chosen was that at which the absorbance at 360 nm reached 1.3, by which time aqueous oxygen levels had declined by 2.24% at $I = 0.2$ M and by 2.45% at $I = 0.16$ M, although it is doubtful if the difference is statistically significant, since noise in the oxygen traces might account for much of the disparity. The data at $I = 0.08$ M show an increase in the time before oscillations appeared over the case of lowest ionic strength, and the steady-state level of NADH was consequently higher throughout the experiment, as was the influx rate. Oscillations were sustainable at an influx rate of 1.0 mM/h at $I = 0.02$ M for a little over three and a half hours, one of the longest trains of oscillations observed in this laboratory. The oscillations spontaneously ceased, with the dissolved oxygen concentration returning to equilibrium. The oscillations at the lowest ionic strength were larger than those of the next in the series, the ratio of their periods being 4:5.

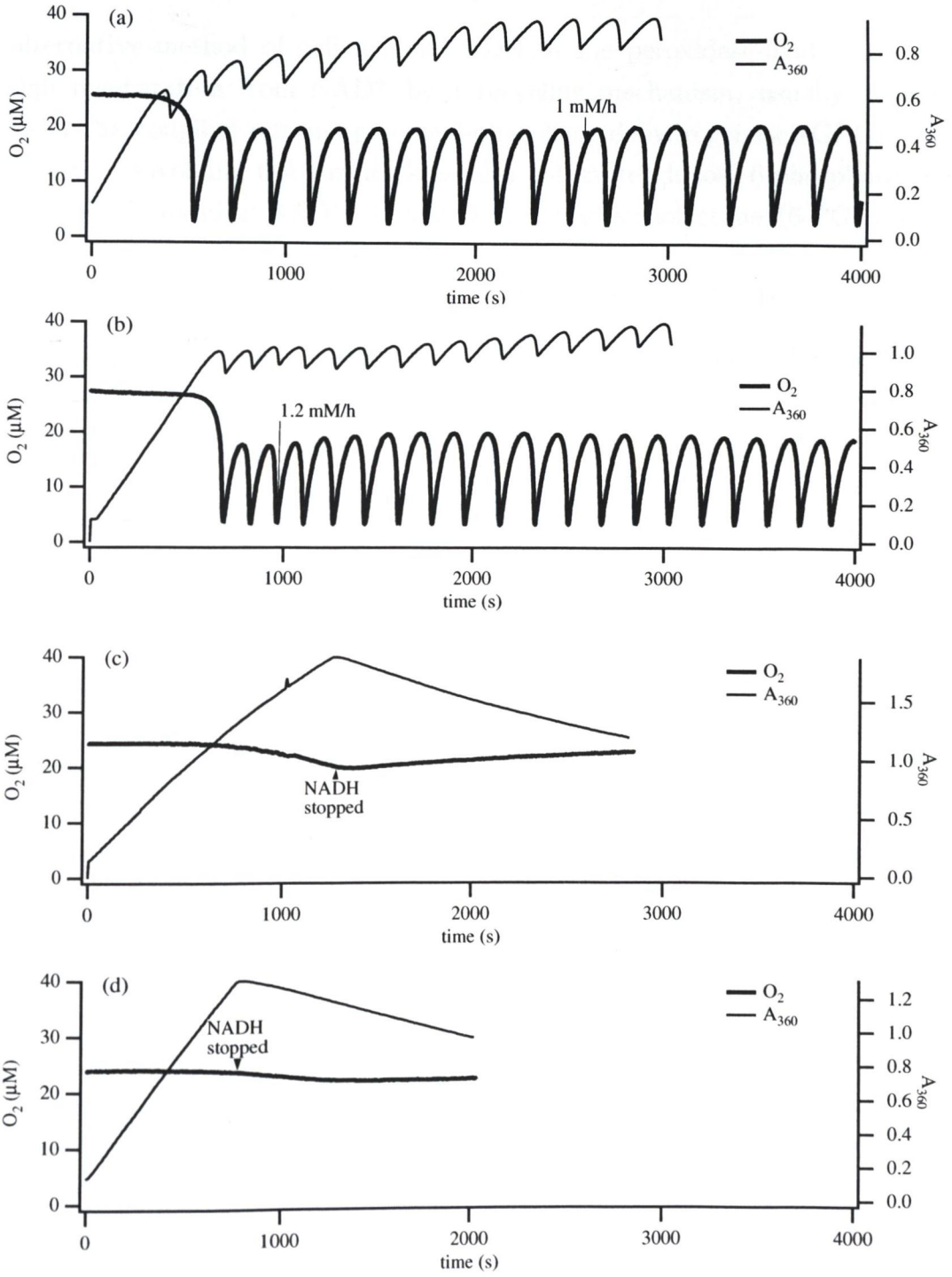

Figure 5.9: Ionic strength effects. Four experiments were performed at standard conditions using potassium phosphate buffer. (*a*) $I = 0.02$ M; (*b*) $I = 0.08$ M; (c) $I = 0.16$ M; (*d*) $I = 0.20$ M. NADH influx rates were changed at the times indicated on each graph. Zero time has been chosen as the time at which NADH infusion was started.

5.5 A coupled enzyme system

An alternative method of delivery of NADH to the peroxidase-oxidase reaction is through regeneration from NAD^+ by a recycling mechanism, usually effected by means of the coupling enzyme glucose-6-phosphate dehydrogenase (GPD) [41, 27], in a reaction involving the enzyme's natural substrate glucose-6-phosphate (G6P), and $NAD(P)^+$, forming NAD(P)H and 6-phosphogluconolactone (6-PGL) as products:

$$\text{G6P} + \text{NAD(P)}^+ \xrightarrow{\text{GPD}} \text{6-PGL} + \text{NAD(P)H} + \text{H}^+$$

An attempt was made to reproduce the conditions of Hauck and Schneider [41], and in preparation for this the influence of G6P on the peroxidase-oxidase reaction was examined, since the concentration of this species was second only to the buffer in that study. A control experiment was first performed using standard conditions, except that pH 4.8 potassium phosphate buffer replaced sodium acetate/acetic acid at pH 5.1 (refer to Table 2.1). A second experiment was done with G6P present at a concentration of 25 mM, the value used in the Hauck and Schneider paper. The two sets of results so obtained are compared in Figures 5.11 and 5.10. The concentration of G6P stock was 250 mM and its pH was determined to be 6.7. Since this may have altered the pH of the PO oscillator medium, the experiment was repeated with a glucose-6-phosphate stock that was pH-adjusted to 4.8 with 5 M HCl before being diluted 10-fold in the PO reaction mixture. Strongly damped oscillations were observed, and their late arrival after the start of NADH infusion accounts for the high concentration of NADH. The pH of the reactor contents was 4.8 before, and 5.0 after the addition of 25 mM G6P. A further replication of the experiment was made, and the results showed a period of sustained oscillations when in the presence of G6P, followed by a linear damping to a steady state of low oxygen concentration. The results are not conclusive, but tend not to support the assertion by Hauck and Schneider [41] that glucose-6-phosphate does not interfere with the PO reaction. As indicated above, the pH of the reaction medium can be influenced by this compound, and the combination of 0.1 M potassium phosphate and 25 mM G6P would increase the ionic strength from 0.1 to 0.175 M. Interestingly, this exceeds the limit at which oscillations are no longer observed (see previous section).

The coupling enzyme method was tested with NAD^+, in a batch system consisting initially of 1.5 mM NAD^+ and 25 mM G6P in 0.1 M phosphate buffer and pH 4.8. The temperature was maintained at 25°C and the stir speed was 1155 ± 69 rpm. Glucose-6-phosphate dehydrogenase had a specific activity of 305 U/mg protein, where 1 unit is defined as the amount of enzyme that will oxidise 1.0 μmol glucose-6-phosphate

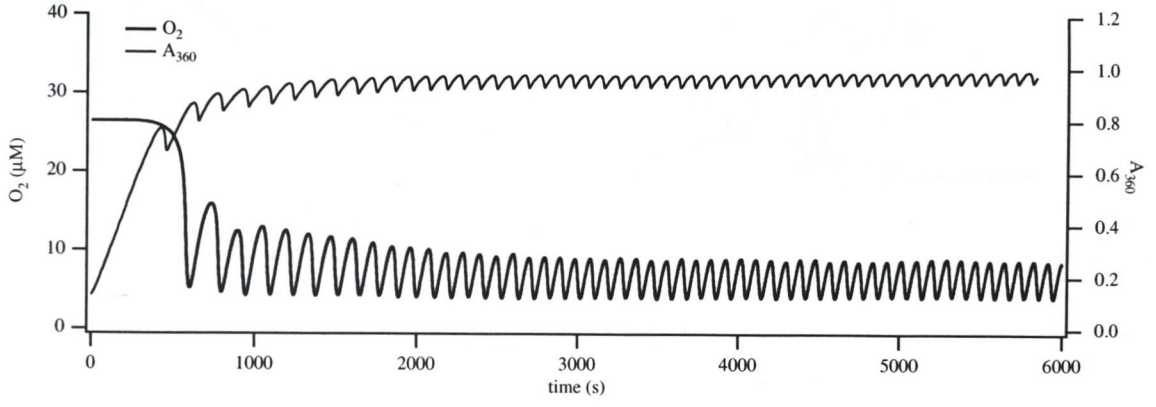

Figure 5.10: Effect of glucose-6-phosphate. Standard conditions applied, except for the buffer which was 0.1 M phosphate at pH 4.8, and the inclusion of 25 mM glucose-6-phosphate in the reaction mixture. Oscillations were smaller in size than the control experiment (Figure 5.11).

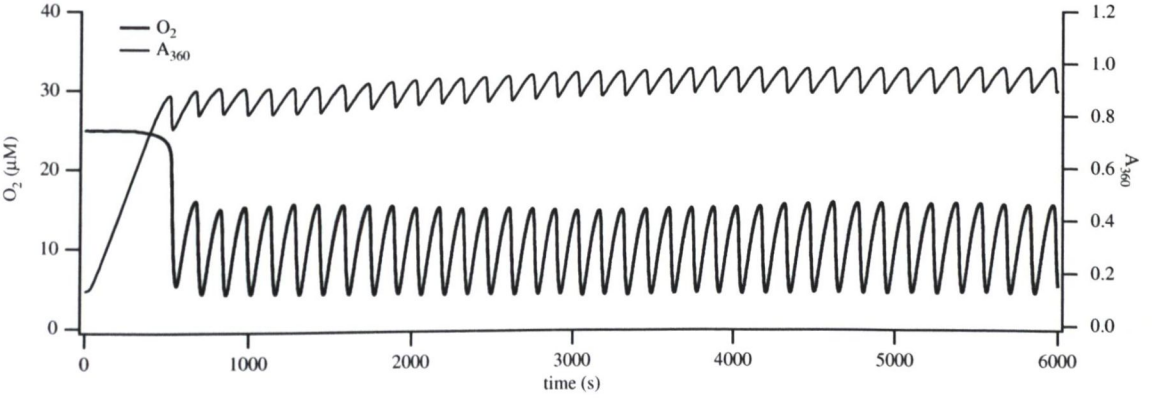

Figure 5.11: Effect of glucose-6-phosphate (control). Experimental parameters were those of Figure 5.10, with G6P omitted. Oscillations were smaller in size than the control experiment (Figure 5.11).

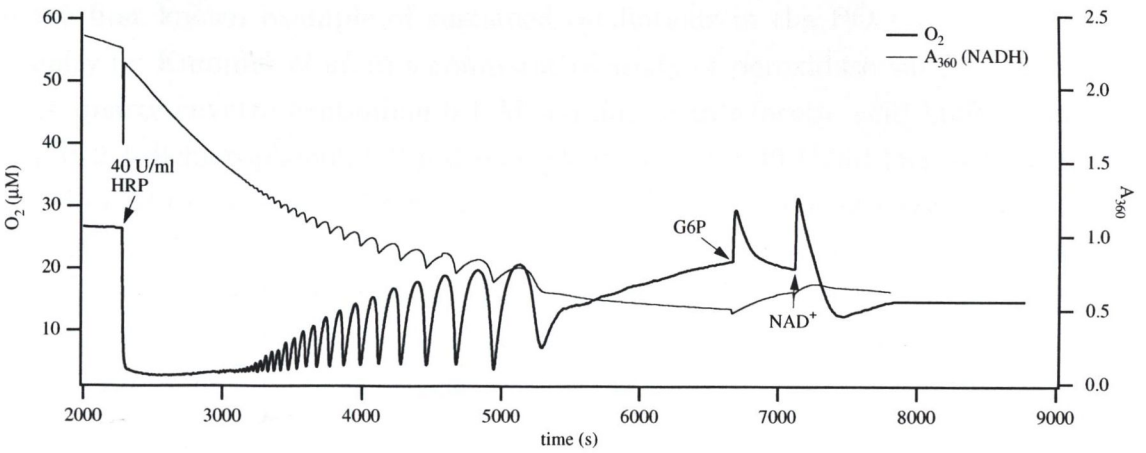

Figure 5.12: NAD^+-NADH recycling mechanism.

to 6-phosphogluconolactone per minute at pH 7.4 at 25°C, in the presence of NADP. It was assumed that the unit definition was the same as that of Hauck and Schneider. 5 U of the enzyme were added to the solution, to give a final concentration of 2.5 U/ml in a total volume of 2.0 ml. The NADH concentration, as measured spectrophotometrically at 340 nm, rose rapidly, A_{340} reaching a value of 2.0 in under two minutes. The mixture was equilibrated with a 2% O_2/N_2 gas stream, bubbled into the liquid at 20 ml/min. After equilibration, which yielded a mass-transport constant of 0.62 min^{-1}, 19 μM 2,4-dichlorophenol and 0.19 μM methylene blue were added. The peroxidase-oxidase reaction was started by the addition of 40 U/ml horseradish peroxidase, which brought the total solution volume to 2.12 ml. Oxygen and NADH time-series data are shown in Figure 5.12, from which it can be seen that dissolved oxygen levels dropped immediately to near zero and NADH concentration (A_{360}) declined gradually thereafter. Oscillations commenced through negative damping away from the low steady state position of dissolved oxygen, and were superimposed on the decay curve of NADH, which continued to decline as the amplitude of the oscillations increased. The behaviour changed to a steady state of high oxygen concentration as the NADH concentration fell below 0.15 mM. A pulse of G6P was added to increase the NADH concentration of the reactor, however, a pulse of NAD^+ had a greater effect, and oxidation recommenced temporarily.

5.6 Lactoperoxidase

The enzyme lactoperoxidase was used as a replacement for horseradish peroxidase in one study in this laboratory. This enzyme was also used by Nakamura *et al.* [27]

in the first known example of sustained oscillations in the PO reaction, and more recently by Kummer *et al.* in a comparative study of peroxidase variants [47].

A quartz cuvette containing 0.1 M sodium acetate/acetic acid buffer at pH 5.1, 20 μM 2,4-dichlorophenol, 0.2 μM methylene blue and 40 U/ml lactoperoxidase was equilibrated to 25°C in a thermostated cell holder. The unit of enzyme activity was the same as for the horseradish species [55]. The solution was stirred continuously from beneath at 1155 $\pm$ 69 rpm. The stock NADH concentration was 80 mM, dissolved in distilled, deionised water. The solution was equilibrated with a 2% O_2/N_2 gas stream, bubbled into the liquid at 20 ml/min, with a mass transport constant of 0.58 min^{-1}.

NADH infusion was started at a rate of 40 μl/h (1.6 mM/h). Oscillations began at an absorbance at 360 nm of approximately 1.5, and were sustained for around 40 minutes, the oscillations began to damp with increasing rapidity thereafter, eventually settling to a steady state of low dissolved oxygen concentration. The data are shown in Figure 5.13 and Figure 5.14 show absorbance spectra taken before and after the experiment.

The initial spectrum of lactoperoxidase has an absorbance maximum at 412 nm, which may be compared with the case of horseradish peroxidase (Figure 2.7) where the corresponding peak occurs at 402 nm.

The upper peak in the spectrum taken at the end of the experiment (the trace marked 'final' in Figure 5.14) may be partly due to the lactoperoxidase Compound III since it appears at 420 nm when the absorbance of the native enzyme is lowered. The data may be compared with those described in Section 4.2.5, and in particular, Figure 4.10 therein. Nakamura *et al.* [27] took 433 nm to be Compound III absorbance maximum, and followed the reaction at that wavelength. The authors also claimed in that paper that methylene blue promoted the decomposition of Compound III, and the concentration of that reagent was 1 μM.

The experiment on lactoperoxidase presented earlier in this section was repeated at the higher methylene blue concentration with the results shown in Figure 5.15. Oscillations damped out within 15 minutes of their commencement. The NADH influx rate was lowered slightly from 1.6 to 1.52 mM/h after 1278 s. NADH oxidation increased as the oscillations declined to a fixed point in phase space, as may be seen from the reduction in absorbance at 360 nm. The phase portrait is shown in Figure 5.16.

Two attempts were made to restart oscillations: in the first instance, NADH levels were raised to their previous maximum level and the gas stream was switched to pure nitrogen to purge the solution of oxygen, during which time some of the NADH was

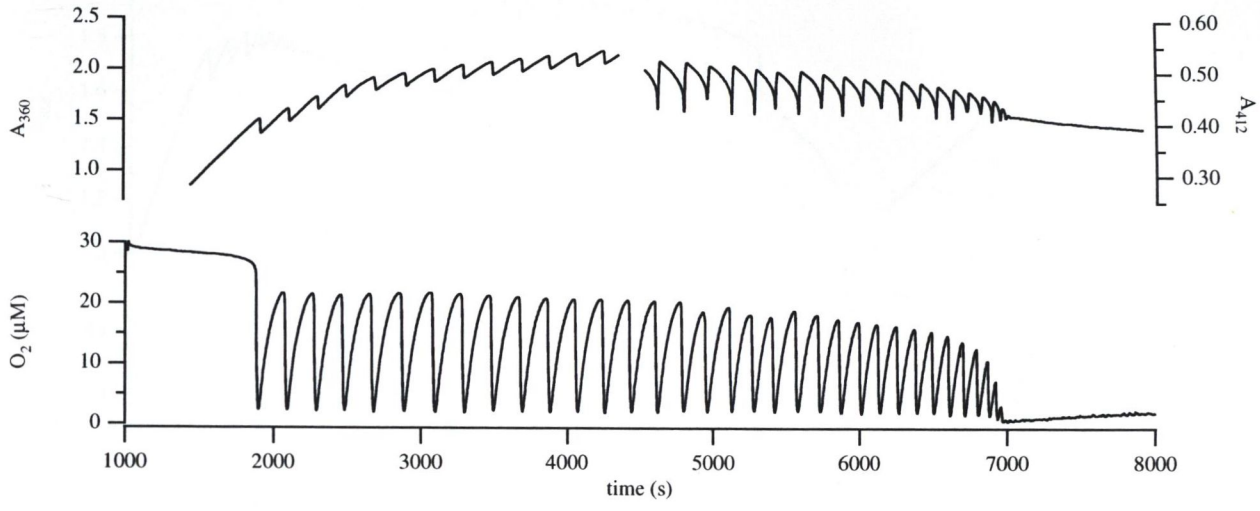

Figure 5.13: Oscillations with lactoperoxidase (1). 20 μM 2,4-dichlorophenol, 0.2 μM methylene blue and 40 U/ml lactoperoxidase were dissolved in 0.1 M sodium acetate buffer at pH 5.1. The temperature was 25°C and the stirring speed was 1155 $\pm$ 69 rpm. Total reaction mixture volume was 2.0 ml. A 2% O_2/N_2 gas mixture was bubbled into the solution at 20 ml/min. Initial NADH infusion rate was 1.6 mM/h, reduced to 1.2 mM/h and 1.12 mM/h at 2535 and 4516 seconds, respectively.

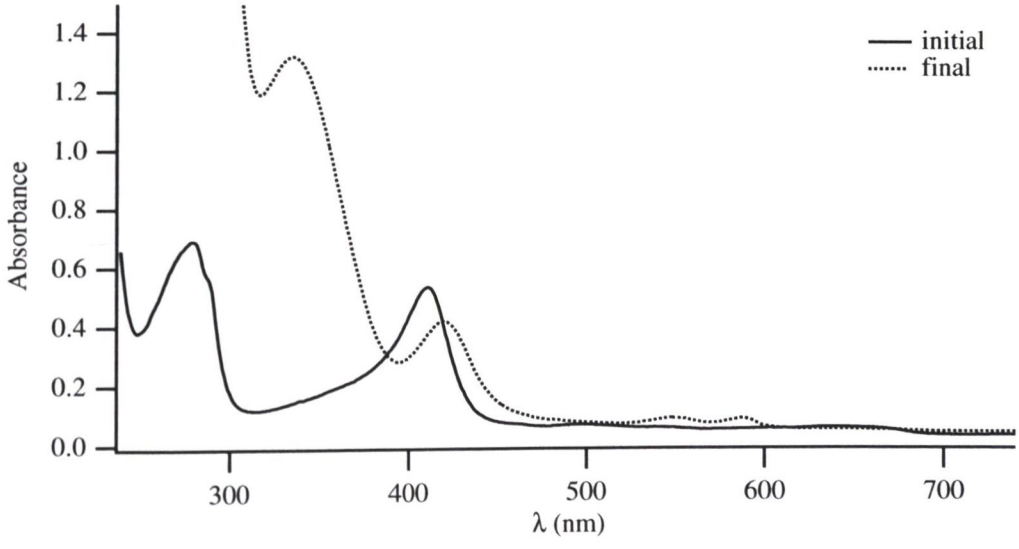

Figure 5.14: Absorbance spectra of lactoperoxidase, taken before and after the oscillatory run of Figure 5.13. In the initial trace, peaks appear at 280 and 412 nm. The peak at 420 nm in the final trace denotes a mixture of lactoperoxidase Compound III and the native enzyme.

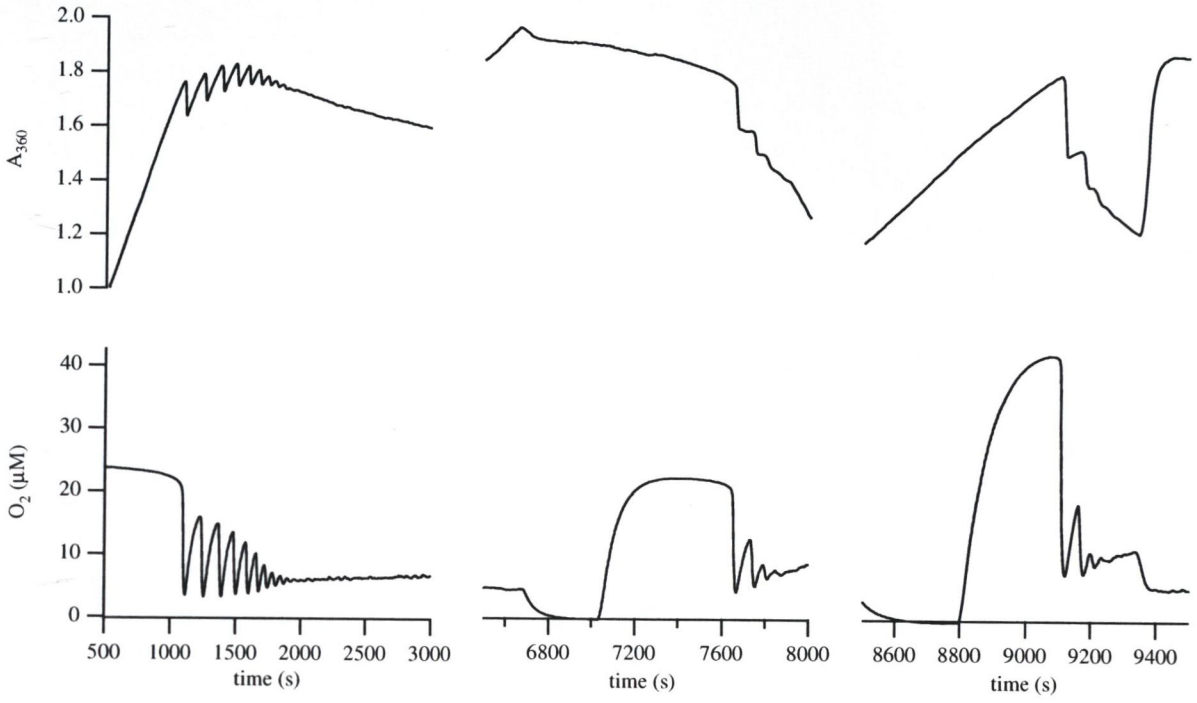

Figure 5.15: Oscillations with lactoperoxidase (2). Initial conditions were those of Figure 5.13 except that [MB] = 1 μM.

consumed (see central graphs in Figure 5.15; the NADH influx rate was increased to 2.0 mM/h, and shortly after, at around 7000 s, 2% oxygen was reintroduced at the same flow rate as before. Oscillations recommenced after oxygen equilibration, though they displayed stronger damping. The NADH oxidation rate was considerably higher, since even at the higher infusion rate, the A_{360} dropped from 1.93 to 1.62 during this period, a decline of 31%. The final set of data in Figure 5.15 shows a repeat of this last procedure, only with a final oxygen composition of 4%, and in this case the pattern of the results was similar.

5.7 Discussion

The fact that the pH indicators studied in this work have been shown to be inhibitors of the PO reaction serves to underline the importance of testing additives to the standard reagent profile, giving particular attention to their possible effect on the dynamics of NADH oxidation. The titration curves of methyl red were not attempted once a pattern of inhibition of the oscillator had begun to emerge. The mechanism of inhibition is unknown, but quenching of the free radical reactions that are implicated in the mechanism cannot be ruled out (see Chapter 6). A more costly, but chemically

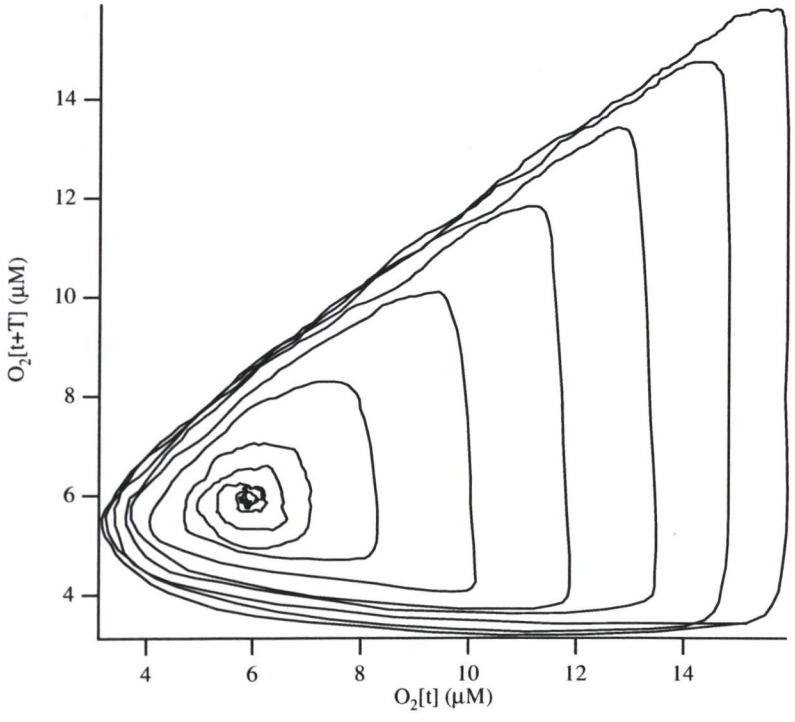

Figure 5.16: Phase plot of lactoperoxidase oscillations showing, by means of a reconstructed attractor using the oxygen data of Figure 5.15 with delay time, $T = 15s$, the damping of oscillations towards a fixed point at 6 μM.

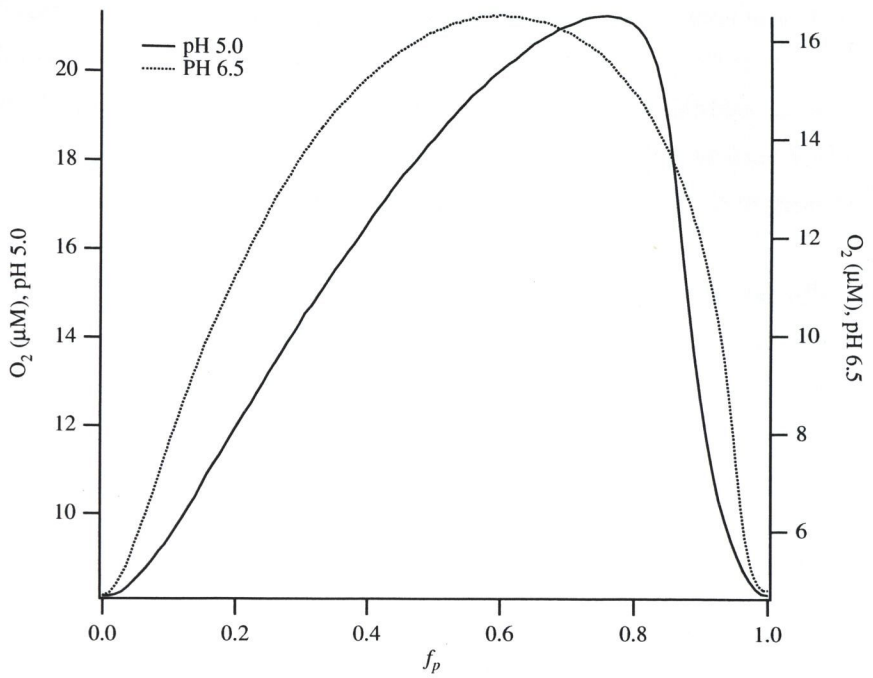

Figure 5.17: Comparison of oscillation shapes. Single oscillations, extracted from the data in Figure 5.7 at pH 5.0 and 6.5, are plotted on the same abscissa for direct comparison. The data from the pH 5.0 trace show a sharper character of oscillation. Those data obtained at pH 6.5 have a round-topped appearance and display a tendency to symmetry about a vertical axis drawn through the peak.

less invasive approach would be the use of a dedicated pH microelectrode, and this may be the direction for future work in this area.

These studies have shown that lower ionic strengths and pH values favour oscillatory oxidation of NADH catalysed by horseradish peroxidase. The manner in which pH affects the type of oscillations is evident from an examination of the individual traces in Figures 5.7 and 5.8, where one of the prominent features is the sharpness of the oscillation peaks. Oscillations had sharpest peaks at pH 5.0 in phosphate buffer, with a progressively more rounded appearance at higher pH values as well as at the lower pH of 4.5. Though perhaps less markedly, the trend is also evident in the sodium acetate buffer traces. Individual oscillations in dissolved oxygen from the data sets at pH 5.0 and 6.5 are shown for comparison in Figure 5.17. The time axes have been normalised to make comparison easier; the abscissa of the graph is the fractional period of the oscillation, denoted f_p. Both oscillations were selected from their respective data sets at approximately 3000 seconds from the start of NADH infusion. The length of the actual period of the pH 5.0 oscillation was 37% of that of

the pH 6.5 data, and the amplitude of the pH 5.0 oscillation was slightly higher than the pH 6.5 oscillation in this region.

In general, sharper oscillations were found to be an indication of stability of the oscillatory mode, and a tendency towards symmetrical appearance indicated to the contrary, or at least that the system was closer to steady state region of parameter space than otherwise.

Increasing the ionic strength has been shown to have an adverse effect on the PO reaction. The experiment described in Section 5.4 was performed over two consecutive days using the same reagent stocks, and not in linear order, which would seem to preclude the possibility of any deterioration of either enzyme or some other reagent as being responsible for the change in behaviour. Further experiments could be performed to extend this work. The ionic strength could be changed by means of a salt such as KCl, at a fixed buffer concentration of, for example, 0.05 M; the pH variation study might be repeated at different ionic strengths; and the region of pH between 6.5 and 7.0 explored for evidence of damped behaviour, which would confirm the presence of a subcritical Hopf bifurcation.

Although sustained oscillations were not obtained using the coupling enzyme method, the results could be viewed as a qualified success, given the fact that the only mass transfer was due to dioxygen gas, and therefore the auxiliary reagents glucose-6-phosphate and NAD^+ could become rate limiting. One experiment that has yet to be attempted with the present apparatus is that wherein the substrates of the glucose-6-phosphate dehydrogenase reaction are fed into the reaction medium continuously, which would affirm or negate the hypothesis that either one of these species caused the cessation of the reaction depicted in Figure 5.12. An preferable scenario is one where all reacting species and their catalysts are infused continuously, and removed as products are formed, effectively a continuously-stirred tank reactor (CSTR). This was the approach taken by Hauck and Schneider in their 1993 paper [41], where both the subtrates and the enzymes were continuously supplied to the stirred reaction medium, and the excess liquid drained passively through an overflow hole in the side of the vessel. As was noted in Section 3.5, the total volume decrease through water evaporation was roughly balanced by the increase due to NADH infusion in experiments using the semi-batch method in this laboratory. Little or no consideration has been given to the phenomenon of evaporation in published accounts of this oscillator, and questions can be raised as to the method of volume preservation, which is seldom stated.

Whether the glucose-6-phosphate concentration has any significant effect on the viability of oscillations remains to be verified, and a repetition of those experiments

would be a valuable exercise, in particular since the results of Section 5.4 demonstrate inhibition of oscillations at $I = 0.16$ M, and under otherwise standard conditions. The metastable nature of the reaction may well be contributing to the apparent contradiction however.

As with so many of the exotic behaviours reported in the literature, in which are included the mixed-mode oscillations of Hauck and Schneider and the period-doubling bifurcations of Geest, *et al.*, their replication in this laboratory was unsuccessful. This was due in part due to insufficient information being supplied, but occasionally, as in the case of the Hauck and Schneider work, one or other parameter was outside the range of values attainable with the present apparatus. In particular, for proper replication of the Hauck and Schneider conditions, a gas stream of oxygen composition 15-17% was needed. This condition could be met by the use of a gas cylinder of higher oxygen composition, and this merits further study.

Finally, the use of lactoperoxidase in place of that from horseradish has demonstrated that peroxidases from entirely disparate species are capable of displaying oscillatory NADH-oxidase activity. This work could be extended by means of the spectral time-series method described in Section 4.2.5, which could be used to follow the different enzyme forms throughout an experiment. One other haem-peroxidase that has not, to the author's knowledge, yet been studied for NADH-oxidase activity is the cytochrome *c* peroxidase variety from yeast. Since the mechanism of peroxidative activity appears to be very similar to the horseradish type there is a possibility that this too will exhibit oscillations of the kind hitherto described in this volume.

Chapter 6

Of Phenols and Free Radicals

6.1 Introduction

This chapter deals with the effects of various phenolic compounds on the peroxidase-oxidase oscillator, and provides indirect experimental evidences for the involvement of free radicals in the reaction mechanism. The phenol 2,4-dichlorophenol has been frequently used as a stabilising additive to the PO reaction, often in conjunction with the electron acceptor methylene blue. The mechanisms of action of both these compounds are still unclear at the time of writing, but two recent papers have been published which deal with this issue; the first, by Hauser and Olsen [1], investigated the use of naturally-occurring phenols other than 2,4-dichlorophenol in the PO reaction, and attempted to relate higher electrochemical potentials of phenolic free radicals with better performances as inducers of oscillations. The second, by Olson and Scheeline [62], examined the role of methylene blue. Both 2,4-dichlorophenol and methylene blue have been implicated in prolonging or stabilising oscillatory behaviour of the reaction, and in this chapter the effects of 2,4-dichlorophenol, 2.6-dichlorophenol, tyramine and an analogue of tyramine, 4-aminophenol, will be examined in this regard. Free radicals are thought to play an active role in the mechanism of peroxidase-catalysed NADH-oxidation, and this was investigated through the use of free radical scavengers, such as superoxide dismutase (SOD) and ascorbic acid. A parenthetic section has been included to discuss results that were obtained for an attempted repetition of one of Hauser and Olsen's published experiments [1] using their method of initiation of oscillations.

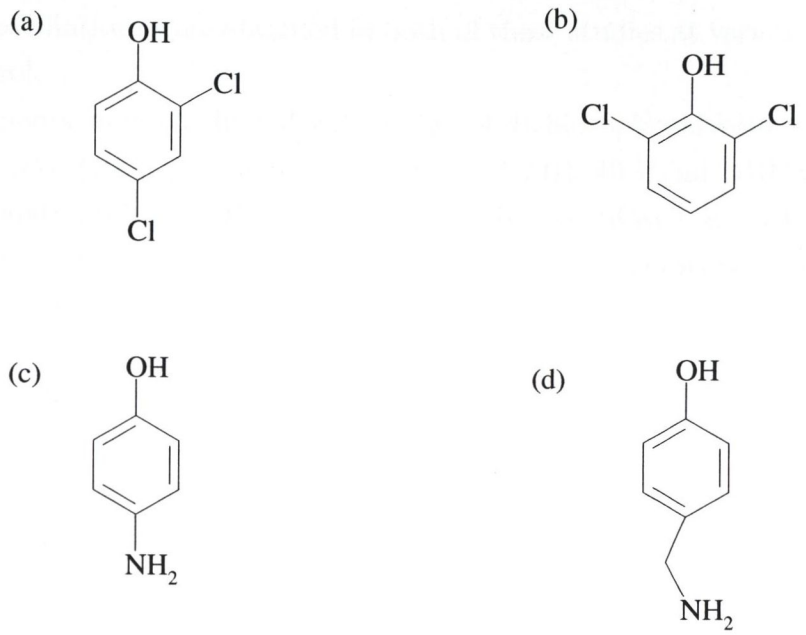

Figure 6.1: Chemical structures of phenolic compounds. (a) 2,4-dichlorophenol; (b) 2,6-dichlorophenol; (c) 4-aminophenol; (d) 4-[2-aminoethyl]phenol (tyramine).

6.2 Reagents

Tyramine (4-[2-aminoethyl]phenol), 2,6-dichlorophenol and L-ascorbic acid were purchased from Sigma. 4-aminophenol was purchased from Aldrich. Superoxide dismutase (EC 1.15.1.1), purified from bovine erythrocytes, was purchased from Sigma as a lyophilised powder. The chemical structures of the phenolic compounds used are drawn in Figure 6.1.

6.3 Variation of [2,4-dichlorophenol]

The experiments in this section were prompted by the observation on two separate occasions of the inhibition of oscillations when 2,4-dichlorophenol and methylene blue were present at concentrations of, respectively, 50 μM and 1 μM. All of the experiments in this study of inter-experimental variation of 2,4-dichlorophenol concentration were conducted with 0.2 μM methylene blue present in the reaction mixture. This compound, shown in Section 4.7 to be a promoter of sustained oscillations at a concentration of 0.1 μM, and elsewhere at 0.2 μM, was also used by Geest *et al.* [38] in their study of period-doubling bifurcations arising from [2,4-dichlorophenol] varia-

tion, though omitted by Watanabe and Inaba in their chemiluminescence studies [44]. Sustained oscillations were obtained in both of these studies at various concentrations of the phenol.

Experiments were conducted with final 2,4-dichlorophenol concentrations in the range 0–50 μM. Other parameters were: 0.2 μM MB, 40 U/ml HRP in 0.1 M potassium phosphate buffer at pH 4.8; 80 mM NADH was infused at 1.44–1.6 mM/h into the reaction mixture of total volume 2.0 ml. The temperature was 25°C and the solution was stirred at 1155 $\pm$ 69 rpm. Figure 6.2 shows the results of five oscillatory runs at different concentrations of 2,4-DCP. In the absence of the phenol, oscillations were seen to damp out under conditions of balanced NADH influx and degradation rates.

At the point indicated by the arrow in sub-figure (a), a small aliquot of 2,4-dichlorophenol (5 μl of a 2 mM stock dissolved in buffer) was added to the reaction mixture to give a final concentration of 5 μM. The effect was to immediately restart oscillations, which thereafter settled to a steady-state of approximately 10 μM amplitude in aqueous oxygen. In the same figure are plotted representative oxygen and compound III (A_{418}) data from the steady state regions of each data set. The amplitudes appear to increase as the concentration of the phenol was raised, although a decline was observed at the highest value of 50 μM. The wavelengths of individual oscillations varied in the same manner. Clearly, concentrations of 2,4-DCP higher than the standard value of 20 μM do not inhibit oscillations in the reaction, and as little as 5 μM is sufficient to promote stable oscillations in the presence of 0.2 μM methylene blue. None of the dynamics that were observed during this study resembled the period-doubling behaviour reported by Geest *et al.* [38].

6.3.1 2,6-dichlorophenol

In the first of two experiments testing the effect of substituting 2,6-dichlorophenol for 2,4-dichlorophenol standard conditions were used, the only deviation being the phenol type, resulted in non-oscillatory NADH oxidation. In a second experiment 2,4-dichlorophenol was again omitted, and strongly damped oscillations were seen. A pulse of 2,6-DCP was made to give a final concentration of 20 μM, and this immediately transferred the system into an oscillatory mode. The data for this second experiment are shown in Figure 6.3. The strong damping apparent in the first portion of the data was typical of a run in the absence of the phenolic compound. The rate of attainment of a non-oscillatory steady state is much faster than for the corresponding experiment in the previous section where the buffer and pH were different

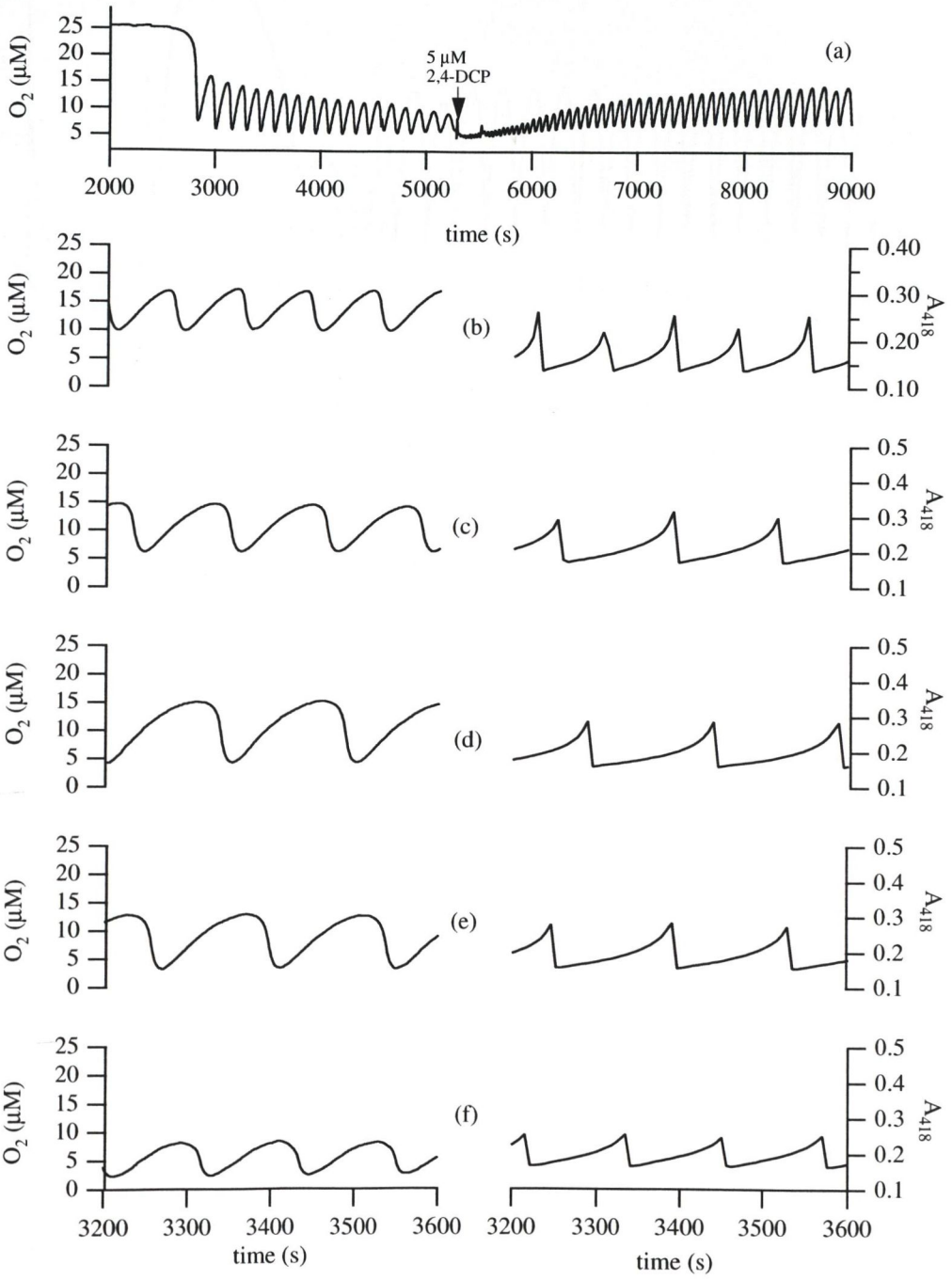

Figure 6.2: Variation of 2,4-dichlorophenol concentration showing time-series data of dissolved oxygen (left-hand axes) and absorbance of CoIII at 418 nm (right-hand axes). The concentrations were (a) 0, 5 μM, (b) 10 μM, (c) 20 μM, (d) 30 μM, (e) 40 μM, (f) 50 μM. Other experimental parameters are given in the text (Section 6.3). In (a), 5 μM 2,4-DCP were added at the time indicated by the arrow.

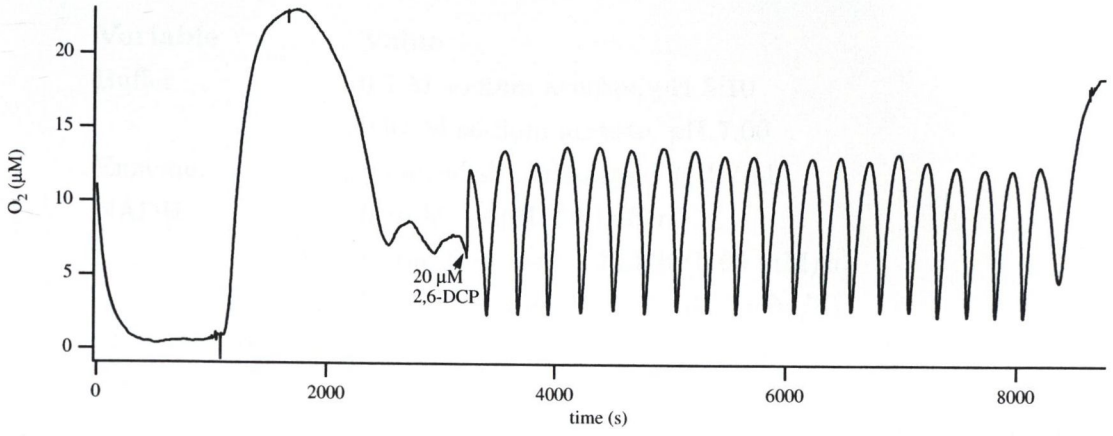

Figure 6.3: Addition of a 20 μM 2,6-DCP pulse to a PO reaction system containing no 2,4-DCP at start. Conditions were otherwise those of the standard set (Table 2.1).

(Figure 6.2(a)).

6.3.2 Initiation of oscillations

The usual method of initiation of the peroxidase-reaction was that described in Chapter 2, Section 2.3.3, where NADH delivery was started after the reaction mixture had equilibrated with the oxygen/nitrogen gas stream. In the method used by Hauser and Olsen [1], the solution of peroxidase enzyme and other reagents was first equilibrated with a pure nitrogen gas stream, then NADH infusion commenced. After the absorbance at 360 nm had reached a value of between 0.9–1.1, the gas composition was switched to a mixture of oxygen and nitrogen and the NADH influx rate adjusted to maintain a constant average NADH concentration.

An attempt was made in this laboratory to reproduce the results published by Hauser and Olsen for one set of experimental conditions in which period-2 oscillations were obtained using 2,4-dichlorophenol as the phenolic compound. The experimental parameters are detailed in Table 6.1 and should be compared with the relevant column in Table 4.1 (where see Reference [1]). The results of the experiment are shown in Figure 6.4. In contrast with the Hauser and Olsen results, period-1, and not period-2 oscillations were obtained under these conditions. The amplitudes of the oscillations were larger than those observed by Hauser and Olsen (see Figure 2 of reference [1]), by a factor of 1.8 at comparable times from the start of each experiment (6000 s).

The following values or conditions differed between the two sets of parameters in Section 6.3.2, and are also collated in Table 6.2 for ready comparison. Hauser and Olsen used ethanol as the 2,4-dichlorophenol solvent, whereas in this work, the buffer

Variable	Value
Buffer	0.1 M sodium acetate, pH 5.10
	0.01 M sodium acetate, pH 7.00
Enzyme	horseradish peroxidase, 37 U/ml
NADH	0.10 M, in pH 7.0 buffer
	Initial flow rate: 12 μl/h (0.60 mM/h)
	Final flow rate: 11 μl/h (0.55 mM/h)
Methylene blue	0.1 μM
2,4-dichlorophenol	25 μM
Gas	Flow rate: 2.5 ml/min (O_2), 9.5 ml/min (N_2), bubbled
	Composition: 1.04% in O_2
Stir speed	1155 $\pm$ 69 rpm
Solution Volume	2.0 ml
Temperature	28°C

Table 6.1: Parameters of an experiment in which the procedure of Hauser and Olsen [1]. See text for further details.

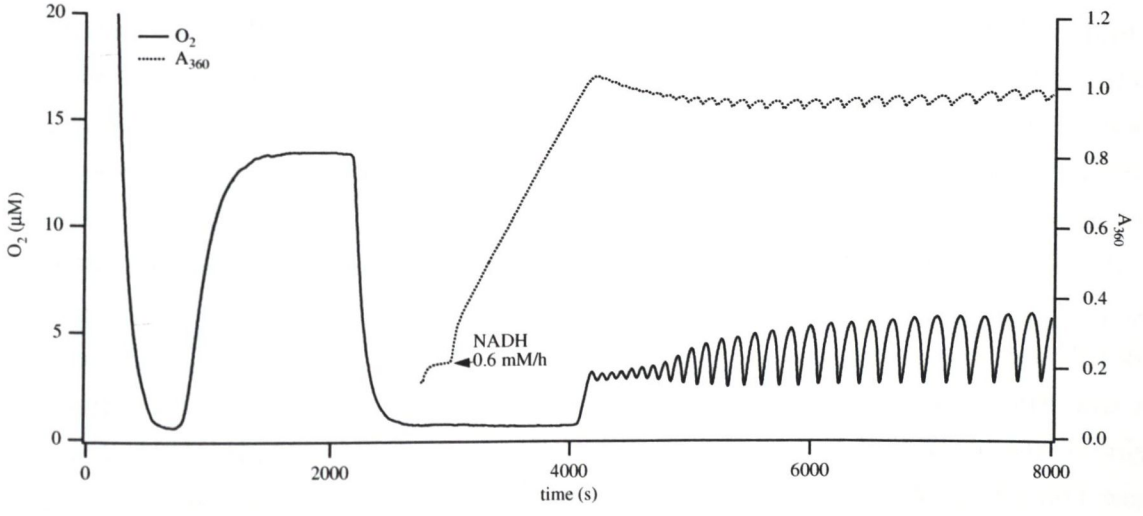

Figure 6.4: Initiation of oscillations by the method of Hauser and Olsen (see Reference [1]. A solution, of volume 2.0 ml, stirred at 1155 $\pm$ 69 rpm, containing 37 U/ml HRP, 0.1 μM MB and 25 μM 2,4-DCP in 0.1 M sodium acetate buffer at pH 5.10 was equilibrated with a pure nitrogen stream, bubbled at 12 ml/min. At 2988 s infusion of a 0.1 M solution of NADH in 0.01 M sodium acetate at pH 7.00 commenced at a rate of 0.6 mM/h. At 4050 s the gas stream was switched to a 1.04% oxygen/nitrogen mixture. After the oxygen concentration had risen to 2.8 μM, period-1 oscillations appeared in both measured components.

Variable	Value	Hauser & Olsen [1]
Peroxidase (U/ml)	37	n/a
Peroxidase (μM)	4.7	1.2–1.5
A_{418} (initial/baseline)	0.158	0.16
O_2 Composition	1.04%	1.05%
Stir speed (rpm)	1155 ± 69	1050
Solution Volume (ml)	2.0	10
k_{-t} (s^{-1})	$(6.40 \pm 0.02) \times 10^{-3}$	$(6.0 \pm 0.2) \times 10^{-3}$

Table 6.2: Detailed comparison of the Hauser and Olsen parameters with those used in the experiment of Section 6.3.2.

was used. The discrepancy, albeit a minor one, between the oxygen gas compositions was unavoidable and was owing to the limited resolution of the mass flow controller devices (Section 2.2.5). The solution volumes, gas delivery methods and stirring speeds also differed to varying degrees. The most difficult parameter to reproduce was the HRP concentration, since an activity unit was not quoted in their paper. An estimate of the enzyme concentration used in these experiments was made, based on the mass of protein weighed and the molecular weight of the horseradish peroxidase, here taken to be 40 kD [65]. This is the value that is quoted in the first column of Table 4.1, which outlines the standard set of experimental conditions. The molar absorbance coefficient of HRP at 402 nm was determined to be $6.3 \times 10^4 M^{-1} cm^{-1}$, and the value of A_{402} being equal to 0.30 at the start of the experiment, which by the Beer-Lambert Law would give a value of 4.7 μM as the concentration of the peroxidase, up four times higher than the minimum value of 1.2 μM quoted by Hauser and Olsen.

The baseline absorbance at 418 nm was close to 0.16 (as shown in Figure 2 of reference [1]), and the corresponding value obtained in this laboratory was 0.158. The buffer was used as a blank, so that the absorbance at this wavelength was a composite of the those of the reagents HRP, MB, 2,4-DCP and NADH, of which only the enzyme absorbs significantly at this wavelength. A value for A_{418} of 0.003 was obtained with a buffered solution of 0.31 mM NADH, compared with 0.158 for HRP at the start of the experiment. Thus the value of A_{418} may be used to compare enzyme concentrations, which by this criterion was accurately reproduced in this experiment. This situation serves to emphasise the usefulness of the activity as a quantitative measure of enzyme.

Although the method of gas delivery was different, the 'oxygen transfer constant' of $(6.0 \pm 0.2) \times 10^{-3}$ s^{-1} quoted in [1] was similar to the mass-transport constant com-

puted from the present data, for which the value $(6.40\pm0.02)\times10^{-3}$ s^{-1} was obtained.

One criticism which can be made of the Hauser and Olsen procedure is that it takes longer for the system to settle to a steady oscillatory regime when compared with the method used in this laboratory, which is modelled on that of Olson [40]. The use of a higher NADH stock concentration would dictate lower volume-influx rates, which while allowing for greater quantities of NADH to be stored in the delivery vessel (a Hamilton syringe in this case: see Section 2.2.4) would possibly not compensate sufficiently for water evaporation from the reaction solution. Hauser and Olsen accounted for this effect by humidifying their gas stream. The topics of water evaporation and humidification are discussed in Chapter 3.

6.4 Tyramine and 4-aminophenol

Tyramine and 4-aminophenol were chosen as replacements for 2,4-dichlorophenol in the oscillator, and their efficacies as promoters or inhibitors of an oscillatory state was examined. Aminophenol was chosen for comparison with tyramine because of its shorter alkyl chain, since the closer proximity of the amino group with the phenol ring might influence the formation of a phenoxyl radical. The readiness of a phenol to form such a species, based on the electrochemical potential of its formation, has been proposed by Hauser and Olsen as key to its function in the PO reaction [1].

6.4.1 Tyramine

Similar experiments to those of Section 6.3 were conducted using initial concentrations of tyramine in the range 0–120 μM, in which the tyramine replaced 2,4-DCP. All other experimental parameters and reagent concentrations were those of the standard set (Table 2.1). Dissolved oxygen-time series are shown in Figure 6.5. In all cases where oscillations were present they were damped, the rate of damping decreasing with increasing concentration of tyramine. This would seem to indicate that tyramine is a positive, though weak, promoter of oscillatory behaviour in the peroxidase-oxidase reaction. The overall rate of oxidation in each run was higher than the average obtained with 2,4-DCP as the phenol, the concentration-influx rates used in each case of the figure were, in units of mM/h, (*a*)-(*d*) 1.6, (*e*) 2.0 and (*f*) 1.6. The oxygen mass-transport constants for the series, computed by the method of nonlinear curvefitting (Section 3.3.2) had a mean value of 0.71 $\pm$ 0.10 min^{-1}. The corresponding NADH concentrations, as measured by the absorbance at 360 nm, are shown in Figure 6.6 Phase plots of NADH (A_{360}) against oxygen concentration are shown in Figure 6.7.

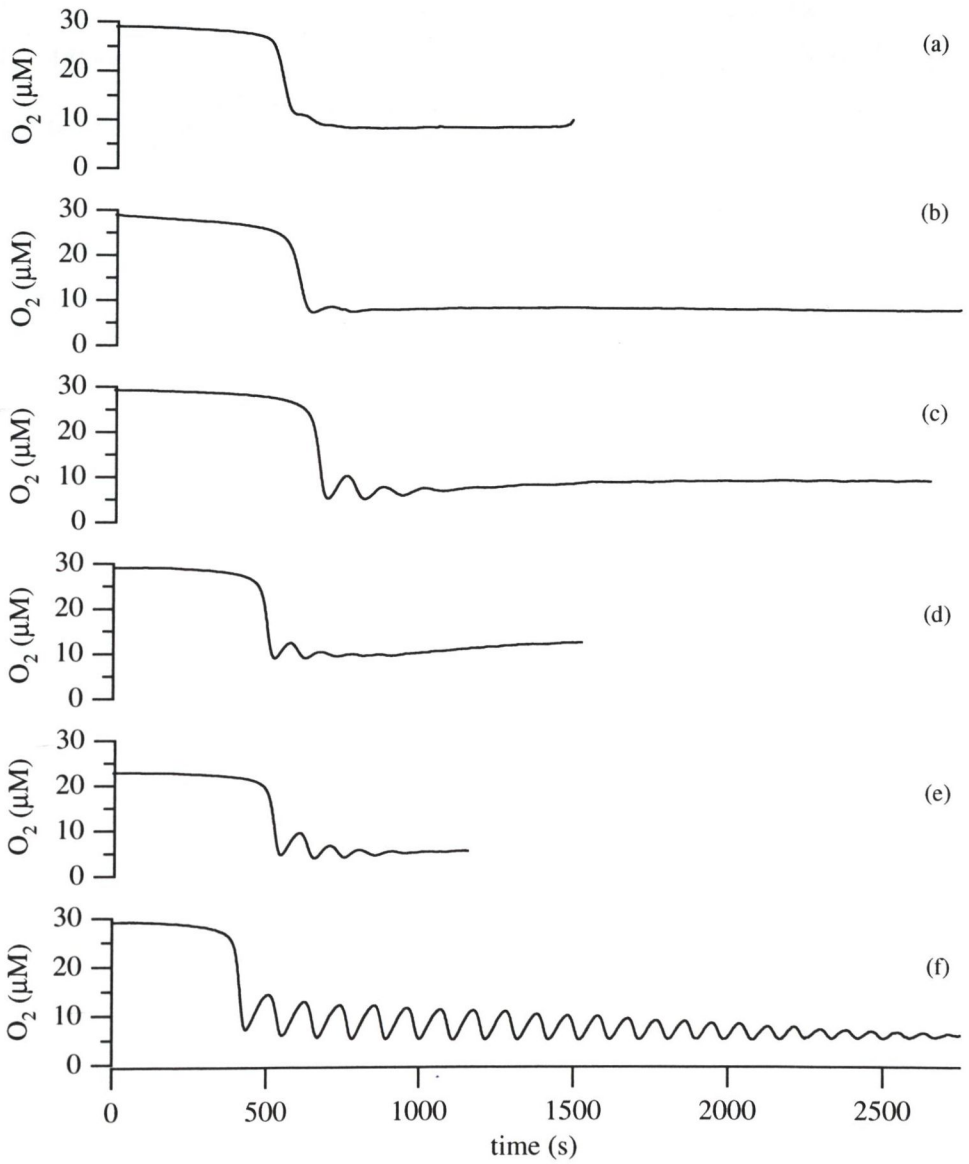

Figure 6.5: Tyramine-induced oscillations in dissolved oxygen. Standard conditions were used, the only deviation from which being the phenol type and concentration, where 2,4-dichlorophenol was replaced by tyramine at final concentrations of (*a*) 0 μM, (*b*) 20 μM, (*c*) 40 μM, (*d*) 60 μM, (*e*) 80 μM and (*f*) 120 μM. Zero time marks the start of NADH infusion.

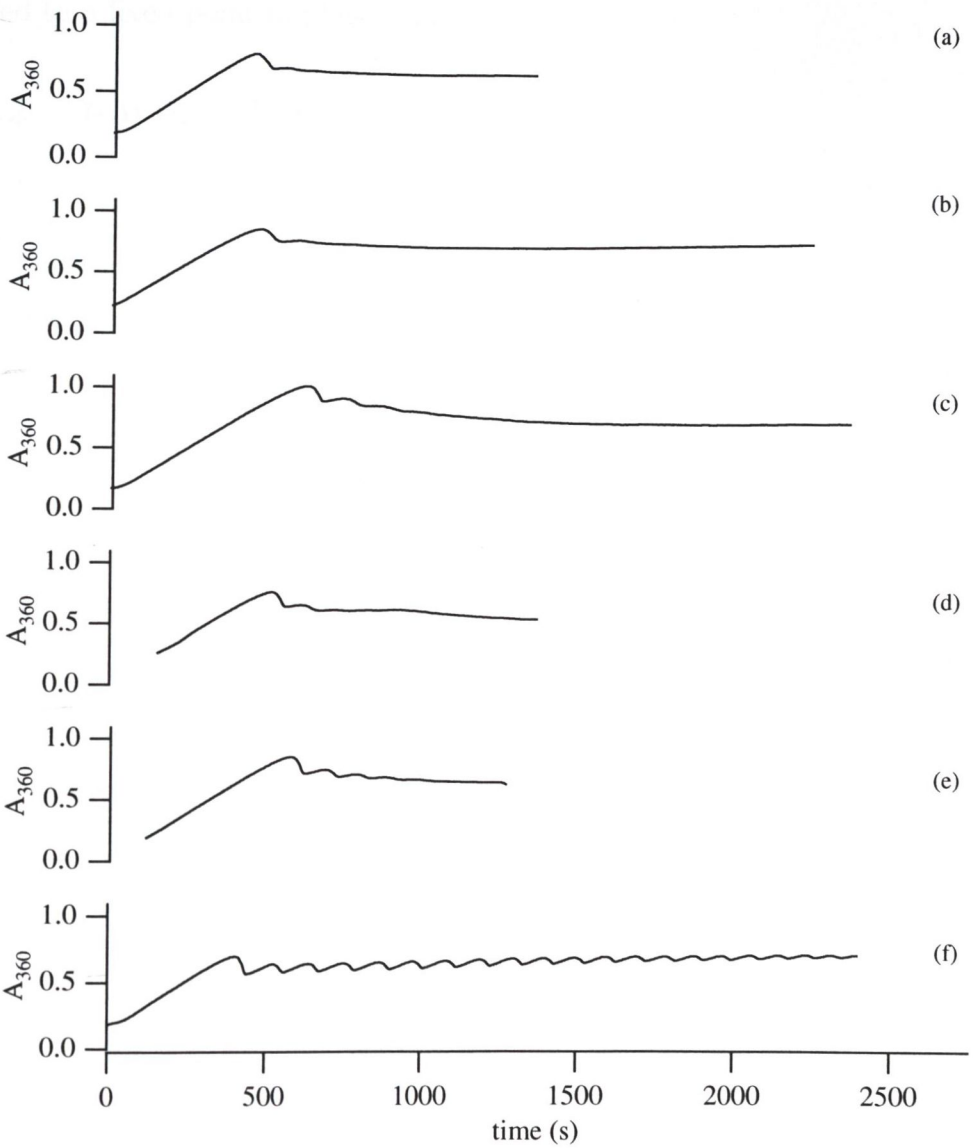

Figure 6.6: Tyramine-induced oscillations in A_{360}. The data were generated from the same series of experiments as those shown in Figure 6.5, in which the concentrations of tyramine were: (*a*) 0 μM, (*b*) 20 μM, (*c*) 40 μM, (*d*) 60 μM, (*e*) 80 μM and (*f*) 120 μM. Zero time marks the start of NADH infusion.

With reference to the oxygen data, which are shown in Figure 6.5, no oscillations were observed in the absence of tyramine, and 24 oscillations were observed at at 120 μM. In between those values an overall increase in the number of oscillations was observed. At each concentration, 1 to 4 oscillations were obtained before the system settled to a fixed point in phase space.

6.4.2 4-aminophenol

The effect of 4-aminophenol on the PO reaction was very different from that of tyramine. Three separate experiments were conducted: the first using 4-aminophenol as a replacement for 2,4-DCP; the second was a control which used 2,4-DCP under otherwise similar conditions; the third experiment investigated the effect of adding a pulse of 4-aminophenol to a working oscillator. The results of each are displayed in Figures 6.8, 6.9, and 6.10. Standard conditions applied, except for the phenol type and concentration.

In Figure 6.8, 4-aminophenol was present initially at a concentration of 25 μM, and 2,4-DCP was omitted. Little oxidation of NADH was observed, and when the NADH supply was cut off at 2644 s, the absorbance at 360 nm went into a steady decline. The NADH consumption may not be solely due to acidic degradation: using a value of 3950 $M^{-1}s^{-1}$ for ϵ_{360}, the rate of decline was calculated to be 95.1 μM/h, nearly 7 times higher than the equivalent value shown in Table 3.1. The control for this experiment is shown in Figure 6.9, where oscillations were observed under standard conditions using the same stock preparations of the reagents.

In Figure 6.10 oscillations were once again obtained. All oscillations immediately ceased after addition of a pulse of 25 μM 4-aminophenol (final concentration). Thus it has been shown from these results that 4-aminophenol is a strong inhibitor of oscillatory oxidation of NADH.

6.4.3 Peroxidase-catalysed dityramine formation

Peroxidases are capable of catalysing oxidative ring-coupling of some substituted phenolic compounds, including tyramine, for which a mechanism has been proposed by Gross and Sizer [66], as shown in Figure 6.11. In this scheme the phenol passes through an initial phenoxyl free radical state in a reaction catalysed by peroxidase. The production of the dityramine species that is ultimately formed can be followed spectrophotometrically in the ultraviolet region, a method that has been used previously by Valoti *et al.* [67] in their study of oxidative ring-coupling using rat intestinal peroxidase. A phenolic free radical has been assumed to play an active role in the

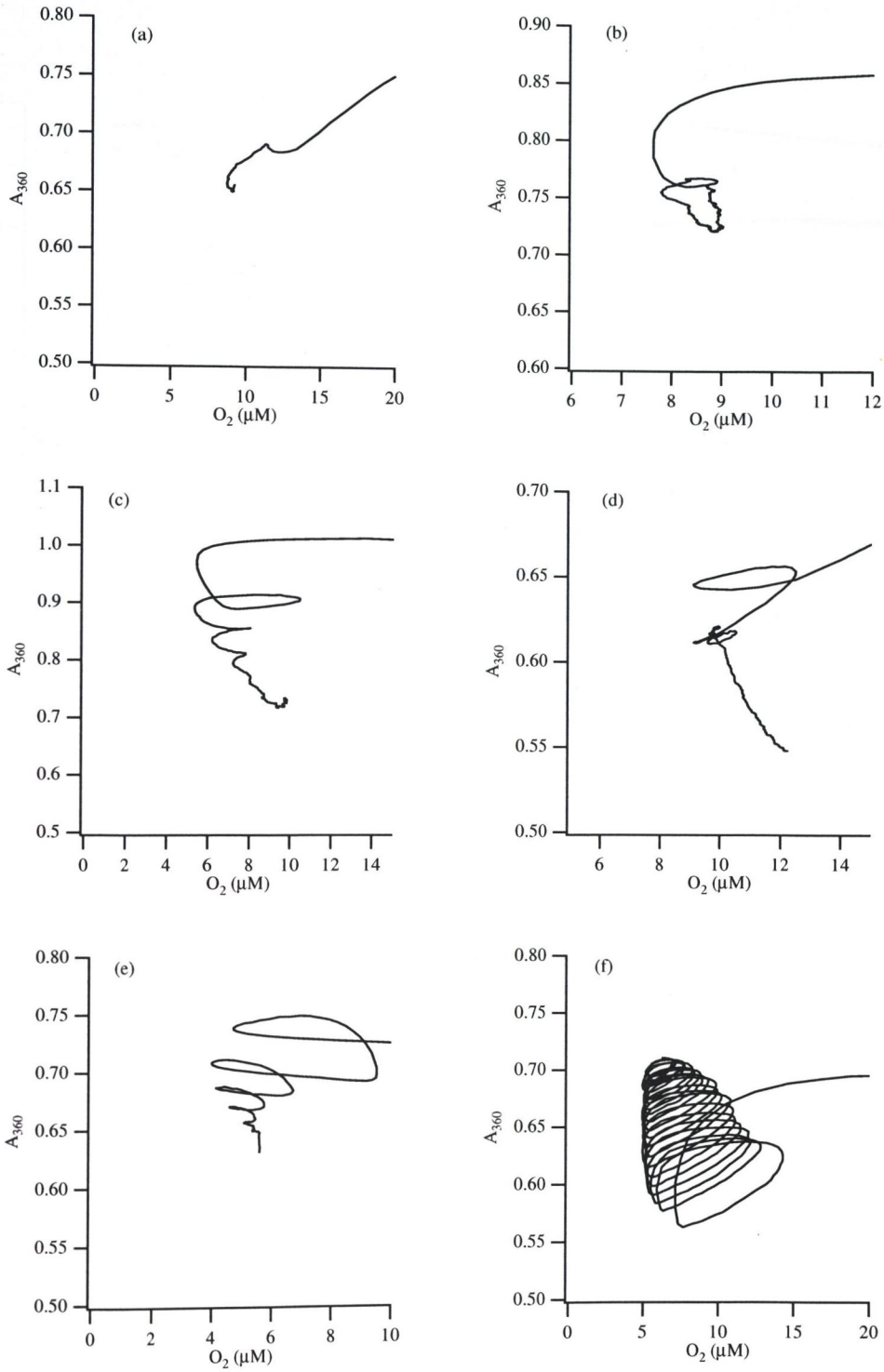

Figure 6.7: Phase plots of tyramine-induced oscillations, which are replots of the data shown in Figures 6.5 and 6.6, in which the concentrations of tyramine were: (*a*) 0 μM, (*b*) 20 μM, (*c*) 40 μM, (*d*) 60 μM, (*e*) 80 μM and (*f*) 120 μM.

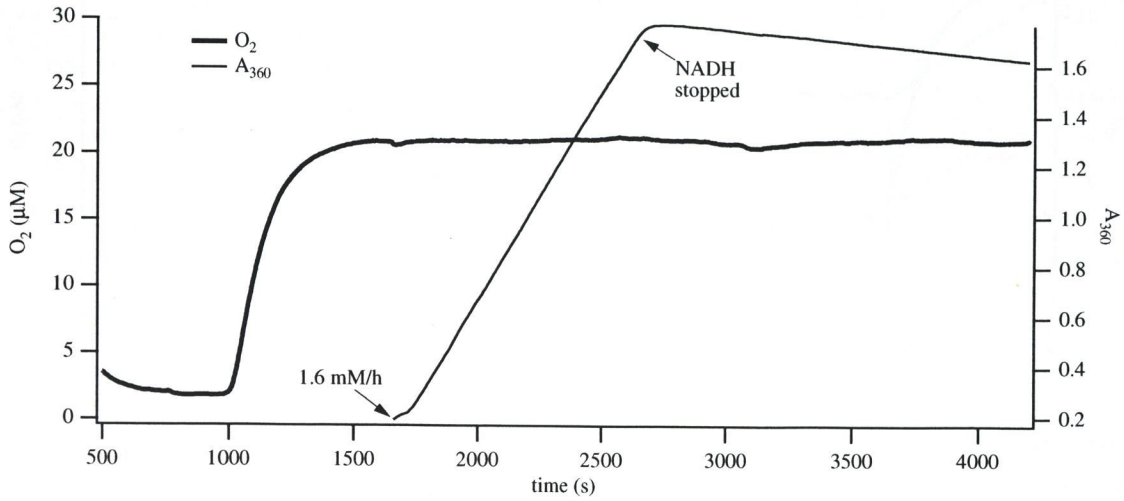

Figure 6.8: Replacement of 2,4-DCP with 4-aminophenol. 4-aminophenol was present initially at 25 μM. Other conditions were as standard (Table 2.1).

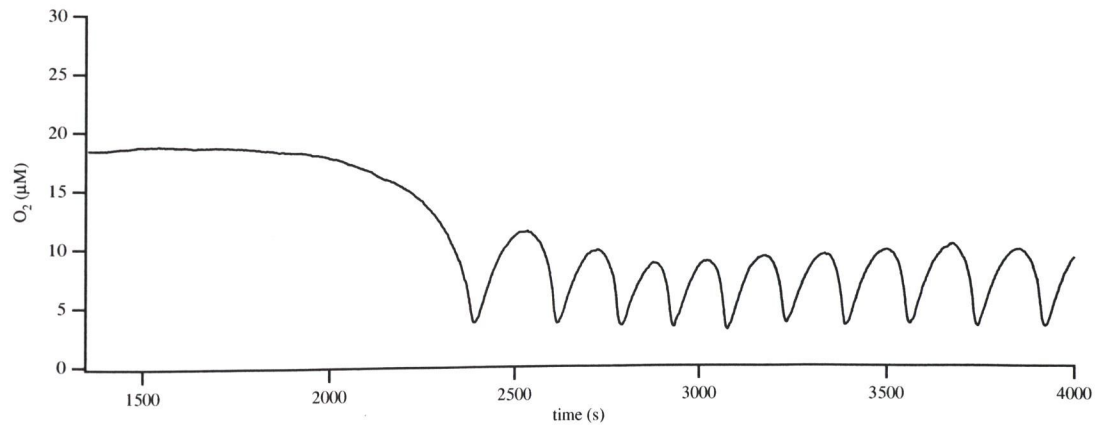

Figure 6.9: Replacement of 2,4-DCP with 4-aminophenol (control). Conditions were those of the standard set (Table 2.1).

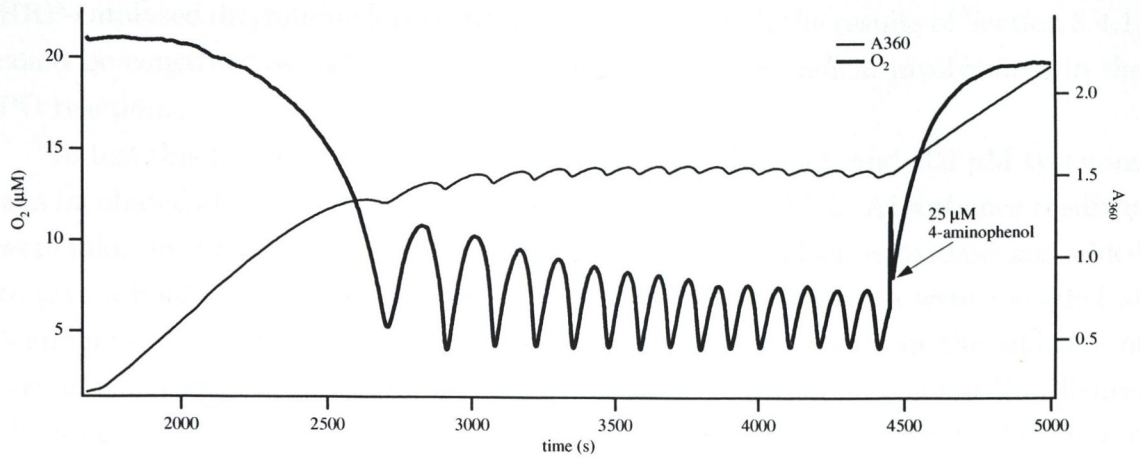

Figure 6.10: Addition of 4-aminophenol pulse to an oscillatory run. Experimental conditions were those of the standard set (Table 2.1). At the point indicated by the arrow, 4-aminophenol was injected into the reaction mixture to give a final concentration of 25 μM.

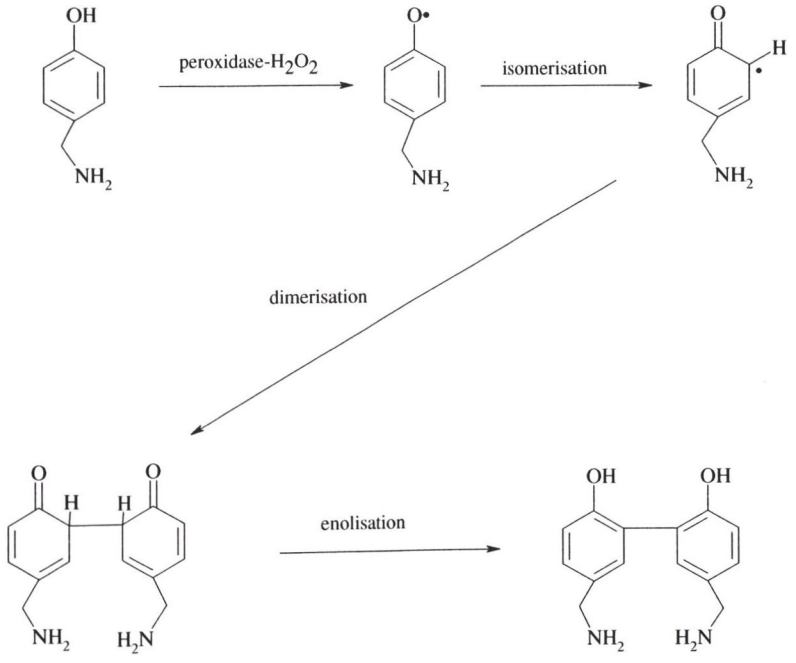

Figure 6.11: Possible mechanism of dityramine formation, as proposed by Gross and Sizer [66].

mechanism of oscillatory oxidation of NADH [1, 44]. Therefore, an observation of HRP-catalysed dityramine formation, taken together with the results of Section 6.4.1, could be construed as indirect evidence for phenoxyl free radical involvement in the PO reaction.

To test this hypothesis, a solution containing 300 μM H_2O_2 and 100 μM tyramine was incubated at 25°C in 0.1 M sodium acetate buffer at pH 5.1. Absorbance readings were taken over the wavelength range 230–400 nm. Horseradish peroxidase was added to give a final concentration of 0.8 μg/ml and absorbance spectra were recorded at 5-minute intervals thereafter. The experiment was repeated without the addition of enzyme, and both sets of results are shown in Figure 6.12. In part (*a*) of that figure, the absorbances at all wavelengths studied increased over the 45-minute duration of the experiment. A further experiment, this time omitting hydrogen peroxide but not the enzyme, gave rise to the same behaviour as that shown in Figure 6.12(*b*). The results are similar to those observed by Valoti *et al.* in the oxidative ring-coupling of tyrosine. Thus the reaction is a H_2O_2-requiring, HRP-catalysed oxidation of tyramine to dityramine, which may have a function in the peroxidase-oxidase oscillator through the generation of free-radical intermediates.

An interesting development arose when the tyramine concentration was increased to 200 and 300 μM. The conditions were otherwise the same as those of Figure 6.12(a), and the results of two separate experiments are shown in Figure 6.13. At 200 μM tyramine little change was observed in the spectra, and at 300 μM a decrease in absorbance at all wavelengths shown in Figure 6.13(b) was noted.

Oxidative ring-coupling experiments were also done using 4-aminophenol as the HRP substrate; the uv absorbance spectrum of a 100 μM solution of 4-AP, which has an absorbance maximum at 271 nm, is shown in Figure 6.14. At this concentration and in the presence of 300 μM H_2O_2 and 0.8 μg/ml enzyme, the character of the absorbance spectrum shifted rapidly to a form a new peak at 244 nm. The reaction was slowed by a ten-fold reduction of the amount of enzyme. Four further oxidative ring-coupling experiments were attempted using 0.08 μg/ml HRP, the data from which are shown in Figure 6.15. Subfigure (*b*) therein shows that some product is formed non-enzymatically, which is in contrast with the corresponding tyramine experiment. From graph (*c*) it is evident that no autoxidation of 4-aminophenol occurs, and graph (*d*) shows the enzyme-catalysed reaction proceeding more slowly at a lower concentration of 4-aminophenol.

In order to slow the reaction still further, and test for the presence of free radicals, 100 μM ascorbic acid was added to a solution of 300 μM H_2O_2 and 25 μM 4-aminophenol in buffer before the addition of the enzyme; scans were taken every

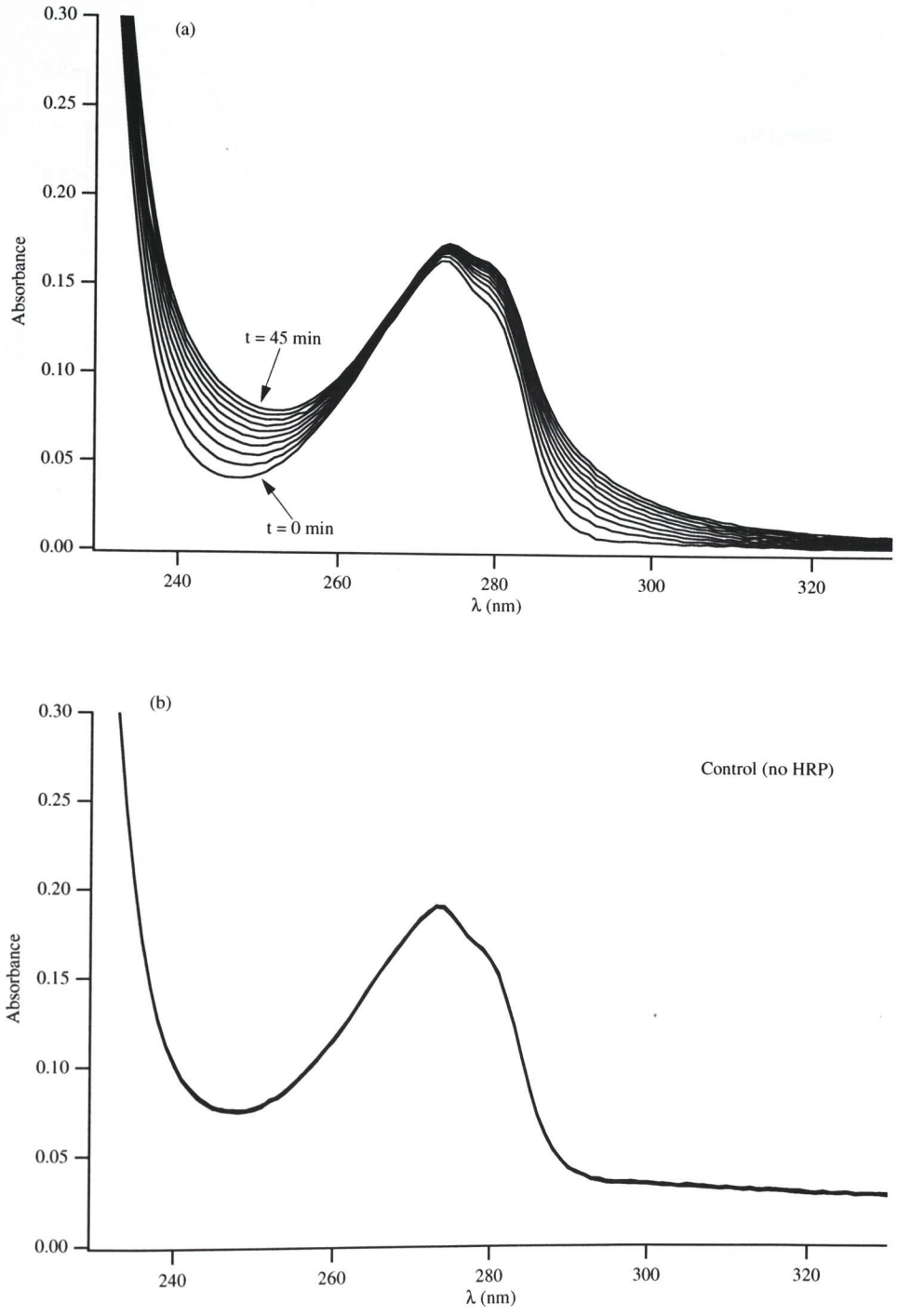

Figure 6.12: Oxidative ring-coupling of tyramine catalysed by HRP. 1.6 μg peroxidase (Type VI, from horseradish) were added to a 0.1 M sodium acetate buffer solution, of pH 5.1, containing 100 μM tyramine and 300 μM hydrogen peroxide. The temperature was 25°C.

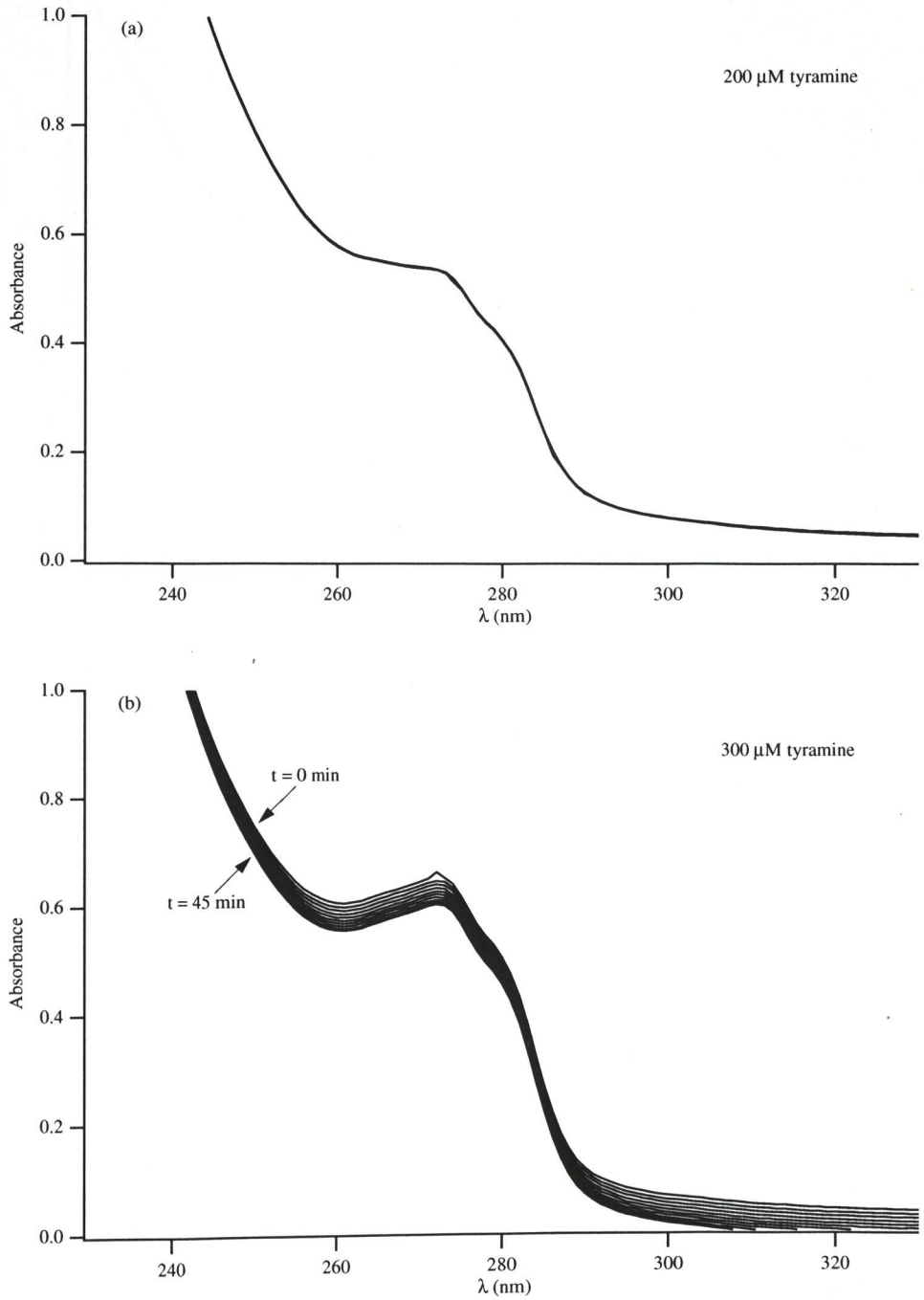

Figure 6.13: Tyramine spectral time series at initial concentrations of (*a*) 200 μM and (*b*) 300 μM. Other experimental parameters were those of Figure 6.12.

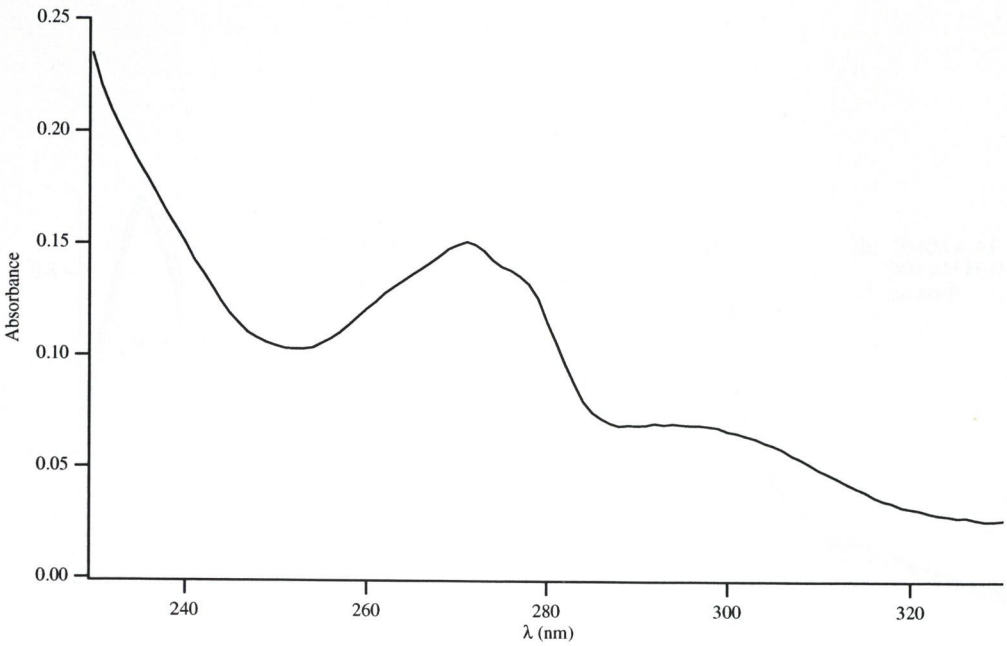

Figure 6.14: Absorbance spectrum of 100 μM 4-aminophenol in 0.1 M acetate buffer at pH 5.1.

two minutes thereafter, giving rise to the results displayed in Figure 6.16. The reference cell in the spectrophotometer contained a solution of 100 μM ascorbic acid in sodium acetate buffer, the spectral properties of which did not alter throughout the experiment. This would seem to suggest that the ascorbate was participating in the reaction. The inset to the figure shows that the absorbance changed in a nonlinear fashion with time, first decreasing and then changing direction abruptly after 8 minutes had elapsed, a peak appearing once again at 244 nm.

6.4.4 Ascorbic acid and the PO reaction

Figure 6.17 shows the results of addition of 10 μl of a 0.2 M stock of ascorbic acid in phosphate buffer to a working oscillator. The reagent concentrations were: [2,4-DCP]=40 μM, [MB]=0.1 μM, and [HRP]=40 U/ml. The buffer was 0.1 M potassium phosphate at pH 4.8. The physical parameters were those of Table 2.1. Ascorbic acid was added at the time indicated by the arrow, to give a 10 mM concentration, and all oxidation of NADH ceased immediately, the dissolved oxygen re-equilibrating with the gas phase. Since ascorbate is known to be a free radical scavenger, this result would seem to support the view that free radicals are essential to the mechanism of NADH-oxidation.

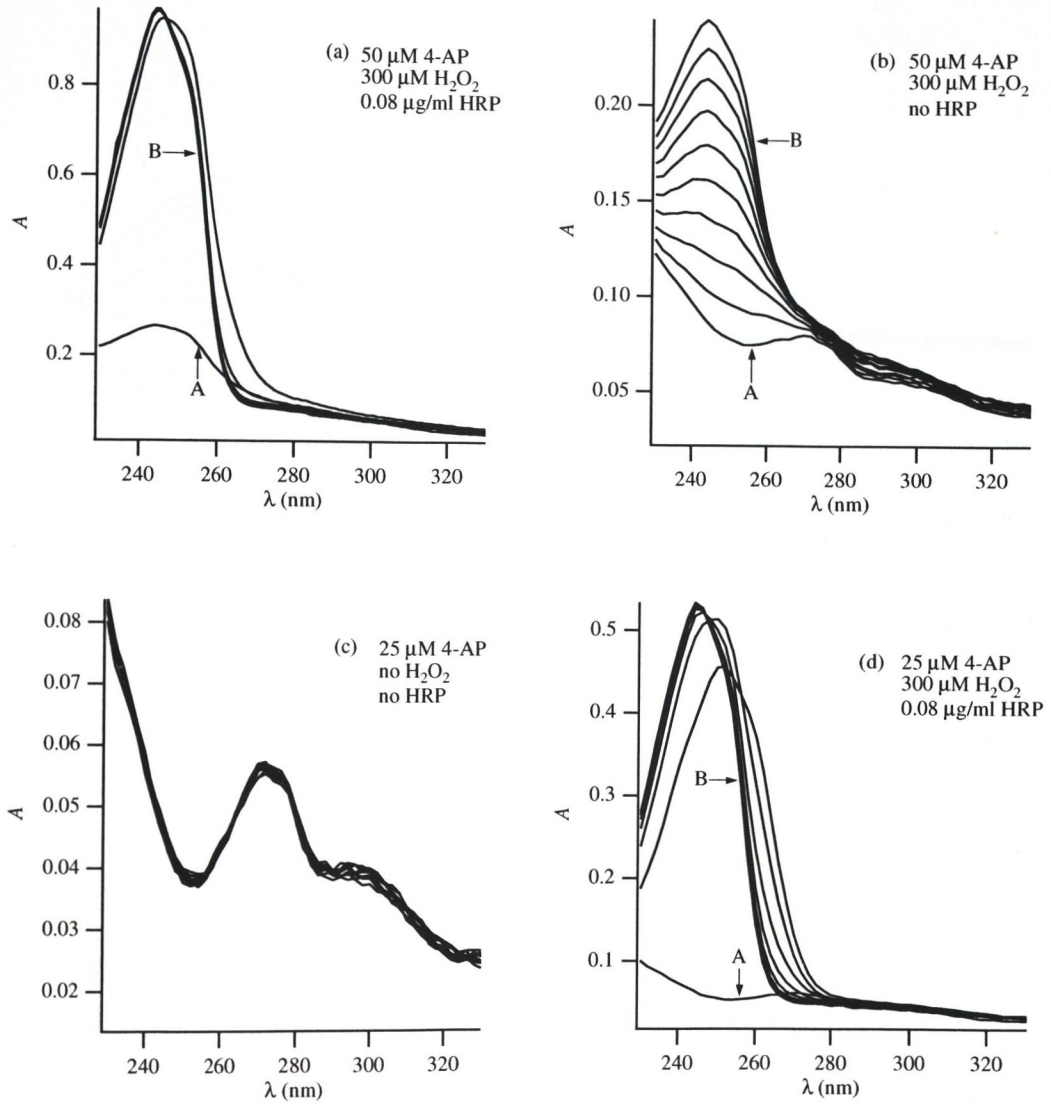

Figure 6.15: Oxidative ring-coupling of 4-aminophenol. All reagents were dissolved in 0.1 M sodium acetate buffer at pH 5.1. Absorbance spectra were taken at five-minute intervals. Curves marked A and B were obtained at $t = 0$ and $t = 45$ minutes, respectively. Graph (*b*) shows the reaction proceeding in the absence of enzyme; in (*c*) no reaction took place when H_2O_2 was omitted; graph (*d*) was generated using 25 μM 4-aminophenol.

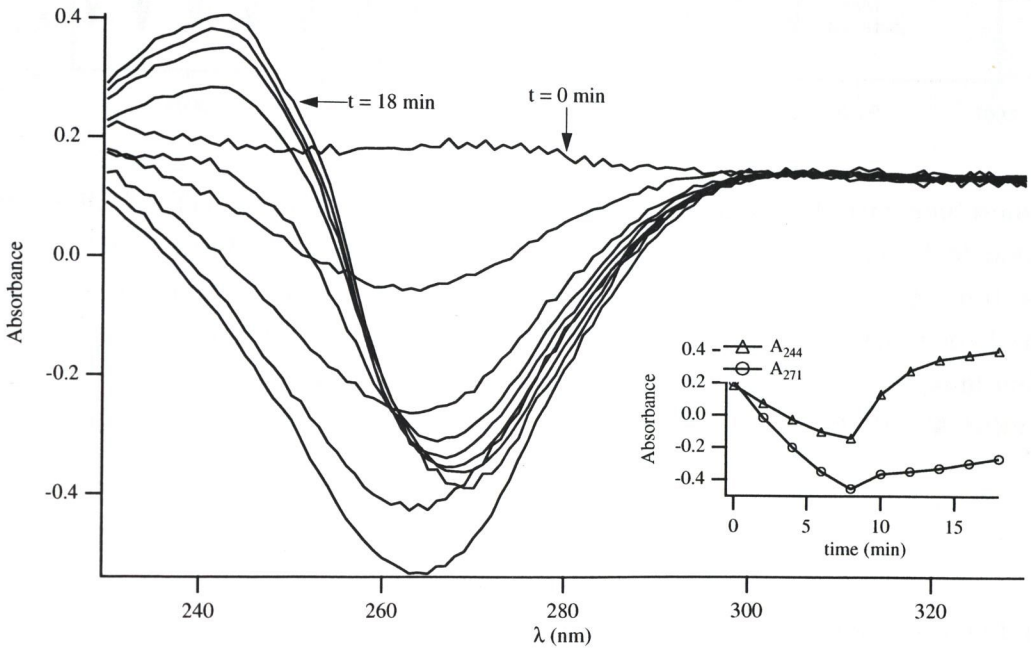

Figure 6.16: The effect of ascorbic acid on HRP-catalysed ring coupling of 4-aminophenol. Shown are ten wavelength scans of a solution containing 300 μM H_2O_2, 25 μM 4-aminophenol and 100 μM ascorbic acid taken over a period of 45 minutes, with the initial and final scans as indicated. The addition of enzyme (to a final concentration of 0.08 μg/ml) was made after the first wavelength scan was taken. The absorbances are relative to a 100 μM solution of ascorbic acid, as stated in the text. Inset is graph of two time courses: the absorbance at 244 and 271 nm, respectively. Notable is a sudden switch after 20 minutes, from a monotonic decline to an increase in absorbances.

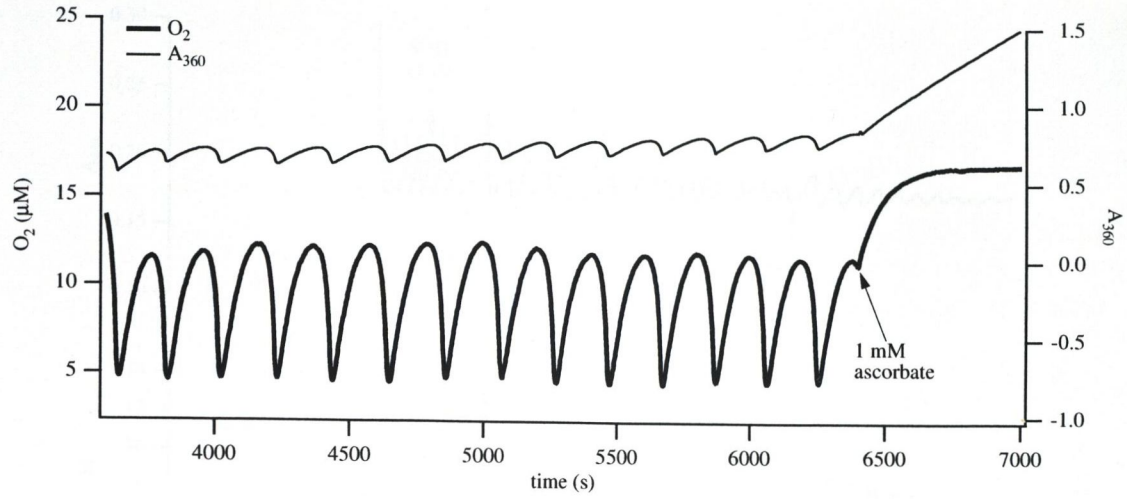

Figure 6.17: The effect of ascorbic acid on the PO reaction. Initial conditions were: 40 U/ml HRP, 40 μM 2,4-dichlorophenol and 0.1 μM methylene blue in 0.1 M potassium phosphate buffer at pH 4.8, of total volume 2.0 ml. Temperature, stirring speed and gas parameters were those given in Table 2.1. NADH was infused from a 80 mM stock solution in 0.01 M buffer (pH 7.0) into the solution at a rate of 1.28 mM/h. At the point indicated by the arrow ascorbic acid was added to give a final concentration of 10 mM, after which NADH oxidation ceased.

6.5 Superoxide radical involvement

A more specific test was performed to check for superoxide radical involvement. To this end, superoxide dismutase was added to a working oscillator. A 2.0 ml solution of 40 U/ml HRP, 40 μM 2,4-dichlorophenol and 0.1 μM methylene blue in 0.1 M potassium phosphate buffer at pH 4.8 was stirred at 1155 $\pm$ 69 rpm and thermostated at 25°C. NADH was infused at 1.28 mM/h (final). Dissolved oxygen concentration and the absorbance at 418 nm were monitored, the data for which are shown in Figure 6.18.

10 μl of a 100 U/ml[1] solution of superoxide dismutase were added to the oscillator at the point indicated. No change was noted in the dynamics. 10 μl of a 1400 U/ml stock were added shortly after, to give 15 U/ml total SOD, which induced damping of the oscillator. A repeat addition of the same number of units of SOD transiently increased the amplitude of oscillations, which damped out thereafter. The total SOD added was 29 U. This result is evidence for participation of superoxide radicals in the mechanism of the oscillator.

[1]The unit is defined as that amount of SOD which will decrease the reduction of cytochrome *c* by 50% in 3.0 ml in the presence of xanthine and xanthine oxidase at pH 7.8 at 25°C.

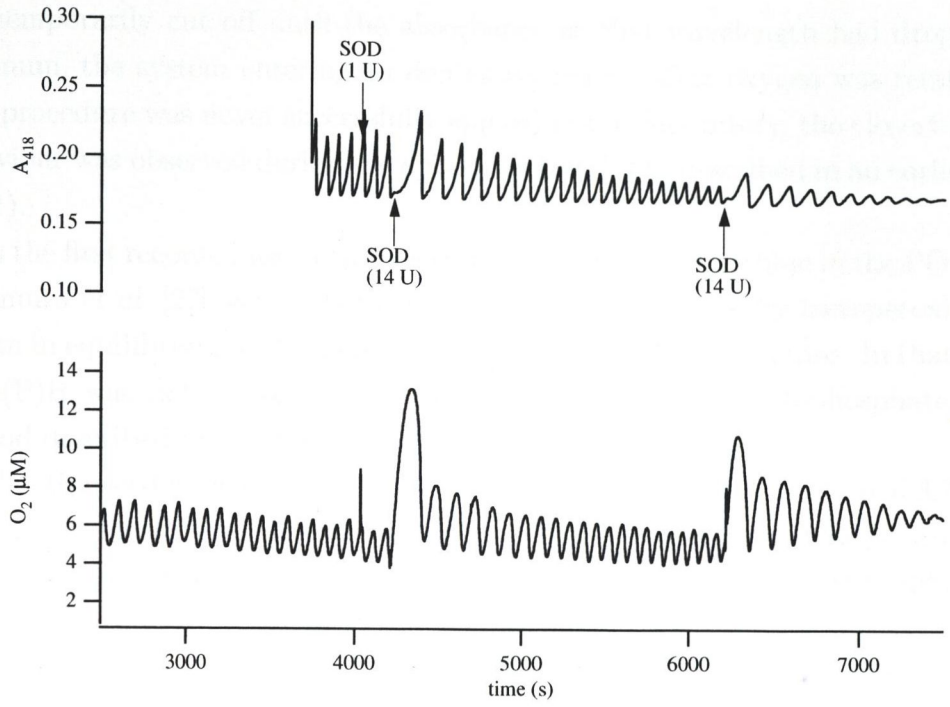

Figure 6.18: The effect of superoxide dismutase on the PO reaction. Initial conditions were: 40 U/ml HRP, 40 μM 2,4-dichlorophenol and 0.1 μM methylene blue in 0.1 M potassium phosphate buffer at pH 4.8, of total volume 2.0 ml. Temperature, stirring speed and gas parameters were those given in Table 2.1. NADH was infused from a 80 mM stock solution in 0.01 M buffer (pH 7.0) into the solution at a rate of 1.28 mM/h. At the point indicated by the arrow ascorbic acid was added to give a final concentration of 10 mM, after which NADH oxidation ceased.

In a repeat of this experiment, a single pulse of SOD was made to give a total SOD concentration of 30 U/2 ml, the result of which was immediate and complete inhibition of the reaction.

6.6 Discussion

Various methods of initiation of oscillations have been reported in the literature; two of these have been successful when used in this laboratory. Some workers have taken advantage of the inherent multistability of the peroxidase-oxidase reaction to switch between different steady-state behaviours that may coexist in parameter space. For example, Rys and Wang [39] used an oxygen perturbation method to induce oscillations, in which the absorbance at 418 nm was monitored after NADH infusion had commenced, and when this had reached a constant value, the oxygen supply

was temporarily cut off until the absorbance at that wavelength had dropped to a minimum, the system entering an oscillatory regime after oxygen was reintroduced. This procedure was never successfully applied in this laboratory, the closest matching behaviour was observed during the episode of bistability described in an earlier section (4.2.1).

In the first recorded use of the electron acceptor methylene blue in the PO reaction, Nakamura *et al.* [27] were able to start oscillations catalysed by lactoperoxidase to a system in equilibrium with gaseous oxygen, by adding MB as a pulse. In that instance NAD(P)H was not infused, but was recycled by the glucose-6-phosphate/G6PDH method described in Chapter 5.

The Hauser-Olsen method followed in the experiment of Section 6.3.2 has the disadvantage that it takes longer to reach a stable (oscillatory) steady-state than by the method generally employed here. In any case, it does not appear to influence the observed dynamical behaviour of the system.

Of the phenols studied in the experiments described in this chapter, 2,4-DCP has proved to be the most useful in maintaining sustained oscillations in the PO reaction, followed by 2,6-dichlorophenol. The period-doubling phenomena observed by Geest *et al.*[38] when 2,4-DCP concentration was varied were never reproduced in this laboratory, a fact that may be due to discrepancies between the parameter sets.

Tyramine and 4-aminophenol, which were shown to have dissimilar effects on the PO reaction, were both substrates for peroxidase/H_2O_2 oxidative ring-coupling. This may explain why tyramine is only a weak promoter of oscillations, since it is likely that it is consumed during an oscillatory run. Continued infusion of tyramine with the NADH might lead to sustained behaviour, and this deserves further study. The action of the dichlorophenols would suggest that these are not consumed during the PO reaction. If phenols pass through a free radical state, as the tyramine oxidative ring coupling results suggest, then successful effectors of oscillations would need to be regenerated during the course of the reaction. A role for 2,4-dichlorophenol has been suggested by Watanabe and Inaba [44] in catalysing the formation of the NAD radical (see Chapter 1, page 12. In their mechanism, superoxide formed from NADH and oxygen reacts with the phenol to form a phenolic radical, which in reacting with NADH forms NAD radical and the original phenol compound.

The reason for the strong inhibition exhibited by 4-aminophenol is not understood, although it has been shown to react with peroxide, and even more quickly when catalysed by HRP than does tyramine (Section 6.4.3, which may also be taken as evidence for a free radical state catalysed by HRP). Ascorbic acid only temporarily suspended oxidation of 4-AP by peroxidase/H_2O_2; it appears that the reaction

recommenced abruptly after some reaction involving ascorbate had taken place (see inset to Figure 6.16), an intriguing result. Less ambiguous was the effect its addition (at 100 μM) to a working PO oscillator, however, which completely inhibited all NADH oxidation by peroxidase. From both this result, and the more specific inhibition demonstrated by superoxide dismutase, it is evident that free radical species are essential to the chemical mechanism of the peroxidase-oxidase oscillator.

Chapter 7

Mathematical Modelling

7.1 Introduction

Mathematical modelling of an observable dynamical system is often key to a full understanding of the mechanisms underlying data observed in the laboratory. The results of simulation data may be used to test hypotheses about various aspects of the dynamics, which, by confirming or denying the experimental observations, may lead the researcher on to further fruitful avenues of inquiry through either new theories or experiments.

An important part of this work was the development of a new model of the peroxidase-oxidase reaction, the aim of which was to show how a relatively simple biochemical system such as that described in the preceding experimental sections may give rise to oscillatory behaviour. The theoretical development will be presented in three stages; the first stage will create a model from known reactions of substrates and possible intermediates, among which will be included various oxidation states of the enzyme. This will be called Model 1; in the second stage a simpler, more abstract model will be developed from the first, with which it will be shown that oscillations can arise from autocatalytic production of an intermediate compound through the action of an enzyme existing in two active states. This will be referred to as Model 2. The final stage will proceed by making a further reduction to the number of state variables in Model 2 and a linearised stability analysis of the system will be used to make predictions about the existence of oscillations. This minimal model will be called Model 3.

7.2 Model 1

The primary model of the PO reaction was developed using as starting point a published collection of known reactions of several implicated species, along with experimentally derived rate constants [53]. A mechanism was proposed involving nine chemical species and twelve steps, which is shown in diagrammatic form in Figure 7.1, in which are involved the substrates NADH and O_2, the intermediates H_2O_2, O_2^- and $NAD^\bullet$, and four oxidation states of haem-peroxidase: native Per^{3+} and so-called Compounds I, II and III. The following table lists the twelve chemical reactions, labelled (Ro), (Rn) and (R1)–(R10) which together compose Model 1:

$$O_{2(g)} \underset{k_{-t}}{\overset{k_t}{\rightleftharpoons}} O_{2(aq)} \qquad \text{(Ro)}$$

$$\xrightarrow{k_f} \text{NADH} \qquad \text{(Rn)}$$

$$\text{NADH} + O_2 + H^+ \xrightarrow{k_1} NAD^+ + H_2O_2 \qquad \text{(R1)}$$

$$Per^{3+} + H_2O_2 \xrightarrow{k_2} \text{CoI} \qquad \text{(R2)}$$

$$\text{CoI} + \text{NADH} \xrightarrow{k_3} \text{CoII} + NAD^\bullet \qquad \text{(R3)}$$

$$\text{CoII} + \text{NADH} \xrightarrow{k_4} Per^{3+} + NAD^\bullet \qquad \text{(R4)}$$

$$Per^{3+} + O_2^- \xrightarrow{k_5} \text{CoIII} \qquad \text{(R5)}$$

$$O_2 + NAD^\bullet \xrightarrow{k_6} O_2^- + NAD^+ \qquad \text{(R6)}$$

$$\text{CoIII} + NAD^\bullet \xrightarrow{k_7} \text{CoI} + NAD^+ \qquad \text{(R7)}$$

$$2NAD^\bullet \xrightarrow{k_8} NAD_2 \qquad \text{(R8)}$$

$$2O_2^- + 2H^+ \xrightarrow{k_9} H_2O_2 + O_2 \qquad \text{(R9)}$$

$$\text{CoII} + H_2O_2 \xrightarrow{k_{10}} \text{CoIII} \qquad \text{(R10)}$$

Reactions (Ro) and (Rn) are involved in the delivery of dioxygen and NADH to the system. The initiation step is the reaction of the substrates to form NAD^+ and H_2O_2 (R1), the former of which is one of the products of the overall reaction (Equations 1.2) and is assumed to be inactive in this system. The hydrogen peroxide so formed combines with native peroxidase enzyme (Per^{3+}) to form CoI (R2), which may in its turn react with NADH to form $NAD^\bullet$ and CoII (R3). CoII goes on to react with NADH to form a further molecule of the NAD radical (R4), and in so doing returns the enzyme to the Per^{3+} form. Although not made explicit in reactions (R3) and (R4), it can be assumed that a molecule of water is released at each of these steps. The NAD radical has three fates in this model, which are (*i*) the formation of an inactive dimer (NAD_2) by reaction (R8), (*ii*) the formation of superoxide radical and NAD^+ by reacting with molecular dioxygen (R6), the former of which may react with Per^{3+} to form the Compound III (R5), and (*iii*) reaction with CoIII to form CoI and NAD^+ (R7). The superoxide radical can dismutate to oxygen and hydrogen peroxide (R9). In addition, CoII can react with H_2O_2 to form CoIII (R10). Both

the initiation step and dismutation of superoxide are explicitly pH-dependent in this model.

The overall reaction can be determined by the following summation of reactions (R1)–(R10):

$$2(\text{R1}) + 2(\text{R2}) + 4(\text{R3}) + 3(\text{R4}) + (\text{R5}) + 3(\text{R6}) + 2(\text{R7}) + (\text{R8}) + (\text{R9}) + (\text{R10})$$

which gives

$$4O_2 + 9\text{NADH} + 4H^+ \longrightarrow 7\text{NAD}^+ + \text{NAD}_2 \,, \tag{7.1}$$

an expression containing only reactants and end products. The equation is not formally charge- and mass-balanced since certain species, such as H_2O, are omitted from the reactions (R1)–(R10) above. Since the reaction occurs in acidic, aqueous medium, adding $3H^+$ to the left hand side and $8H_2O$ to the right hand side gives the final, balanced, overall reaction:

$$4O_2 + 9\text{NADH} + 7H^+ \longrightarrow 7\text{NAD}^+ + \text{NAD}_2 + 8H_2O. \tag{7.2}$$

We can further state that the total amount of peroxidase, P, is conserved, *i.e.*, that $[\text{P}] = [\text{Per}^{3+}] + [\text{CoI}] + [\text{CoII}] + [\text{CoIII}]$ is a constant.

By applying the law of mass action, the rate equations for each of the nine reactants may be written as a set of ordinary differential equations, as follows:

$$\begin{aligned} d[O_2]/dt &= -k_1[\text{NADH}][O_2] + k_t[O_{2(g)}] + k_9[O_2^-]^2 - \\ &\quad k_{-t}[O_2] - k_6[O_2][\text{NAD}^\bullet] \end{aligned} \tag{7.3}$$

$$\begin{aligned} d[\text{NADH}]/dt &= k_f[\text{NADH}]_i - k_1[\text{NADH}][O_2] - k_3[\text{CoI}][\text{NADH}] - \\ &\quad k_4[\text{CoII}][\text{NADH}] \end{aligned} \tag{7.4}$$

$$\begin{aligned} d[\text{CoI}]/dt &= k_2[\text{Per}^{3+}][H_2O_2] - k_3[\text{CoI}][\text{NADH}] + \\ &\quad k_7[\text{NAD}^\bullet][\text{CoIII}] \end{aligned} \tag{7.5}$$

$$\begin{aligned} d[\text{CoII}]/dt &= k_3[\text{CoI}][\text{NADH}] - k_4[\text{CoII}][\text{NADH}] - \\ &\quad k_{10}[\text{CoII}][H_2O_2] \end{aligned} \tag{7.6}$$

$$d[\text{Per}^{3+}]/dt = k_4[\text{CoII}][\text{NADH}] - k_2[\text{Per}^{3+}][H_2O_2] -$$

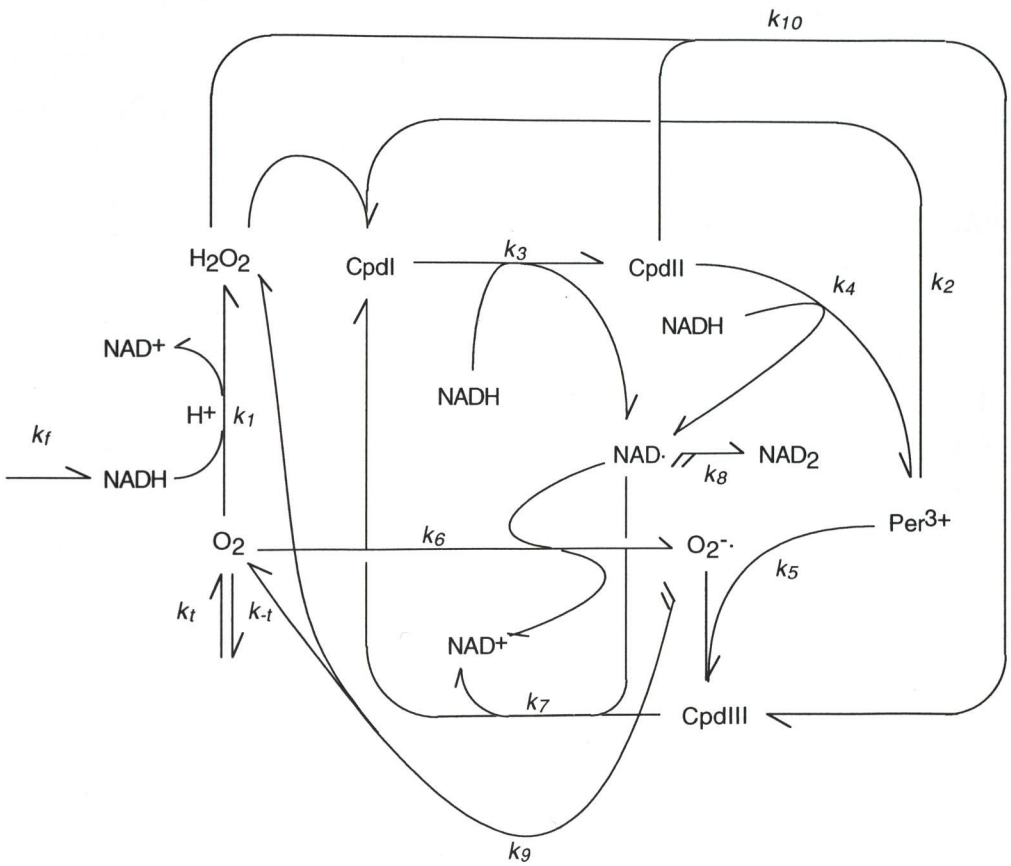

Figure 7.1: Diagram of the full model. The arrow-style adheres to the convention of Aguda and Larter [53] where the number of barbs on an arrowhead denotes the number of molecules of product formed in that step, and similarly, the number of feathers on the tail marks the number of reactants consumed.

$$k_5[\mathrm{Per}^{3+}][\mathrm{O}_2^-] \tag{7.7}$$

$$d[\mathrm{CoIII}]/dt = k_5[\mathrm{Per}^{3+}][\mathrm{O}_2^-] - k_7[\mathrm{NAD}^\bullet][\mathrm{CoIII}] + k_{10}[\mathrm{CoII}][\mathrm{H}_2\mathrm{O}_2] \tag{7.8}$$

$$d[\mathrm{H}_2\mathrm{O}_2]/dt = k_1[\mathrm{NADH}][\mathrm{O}_2] + k_9[\mathrm{O}_2^-]^2 - k_2[\mathrm{Per}^{3+}][\mathrm{H}_2\mathrm{O}_2] - k_{10}[\mathrm{CoII}][\mathrm{H}_2\mathrm{O}_2] \tag{7.9}$$

$$d[\mathrm{O}_2^-]/dt = k_6[\mathrm{NAD}^\bullet][\mathrm{O}_2] - k_5[\mathrm{Per}^{3+}][\mathrm{O}_2^-] - 2k_9[\mathrm{O}_2^-]^2 \tag{7.10}$$

$$d[\mathrm{NAD}^\bullet]/\mathrm{dt} = k_3[\mathrm{CoI}][\mathrm{NADH}] + k_4[\mathrm{CoII}][\mathrm{NADH}] - k_7[\mathrm{CoIII}][\mathrm{NAD}^\bullet] - k_6[\mathrm{O}_2][\mathrm{NAD}^\bullet] - 2k_8[\mathrm{NAD}^\bullet]^2 \tag{7.11}$$

where $[\mathrm{NADH}]_i$ is the concentration of the stock solution of NADH.

These equations were integrated numerically on an Apple Macintosh computer using the simulation program Madonna[1], employing a combination of published values of the rate constants and those obtained from work performed in this laboratory, specifically those pertaining to the rates of entry of substrates into the system. Initial studies of Model 1 used rate constants quoted by Larter and Aguda [53], and a value of k_1 taken from [20]. An example of one such simulation run of the model is shown in Figure 7.3. The values of k_t, k_{-t} and k_f (rate constant of NADH infusion, in units of s^{-1}) are representative of those used in the laboratory experiments. For example, the mass-transport constant used was 0.0091 s^{-1}, or 0.546 min^{-1}, which was close to the average value 0.56 min^{-1} that was obtained over many laboratory experiments in which standard conditions applied (see p. 71). The text input to Madonna which was used to generate the simulation data of Figure 7.3 is shown below.

A feature of note in the above Madonna equation file is the use of the `TIME` variable in the NADH rate equation. Boolean logic was used to mimic the practice of altering the NADH influx rate during the course of a real experiment. The oxygen concentration was zero initially (`INIT O2 = 0`) and NADH influx was not started until the oxygen level had equilibrated with the gaseous phase (`O2g`). When the value of the `TIME` variable lay between 250 and 1500 seconds, the value of the NADH influx rate was `kf*NADHi`. The inequalities `TIME>250` and `TIME<=1500` each evaluated to

[1]Written by Robert I. Macey and George F. Oster, University of California, Department of Molecular and Cellular Biology, CA 94720, USA; http://www.kagi.com/madonna.

```
METHOD Stiff

STARTTIME = 0
STOPTIME = 5000
DT = 0.001
DTOUT = 1
DTMAX = 0.1

INIT O2 = 0
INIT NADr = 0
INIT NADH = 0
INIT Per = 3e-6
INIT Co1 = 0
INIT Co2 = 0
INIT Co3 = 0
INIT SOr = 0
INIT H2O2 = 0.1e-8

kt = 2.54829e-4
k_t = 0.0091
kf = 8.033e-6
k1 = 33
k2 = 1.8e7
k3 = 5.4e3
k4 = 8.0e2
k5 = 1.9e6
k6 = 2.0e9
k7 = 1.3e8
k8 = 3.0e7
k9 = 1.1e7
k10 = 46

O2g = 7.8e-4
NADHi =80e-3

d/dt (O2) = -k1*NADH*O2 + kt*O2g + k9*SOr^2 - k_t*O2 - k6*O2*NADr
d/dt (NADH) = (TIME>250 AND TIME<=1500)*kf*NADHi +
(TIME>1500)*0.6*kf*NADHi - k1*NADH*O2 - k3*Co1*NADH
- k4*Co2*NADH
d/dt (Co1) = k2*Per*H2O2 - k3*Co1*NADH + k7*NADr*Co3
d/dt (Co2) = k3*Co1*NADH - k4*Co2*NADH - k10*Co2*H2O2
d/dt (Per) = k4*Co2*NADH - k2*Per*H2O2 - k5*Per*SOr
d/dt (Co3) = k5*Per*SOr - k7*NADr*Co3 + k10*Co2*H2O2
d/dt (H2O2) = k1*NADH*O2 + k9*SOr^2- k2*Per*H2O2 - k10*Co2*H2O2
d/dt (SOr) = k6*NADr*O2 - k5*Per*SOr - 2*k9*SOr^2
d/dt (NADr) = k3*Co1*NADH + k4*Co2*NADH - k7*Co3*NADr - k6*O2*NADr -
2*k8*NADr^2
```

Figure 7.2: Madonna script used to generate the simulated data shown in Figure 7.3. The numerical integration method is first defined, then the start and end times, the step time (`DT`). Certain integration methods vary the step size automatically, and these cases an upper bound is set by the parameter `DTMAX`. `DTOUT` defines the time interval between recorded (as opposed to calculated) data values; thus, in this example, data output will be recorded every 1 time unit (second). The initial values of each variable are set using the `INIT` command. Values are assigned to each parameter and the rate equations are entered as `d/dt (`<*variable-name*>`) =` <*expression*>.

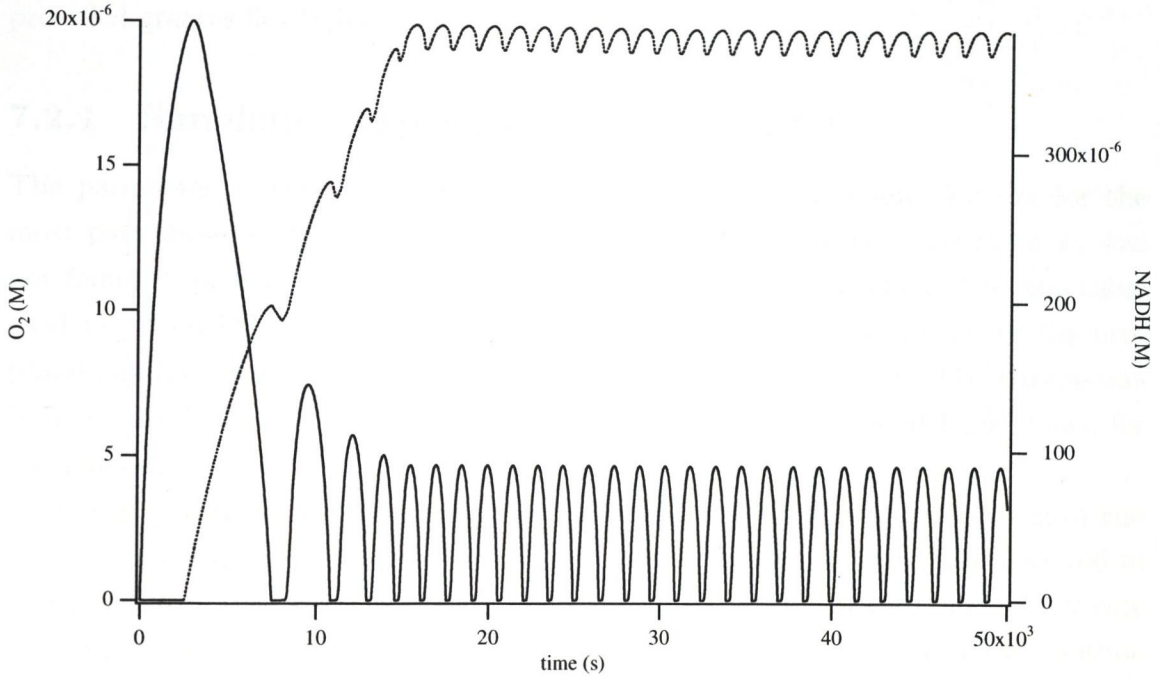

Figure 7.3: Simulated oxygen and NADH traces. Rate constants were as follows: $k_1 = 33\ s^{-1}$; $k_2 = 1.8 \times 10^7\ M^{-1}\ s^{-1}$; $k_3 = 5400\ M^{-1}\ s^{-1}$; $k_4 = 800\ M^{-1}\ s^{-1}$; $k_5 = 1.9 \times 10^6\ M^{-1}\ s^{-1}$; $k_6 = 2.0 \times 10^9\ M^{-1}\ s^{-1}$; $k_7 = 1.3 \times 10^8\ M^{-1}\ s^{-1}$; $k_8 = 3 \times 10^7\ M^{-1}\ s^{-1}$; $k_9 = 1.1 \times 10^7\ M^{-1}\ s^{-1}$; $k_{10} = 46\ M^{-1}\ s^{-1}$; $k_f = 8.033 \times 10^{-6}\ s^{-1}$; $k_t = 2.55 \times 10^{-4}\ s^{-1}$; $k_{-t} = 9.1 \times 10^{-3}\ s^{-1}$. Other parameters were: $[O_{2(g)}] = 7.8 \times 10^{-4}$ M; $[NADH]_i$=0.08 M. The initial concentration of $[Per^{3+}]$ was 3×10^{-6} M, and that of $[H_2O_2]$ was 1×10^{-9} M. All other concentrations were zero initially. The differential equations (7.3)-(7.11) were integrated numerically using a Rosenbrock (auto-stepsize) algorithm.

1 (Boolean TRUE) and therefore their conjunction did likewise. Above this time interval the conjunction evaluated to 0 (Boolean FALSE) and the NADH influx rate was reduced to 60% of the original value by means of the next term in the equation, `(TIME>1500)*0.6*kf*NADHi`.

Model 1 was refined to include a new constant, r_f, which was used to decrease the NADH influx rate to its final value. This general constant replaced the fixed value of 0.6 that was used initially in the second term of the NADH rate equation, and provided greater flexibility.

7.2.1 Simulation experiments with Model 1

The parameter values used in the simulation run shown in Figure 7.3 are for the most part those quoted by Aguda and Larter [53]. However, their value for k_1 was not found to produce oscillations in Model 1, and was instead replaced by the value used by Olson [40] in his "Urbanalator" model[2], which takes into account the proposed catalytic role of MB in H_2O_2 formation (Section 1.2, p.12). The parameters from Figure 7.3, the Aguda-Larter paper and the Urbanalator model are shown for comparison in Table 7.1.

It was discovered that the value for k_4 used in the Urbanalator model gave rise to simulated data from Model 1 that was in better agreement with data observed in this laboratory. With certain other adjustments to the substrate influx/efflux rate constants, a good approximation to the real-world data is given by the simulation results shown in Figures 7.4 and 7.5. In particular, the results of Figure 7.4 compare favourably with, for example, the data shown in Figure 4.5. Figure 7.6 shows the development of a stable limit cycle in NADH-O_2 phase space.

The Per^{3+} and CoIII traces appear to be mirror images of each other, which is also in agreement with experimental observation (see Section 4.2.5). Oscillations in compounds I and II of the peroxidase, and in particular $NAD^{\bullet}$ are very sharp in character. This observation may be accounted for by the fact that $NAD^{\bullet}$ is very reactive: the rate constants of its three removal terms in Equation (7.11) are all of high magnitude (refer to Table 7.1).

[2]The Urbanalator model of the PO reaction was developed by Olson and Scheeline at the University of Illinois at Urbana-Champaign. The naming convention follows that of the Field and Noyes "Oregonator" chemical model, which originated at the University of Oregon, and which in its turn followed the naming convention laid down by Ilya Prigogine at the University of Brussels, whose abstract chemical oscillator was termed the "Brusselator". In keeping with this convention the systems developed here would be called the "Dublinator" models.

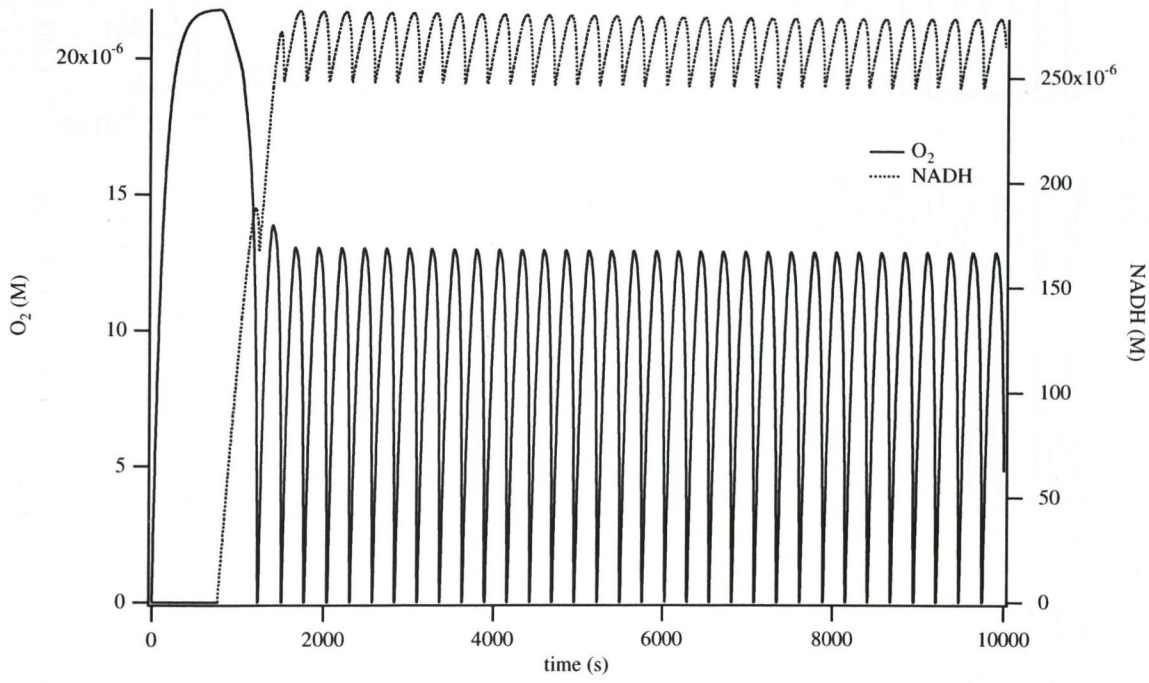

Figure 7.4: Simulated oxygen and NADH traces of the improved Model 1. Rate constants were as follows: $k_1 = 4.0\ s^{-1}$; $k_2 = 1.8 \times 10^7\ M^{-1}\ s^{-1}$; $k_3 = 5400\ M^{-1}\ s^{-1}$; $k_4 = 53700\ M^{-1}\ s^{-1}$; $k_5 = 1.9 \times 10^6\ M^{-1}\ s^{-1}$; $k_6 = 2.0 \times 10^9\ M^{-1}\ s^{-1}$; $k_7 = 1.3 \times 10^8\ M^{-1}\ s^{-1}$; $k_8 = 3 \times 10^7\ M^{-1}\ s^{-1}$; $k_9 = 1.1 \times 10^7\ M^{-1}\ s^{-1}$; $k_{10} = 46\ M^{-1}\ s^{-1}$; $k_f = 8.033 \times 10^{-6}\ s^{-1}$; $k_t = 2.55 \times 10^{-4}\ s^{-1}$; $k_{-t} = 9.1 \times 10^{-3}\ s^{-1}$. Other parameters were: $[O_{2(g)}] = 7.8 \times 10^{-4}$ M; $[NADH]_i$=0.08 M; $r_f = 0.4635$. The initial concentration of $[Per^{3+}]$ was 3×10^{-6} M, and that of $[H_2O_2]$ was 1×10^{-9} M. All other concentrations were set to zero initially. The model equations were integrated numerically using a Rosenbrock algorithm.

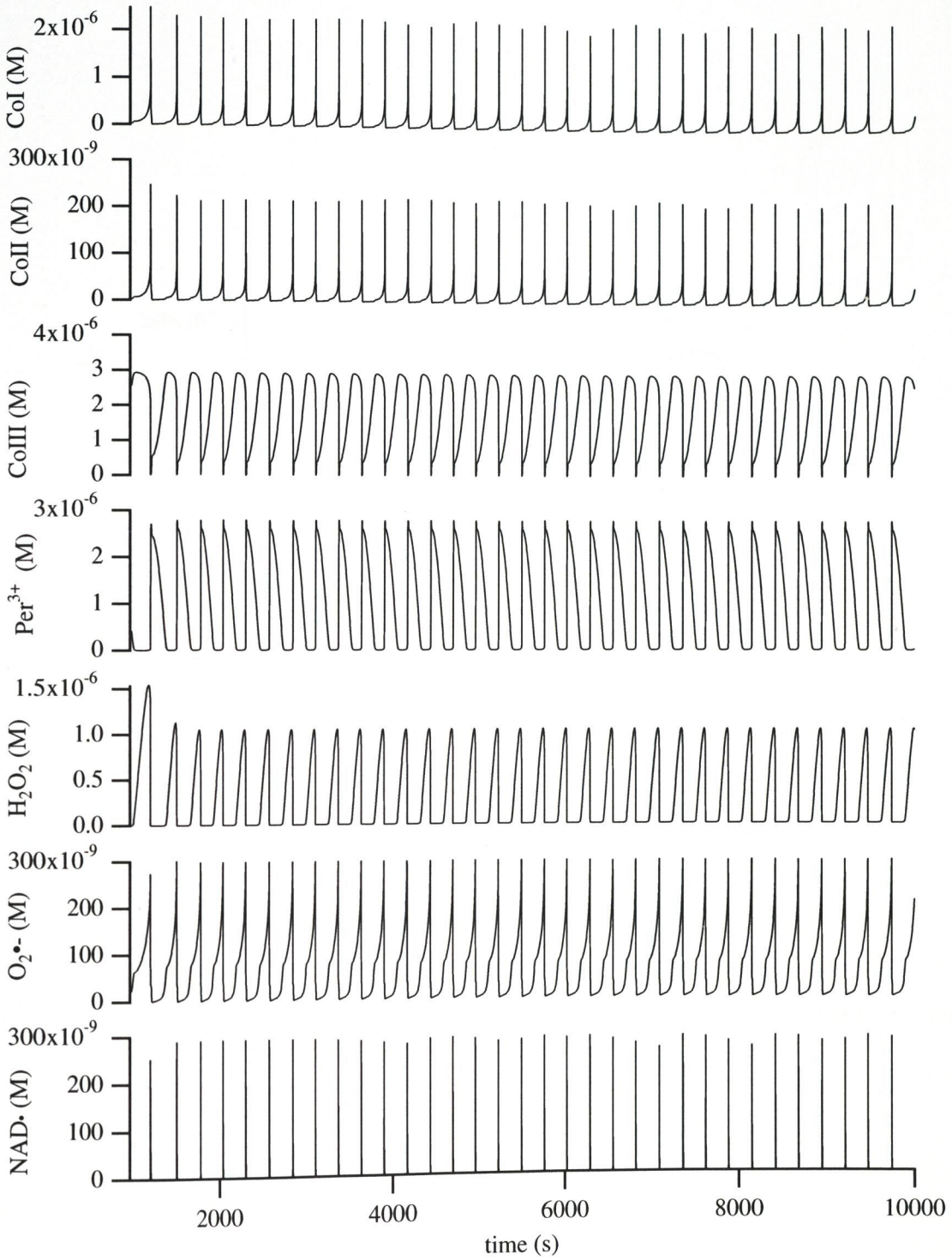

Figure 7.5: Simulated time courses of enzyme compounds and other species. Rate constants and other conditions were those of Figure 7.4.

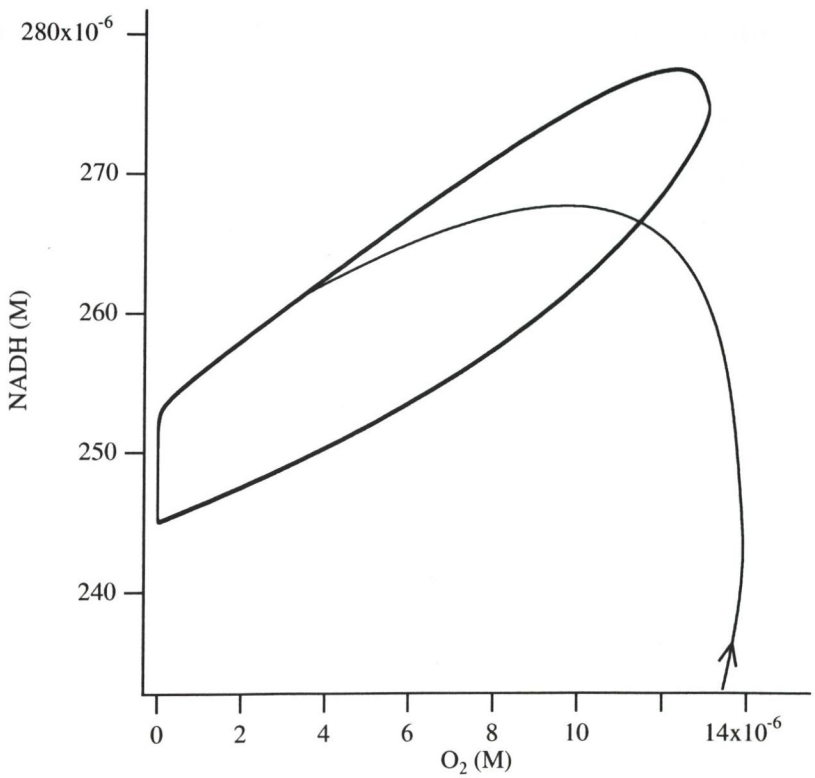

Figure 7.6: Stable limit cycle emerging in NADH-O_2 phase space. Rate constants and other conditions were those of Figure 7.4.

Rate constant	Value			Units
	Model 1	Aguda-Larter [53]	Urbanalator [40]	
k_f	8.033×10^{-6}		1.72×10^{-5}	s^{-1}
k_t	2.55×10^{-4}		7.3×10^{-5}	s^{-1}
k_{-t}	9.1×10^{-3}		2.5×10^{-3}	s^{-1}
k_1	33	3×10^{-6}	33	s^{-1}
k_2	1.8×10^{7}	1.8×10^{7}	9.0×10^{6}	$M^{-1}\ s^{-1}$
k_3	5.4×10^{3}	5.4×10^{3}	9.44×10^{4}	$M^{-1}\ s^{-1}$
k_4	8.0×10^{2}	8.0×10^{2}	5.37×10^{4}	$M^{-1}\ s^{-1}$
k_5	1.9×10^{6}	1.9×10^{6}	1.7×10^{7}	$M^{-1}\ s^{-1}$
k_6	2.0×10^{9}	2.0×10^{9}	2.0×10^{9}	$M^{-1}\ s^{-1}$
k_7	1.3×10^{8}	1.3×10^{8}	1.3×10^{6}	$M^{-1}\ s^{-1}$
k_8	3.0×10^{7}	3.0×10^{7}	5.6×10^{7}	$M^{-1}\ s^{-1}$
k_9	1.1×10^{7}	1.1×10^{7}	2.0×10^{7}	$M^{-1}\ s^{-1}$
k_{10}	46	46		$M^{-1}\ s^{-1}$

Table 7.1: Rate constants compared.

With a standard set of parameter values giving simulated results that are in agreement with the regular sustained oscillations found in the laboratory, it will be instructive to vary certain of these parameters and observe the effects on the dynamical behaviour exhibited by Model 1.

The results obtained from a variation of k_t is shown in Figure 7.7. In fact, these data were generated by varying both k_t and k_{-t} by the same amount, thus fixing the value of K_{eq}. Unlike previous simulation experiments, the rate of influx of NADH was held constant throughout, so that the NADH rate equation in Madonna was simply

```
d/dt (NADH) = kf*NADHi - k1*NADH*O2 - k3*Co1*NADH - k4*Co2*NADH .
```

The oxygen concentration was set initially to that value of $O_{2(aq)}$ which is computable from $[O_{2(aq)}]_{eq} = [O_{2(g)}]_{eq}K_{eq} = [O_{2(g)}]k_t/k_{-t}$. The NADH concentration was 2.0×10^{-4} M at the start of each run, and k_f was chosen so as to minimise the time taken to form a stable limit cycle in NADH-O_2 phase space.

In similar fashion to the experimental results on varying gas flow rates that were described in Section 4.6, the amplitudes of oxygen oscillations appear to increase with increasing k_t. Unlike the data from those experiments, however, the wavelengths of the oscillations appear to decrease, so that the relationship between gas flow rate and oscillation amplitude and period may not be fully explained by the dependency of

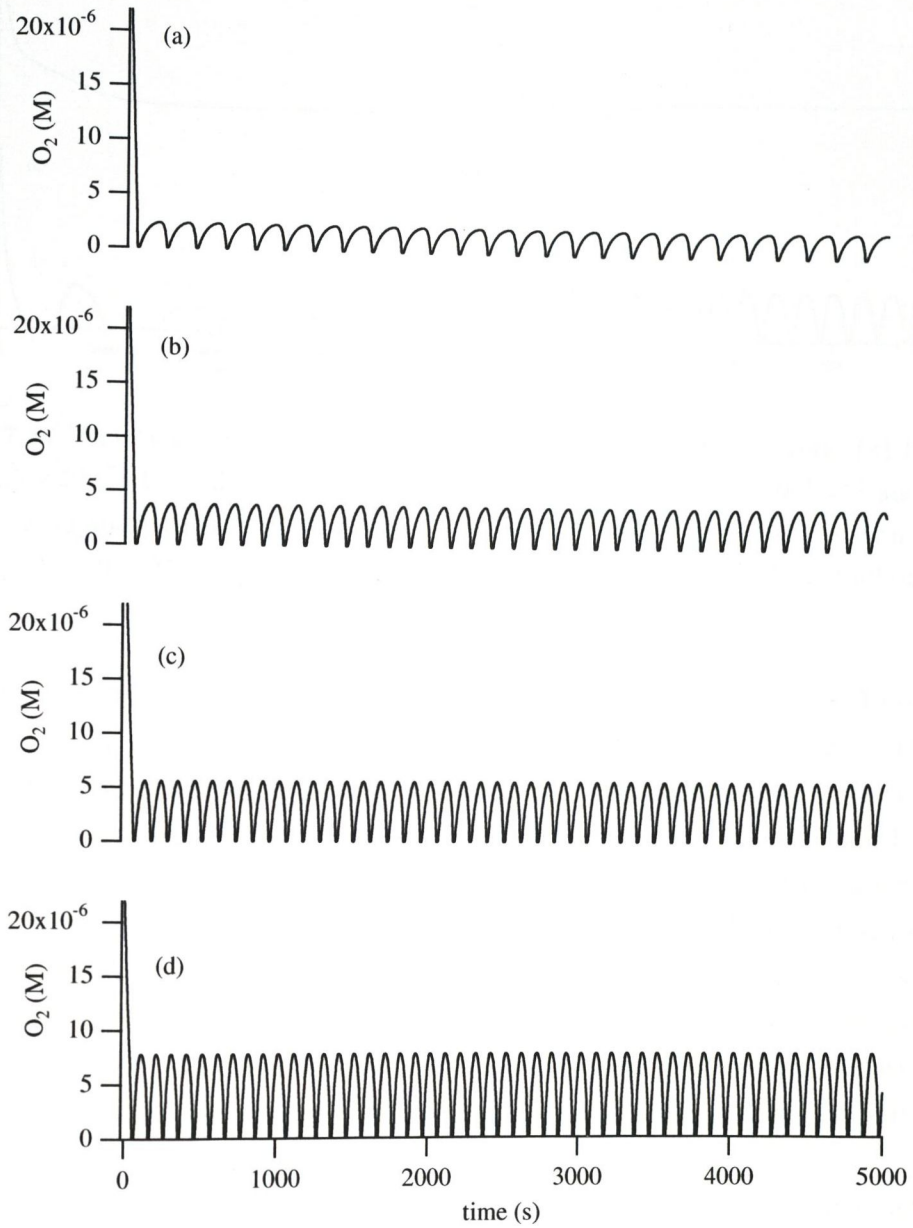

Figure 7.7: Variation of k_t in Model 1. (a) $k_t = 1.27414 \times 10^{-5}$ s^{-1}, $k_f = 1.2394 \times 10^{-6}$ s^{-1}; (b) $k_t = 6.27415 \times 10^{-4}$ s^{-1}, $k_f = 2.38 \times 10^{-6}$ s^{-1}; (c) $k_t = 2.54281 \times 10^{-4}$ s^{-1}, $k_f = 4.42 \times 10^{-6}$ s^{-1}; (d) $k_t = 5.09658 \times 10^{-4}$ s^{-1}, $k_f = 8.065 \times 10^{-6}$ s^{-1}. Other rate constants were: $k_1 = 33$ s^{-1}; $k_2 = 1.8 \times 10^7$ M^{-1} s^{-1}; $k_3 = 5400$ M^{-1} s^{-1}; $k_4 = 53700$ M^{-1} s^{-1}; $k_5 = 1.9 \times 10^6$ M^{-1} s^{-1}; $k_6 = 2.0 \times 10^9$ M^{-1} s^{-1}; $k_7 = 1.3 \times 10^8$ M^{-1} s^{-1}; $k_8 = 3 \times 10^7$ M^{-1} s^{-1}; $k_9 = 1.1 \times 10^7$ M^{-1} s^{-1}; $k_{10} = 46$ M^{-1} s^{-1}; $[O_{2(g)}] = 7.8 \times 10^{-4}$ M; $[NADH]_i$=0.08 M; Initial concentrations were: $[Per^{3+}]_0 = 3 \times 10^{-6}$ M, $[H_2O_2]_0 = 1 \times 10^{-9}$ M, $[O_2]_0 = 2.2 \times 10^{-5}$ M, $[NADH]_0 = 2.0 \times 10^{-4}$ M, all other concentrations were zero.

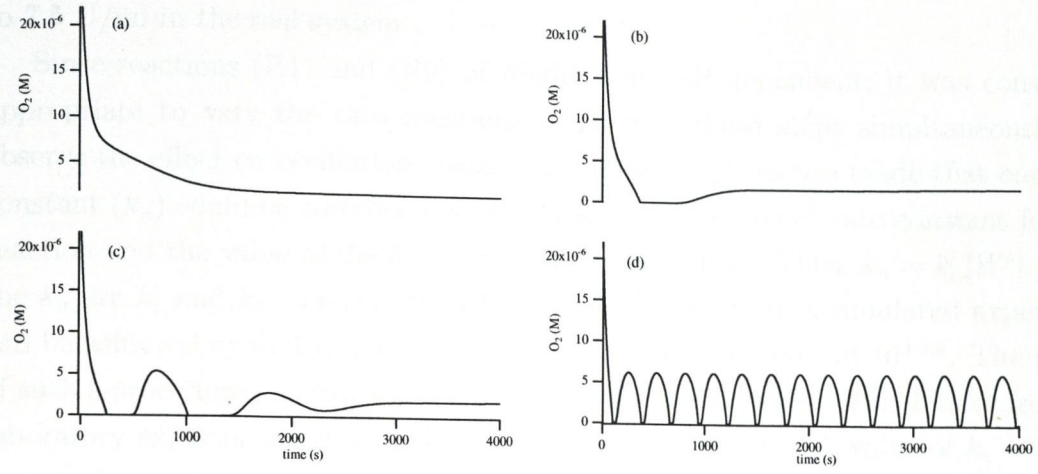

Figure 7.8: Variation of total enzyme. Initial concentrations of Per^{3+} were: (a) 1.25×10^{-7} M; (b) 2.5×10^{-7} M; (c) 3.0×10^{-7} M; (d) 6.0×10^{-7} M. k_f was 4.4×10^{-6} s^{-1} and all other rate constants and parameters were those of Figure 7.7. Initial values of the variables were: $[H_2O_2]_0 = 1 \times 10^{-9}$ M, $[O_2]_0 = 2.2 \times 10^{-5}$ M, $[NADH]_0 = 2.0 \times 10^{-4}$ M, and all others were set to zero.

k_{-t} on gas flow rate that was demonstrated in Section 3.3.2 (where see Figure 3.8).

Variation in peroxidase concentration can be achieved by changing the initial value of Per^{3+} in the present model, provided that the other enzyme species are set to zero concentration at start. The principle of enzyme conservation then holds, *i.e.*, $[Per^{3+}]_0 = [Per^{3+}] + [CoI] + [CoII] + [CoIII]$. The value of $[Per^{3+}]_0$ was varied between 1.25×10^{-7} and 6×10^{-7} M. Four simulated oxygen traces are displayed in Figure 7.8. All other parameters were held constant through this set of simulations. No oscillations are visible at the lowest enzyme concentrations, and damped oscillations occur with $[Per^{3+}]_0 = 3 \times 10^{-7}$, sustained oscillations appearing at twice this value. It is evident that in this region of parameter space the system switches stability from a steady-state to a periodic attractor.

In passing, we note that, in this simulation experiment, sustained oscillations would have been obtained at the lower enzyme concentrations if compensatory changes had been made to k_f in order to balance changes in the overall oxidation rate. The peroxidase concentration was chosen to be the only parameter that should changed between each simulation run. In addition, if we assume that a linear relationship exists between peroxidase concentration and its activity, then an approximate value for the activity may calculated from the ratio of activity and concentration values shown in Table 4.1. There, 40 U/ml HRP corresponds to a concentration of 3.2 μM, so that the value of 0.6 μM HRP used to generate the data in Figure 7.8(d) will correspond

to 7.5 U/ml in the real system.

Since reactions (R1) and (R9) of Model 1 are pH-dependent, it was considered appropriate to vary the rate constants of both of these steps simultaneously and observe the effect on oscillation character. The assumption was made that each rate constant (k_n) could be considered as the product of the "true" rate constant for that reaction and the value of the hydrogen ion concentration. Thus, $k_n = k'_n[H^+]$, where the k_n are k_1 and k_9. Varying the pH by $\pm$ 0.5 pH units in a simulated experiment can be achieved by multiplying both rate constants by a factor of $10^{\pm 0.5}$. The results of such a procedure are shown in Figure 7.9 and may be compared with data from the laboratory experiments that were presented in Section 5.3.2. A value of $k_1 = 33$ s^{-1} was used as a starting point, and since this value was computed by Olson *et al.* [20] for a pH of 5.1, the pH range of the model runs is approximately 4.5–6.5. k_f was chosen in each case so as to minimise the time taken to reach stable limit-cycle in NADH-O_2 phase space.

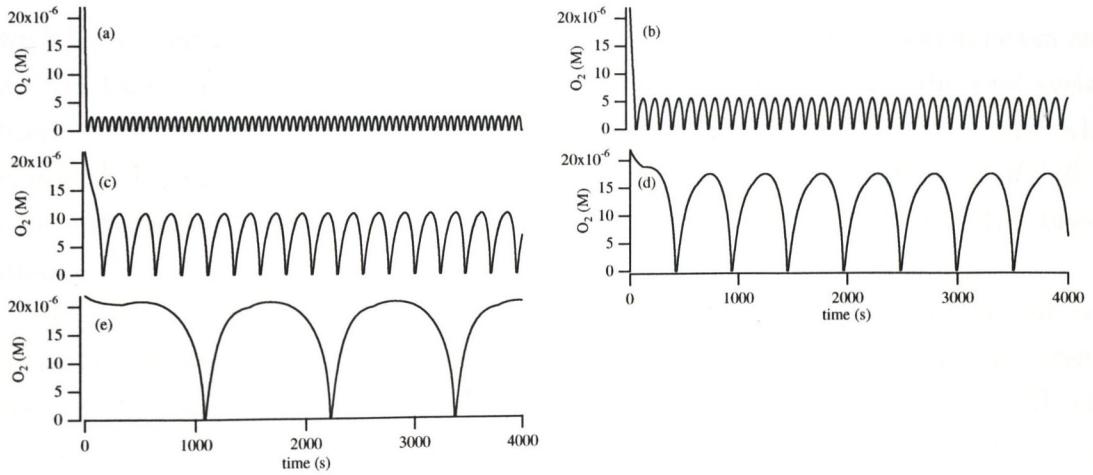

Figure 7.9: Testing pH-dependent steps of Model 1. The values of k_1, k_9 and k_f were as follows: (a) $k_1 = 104.4$ M^{-1} s^{-1}, $k_9 = 3.48 \times 10^7$ M^{-1} s^{-1}, $k_f = 4.95 \times 10^{-6}$ s^{-1}; (b) $k_1 = 33$ M^{-1} s^{-1}, $k_9 = 1.1 \times 10^7$ M^{-1} s^{-1}, $k_f = 4.43 \times 10^{-6}$ s^{-1}; (c) $k_1 = 10.44$ M^{-1} s^{-1}, $k_9 = 3.48 \times 10^6$ M^{-1} s^{-1}, $k_f = 3.45 \times 10^{-6}$ s^{-1}; (d) $k_1 = 3.3$ M^{-1} s^{-1}, $k_9 = 1.1 \times 10^6$ M^{-1} s^{-1}, $k_f = 2.13 \times 10^{-6}$ s^{-1}; (e) $k_1 = 1.044$ M^{-1} s^{-1}, $k_9 = 3.48 \times 10^5$ M^{-1} s^{-1}, $k_f = 1.19 \times 10^{-6}$ s^{-1}; k_f was 4.4×10^{-6} s^{-1} and the values of the other model constants were those of Figure 7.7. Initial values of the variables were: $[Per^{3+}]_0 = 3 \times 10^{-6}$ M, $[H_2O_2]_0 = 1 \times 10^{-9}$ M, $[O_2]_0 = 2.2 \times 10^{-5}$ M, $[NADH]_0 = 2.0 \times 10^{-4}$ M, and all others were zero.

Increasing the pH of the simulated reaction system has the effect of increasing the amplitude, period, and character of the oscillation train, which is largely in agreement

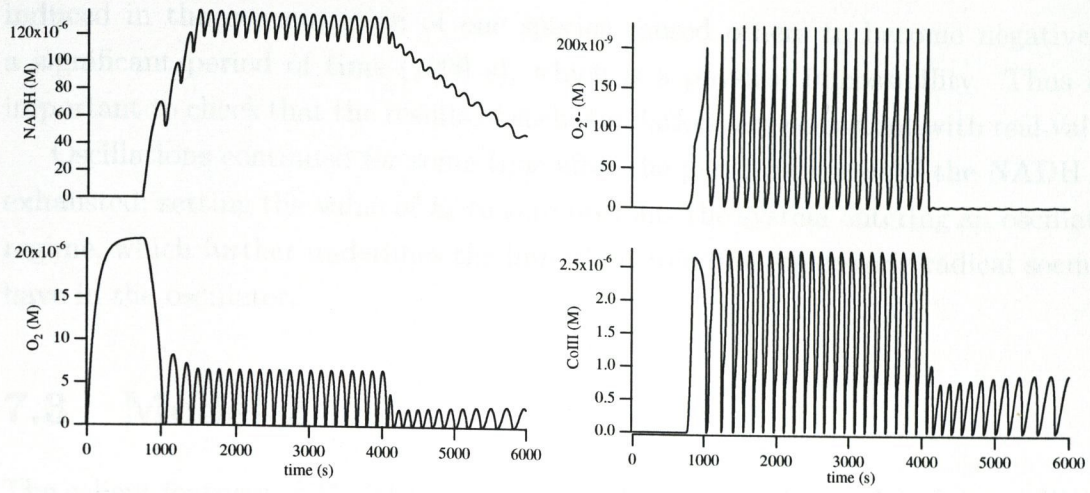

Figure 7.10: Simulated SOD perturbation was made by the method outlined on the text. The value of `sf` was 999, the perturbation was made after 4090 s, $k_f = 6 \times 10^{-6}$ s^{-1} and $r_f = 0.71$. Initial conditions and all other parameters were those of Figure 7.7.

with the experimental results. The initiation and superoxide disproportionation steps do not take into account of the full effect that pH might have on the real system, however; in Model 1 there is no reaction involving any form of the peroxidase which explicitly incorporates [H^+]. The Urbanalator model proposed by Olson *et al.* [40, 20] contains two such steps, which are the equivalent of (R2) and (R5) in the present model.

The final simulation experiment that concludes this section was performed as an investigation into superoxide dismutase inhibition of the model system. The premise behind the procedure which follows is that a pulsatile addition of SOD will affect the rate constant of superoxide disproportionation substantially, and consequently the method of implementation was the addition of a suitable modifying factor to all terms involving [O_2^-] in the Madonna equation file. Each term containing k_9 was multiplied by `(1+sf*(TIME>ADDT))`, where `sf` is a "SOD factor" that mimics such an addition that is made after `ADDT` elapsed seconds.

Figure 7.10 shows sample traces of oxygen, NADH and O_2^- concentrations, with `ADDT`=4090 s, and `sf`=999. The rate constant k_9 was instantaneously changed to 10^3 times its initial value, in this case to 1.1×10^{10} M^{-1} s^{-1}. The [O_2^-] is seen to drop immediately to near zero, and the NADH oxidation rate to decline. This is similar in the main to the laboratory findings, where increased damping was observed with successive additions of SOD.

An important practical issue is one of the stability of the integration procedure to sudden changes in the rate constants. For higher values of `sf` the sudden change

induced in the concentration of one species caused others to become negative for a significant period of time (1000 s), which is a physical impossibility. Thus it is important to check that the results of such simulations are consistent with real values.

Oscillations continued for some time after the perturbation until the NADH was exhausted; setting the value of k_6 to zero prevents the system entering an oscillatory regime, which further underlines the important role that superoxide radical seems to have in the oscillator.

7.3 Model 2

The salient features of Model 1 can be distilled into a simpler model of the oscillatory behaviour of the peroxidase-oxidase reaction. This section is devoted to the exposition and mathematical treatment of such a model.

The basic concepts of Model 1 are: (*i*) the system is held thermodynamically open by the continuous input of substrates, (*ii*) the autocatalytic production of the free radical intermediate $NAD^{\bullet}$, and (*iii*) cycling of the peroxidase enzyme between two main catalytic states that have semi-independent roles in the production of the intermediate.

The reasoning behind the development of Model 2 can be followed by a consideration of the Model 1 reaction network diagram (Figure 7.1). Let A, B denote two reactant species, E and F represent two oxidation states of the enzyme, and X denote an intermediate. Concept (*i*) above defines substrate input, thus we have

$$\xrightarrow{k_1} \mathrm{A} \quad \text{(S1)}$$

$$\underset{k_{-2}}{\overset{k_2}{\rightleftharpoons}} \mathrm{B} \quad \text{(S2)}$$

as the first steps of the Model 2. In Model 1 these substrates go to produce two molecules of the intermediate X in one catalytic cycle involving E, which is reformed in the process. This is effectively the sum of reactions (R1)–(R4) in Model 1, which yields

$$\mathrm{A} + \mathrm{B} \xrightarrow{k_3} 2\mathrm{X} \quad \text{(S3)}$$

The sum of the Model 1 reactions (R5) and (R6) yield CoIII from O_2, $NAD^{\bullet}$ and Per^{3+}, which gives us the fourth reaction of Model 2:

$$\mathrm{B} + \mathrm{X} + \mathrm{E} \xrightarrow{k_4} \mathrm{F} \quad \text{(S4)}$$

The F form of the peroxidase is involved in the autocatalytic production of X, reforming E in the process:

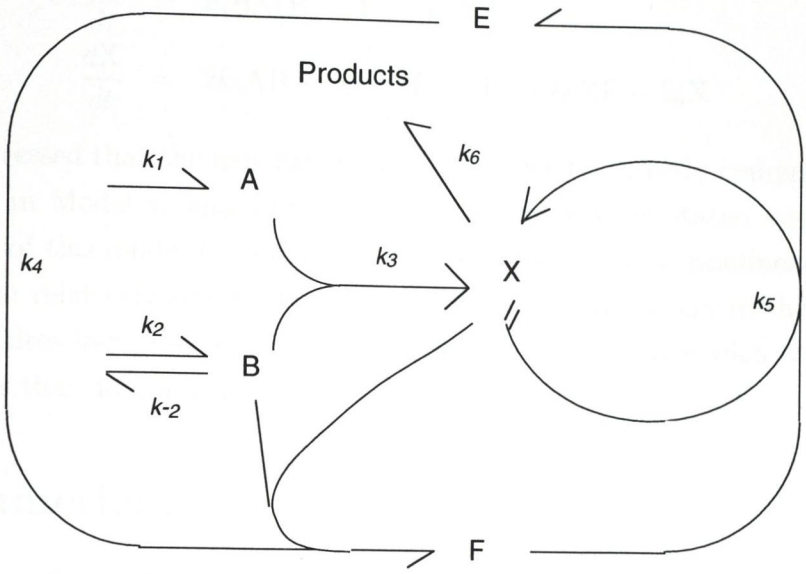

Figure 7.11: Diagram of the 4-variable model.

$$X + F \xrightarrow{k_5} 2X + E \quad (S5)$$

Finally, X is removed from the system:

$$X \xrightarrow{k_6} \text{Products} \quad (S6)$$

which encapsulates all of the reaction steps of Model 1 that produce inactive forms of NAD, (R1), (R6) and (R8). The combined reactions of Model 2 are

$$\xrightarrow{k_1} A \quad (S1)$$
$$\underset{k_{-2}}{\overset{k_2}{\rightleftharpoons}} B \quad (S2)$$
$$A + B \xrightarrow{k_3} 2X \quad (S3)$$
$$B + X + E \xrightarrow{k_4} F \quad (S4)$$
$$X + F \xrightarrow{k_5} 2X + E \quad (S5)$$
$$X \xrightarrow{k_6} \text{Products} \quad (S6)$$

and are depicted in the scheme shown in Figure 7.11.

Applying the law of enzyme conservation, we must have $E + F = E_0$, and so the system of differential equations describing this model may be reduced to four variables, A, B, X and F, where $(E_0 - F)$ replaces E wherever it appears in the rate equations. The model expressed in differential equation form is therefore:

$$\frac{dA}{dt} = k_1 - k_3 AB \quad (7.12)$$

$$\frac{dB}{dt} = k_2 B_0 - k_{-2} B - k_3 AB - k_4 BX(E_0 - F) \quad (7.13)$$

$$\frac{dF}{dt} = k_4 BX(E_0 - F) - k_5 XF \quad (7.14)$$

$$\frac{dX}{dt} = 2k_3 AB - k_4 BX(E_0 - F) + k_5 XF - k_6 X \quad (7.15)$$

It must be stressed that the new rate constants cannot be directly compared to their counterparts in Model 1, and values of the variables will be stated without units. The purpose of this model is to demonstrate the principle that nonlinear behaviour can arise from relatively simple (bio)chemical systems. Reduction in the number of variables requires less processing time, and oscillations can arise with combinations of parameters that do not yield a stiff[3] system.

7.4 Numerical integration of Model 2

The equations (7.12)–(7.15) were integrated numerically in the computer program Madonna using a fourth-order Runge-Kutta algorithm and step-size of 0.01.

Model 2 is capable of showing a variety of dynamical behaviours when certain parameters are varied. The most basic of such behaviours is the bifurcation from an attracting steady-state point in phase space to a limit cycle, which epitomises the behaviour exhibited by Model 1 and the experimental system. A sequence of traces at various values of the parameter k_5 are shown in Figure 7.12. A limit cycle in A-B phase space appears as the parameter k_5 drops below 53.

A finite region of k_5-k_4 parameter space was tested for convergence to a steady-state point or periodic attractor, the results of which are summarised by the contour plot in Figure 7.13, in which the curves mark the approximate boundaries between regions of sustained, damped and no oscillations. All other parameters were as Figure 7.12. Changes to the other parameters give rise to a different distribution pattern.

7.4.1 Complex oscillations

Complex oscillations can be observed for limited set of parameter values in Model 2. For example, oscillations of period 2, 4, 13 and 26 were observed at different E_0 values, as was also a seemingly aperiodic regime. An example of period-4 oscillations is shown in Figure 7.14, along with a 2-dimensional phase plots of B versus A and F

[3] *Stiff* systems of differential equations arise when solutions of the dependent variables exist on very different scales of the independent variable, causing the more basic numerical integration methods to become unstable. For further discussion, see, for example, references [68] and [69].

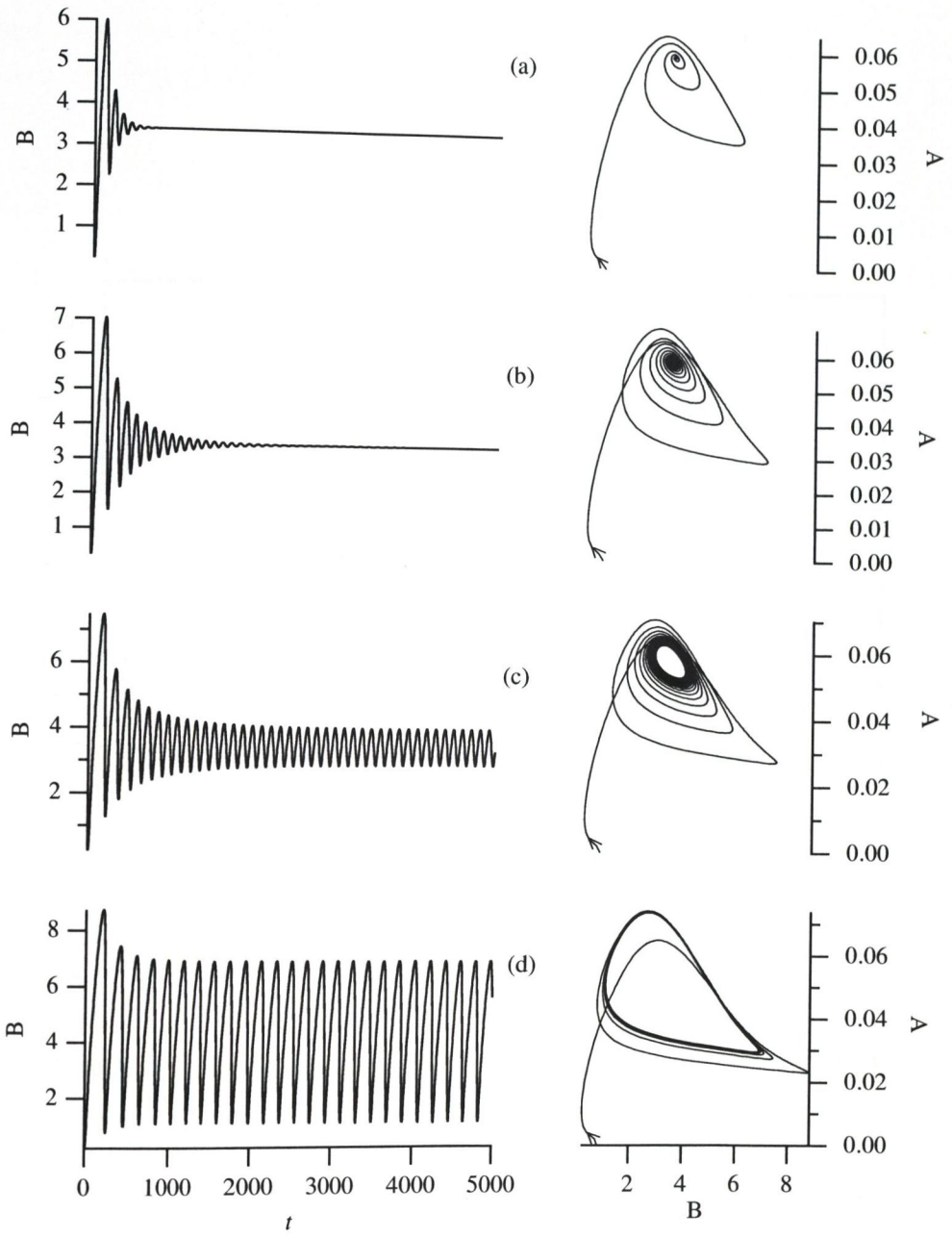

Figure 7.12: Emergence of sustained oscillations in Model 2. Shown are four sets of graphs of B versus time t and A versus B at four different values of k_5, which were (a) 64, (b) 55, (c) 52 and (d) 45. Initial values of the four variables were: A = 0, B = 0.808, F = 0.868475 and X = 0.00452. The values of the remaining parameters were: $k_1 = 0.01$, $k_2 = 0.2$, $k_{-2} = 0.02$, $k_3 = 0.05$, $k_4 = 1$, $k_6 = 1$, $B_0 = 2$ and $E_0 = 5$.

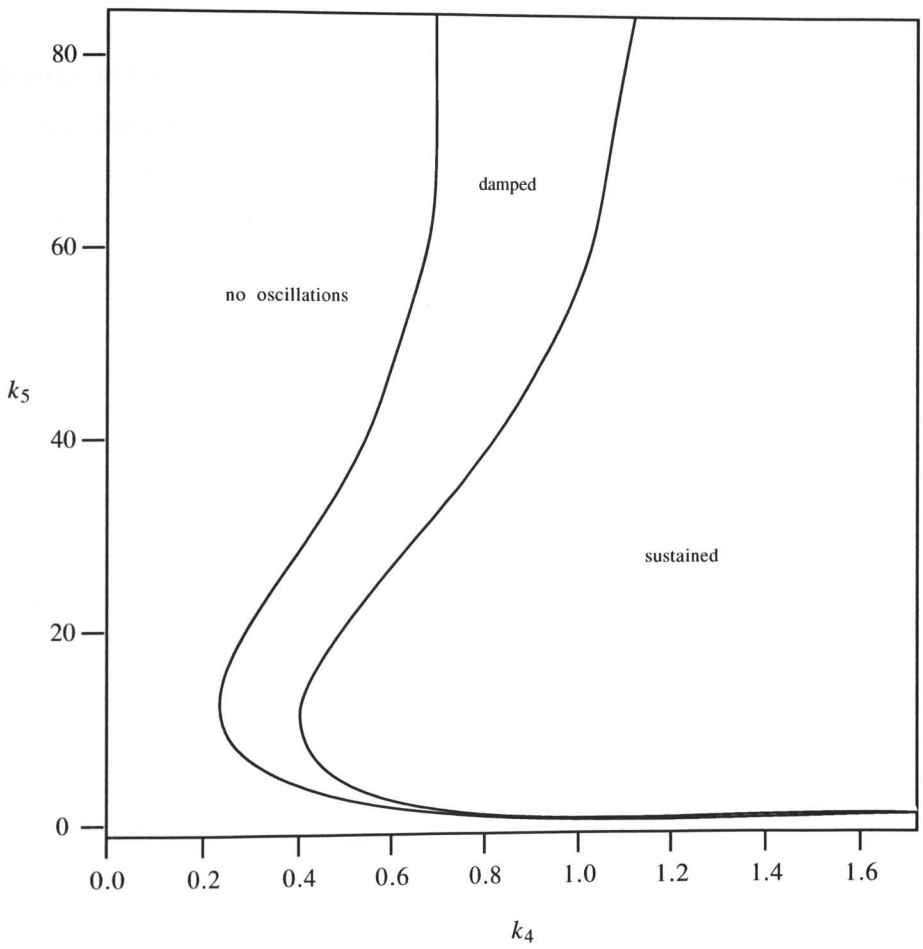

Figure 7.13: Distribution of oscillations in k_5-k_4 space. Other parameters were those of Figure 7.12.

versus X, each of which exhibits a non-simple closed curve in phase space. Figure 7.15 shows an aperiodic regime which appears at $E_0 = 0.64$. The X trace in both Figures shows large and small peaks, the numbers of each kind changing as the parameter E_0 was varied in the region 0.55–1.0. A useful method of describing the pattern of such "mixed-mode" oscillations [70] is with a *firing number*, F, defined as the ratio of small peaks to the total number of peaks in the largest repeating unit. If the number of small peaks is denoted by s and that of the large peaks by L, then we have

$$F = \frac{s}{L+s} \tag{7.16}$$

Hence the firing number of the 2^2 regime in the period-4 example is $F = 0.5$. To obtain the firing numbers of concatenations of repeating units, such as $1^2 1^3$ (one large and two small, followed by one large and three small oscillations), Farey arithmetic [71] must be used. For two rational firing numbers, p_1/q_1, p_2/q_2, the Farey sum ($\oplus$) is taken:

$$\frac{p_1}{q_1} \oplus \frac{p_2}{q_2} = \frac{p_1 + p_2}{q_1 + q_2}$$

Irrational firing numbers cannot be so expressed, and these are likely to give rise to the kinds of non-periodic behaviour evident in Figure 7.15.

The aperiodic regime can be viewed in a number of different ways, one of which is by constructing a *Poincaré first-return map*. The method is illustrated in Figure 7.16 for the case of a trajectory in three dimensions. A Poincaré map plots the points of intersection of the trajectory with a 'surface of section', in this instance a plane. Those points intersecting the chosen plane in phase space which lie on a trajectory passing through that plane in one direction are plotted (these are the filled dots in Figure 7.16). Therefore a trajectory must make a full 'rotation' of one period or more before being plotted as a coordinate of the Poincaré map. Clearly, then, a period-one oscillation will have a Poincaré first-return map consisting of one point; a period-2 trajectory will have two points in the plane, and so on. A chaotic trajectory will often form an distinctive object that characterises the flow. Returning to the notation in Chapter 1, Section 1.1, the action of a flow ϕ_t can be encapsulated by a discrete map Ψ, which maps a point $\mathbf{p}_n$ on the Poincaré surface of section to $\mathbf{p}_{n+1}$. This is an iterative scheme, which can be formalised thus:

$$\mathbf{p}_{n+1} = \Psi(\mathbf{p}_n) \tag{7.17}$$

where $\mathbf{p}_n$, the nth point of the map, is a coordinate on the surface of section. In effect, the four-dimensional attractor arising from numerical integration of the system of continuous differential equations can reduced to an attractor embedded in a two-dimensional space (the Poincaré surface of section).

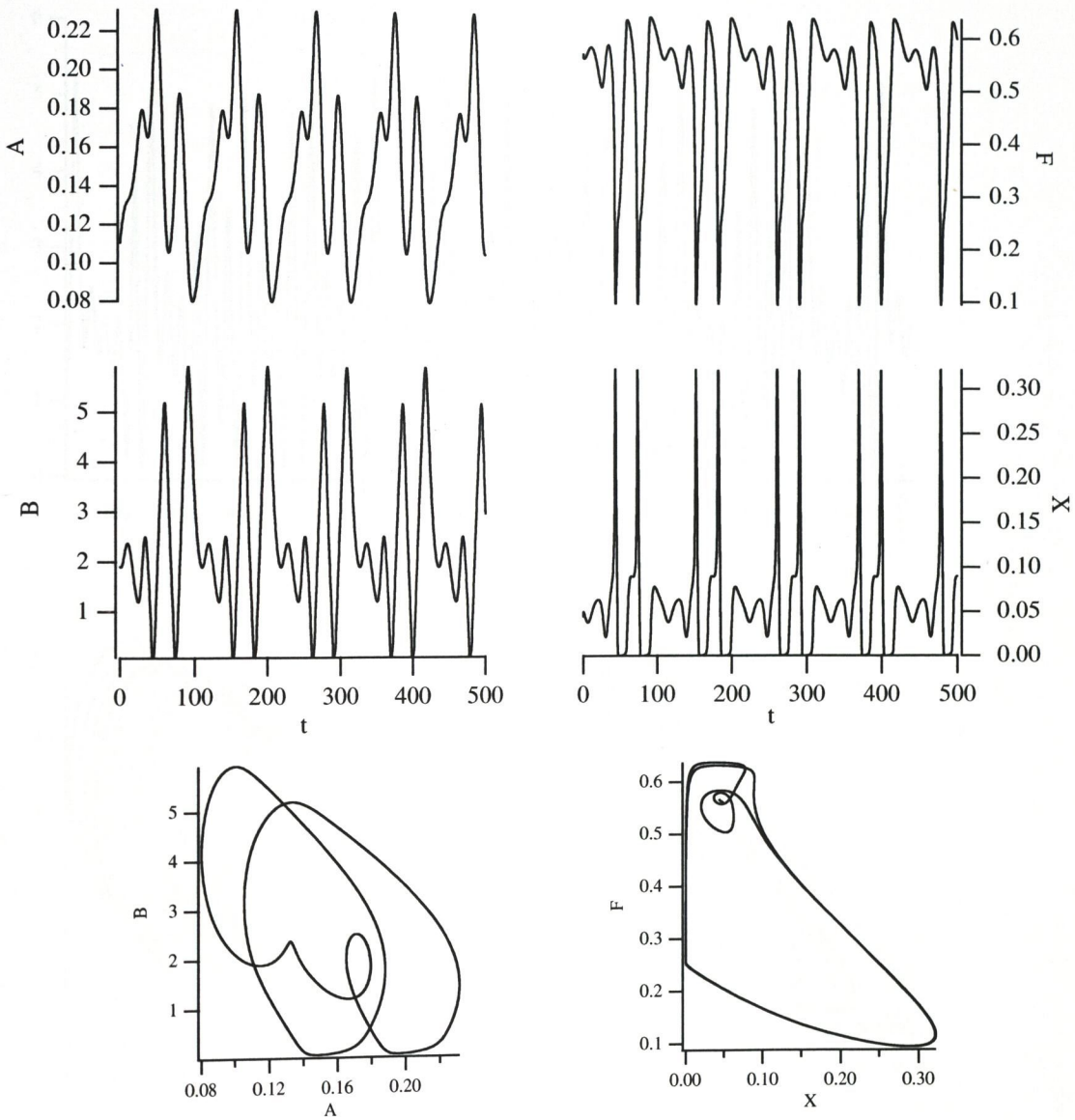

Figure 7.14: Period-4 oscillations in Model 2. Parameters values were: $k_1 = 0.01$, $k_2 = 1.3$, $k_{-2} = 0.007$, $k_3 = 0.03$, $k_4 = 40$, $k_6 = 0.34$, $B_0 = 0.3676$ and $E_0 = 0.683$.

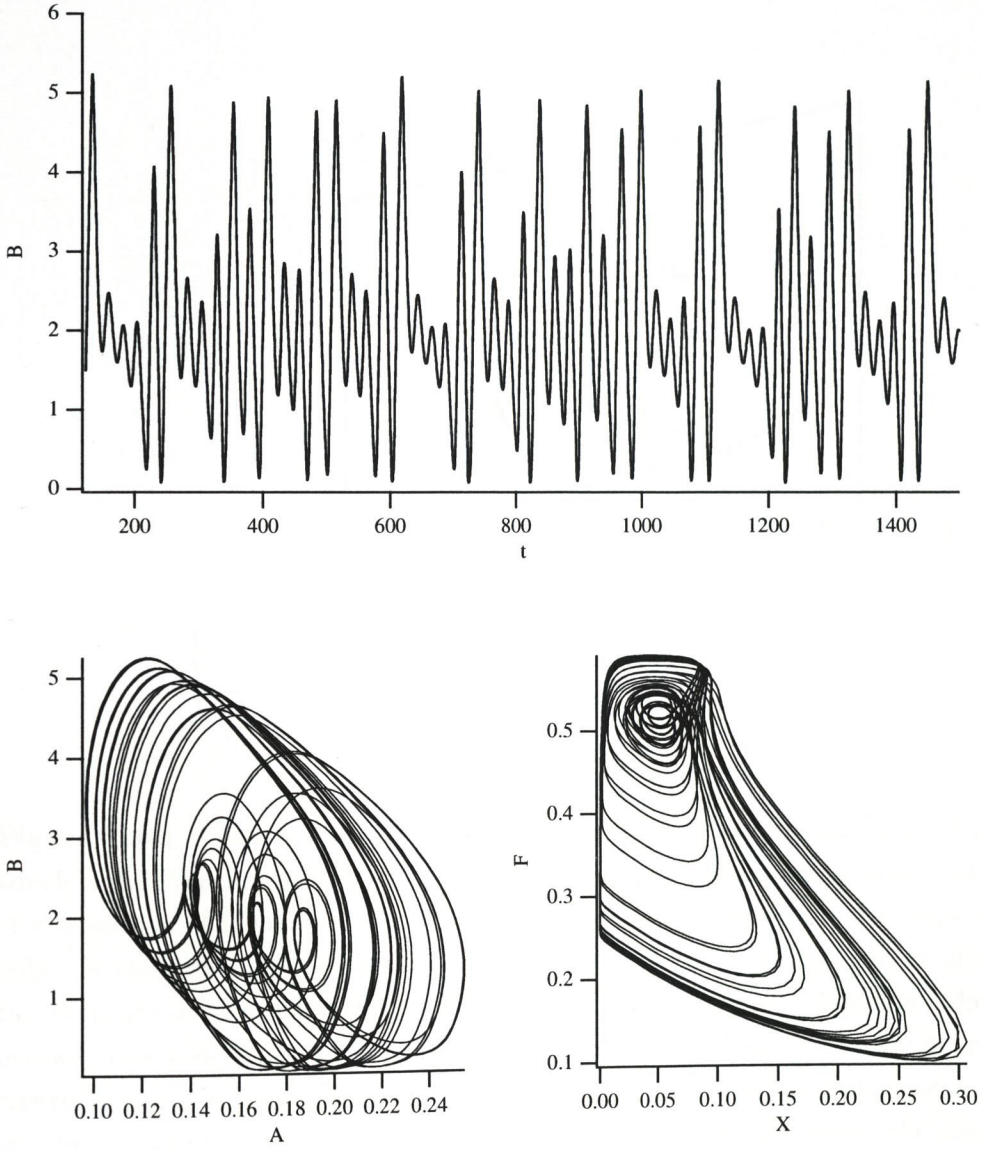

Figure 7.15: Aperiodic oscillations in Model 2. Parameter values were those of Figure 7.14 except that $E_0 = 0.64$.

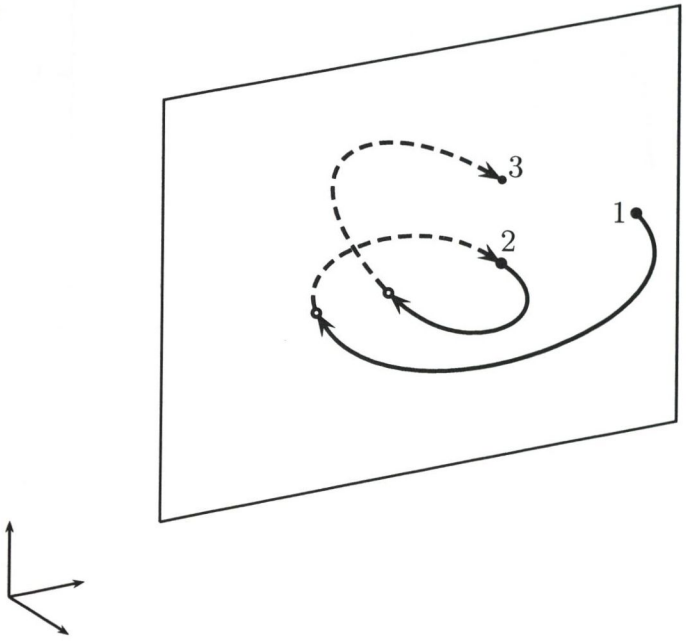

Figure 7.16: Poincaré first-return map. Shown is a plane in phase space (here, 3-space) which is the Poincaré surface of section, and a trajectory of a dynamical system. The points of intersection of the trajectory with the plane are plotted when the flow is in one direction only: in this case, out of the plane of the page. Solid lines are in front of the plane of the Poincaré section, dashed lines are behind it. The direction of flow is indicated by the arrows. The first-return map is so-called because it plots those points which are the first to return to the Poincaré surface of section under the action of the flow. The unfilled circles are the points of intersection of the trajectory with the section where the direction of the flow is into the plane: these are not plotted. The filled circles are the plotted points of the Poincaré map, and the numbers assigned to them are the iteration numbers of the map.

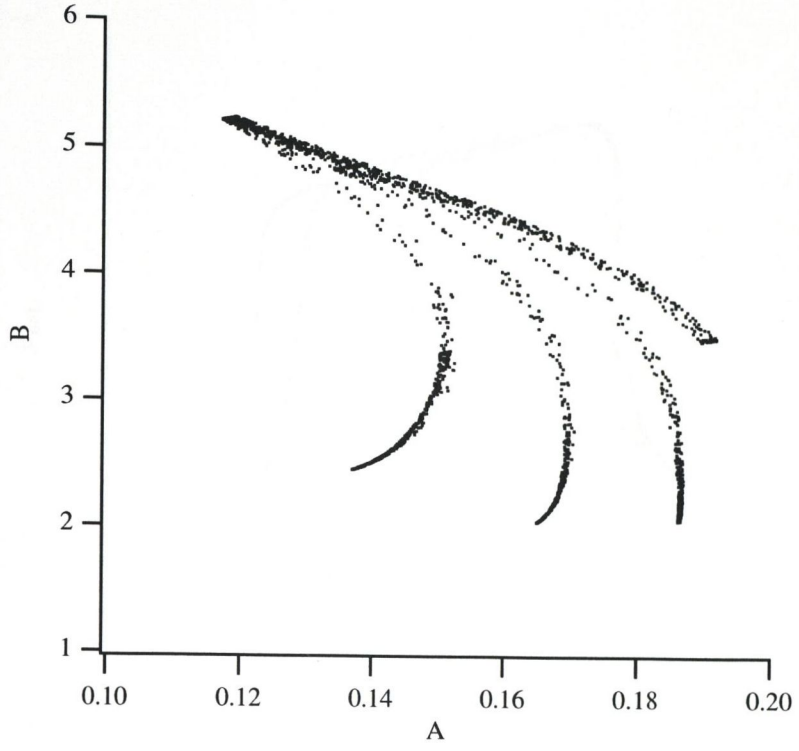

Figure 7.17: Poincaré first-return map of the putative chaotic attractor in Model 2. Data were generated using the parameter values of Figure 7.15 were treated in the manner described in the text. The Poincaré surface of section was a plane, orthogonal to the axis of F in phase space, situated at $F = 0.5$.

In Figure 7.17 a first-return map was plotted in the A-B plane by selecting the coordinates at which F passed through a value of 0.5 in the positive direction. The Equations 7.12–7.15 were integrated in Madonna using the parameters of Figure 7.15, and the data exported as 64,000 coordinates in the four-dimensional phase space. The data were imported into the Igor Pro graphing program, and a Poincaré first-return map was constructed using Igor Pro's built-in programming language. The source code of the program is given in Appendix A.5.

The above method is only a first approximation to the two-dimensional attractor underlying the flow, since the algorithm given in the Appendix does not attempt to interpolate between points not lying directly in the plane of the Poincaré section. The object in Figure 7.17 is thus "smeared" by the resulting error in each point of the map. An better method, suggested by Hénon [72], is to transform one of the dependent variables of an N-variable differential system into the independent variable. All points of intersection with a Poincaré section located at some point in the domain of the new independent variable will be points of integration of the

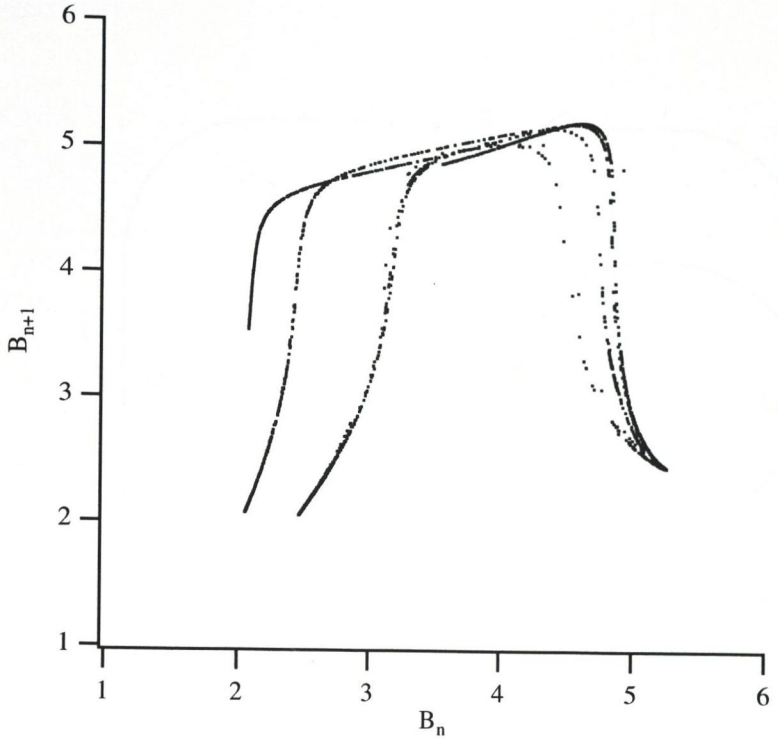

Figure 7.18: Next-amplitude plot showing a complex attractor underlying the data to Figure 7.15. In this graph, successive maxima of the variable B of Model 2 are plotted against each other by the method described in the text.

new system. To implement this, Hénon suggested that when the Poincaré section is perceived to have been crossed under during integration of the original equation set, a period of numerical integration of the transformed equations will bring the system onto the Poincaré section.

A similar technique for capturing low-dimensional behaviour of chaotic attractors is that of next-amplitude plots, where successive maxima of one variable are plotted in two dimensions. The deterministic flow that arises from integration of the describing equations of Model 2 can also be thought of as a map such as that of Equation 7.17. Thus a maximum M_n will be assumed to be mapped, under the action of the flow ϕ_t, to the maximum value of the next oscillation, M_{n+1}. The same data that were used to generate the attractor in Figure 7.17 were used as input to a separate Igor Pro script, written by the author and reproduced in Appendix A.6, which calculates maxima, M_n (for $n = 1, 2, \ldots$), in the time series of one variable and plots a graph of M_{n+1} against M_n for each n. The results are shown in Figure 7.18. In both Figures 7.17 and 7.18 the attractors are apparently complicated objects that display a very high, if not infinite, period order, which is further evidence to support the view that the

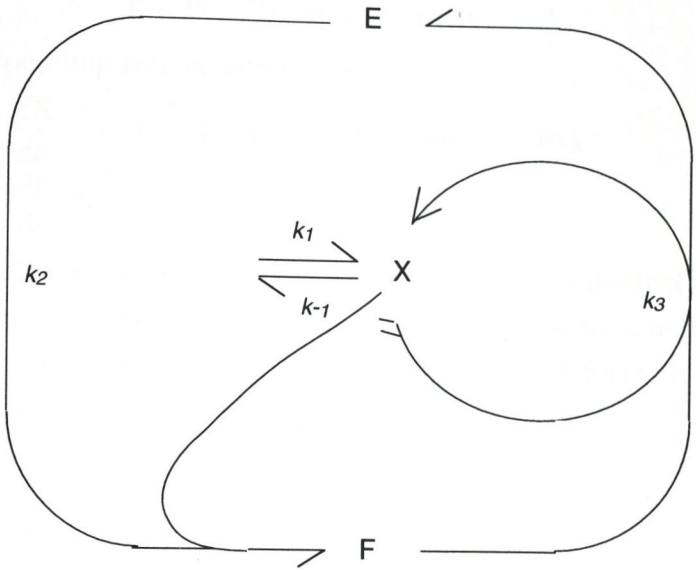

Figure 7.19: Model 3.

data in Figure 7.15 depicts a chaotic attractor. The method of plotting successive amplitudes has been employed by Lorenz [73], who observed a cusp-shaped attractor in numerical solutions of his model of fluid convection. As stated in Section 1.2, Olsen used the method to reveal the presence of a strange attractor in his model of peroxidase-oxidase oscillations [35]. This attractor and the one shown in Figure 7.18 display some topological similarity.

7.5 Model 3

A full mathematical treatment of Model 2 has not been attempted. The steady state values of the variables A, B, F and X were evaluated using Maple V[4]. Conversion to dimensionless units reduced the number of parameters from nine to seven, but the complexity of the steady state expressions was not reduced significantly. These, along with the results of the dimensional analysis, are reproduced in Appendix C. A third model was derived, based on Model 2, in which the two interconverting forms of the enzyme act upon a single substrate that in this case performed the role of all three substrates of Model 2. The model, which we will refer to hereafter as Model 3, is outlined as a scheme in Figure 7.19. The reactions of this system are:

[4]Waterloo Maple Software, 1998

$$\begin{array}{ll} \overset{k_1}{\underset{k_{-1}}{\rightleftharpoons}} \mathrm{X} & \text{(T1)} \\ \mathrm{E} + \mathrm{X} \xrightarrow{k_2} \mathrm{F} & \text{(T2)} \\ \mathrm{F} + 2\mathrm{X} \xrightarrow{k_3} 2\mathrm{X} + \mathrm{E} & \text{(T3)} \end{array}$$

for which the corresponding rate equations are

$$\begin{aligned} \frac{d\mathrm{X}}{dt'} &= k_1 - k_{-1}\mathrm{X} + k_3\mathrm{F}\mathrm{X}^2 - k_2(\mathrm{E}_0 - \mathrm{F})\mathrm{X} \\ \frac{d\mathrm{F}}{dt'} &= k_2(\mathrm{E}_0 - \mathrm{F})\mathrm{X} - k_3\mathrm{F}\mathrm{X}^2 \end{aligned}$$

and where the law of enzyme conservation has been used to substitute for the free native enzyme E wherever it appears. This two-variable model can be converted to dimensionless form by rescaling to a new time t. The final form that the model equations then take is

$$\frac{dx}{dt} = \alpha(1-x) + \alpha^2\gamma x^2 y - \alpha^2\beta x(1-y) \tag{7.18}$$

$$\frac{dy}{dt} = \alpha\beta x(1-y) - \alpha\gamma x^2 y \tag{7.19}$$

where $t = t'\mathrm{E}_0/k_1$, $x = k_{-1}\mathrm{X}/k_1$, $y = \mathrm{F}/\mathrm{E}_0$, $\alpha = k_1\mathrm{E}_0/k_{-1}$, $\beta = k_2/k_1$ and $\gamma = k_3/k_{-1}$.

The steady-state values of the variables (also called the stationary states, or fixed points, of the system; see Section 1.1), written as x_{ss} and y_{ss} are obtained by setting the time derivatives equal to zero and solving for each. It is easy to see that this gives a single stationary state P at

$$x_{ss} = 1, \quad y_{ss} = \frac{\beta}{\beta+\gamma}$$

An analysis of the stability of the steady state with respect to variation of one or more parameters is now much easier than for the preceding four- and nine-variable models. The first step of such a procedure is linearisation about the fixed point P, which is achieved by evaluating the Jacobian matrix $\mathbf{J}$ at P. The underlying principle is that infinitesimally small perturbations of the system about the fixed point(s) will grow or decay over time, and a study of the eigenvalues of $\mathbf{J}$ will indicate whether the system is stable or unstable at P, depending on the values of the parameters [74]. Equations 7.18 and 7.19 describe a nonlinear system of differential equations $\dot{\mathbf{x}} = \mathbf{f}(\mathbf{x})$ where

$$\begin{aligned} \mathbf{f}(\mathbf{x}) &= \begin{pmatrix} f_1(x,y) \\ f_2(x,y) \end{pmatrix} \\ &= \begin{pmatrix} \alpha(1-x) + \alpha^2\gamma x^2 y - \alpha^2\beta x(1-y) \\ \alpha\beta x(1-y) - \alpha\gamma x^2 y \end{pmatrix} \end{aligned}$$

The Jacobian at P is

$$\begin{aligned} \mathrm{J} &= \left(\begin{array}{cc} \partial f_1(x,y)/\partial x & \partial f_1(x,y)/\partial y \\ \partial f_2(x,y)/\partial x & \partial f_2(x,y)/\partial y \end{array} \right) \Bigg|_{(x,y)=(x_{ss},y_{ss})} \\ &= \left(\begin{array}{cc} -\alpha x_{ss} + 2\alpha^2\gamma x_{ss}y_{ss} - 2\alpha^2\beta x_{ss}(1-y_{ss}) & \alpha^2\gamma x_{ss}^2 + \alpha^2\beta x_{ss} \\ \alpha\beta(1-y_{ss}) - 2\alpha\gamma x_{ss}y_{ss} & -\alpha\beta x_{ss} - \alpha\gamma x_{ss}^2 \end{array} \right) \end{aligned}$$

The eigenvalues are the solutions λ to $|\mathbf{J} - \lambda\mathbf{I}| = \mathbf{0}$, where $\mathbf{I}$ is the identity matrix, which for the case of a 2×2 matrix gives the characteristic equation

$$\lambda^2 - \mathrm{tr}(\mathbf{J})\lambda + \det(\mathbf{J}) = 0 \tag{7.20}$$

and therefore

$$\lambda_{1,2} = \tfrac{1}{2}[\mathrm{tr}(\mathbf{J}) \pm (\mathrm{tr}(\mathbf{J})^2 - 4\det(\mathbf{J}))^{\frac{1}{2}})] \tag{7.21}$$

where $\mathrm{tr}(\mathbf{J})$ is the trace of the matrix $\mathbf{J}$, defined as the sum of the elements of the main diagonal, and $\det(\mathbf{J})$ is the determinant. The discriminant Δ is the term under the square root of Equation (7.21), namely $\mathrm{tr}(\mathbf{J})^2 - 4\det(\mathbf{J})$. If $\mathrm{tr}(\mathbf{J}) < 0$, $\det(\mathbf{J}) > 0$ and $\Delta > 0$ then the stationary state is a *stable node*, and all trajectories in some local neighbourhood N of P will decay monotonically to P as $t \to \infty$. If these conditions are altered so that the discriminant becomes negative, then the roots of the characteristic equation are complex, and trajectories will tend to P via damped oscillations. The stationary state P is called a *stable focus*. If $\mathrm{tr}(\mathbf{J}) = 0$ and $\det(\mathbf{J}) > 0$, there is the possibility of a Hopf bifurcation at P and the development of a stable limit cycle as a parameter μ of the linearised system increases through some critical parameter μ^*.

For this model, the value of the determinant is

$$\det(\mathbf{J}) = \alpha^2(\beta + \gamma) \tag{7.22}$$

which will always be positive, since α, β and γ are positive, by definition. The stability is therefore determined by the trace of $\mathbf{J}$:

$$\mathrm{tr}(\mathbf{J}) = -\alpha + 2\frac{\alpha^2\beta\gamma}{\beta+\gamma} - \alpha^2\beta(1 - \frac{\beta}{\beta+\gamma}) - \alpha\beta - \alpha\beta \tag{7.23}$$

Before continuing, we note that the analysis can be simplified by setting $\gamma = \beta$, so that P is now $(1, \frac{1}{2})$. We choose α as our Hopf bifurcation parameter, and set the trace of the Jacobian of Model 3 to zero, solving for α. The choice of α is appropriate, since it is equivalent to a variation of the total enzyme concentration, and provides

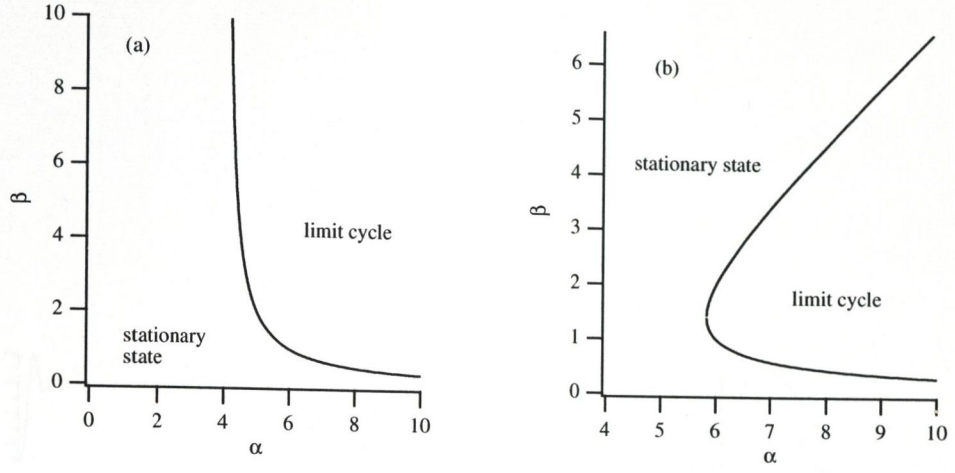

Figure 7.20: Loci of Hopf bifurcation points which demarcate regions of stability in α-β parameter space. In (a), $\beta = \gamma$, and (b), $\gamma = 1$.

a link to earlier simulation experiments with Model 1 and Model 2 (Figures 7.8, 7.14 and 7.15). Equation (7.23) is now

$$\mathrm{tr}(\mathbf{J}) = -\alpha - \frac{1}{2}\alpha^2\beta - 2\alpha\beta \tag{7.24}$$

Setting this equal to zero and solving for β gives

$$\beta = \frac{2}{4-\alpha} \tag{7.25}$$

as the preliminary condition for a Hopf bifurcation when $\beta = \gamma$ and $\alpha <> 4$ in Model 3. The general case is

$$\beta = \tfrac{1}{2}[\alpha\gamma - 2\gamma - 1 \pm \sqrt{\alpha^2\gamma^2 - 4\alpha\gamma^2 - 2\alpha\gamma + 1}] \tag{7.26}$$

The loci of possible Hopf bifurcation points in Model 3 are plotted in the graphs shown in Figure 7.20 for the cases $\beta = \gamma$ and $\gamma = 1$.

It can be easily verified that in the general case the lowest value of α for which a Hopf bifurcation is possible with positive β and γ is

$$\alpha = \frac{2\gamma + 1 \pm 2\sqrt{\gamma^2 + \gamma}}{\gamma}$$

In particular, at $\gamma = 1$, $\alpha^* = 3 + 2\sqrt{2} \approx 5.828\ldots$.

Although the stability analysis has not proven the existence of a stable limit cycle, computer simulation of Model 3 shows that stable oscillations do in fact appear as the Hopf locus is crossed in the direction of increasing α, some examples of which are

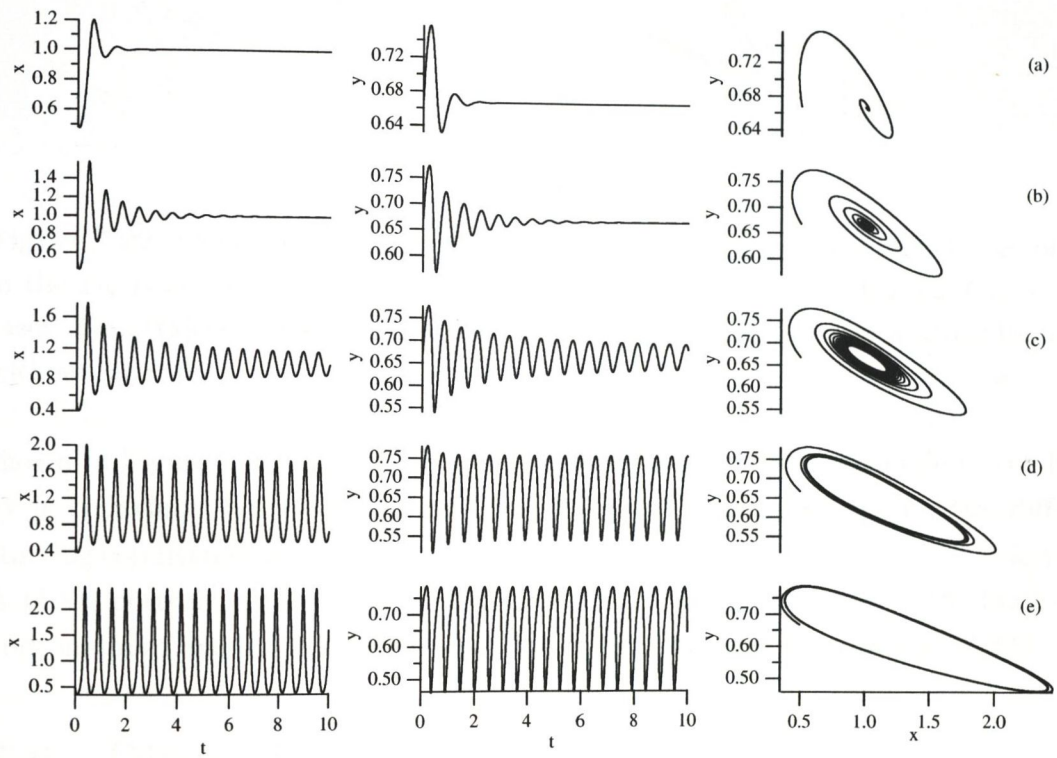

Figure 7.21: Computer simulation of Model 3. Graphs of x and y are plotted in the first two columns and the phase portrait of x and y is plotted in the last column. The values of β and γ were 2.0 and 1.0 respectively, and the values of the parameter α were (a) 4.2, (b) 5.6, (c) 6.0, (d) 6.4, and (e) 7.0. Between (c) and (d), a bifurcation occurs, with an exchange of stability between a stationary state in (c), and a limit cycle in (d).

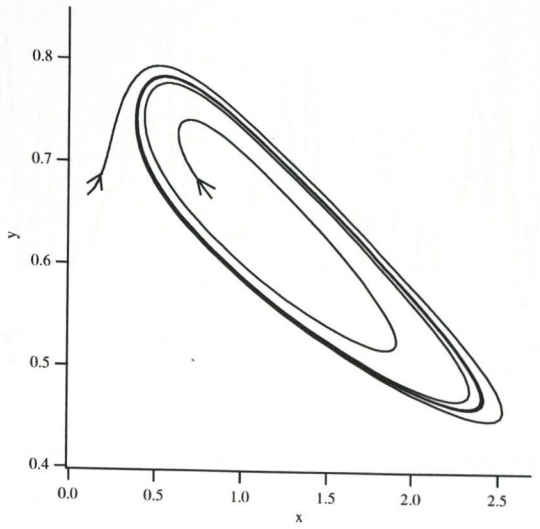

Figure 7.22: Example of a limit cycle in Model 3. Two trajectories of Model 3 are plotted in the x-y plane, with $\alpha = 7$, $\beta = 2$ and $\gamma = 1$. The initial value of y was 0.25 in both cases. Both trajectories settle to a stable limit cycle in phase space when starting from both without ($x_0 = 0.1$) and within ($x_0 = 0.82$) the region bounded by the closed curve.

shown in Figure 7.21 for $\beta = 2, \gamma = 1$ and $4.2 \leq \alpha \leq 7$. As an example of the limit-cycle behaviour illustrated in Figure 1.2, the model was integrated for two different starting conditions: $x = 0.1$ and $x = 0.82$, with $y = \beta/(\beta+\gamma)$ and $\alpha = 7, \beta = 2, \gamma = 1$. A phase portrait of the two trajectories, one emanating from outside the limit cycle and one from inside are shown in the phase portrait displayed in Figure 7.22.

7.6 Discussion

The PO reaction has been the subject of several theoretical papers in the period since its discovery. Among the earliest of the models developed is that of Yokota and Yamazaki [28], who studied the reaction experimentally in a closed system, and derived an eight-variable model which accounted for the four observable phases of the reaction which were, in order: an initial burst in oxyperoxidase (CoIII) formation, a short exponential induction phase, a steady state phase in which oxygen was consumed and hydrogen peroxide accumulated, and a termination phase which proceeded rapidly once oxygen had dropped below a critical level.

The Degn-Olsen-Perram model [33], and its later revision, the Olsen model [35] are four-variable models which give rise to a wide variety of behaviours, including chaos. Several oscillatory modes of the revised model have been shown to bear a marked similarity to patterns of oscillations observed in the real system [35]. The Olsen

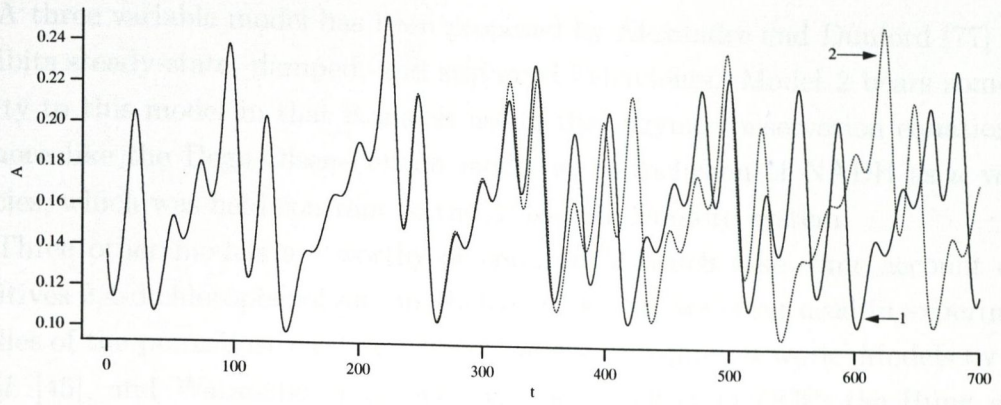

Figure 7.23: Sensitivity to initial conditions in Model 2. Two trajectories are plotted with initial conditions differing by only 1×10^{-5}. The trace labelled (1) started at A=0.13675 and trace (2) was begun at A=0.13676. The traces diverge after a few hundred time units have elapsed and behave independently thereafter.

models [33, 35] do not use rate constants that relate to known elementary reactions, but since they are dimensionless, reconstruction of real data would be a matter of rescaling were it not for the fact that two of the variables are without explicit physical counterparts, in contrast with Model 2, where each species is shown to have direct counterpart in the full model (Model 1). One of the hallmarks of chaotic behaviour is sensitivity to initial conditions, and in the 1983 paper [35], Olsen provides evidence for chaos through the assertion that small perturbations are absorbed by the system in periodic regimes, but that in those simulated time series which are apparently non-periodic two initial conditions separated by very small distances give rise eventually to completely different aperiodic trajectories. This phenomenon, described elsewhere as "sensitivity to initial conditions" [75], is apparent in Model 2: in Figure 7.23 the equations (7.12)-(7.15) are integrated numerically for two different values of A, but under otherwise identical conditions. The trajectories stay together for a limited period of time before diverging and taking wholly different paths in phase space. It is debatable whether the computer simulation in fact captures the chaotic attractor, since by definition errors are magnified through the action of the flow, and thus the computer's finite numerical precision entails that it will quickly become unable to follow the original trajectory; however, the fact that the error propagation occurs at all is sufficient reason to believe that data in Figures 7.15 and 7.23 are from a chaotic regime. Other numerical methods can be used to test for chaotic behaviour, perhaps the most widely known of these is the calculation of Lyapunov exponents of the system [76]. This has yet to be applied to Model 2, for want of an suitable algorithm.

A three variable model has been proposed by Alexandre and Dunford [77] which exhibits steady-state, damped, and sustained behaviours. Model 2 bears some similarity to this model in that it makes use of the enzyme conservation equation, but is more like the Degn-Olsen-Perram model in its inclusion of NADH as a varying species, which was held constant in the Alexandre-Dunford system.

Three other models are worthy of note, all of which take some account of the additives 2,4-dichlorophenol and methylene blue that are often used in experimental studies of the peroxidase-oxidase reaction, and in this present work. Models by Hung *et al.* [45], and Watanabe *et al.* [44] explore the effect of DCP; the Hung model, which comprises 18 chemical steps and 12 chemical species, employs the phenol in the generation of $NAD^{\bullet}$ from NADH via a two-step mechanism:

$$\mathrm{CoIII} + \mathrm{DCP} \longrightarrow \mathrm{Per}^{2+} + \mathrm{O}_2^- + \mathrm{DCP}^{\bullet}$$
$$\mathrm{DCP}^{\bullet} + \mathrm{NADH} \longrightarrow \mathrm{DCP} + \mathrm{NAD}^{\bullet}$$

The role of the Per^{2+} was not considered in Model 1, since the known rate constants of the reactions published in [53] that were used as a basis for the model seemed to indicate that this form of the enzyme will not play a significant part, the reasoning for which was as follows. In Table 2 of [53] rate of production of Per^{2+} by the reaction of $NAD^{\bullet}$ and CoIII, is described as "very slow", and can be removed in two reactions, the first by oxidation to CoIII at a rate of 5.8×10^{-4} M^{-1} s^{-1} and the other is a "very fast" reaction between Per^{2+} and CoIII to yield native peroxidase and CoI [28, 78, 79]. Therefore this enzyme species is likely to remain at a very low steady-state level in the oscillator. The main function of Per^{2+} in the Hung model is to increase the levels of $NAD^{\bullet}$, and it is doubtful if by this process DCP would facilitate the break down of CoIII, a role for DCP that has been postulated before by Olsen *et al.* [19]. If the Per^{2+} species could be experimentally distinguished from the other oxidation states of the peroxidase, then this might be a way to follow the DCP reaction(s) in a laboratory setting.

The Watanabe-Inaba model [44] also incorporates DCP into the reaction mechanism of the peroxidase-oxidase oscillator, and that towards a similar end, namely, the catalysis of NAD radical formation, though in this case non-enzymatically.

The closest model to that of Model 1 is the Urbanalator model, which involves 10 chemical steps, and employs the electron acceptor methylene blue as a mediator of the initiation step ((R1) in Model 1) in which MB cycles between the oxidised and reduced forms MB^+ and MBH.

Although at the expense of some realism, Model 3 has reduced the number of variables in a model of the PO reaction to two, in which the minimal conditions for

oscillations now appear to rely on a nonlinear rate law describing the time-evolution of a "lumped-substrate" species X catalysed by a cycling enzyme system. This is simply a truncation of Model 2 with the addition of a squared term to retain some of the nonlinearity of the four-variable model. It would be interesting to compare this model with the modified Lotka-Volterra model proposed by Degn and Mayer [80], which was found to only exhibit damped oscillations.

To summarise, a new 9-variable, 12-step model (Model 1) has been derived using a subset of the known reactions of substrates, proposed free radical intermediates and various oxidation states of haem peroxidase based on a combination of published and experimentally verifiable rate constants, and this model is in good quantitative and qualitative agreement with the various behaviours of the laboratory system described in earlier chapters. Furthermore, two successively truncated versions of this model (Model 2 and Model 3) have been developed which also exhibit oscillations. For the case of the simplest model, good evidence has been provided for a division of parameter space into regions of stable points and stable limit cycles. As one or more parameters of Model 3 are varied, there is reason to believe that a Hopf bifurcation occurs at points defined by the relationship expressed in Equation (7.26). To the author's knowledge, this is the first attempt to derive low-dimensional models from a more quantitatively accurate models in order to distil the essential features of the oscillator into simpler form. This concludes our experimental and theoretical treatment of the peroxidase-oxidase oscillator.

Chapter 8

General Discussion

8.1 In review

This study of the peroxidase-oxidase reaction has been successful in its aim of constructing a new laboratory system of apparatus for its study, and with it have been reproduced some of the behaviours typical of nonlinear chemical systems, such as bistability and damped and sustained oscillations. The apparatus has been characterised and the methodologies validated, and several physical and chemical properties of the experimental system have been elucidated. The apparatus makes use of standard 4 ml quartz cuvettes, which obviates the need for custom solutions that can be expensive to manufacture. This imparts a greater level of convenience to the study of what is, as yet, a relatively little studied oscillator.

Several novel discoveries have been made, experiments attempted, and theoretical avenues explored. To the author's knowledge, this is the first time that pH indicators were tested for use in the PO reaction. It has been shown that those chosen for this study strongly inhibited NADH oxidation, and although the mechanism was not clear, this may have been simply due to scavenging free radicals, the mechanistic importance of which were suggested by the similar effects of ascorbate and superoxide dismutase. Although the effect of pH on the PO reaction has been described in broad outline previously [24], this is the first time that a systematic study using two buffers has been made and the results presented graphically. Also novel is the study on ionic strength, which has shown the reaction to be non-oscillatory at values of 0.16 and above.

The use of tyramine, 4-aminophenol, and ascorbate as effectors has also not been published in the literature, and the results obtained with these agents tend to support the conclusions reached by Hauser and Olsen [1] in their study of naturally-occurring

phenols (see p.13). A new application of the tyramine-dityramine assay [67] to the mechanism of phenol-promoted oscillations has been reported here to be indirect evidence for the involvement of phenoxyl radical in promoting oscillatory activity of the PO reaction.

Various physico-chemical experiments were done that followed the groundwork laid down by Olson [40]. A statistical analysis of the oxygen mass-transport constant values obtained over many experiments performed using standard conditions (See Table 2.1) showed a gaussian distribution: an important observation, since variation of this physical parameter was shown to have a pronounced effects upon the dynamics.

Several theoretical models have been derived to account for various phenomena observed. The lag time visible in some of the oxygen data following a switch from zero oxygen at low total gas flow rates was modelled using two equilibrium steps. Although its appears to be difficult to fit such a model to some of these data, the new theory is nevertheless a starting point for future investigations. The PO reaction has been modelled afresh using known elementary reactions [53] and a selection of the published literature rate constants collated in two separate sources [53, 20]. The full model (Section 7.2) has been able to reproduce the type of oscillations observed in this laboratory, including the effect of pH on oscillation character, if not on their viability, and the influence of free radical scavengers. The successive reductions of the nine-variable model to four and two variables have elucidated one of the basic features of the PO reaction mechanism, which is the ability of the enzyme to switch between two catalytic states, both of which are involved in the production of free radical intermediates. It must be stressed that this is the first time that such an approach has been taken, and it provides a link between the lower-variable models favoured by Degn, Olsen and coworkers [80, 33, 35] and Larter *et al.* [42, 43] and the more complex, though ultimately more realistic, models of Olson, Williksen and Scheeline [20] and Hung, Schreiber and Ross [45]. The four-variable model evinces some of the more complicated behaviours that are possible in nonlinear systems, which in this instance may include a chaotic regime. The two-variable model derived here has been used to show how instabilities can arise through the variation of a parameter, such as the concentration of total enzyme, in which it predicts the existence of a Hopf bifurcation.

8.2 Reproducibility and the PO reaction

In the discussion of Chapter 4, it was stated that some dynamical behaviours were only rarely observed, such as the highly regular, sustained oscillations that were obtained on two successive occasions (see Figure 4.22) and which displayed a notably sharp

turning points. A partial explanation for appearance of the waveform is provided by the pH study described in Section 5.3.2 which displayed sharper oscillations at pH 4.5–5.0, in phosphate buffer. As a rule, the pH of the buffer was verified and adjusted before use, and it is unlikely that a deviation of small magnitude (0.1 pH units, for example) would be likely to completely account for both the change in appearance of the oxygen and enzyme traces. This illustrates the fact that the experimenter may not have complete knowledge of, or control over, the parameters influencing the reaction, which has particular significance for a nonlinear multistable system such as this, and it should not be surprising that inexplicable behaviours may observed on occasion. The fact that this particular observation was made on two successive runs with the same preparation of the enzyme and auxiliary reagents shows that it was not an artefact imposed by external agencies alone.

The importance of reproducibility has been emphasised by Olson [40], who has pointed out many of the deficiencies of the methods published in the literature, particularly the lack of critical experimental details necessary for accurate reproduction of the conditions under which reported behaviours were observed. An examination of both Table 4.1 and the literature cited therein sometimes will reveal the omission of important details, such as gas flow rate and buffer concentration, both of which have been shown in this study to influence the kinetic behaviour (see Chapter 3); researchers often do not quote the type of gas delivery apparatus used, the methods of calculating enzyme concentration (where activity units are not quoted) and the value of mass-transport constant. In the latter instance, even the underlying models of oxygen transport are not quoted, or have been shown by Olson to be based on the false assumption that the rate of oxygen entry is diffusion-controlled [40]. Nevertheless, even where such experimental details have been given, none of the work on higher-order dynamics was reproduced in this laboratory, and so it would appear that the results obtained are unique to apparatus and methodology of a particular group, and there are no attempts in the literature to corroborate other researchers' results, something that must surely be an important part of the scientific process. The sometimes paradoxical values that have been quoted for NADH influx rate [39] and gaseous oxygen composition [41] can only serve to inhibit independent replication of the data. It is hoped that the description of the methods employed in this laboratory gives experimental detail of sufficient quantity and reliability as to facilitate independent repetition of the results obtained here.

8.3 Directions for future work

Before discussing various experiments that might be performed to extend this study of the peroxidase-oxidase reaction it is important to mention one experiment that was not performed, which was the use of xanthine oxidase as a coupling enzyme to generate superoxide radicals and observe the effect on the character or durability of HRP-catalysed oscillations. Xanthine oxidase (for review, see [81]) has been used by Olsen [29] to predict the rate constant of Compound III formation from ferroperoxidase and O_2^- (see Chapter 7, p.121; reaction (R5) of Model 1). It was not used with the standard experimental system described in Chapter 2, since this system has included the auxiliary reagent, methylene blue, which has elsewhere been shown to be an inhibitor of the superoxide radical formation catalysed by xanthine oxidase [82], with the result that an experiment coupling the PO reaction under standard conditions was deemed likely to give negative or misleading results. It would be interesting to see if brilliant cresyl blue has a similar effect upon xanthine oxidase as does methylene blue. An interesting aspect to this problem is apparent in the proposed pharmaceutical use to which MB might be put, some seeing it as a potential antioxidant (described as a "parasitic" electron acceptor in [82]). At the same time, MB is seen in this and other studies as stabilising an oscillatory reaction which has at its core the production of free radicals, including superoxide anion. Although the reactions studied here have mainly involved a plant peroxidase, peroxidases from mammalian sources can also exhibit periodic behaviour (Section 5.6 and also Reference [47]) and this fact might have implications for the use of MB as a drug to relieve the effects of ischaemia and other similar pathological conditions.

A study of the interactions of methylene blue and brilliant cresyl blue with the peroxidase enzyme would help in the deduction of the mechanistic role that this species plays in prolonging oscillations, possibly by means of spectrophotometric methods. The work of Olsen [29] could be extended by testing for any influence that MB might have on the rate of decay of the Compound III formed through the action of xanthine oxidase. It is possible that methylene blue might prove to be an attenuator the rate of formation of CoIII.

While the recent study by Kummer *et al.* [47] on peroxidases from species other than horseradish has covered much new ground, it has not been exhaustive. Two other haem-peroxidases that have yet to be studied in this regard are cytochrome *c* peroxidase [83], and myeloperoxidase. The former of these has a peroxidatic mechanism that appears to be very similar to that of the horseradish variety [83]; if this can form an oxyperoxidase species (CoIII) then it might enable it to catalyse oscillatory

NADH oxidation.

Experiments with NAD-analogs, such as those studied by Kaplan *et al.* [84] would be another avenue of investigation. The reduced versions of these compunds, originally developed for the study of animal tissue NADases [84, 85], might show altered dynamics, or perhaps no oscillatory behaviour. Examples of such compounds are 3-acetylpyridine-adenine dinucleotide and thionicotinamide-adenine dinucleotide, which vary in the 2′- substituents of the pyridine ring. The theoretical work in Chapter 7 has demonstrated that NAD radical plays a central role in the nonlinearity of the reaction, and it may therefore be predicted that the readiness of these NAD analogs to form such radicals is likely to be an important determinant of the type of dynamics observed. Once again, careful attention would have to be paid to the reproducibility of the results in order to make valid comparison with to those obtained using NADH.

As stated in the discussion to Chapter 5, a closer examination of the pH region in which oscillatory motion becomes unstable (between pH 6 and 7) would be an interesting study; such an experiment would require several repetitions at each pH value to determine the average behaviour there. Also of interest would be pH experiments using lactoperoxidase, or perhaps of myeloperoxidase or cytochrome *c* peroxidase, should these prove to be capable of participating in the PO reaction. The incompatibility of both of the pH indicators tested in this study with the NADH-oxidation reaction leaves open only the use of a pH electrode for the study of pH changes during the course of an oscillatory reaction.

Further work is needed to determine the reason for the failure of the glucose-6-phosphate dehydrogenase NADH-recycling mechanism that was described in Section 5.5. It is possible that depletion of glucose-6-phosphate was the cause, and if this is correct, then continuous infusion of this reagent would prolong the lifetime of oscillations.

That free radicals are involved in the mechanism of the oscillator is clear from the work described in Chapter 6. Tyramine has been shown to be a weak promoter of oscillations but, since it is likely to be removed through dimerisation, the resultant behaviour was always damped oscillations. The mechanism of inhibition by the tyramine analogue 4-aminophenol is unclear, but may be due to free radical scavenging, in the manner of ascorbate. An examination of other classes of phenols that have not already been tested by other groups would be a logical extension of the phenol experiments described here.

The theoretical work of Chapter 7 can be built upon in several areas. The simulation model, Model 1, is the most realistic, since it is based on elementary reactions with experimentally-derived rate constants. Models 2 and 3 are mathematical analo-

gies of Model 1, and were derived for the value for their qualitative, rather than quantitative, similarity to the behaviour of the peroxidase-oxidase reaction. Model 1 may be extended in several ways. No model has yet incorporated both 2,4-DCP and MB explicitly in its reaction mechanism. Although these compounds have been variously omitted in two previous experimental studies: 2,4-DCP by Olson and Scheeline [62] and MB by Watanabe and Inaba [44], both were found to be necessary for sustained oscillations in the experimental studies carried out in this laboratory, and their inclusion together in a realistic model would be desirable. The results of the experiment suggested above that would test for any interaction between methylene blue and CoIII would aid in constructing a new role for MB, in keeping with the experimental findings of Olson and Scheeline [62] but also separate from that proposed for it by their Urbanalator model (see Section 1.2). It is significant to note, however, a point made in the development of Model 1, that in using the Urbanalator value for k_1 (of Model 1) a mechanistic role for MB can be said to have been implicitly assumed. Perhaps a dual function of this electron acceptor is possible in the real system, which would justify an expansion of its present role in an extended version of the simulation model.

The only parameters that were varied in the exposition of Model 1 were those which were linked to pH, NADH influx rate and oxygen transfer, all of which are under the control of the experimenter. It might be useful to observe the effect of varying one or more of the other parameters away from their measured values, which might give some indication of the importance of such steps to the reaction mechanism, and possibly improve on the likeness to the waveform data gathered experimentally. An obvious extension of the simulation experiment on pH is that the rate constants of reactions (R2) and (R5) (see Chapter 7, p.121) be included in further studies, since these are pH-dependent in the Urbanalator model [40, 20].

The development of the simpler four- and two-variable models by derivation from a realistic reaction scheme has also reduced in complexity the mathematical analysis. Some questions remain to be answered regarding the nature of the complex, aperiodic, oscillations of Model 2, for instance, which could be addressed by calculating a Lyapunov exponent for the time series data shown in Figure 7.15. A mathematical treatment of this model is also possible. For example, the steady state values of the variables in terms of the rate constants was determined using Maple V, but the resulting expressions were quite complex and for this reason were not included in the exposition of the model. The enzyme cycling mechanism which is at the heart of models 2 and 3 has been proposed in this work as key to a proper understanding of the oscillator. It would be interesting to develop a new model which incorporates

this concept with the mechanism for substrate inhibition and bistability in an open system that was the subject of an early paper by Degn [25].

Model 3, being the simplest of the PO reaction models that exhibits sustained oscillations, is perhaps suitable as a generator of oscillations in studies of the dynamics of generalised schemes of metabolism, and as such could be treated as a "black box" used for the effects of the transmission of an oscillating signal through branched or unbranched pathways.

8.4 Conclusion

Interest in oscillations in biochemistry is growing as it is fuelled by the discoveries that are continually being made in diverse areas of this subject. Cycling behaviours are ubiquitous: nerve impulses, the endocrine system, glycolysis, cell signalling, and cell division all have biochemical bases that may exhibit some of the properties that are common to chemical oscillators and the peroxidase-oxidase reaction. The peroxidase-oxidase reaction has proved a useful laboratory model of these time-periodic phenomena, and though its specific physiological role may not be clear, or even exist, it displays the necessary nonlinearities, through autocatalysis and bistability, that underlie many oscillating chemical systems. It is interesting to note that the behaviour in the laboratory is observed at low oxygen tensions, which is where the free radicals so inimical to the cell and its environment are generated in conditions of ischaemia and oxygen reperfusion.

Whatever that application, the dynamical behaviour that has been observed, is indication of the complexity of living systems that lies hidden at the molecular level. It is hoped that this experimental and theoretical exposition of a single-enzyme oscillator has brought us closer to an understanding of their mechanism.

Appendix A

Computer Program Source Codes

A.1 Source code of K_M.C

The following C source code is that of a program written by the author to compute, from dissolved oxygen data, the mass-transport constant defined in Chapter 2. The algorithm is an iterative fitting of the log-linear model of oxygen mass transport, derived in Section 2.3.2 as

$$\ln([O_{2(aq)}]_{eq} - [O_{2(aq)}]) = \ln[O_{2(aq)}]_{eq} - k_{-t}t. \tag{A.1}$$

to dissolved oxygen data sets. In the model equation, $[O_{2(aq)}]$ is the dependent variable and the time, t, is the independent variable. There are two unknowns, $[O_{2(aq)}]_{eq}$ and k_{-t}. The `n` measured dissolved-oxygen concentration values are stored in the array `c[]`. The program takes the last data point of the array `c[]` to be the closest to the true value of $[O_{2(aq)}]_{eq}$. This first approximation we denote C_1. The oxygen data is transformed to a new variable `y` by means of the left-hand side of the above equation:

$$y = \ln(C_1 - \texttt{c[]})$$

A new estimate of $[O_{2(aq)}]_{eq}$, which we will call C_2, is obtained through linear regression, along with a value for the mass-transport constant, k_{-t}. The process is repeated, with C_2 in place of C_1, etc., until the tolerance condition $|C_i - C_{i-1}|/C_i < \delta_c$ holds, with δ_c a small number (called `tol` in the source code), for some iteration step i. If the iteration process is convergent, and tolerance is achieved, the mass-transport constant is taken to be the negative of the slope of linear regression line.

With real data, the process may not be convergent, *i.e.*, the set maximum number of iterations may be exceeded before tolerance is achieved, which is sometimes the case with data which do not transform linearly, such as those displaying a lag time

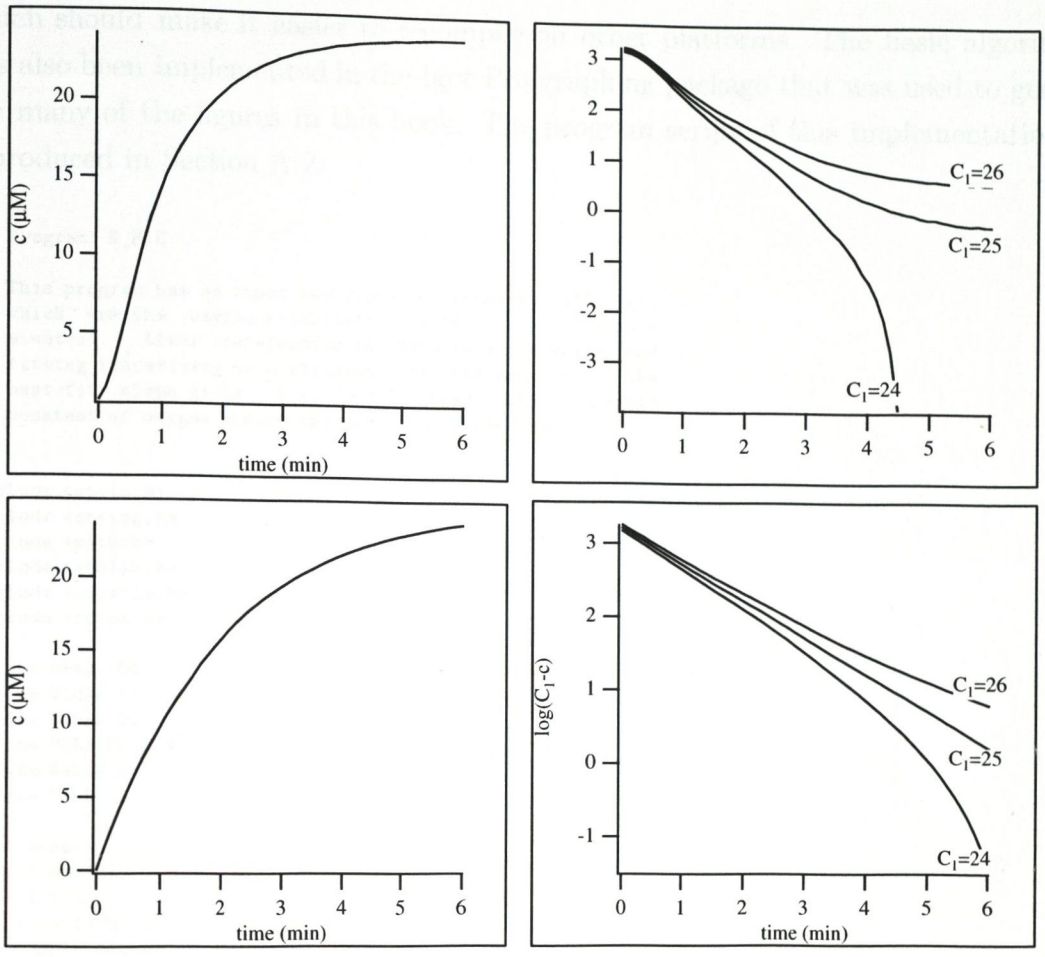

Figure A.1: Log-linear analysis of k_{-t} data. (a) Experimental k_{-t} data; (b) semi-log plot of the data in (a) at three different values of C_1, the initial estimate of $[O_{2(aq)}]_{eq}$; (c) idealised data, with $[O_{2(aq)}]_{eq} = 25$ μM; (d) semi-log plot of data in (c) at three values of C_1.

(see Section 3.3.2), and such data have been analysed using the optimised nonlinear regression method described in Chapter 3. Even with idealised data, the transformed data are not linear at long times when C_1 is not close to the true value of $[O_{2(aq)}]_{eq}$, and for this reason it is best to use the first two-thirds of the time-series data when using the iterative linearisation method, ignoring the approach to equilibrium altogether. By this means, lack of convergence can be avoided.

A sample, idealised dataset was generated from the equation $y = 25(1-\exp(-0.5t))$. This, and its log-linear transforms for C_1 =24, 25 and 26, are shown in Figure A.1.

The computer program is written in the C programming language, and was originally intended to run on an IBM-compatible PC running MS-DOS. The version reproduced below has been adapted by the author to comply with the ANSI C standard,

which should make it easier to recompile on other platforms. The basic algorithm has also been implemented in the Igor Pro graphing package that was used to generate many of the figures in this book. The program script of this implementation is reproduced in Section A.2.

```
/*
    Program: K_M.C

    This program has as input two arrays of numbers:  c[], t[],
    which  are the  oxygen solubility c, with time  t  (units =
    minutes).   After transforming the data to a log scale, and
    fitting iteratively to a straight line, the negative of the
    best-fit  slope gives  -k_m,  the (inverse)  mass-transport
    constant of oxygen across the gas-liquid interface.
*/

#include <stdio.h>
#include <string.h>
#include <math.h>
#include <stdlib.h>
#include <console.h>
#include <ctype.h>

#define NMAX 100                    /* up to 100 experimental points */
#define XCHAR 60
#define YCHAR 20
#define VERSION 2.0                 /* command line functionality */
#define FALSE 0
#define TRUE -1

float mean();
float fnmin();
float fnmax();
void transform();
void sample_data();
void char_graf();
void welcome();
void sample_data();
void menu();
int load_data();
int enter_data();


main(argc,argv)
    int argc;
    char *argv[];
{
    /* DECLARE VARIABLES */

    float x[NMAX],y[NMAX],c[NMAX],t[NMAX];
    float xx,yy,b0,b1,num,denom,rx,ry,cmax,cmax1,tol=0.01;
    int i,j,k,n=0,maxiter=20,file_error=FALSE,file_flag=FALSE;
    char key,number[30],command[30],datfile[13];


    /* PRINT WELCOME MESSAGE */
    welcome();

    if (argc>1)                     /* at least one argument passed */
    {
        for (i=1; i<argc; i++)
        {
            strcpy(command,argv[i]);  /* get the string to
                                         analyse */
            if (command[0] == '-')    /* command is a switch */
```

```
        {
            switch(command[1])
            {
                case 'm' :        /* maxiter is changed */
                    for (k=2; k<strlen(command); k++)
                        number[k-2]=command[k];
                    number[strlen(command)-2]='\0';
                    maxiter=atoi(number);
                    if (maxiter < 1)
                        {
                            puts("Maximum number of iterations can't be less than 1 !");
                            break;
                        }
                    printf("Maxiter set to %d\n",maxiter);
                    break;
                case 't' :              /* tol is changed */
                    for (k=2; k<strlen(command); k++)
                       number[k-2]=command[k];
                    number[strlen(command)-2]='\0';
                    tol=atof(number);
                    printf("Tolerance set to %f\n",tol);
                    break;
            }
        }
        else
        {
            strcpy(datfile,argv[i]);   /* else it's a
                                          filename */
            file_flag=TRUE;            /* we do not need the
                                          menu() */
        }
    }
    if (file_flag==FALSE)
        menu(t,x,c,&n);
    else
    {
        if ((file_error=load_data(t,x,c,&n,datfile)) == TRUE)
            exit(1);
    }
}
else
    menu(t,x,c,&n);

cmax1=c[n-1]+0.1;
puts("\nGraph the data (y/n)?");
key=getch();
if (key=='y' || key=='Y')
    char_graf(t,c,n);
puts("\n");

/* START MAIN LOOP */
j=0;
do
{
    cmax=cmax1;

    /* TRANSFORM DATA TO LOG SCALE */
    transform(c,y,cmax,n);

    /* OBTAIN MEANS OF x() AND y() */
    xx=mean(x,n);
    yy=mean(y,n);
    num=0;
    denom=0;
    for (i=0; i<n; i++)
    {
        rx=(x[i]-xx);
```

```
            ry=(y[i]-yy);
            num+=rx*ry;
            denom+=rx*rx;
        }
        if (denom!=0)
            b1=num/denom;
        else
        {
            puts("Division by zero!");
            exit(1);
        }
         b0=yy-b1*xx;
        printf("Iteration %d\tlog(cinf)=%f\t-k_m=%f\n",j,b0,b1);
        cmax1=exp(b0);
        j++;
    }
    while (fabs(cmax-cmax1)/cmax>tol && j<maxiter);

    if (j<maxiter)
    {
        printf("\nTolerance achieved in %d iterations\n\n",j);
        printf("k_m = %f (1/min)\n\n",-b1);
        puts("Graph the transformed data (y/n)?");
        key=tolower(getch());
        if (key=='y')
            char_graf(x,y,n);
    }
    else
    {
        puts("Convergence too slow!\n");
        puts("Do you want a post mortem graph of the transformed data?");
        key=tolower(getch());
        if (key=='y')
            char_graf(x,y,n);
        puts("\n");
    }
return(NULL);
}


void transform(c,y,max,n)
    float *c,*y,max;
    int n;
{
    int i;

    for (i=0; i<n; i++)
    {
        if (max > c[i])
            y[i]=log(max-c[i]);
        else
        {
            puts("Cannot take logarithm of negative number...");
            exit(1);
        }
    }
}

float mean(array,size)          /* computes mean of n numbers */
    float *array;
    int size;
{
    float sum=0;
    int i;

    for (i=0; i<size; i++)
    {
```

```
        sum+=*(array+i);
    }
    return(sum/size);
}


void char_graf(x,y,size)
        float *x,*y;
        int size;
{
        float xmin,ymin,xmax,ymax,m,n;
        int i,j,ln;          /* cl,l are points in XCHAR,YCHAR */
        char line[XCHAR];     /* holds a line of chars to print */

        xmin=fnmin(x,size);
        ymin=fnmin(y,size);
        xmax=fnmax(x,size);
        ymax=fnmax(y,size);
        m=(XCHAR-1)/(xmax-xmin);   /* XCHAR-1 to preserve end \0 */
        n=(YCHAR-1)/(ymax-ymin);

        puts("\n\n");
        for (ln=YCHAR-1; ln>=0; ln--) /* ln goes from top to bottom */
        {
                for (j=0; j<XCHAR; j++)
                        line[j]=' ';
                for (i=0; i<size; i++)
                {
                        if ((int)(n*(y[i]-ymin))==ln)
                                line[(int)(m*(x[i]-xmin))]='*';
                }
                if ((YCHAR-1)==ln)
                        printf("%8.3f|%.60s\n",ymax,line);
                else
                        printf("\t|%.60s\n",line);
                /* getch(); */
        }
        for (j=0; j<XCHAR; j++)
                line[j]='-';
        printf("%8.3f+%.60s\n",ymin,line);
        for (j=0; j<XCHAR-8; j++)
                line[j]=' ';
        line[XCHAR-8]='\0';
        printf("     %8.3f%.60s%8.3f\n",xmin,line,xmax);
        getch();
}


float fnmax(array,size)
    float *array;
    int size;
{
    float max;
    int index;

    max=array[0];
    for (index=1; index<size; index++)
    {
        if (max<array[index])
            max=array[index];
    }
    return(max);
}


float fnmin(array,size)
    float *array;
```

```
    int size;
{
    float min;
    int index;

    min=array[0];
    for (index=1; index<size; index++)
    {
        if (min>array[index])
            min=array[index];
    }
    return(min);
}

void sample_data(t,x,c,n)
    float *t,*x,*c;
    int *n;
{
    int i;

    *n=30;                  /* pass by reference enables init */
    for (i=0; i<*n; i++)    /* array indices start at 0 */
    {
        t[i]=(float)i/2;
        c[i]=1.5*(1-exp(-0.15*t[i]));
        x[i]=t[i];
    }
}


void welcome()
{
    puts("\n\n\n\n\n\n\n\n\n\n");
    puts("\t\t     Dissolved Oxygen Data Analysis\n\n\t\tMass-Transport Constant Determination\n");
    printf("\n\t\t\t   Version %1.2f %s\n",VERSION,DATE);
    puts("\n\n\n\n\n\n\n\n\n");
}


int load_data(t,x,c,n,fname)
    float *t,*x,*c;
    int *n;
    char *fname;

{
    int i;
    FILE *fp_in;
    float val1,val2;

    if (strcmp(fname,"") != 0)
        printf("Now loading %s...\n",fname);
    else
    {
        printf("\n\nGive the name of a file to load: ");
        scanf("%s",fname);
    }
    if ((fp_in=fopen(fname,"r")) != NULL)
    {
        i=0;
        while ((fscanf(fp_in,"%f\t%f",&val1,&val2)) != EOF)
        {
            t[i]=val1;
            c[i]=val2;
            x[i]=t[i];
            i++;
        }
        *n=i;       /* get the size of the array */
```

```
        fclose(fp_in);
    }
    else
    {
        puts("Can't open that file!");
        return(TRUE);
    }
    return(FALSE);       /* no error generated */
}

int enter_data(t,x,c,n)
    float *t,*x,*c;
    int *n;
{
    float tmax,dt,zero,factor;
    int index;
    char keypress,filename[13];
    FILE *fp_out;

    puts("\n\n\nChart Recorder Oxygen Data Entry\n");
    printf("Please enter the following information...");
    printf("\nMaximum time value = ");
    scanf("%f",&tmax);
    printf("Step time = ");
    scanf("%f",&dt);
    printf("Percentage of f.s.d. corresponding to 0 per cent 02 = ");
    scanf("%f",&zero);
    printf("Percentage of oxygen which gives 1 per cent of f.s.d. = ");
    scanf("%f",&factor);
    puts("\n");
    if (dt!=0)
    {
        *n=tmax/dt+1;
        if (*n>NMAX)
        {
            printf("Number of data points must not exceed 100! (%f,%f,%d)",tmax,dt,*n);
            exit(1);
        }
    }
    else
    {
        puts("Division by zero!\n");
        exit(1);
    }
    puts("Now enter oxygen data in the range 0<y%<100\n");
    for (index=0; index<*n; index++)
    {
        t[index]=tmax*index/(*n-1);
        printf("t(%d)=%f\tc(%d)=",index,t[index],index);
        scanf("%f",&c[index]);
        c[index]=factor*(c[index]-zero);
        x[index]=t[index];
    }
    puts("Save this data (y/n)? ");
    if ((keypress=getch()) == 'y' || (keypress=getch()) == 'Y')
    {
        printf("\nGive a filename for this data: ");
        scanf("%s",filename);
        if ((fp_out=fopen(filename,"w")) != NULL)
        {
            for (index=0; index<*n; index++)
            {
                fprintf(fp_out,"%f\t%f\n",t[index],c[index]);
                printf("%f\t%f\n",t[index],c[index]);
            }
            fclose(fp_out);
            puts("Data saved to disk");
```

```
            return(FALSE);
        }
        else
        {
            puts("Error in opening file for output");
            return(TRUE);
        }
    }
    return 0;
}

void menu(t,x,c,n)
    float *t,*x,*c;
    int *n;
{
    char key;
    int i,error;

    /* DISPLAY MENU LINE */
    do
    {
        printf("\nOptions :- (L)oad data, (E)nter data, Use (S)ample data");
                key=toupper((char)getch());
    }
    while (key!='L' && key!='E' && key!='S');
    switch(key)
    {
        case 'L' :
            if ((error=load_data(t,x,c,&*n,"")) == TRUE)
            exit(1);
            break;
        case 'E' :
            enter_data(t,x,c,&*n);   /* ENTER data */
            for (i=0; i<*n; i++)
            printf("%f\t%f\t%d\n",t[i],c[i],*n);
            break;
        default :
            sample_data(t,x,c,&*n);  /* SAMPLE data */
            break;
    }

}
```

A.2 Igor Pro script version of K_M.C

```
Function kt_iter(w,tol,maxiter)
Wave w
Variable tol,maxiter

WAVE gCoef = W_coef
WAVE gErr = W_sigma
Variable/G cmax
Variable old_cmax,iter,kt,kt_av
Duplicate/O w transform
Display transform as "Display Window"
DoWindow/C theWindow
WaveStats w
cmax = V_max
tol = 0.001
if (maxiter==0) then
maxiter=100
endif
iter = 0
kt_av=0
```

```
do
old_cmax = cmax
transform = ln(cmax-w)
CurveFit/Q line transform /D
cmax = exp(gCoef[0])
kt=-gCoef[1]
kt_av=kt_av+kt
iter = iter + 1
print iter,cmax,gErr[0],kt,gErr[1]
while ((abs(cmax-old_cmax)/cmax>tol) %& (iter<maxiter))
DoWindow/K theWindow
print kt_av/iter
End
```

A.3 Source code of MIXTIMES.BAS

A program written in Microsoft QuickBasic™ was used to generate the data shown in Figure 3.2. Spectrophotometric data was saved as a series of files with a standardised nomenclature. The program reads each file in turn and finds the time of addition of dye, the point of maximum absorbance and the final resting value. An example is shown in Figure A.2 below. When all the files are processed by the method described in Section 3.2, the mixing times and associated errors are output to disk as a plain text file.

```
DECLARE SUB save.data ()
REM *** MIXTIMES.BAS - a program to calculate mixing time from
   saved data ***
REM *** written by Andrew McDonald v2.0 24/4/95 ***
REM *** Modified - 5/5/95 ***

REM *** Mixing time is defined as the time taken to reach 5% of the
   equilibration ***
REM *** level from the time of injection ***

DECLARE SUB print.it ()
DECLARE SUB open.file (num%)
DECLARE SUB graph.it ()
REM Set up for VGA graphics
SCREEN 12
OPTION BASE 1

DIM SHARED t(600), a(600), winx%, winy%, winw%, winh%, windx%,
   windy%, windw%, windh%
DIM SHARED mint, maxt, mina, maxa, n%, counter%, r%, i.first%,
   i.last%
DIM SHARED tau(50, 3), slope(50, 3), max.dy, max.record%, range
DIM SHARED df(600), maxd, mind
DIM SHARED the.beginning%, the.end%, aver(600)

REM df() holds the derivatives, maxd and mind define its range,
   windw/h its width/height
REM max.dy holds the highest absorbance change recorded
REM n% is the number of points loaded...

winx% = 340
winy% = 360
winw% = 240
winh% = 200
```

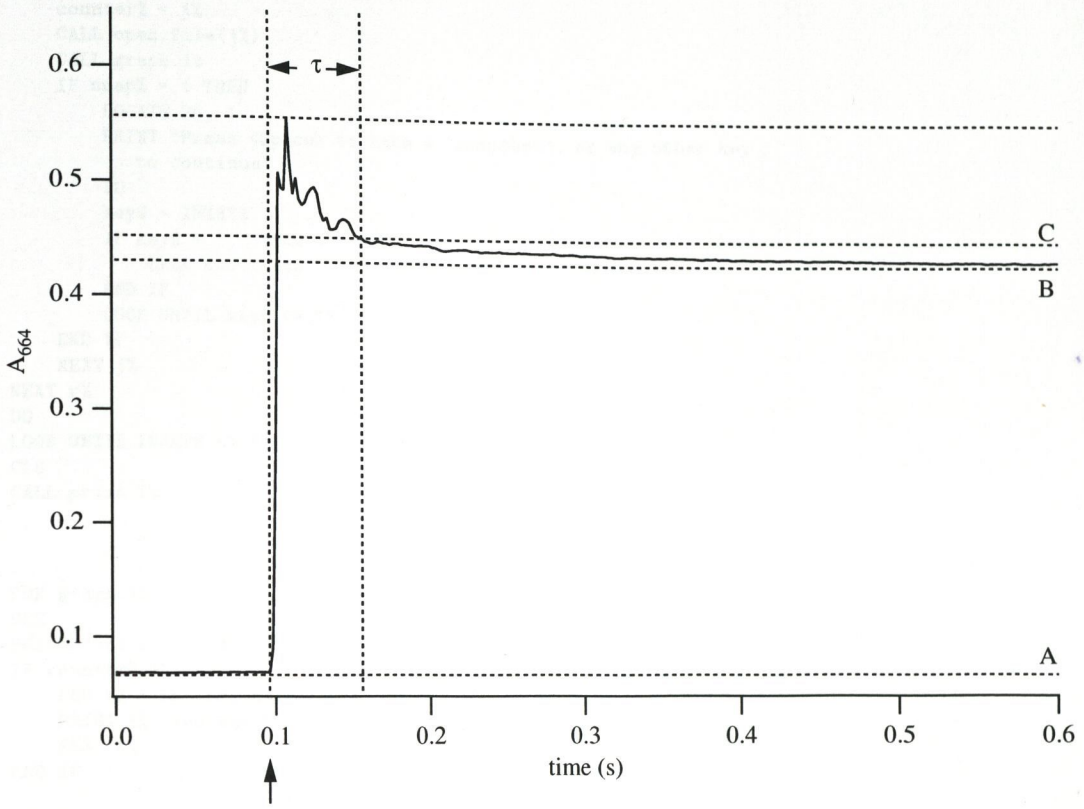

Figure A.2: Sample time-series data showing the calculation method defining τ, the mixing time. Line A denotes the baseline absorbance, B, the equilibrium absorbance, and C, a small percentage above the equilibrium position, usually 5% of $(A^B_{664} - A^A_{664})$. See Section 3.2 for experimental details.

```
windx% = 400
windy% = 150
windw% = 180
windh% = 120
winvx% = 400
winvy% = 150
winvw% = 180
winvh% = 120

dy% = 55

INPUT "Do you want to take snapshots of the data (y/n)?", p$
IF p$ = "y" THEN
    snap% = 1
ELSE
    snap% = 0
END IF
p% = 0
PRINT "Printing is OFF..."

the.beginning% = 5
the.end% = 20
REM main loop
FOR r% = 1 TO 3
    FOR j% = the.beginning% TO the.end%
```

```
    counter% = j%
    CALL open.file(j%)
    CALL graph.it
    IF snap% = 1 THEN
        LOCATE 24, 1
        PRINT "Press <Space> to take a 'snapshot', or any other key
          to continue"
        DO
        key$ = INKEY$
        IF key$ = " " THEN
            CALL save.data
        END IF
        LOOP UNTIL key$ <> ""
    END IF
    NEXT j%
NEXT r%
DO
LOOP UNTIL INKEY$ <> ""
CLS
CALL print.it


SUB graph.it
CLS
PRINT "set #", "tau", "slope"
IF counter% > 1 THEN
    FOR k% = the.beginning% TO counter% - 1
    PRINT k%, tau(k%, r%), slope(k%, r%)
    NEXT k%
END IF

REM The main window
LINE (winx%, winy%)-(winx% + winw%, winy%)
LINE (winx%, winy%)-(winx%, winy% - winh%)

REM The upper window (the first derivative)
LINE (windx%, windy%)-(windx% + windw%, windy%)
LINE (windx%, windy%)-(windx%, windy% - windh%)

REM scaling factors follow
IF mint <> maxt AND mina <> maxa AND mind <> maxd THEN
    mx = winw% / (maxt - mint)
    my = winh% / (maxa - mina)
    mdx = windw% / (maxt - mint)
    mdf = windh% / (maxd - mind)
ELSE
    PRINT "Fatal Error - division by zero!"
    STOP
END IF

FOR i% = 2 TO n% - 2
    LINE (mdx * t(i%) + windx%, -mdf * (df(i%) - mind) + windy%)-
    (mdx * t(i% + 1) + windx%, -mdf * (df(i% + 1) - mind) +
    windy%)
    IF i% = i.first% THEN
        REM Draw an arrow
        LINE (mx * t(i%) + winx%, 4 + winy%)-(mx * t(i%) + winx%,
          4 + 8 + winy%)
        LINE (mx * t(i%) + winx%, 4 + winy%)-(mx * t(i%) + 4 +
          winx%, 4 + 3 + winy%)
        LINE (mx * t(i%) + winx%, 4 + winy%)-(mx * t(i%) - 4 +
          winx%, 4 + 3 + winy%)
    END IF
    REM Vertical line at the maximum
    IF a(i%) = maxa THEN
        i.max% = i%
```

```
    LINE (mx * t(i%) + winx%, -my * (a(i%) - mina) + winy%)-
       (mx * t(i%) + winx%, winy%), , , &HC3C3
    END IF
NEXT i%

REM *** BEGIN AVERAGING ***
d.i% = 5
maxy = -10000
miny = 10000
FOR i% = 1 TO n% - d.i%
    IF i% < i.max% THEN
        aver(i%) = a(i%)
    ELSE
        sum = 0
        FOR j% = i% - d.i% TO i% + d.i%
            sum = sum + a(j%)
        NEXT j%
        aver(i%) = sum / (2 * d.i% + 1)
    END IF
    IF aver(i%) > maxy THEN
        maxy = aver(i%)
    END IF
    IF aver(i%) < miny THEN
        miny = aver(i%)
    END IF
NEXT i%

REM scaling factors for the averaged data
IF miny <> maxy THEN
    mvf = winh% / (maxy - miny)
ELSE
    PRINT "Fatal Error - division by zero!"
    STOP
END IF
FOR i% = 2 TO n% - d.i%
    LINE (mx * t(i% - 1) + winx%, -my * (aver(i% - 1) - mina) +
       winy%)-(mx * t(i%) + winx%, -my * (aver(i%) - mina) + winy%)
NEXT i%

REM Draw a horizontal line at the equilibrium position
LINE (mx * t(n% - d.i%) + winx%, -my * (aver(n% - d.i%) -
   mina) + winy%)-(mx * t(i.first%) + winx%, -my * (aver(n% -
   d.i%) - mina) + winy%), , , &HC3C3

REM *** END AVERAGING ***

i.last% = n% - d.i%
percent = .05
IF i.max% <> 0 THEN
    range = aver(i.last%) - a(1)
    target = aver(i.last%) + percent * range
    tol = .001 * range
    i% = i.max% + d.i%
END IF

REM Draw a horizontal line at the equilibrium position
LINE (mx * t(n% - d.i%) + winx%, -my * (target - mina) + winy%)-
   (mx * t(i.first%) + winx%, -my * (target - mina) + winy%), ,
   , &HC3C3

hit% = 0
WHILE i% < i.last% AND hit% = 0
    IF aver(i%) < target THEN
        hit% = 1
        i% = i% - 1
    ELSE
        i% = i% + 1
```

```
    END IF
WEND
tau(counter%, r%) = t(i%) - t(i.first%)
REM Mark the position of tau on the graph
LINE (mx * (t(i.first%) + tau(counter%, r%)) + winx%, -mvf *
   (aver(n% - d.i%) - miny) + winy%)-(mx * (t(i.first%) +
   tau(counter%, r%)) + winx%, winy%), , , &HC3C3
END SUB



SUB open.file (num%)
rep% = r%
REM ****************************
REM *** Pathname defined here ***
REM ****************************
drive$ = "C:"
path$ = "\WORK\"
n$ = STR$(num%)
IF num% < 10 THEN
    number$ = "0" + RIGHT$(n$, LEN(n$) - 1)
ELSE
    number$ = RIGHT$(n$, LEN(n$) - 1)
END IF
extension$ = ".ASC"
replicate$ = RIGHT$(STR$(rep%), LEN(STR$(rep%)) - 1)
filename$ = "MBST"
full.path$ = drive$ + path$ + filename$ + number$ + "-" +
replicate$ + extension$

REM rep% is the replicate number (1..3)
REM winx and winy are the screen coords of the origin of the graphs
REM winw and winh are the width and height (in pixels) of the
   window

OPEN full.path$ FOR INPUT AS #1
REM define min and max values for two sets of data
maxt = -1000
maxa = -1000
mint = 1000
mina = 1000
max.dy = -1000
l% = LOF(1)
REM Only load the following number of records:
max.record% = 200
record.length% = 23
IF l% / 23 >= max.record% THEN
    skip% = l% / (23 * max.record%)
ELSE
    skip% = 1
END IF

i% = 1
j% = 1
REM input the first point
INPUT #1, t(i%), a(i%)
WHILE j% < 600 AND EOF(1) = 0
    IF j% MOD skip% = 0 THEN
        i% = i% + 1
        INPUT #1, t(i%), a(i%)
        dy = a(i%) - a(i% - 1)
        IF dy > max.dy THEN
            max.dy = dy
            i.first% = i% - 1
        END IF
    ELSE
        INPUT #1, dummy1, dummy2
```

```
    END IF
    IF t(i%) < mint THEN
        mint = t(i%)
    END IF
    IF t(i%) > maxt THEN
        maxt = t(i%)
    END IF
    IF a(i%) < mina THEN
        mina = a(i%)
    END IF
    IF a(i%) > maxa THEN
        maxa = a(i%)
        time% = i%
    END IF
    j% = j% + 1
WEND
n% = i% - 1
CLOSE #1

REM *** BEGIN NUMERICAL DIFFERENTIATION ***
REM h is the step time
h = .1
REM calculate new max/mina's
maxd = -100000
mind = 100000
FOR i% = 2 TO n% - 1
    df(i%) = (a(i% + 1) - a(i% - 1)) / 2 / h
    REM find the range
    IF df(i%) > maxd THEN
        maxd = df(i%)
    END IF
    IF df(i%) < mind THEN
        mind = df(i%)
    END IF
NEXT i%
REM *** END NUMERICAL DIFFERENTIATION ***

END SUB



SUB print.it
OPEN "MBSTIR.LOG" FOR OUTPUT AS #1
PRINT "RESULTS"
PRINT "-------"
PRINT "set #"; "    "; "rep 1"; "   "; "rep 2"; "   "; "rep 3";
"   "; "avg"; " "; "+/- s.d."
PRINT #1, "RESULTS"
PRINT #1, "-------"
PRINT #1, "set #"; "    "; "rep 1"; "   "; "rep 2"; "   "; "rep 3";
"   "; "avg"; " "; "+/- s.d."
IF p% = 1 THEN
    LPRINT "RESULTS"
    LPRINT "-------"
    LPRINT "set #"; "   "; "rep 1"; "   "; "rep 2"; "   "; "rep 3";
    "   "; "avg"; " "; "+/- s.d."
END IF
FOR i% = the.beginning% TO the.end%
    PRINT i%; " ";
    PRINT #1, i%; " ";
    IF p% = 1 THEN
        LPRINT i%; "    ";
    END IF
    sum = 0
    FOR r% = 1 TO 3
        t = tau(i%, r%)
        LOCATE i% - the.beginning% + 4, 8 * r% + 2
```

```
            PRINT USING "#.####"; t
            PRINT #1, USING "#.####"; t;
            PRINT #1, " ";
            IF p% = 1 THEN
                LPRINT USING "#.####"; t
            END IF
            sum = sum + t
        NEXT r%
        avg = sum / 3
        LOCATE i% - the.beginning% + 4, 37
        PRINT USING "#.####"; avg
        PRINT #1, USING "#.####"; avg;
        PRINT #1, " ";
        IF p% = 1 THEN
            LPRINT USING "#.####"; avg
        END IF
        sum = 0
        FOR r% = 1 TO 3
            t = tau(i%, r%)
            sum = sum + (t - avg) ^ 2
        NEXT r%
        sd = SQR(sum) / 2
        REM divided by rep%-1 (=3-1)
        LOCATE i% - the.beginning% + 4, 46
        PRINT USING "#.####"; sd
        PRINT #1, USING "#.####"; sd
        IF p% = 1 THEN
            LPRINT USING "#.####"; sd
        END IF
    NEXT i%
    DO
    LOOP UNTIL INKEY$ <> ""
    END SUB


    SUB save.data
    OPEN "snapshot.dat" FOR OUTPUT AS #1
    PRINT #1, "Data Set #: ", counter%
    PRINT #1, "Number of points: "; n% - d.i%
    PRINT #1, "Calculated mixing time (sec): "; tau(counter%, r%) * 60
    FOR i% = 1 TO n% - d.i%
        PRINT #1, t(i%), aver(i%)
    NEXT i%
    CLOSE #1
    END SUB
```

A.4 Optimisation procedure

The following function was used in Igor Pro (Wavemetrics Inc., USA) to optimise the computed mass-transport constant by searching for a minimum value of the goodness-of-fit parameter, χ^2. The model equation was Equation 2.6. The k_t is also estimated by the half-life; both of these methods are discussed in Section 3.3.2.

```
#pragma rtGlobals=1 // Use modern global access method.
Function Optimize_k_m(wave0,coeff,chi_store,km_store,a, delta)
Wave wave0, coeff,chi_store,km_store
Variable a,delta

Variable oldchisq,counter,t,tmin,tmax,thalf,whalfmax,wmax,wmin,tol
if (delta<=0)
```

```
Abort "Time increment must be greater than zero!"
endif
tol=0.01
chi_store = 0 //inititialise chi_store
km_store = 0 //inititialise km_store
SetScale/P x 0,delta,"", chi_store //set X scale
SetScale/P x 0,delta,"", km_store //set X scale
Duplicate/O/D/R=(xcsr(A),xcsr(B)) wave0,workwave // make a copy
//of data wave between cursors
Display workwave as "Display Window"
DoWindow/C theWindow
SetScale/P x 0,1,"", workwave
WaveStats workwave
tmin=0
tmax=V_npnts
wmax=workwave[tmax]
t=tmin
do //step along the time axis to get tmin
t=t+1
while ((workwave[t]-workwave[tmin]) < tol*(wmax-wmin))
tmin=t
wmin=workwave[tmin]
whalfmax=workwave[tmin]+(workwave[tmax]-workwave[tmin])/2
do step along from
t=t+1
while ((workwave[t]-whalfmax) < tol*(wmax-wmin))
thalf=t
counter=0
FuncFit/Q k_m_func coeff workwave(a,) /D
do
oldchisq=V_chisq
FuncFit/Q k_m_func  coeff workwave(a,) /D
a += delta
K4 = a
chi_store[counter]=V_chisq
km_store[counter]=coeff[1]
counter += 1
while ((oldchisq >= V_chisq) %| (counter<(100/delta)-1))
DoWindow/K theWindow
WaveStats/R=(20,80) chi_store
Printf "Predicted k_t : %f",60*ln(2)/thalf;
Print " per min (half-life method)"
Printf "Optimised k_t: %f",60*km_store[V_minloc/delta];
Print " per min"
End
```

A.5 Generation of Poincaré maps

The Igor Pro script below generates a Poincaré map from three coordinates of a dynamical system, by plotting a point in the space of the first two variables when the third increases through a specific value. The increment ensures that the directionality criterion is satisfied (see Figure 7.16).

```
#pragma rtGlobals=1 // Use modern global access method.
Function Poincare(w1,w2,w3,z,labelx,labely)
Wave w1,w2,w3
Variable z // z holds the w3 intercept value
String labelx,labely // the axis labels
```

```
// Plot points in the w1,w2 plane, based on the value of w3 passing through z
Variable i,n,count
Make/N=5000/D/O px=0,py=0 // px and py hold the x and y coordinates
n=min(min(numpnts(w1),numpnts(w2)),numpnts(w3)) //
i=1 //
count=0
DoWindow/K PoincareSection // close previous window, if it exists
do
if (((w3[i]>z) %& (w3[i-1]<z)) %| (w3[i]==z)) then
// w3 has passed through, or is in, the w1-w2 plane at z
px[count]=w1[i] // store x-value
py[count]=w2[i] // store y-value
count=count+1
endif
i=i+1
while (i<n)
Redimension/N=(count,0) py,px
Display py vs px as "Poincare Section" // Plot py vs py
ModifyGraph mode(py)=2 // as discrete points
ModifyGraph rgb=(0,0,0) // set colour to black
Label left labely // label axes
Label bottom labelx
DoWindow/C PoincareSection
End
```

A.6 Generation of next-amplitude plots

The following Igor Pro script generates a next-amplitude plot from the time-series of a single variable. See Section 7.4.1 for further details.

```
#pragma rtGlobals=1 // Use modern global access method.
Function NextAmp(w,labelx,labely)
Wave w
String labelx,labely

Variable i,n,count,prevmax
Make/N=5000/D/O qx=0,qy=0 // px and py hold the x and y coordinates
n=numpnts(w)
i=2 // start at the third point of the data
count=0
prevmax=0
DoWindow/K NextAmplitudePlot // close previous window, if it exists
do
if ((w[i-2]<=w[i-1]) %& (w[i-1]>w[i])) then
// w is at a local maximum
qx[count]=prevmax // store previous maximum in px
qy[count]=w[i-1] // store current max in py
count=count+1
prevmax=w[i-1]
endif
i=i+1
while (i<n)
Redimension/N=(count,0) qy,qx
DeletePoints 0,1, qy,qx
Display qy vs qx as "Next-Amplitude Plot" // Plot qy vs qy
ModifyGraph mode(qy)=2 // as discrete points
ModifyGraph rgb=(0,0,0) // set colour to black
Label left labely // label axes
Label bottom labelx
DoWindow/C NextAmplitudePlot
End
```

A.7 Source code of `PO_Control.vi`

Figures A.3 and A.4 show the main routine and subroutine hierarchy, respectively, of the LabVIEW program `PO_Control.vi`, which was used to sample voltage data from the oxygen meter and also control the syringe infusion pump and spectrophotometer from a single computer. Further details are to be found in Chapter 2.

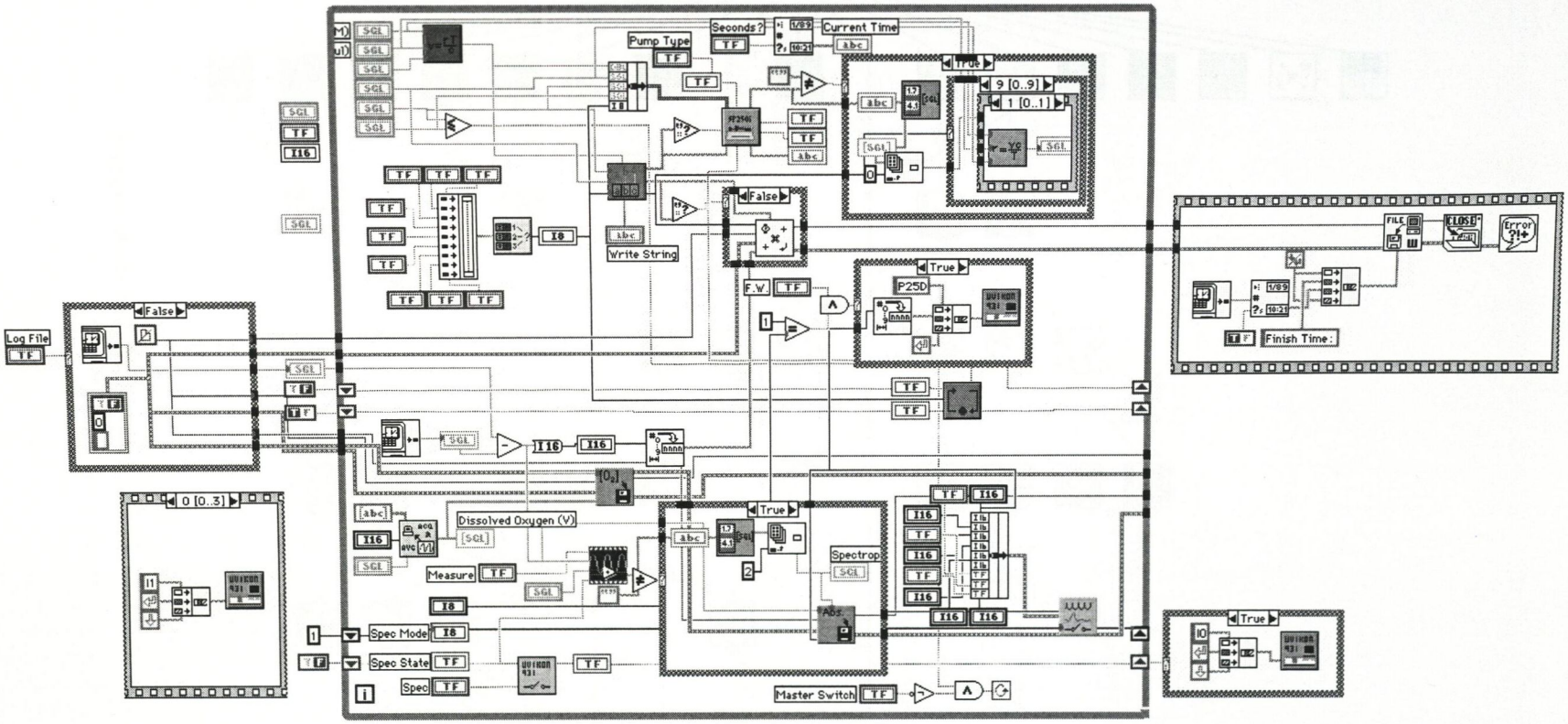

Figure A.3: Source code of `PO_Control.vi`. For simplicity only the top level is shown. See Figure A.4 for a tree of the entire program subroutines.

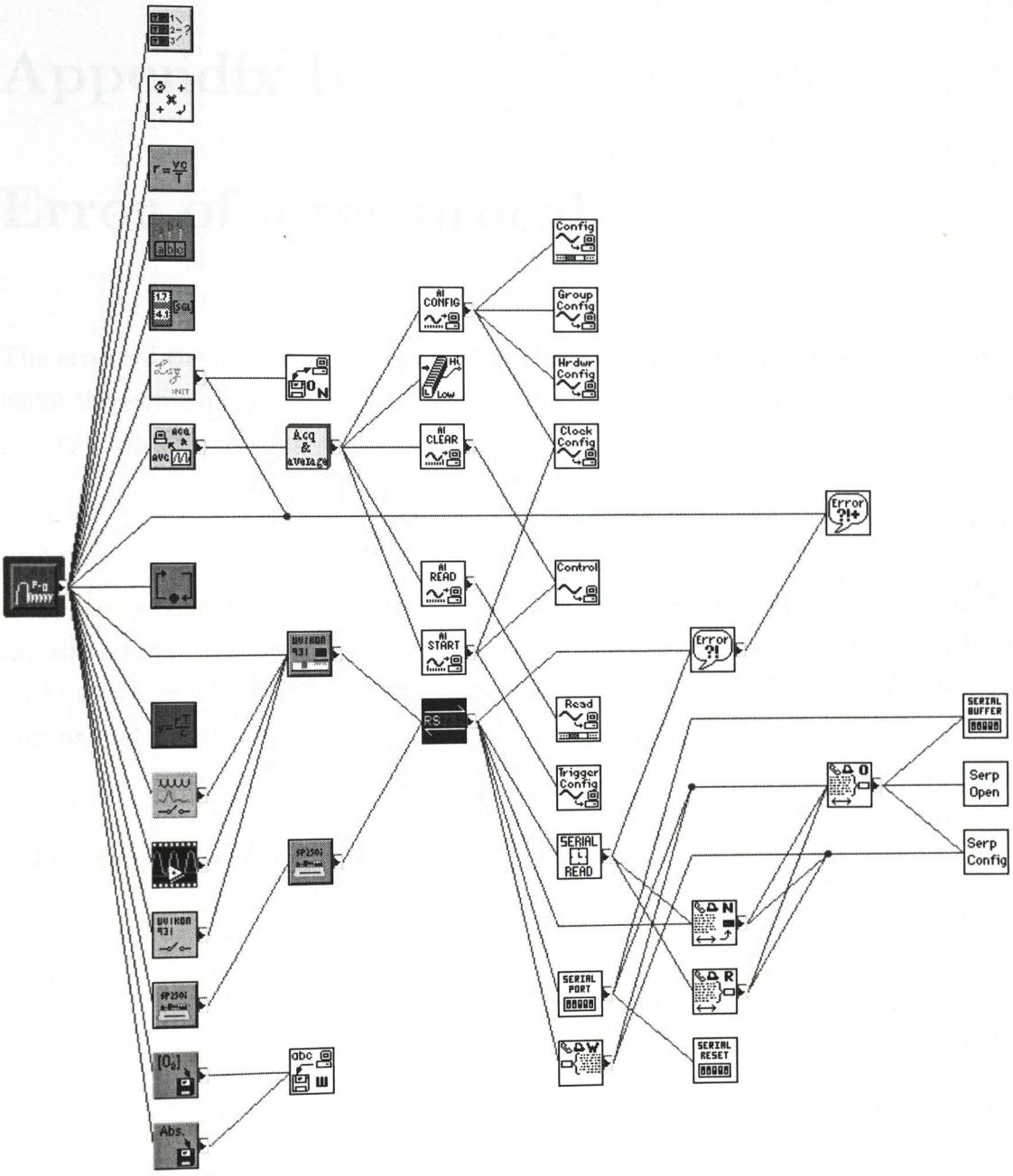

Figure A.4: Sub-VI hierarchy of `PO_Control.vi`.

Appendix B

Error of a reciprocal

The errors of the reciprocal values of mixing time (used in Figure 3.2) were calculated using the formula derived below. The equation for the propagated error of a quotient $z = x/y$ can be expressed in the form

$$\left(\frac{\sigma_z}{z}\right)^2 \simeq \left(\frac{\sigma_x}{x}\right)^2 + \left(\frac{\sigma_y}{y}\right)^2 \tag{B.1}$$

where the σs denote the standard error of the mean of each variable, and x, y and z are the means. The error, σ_y, of the reciprocal $y = 1/x$ can be shown to follow from (B.1) as a special case. Rewriting (B.1) with $x = 1$ and $\sigma_x = 0$, and neglecting the approximation, gives

$$\left(\frac{\sigma_z}{z}\right)^2 = \left(\frac{0}{1}\right)^2 + \left(\frac{\sigma_y}{y}\right)^2.$$

Taking the square root of both sides, and since $y = 1/z$, we have

$$\sigma_z = \frac{\sigma_y}{y^2}. \tag{B.2}$$

Appendix C

Further analyses of Model 2

The system of differential equations which comprise the peroxidase-oxidase Model 2, defined in Chapter 7, are as follows:

$$\frac{d\mathrm{A}}{dt} = k_1 - k_3\mathrm{AB} \tag{C.1}$$

$$\frac{d\mathrm{B}}{dt} = k_2\mathrm{B}_0 - k_{-2}\mathrm{B} - k_3\mathrm{AB} - k_4\mathrm{BX}(\mathrm{E}_0 - \mathrm{F}) \tag{C.2}$$

$$\frac{d\mathrm{F}}{dt} = k_4\mathrm{BX}(\mathrm{E}_0 - \mathrm{F}) - k_5\mathrm{XF} \tag{C.3}$$

$$\frac{d\mathrm{X}}{dt} = 2k_3\mathrm{AB} - k_4\mathrm{BX}(\mathrm{E}_0 - \mathrm{F}) + k_5\mathrm{XF} - k_6\mathrm{X} \tag{C.4}$$

The aim of this section is to derive a set of equations which are truly dimensionless and to obtain expressions for the steady-state values of each of the variables, in terms of dimensionless rate constants. First, we define some notation. We recognise the symbols L and T as representing unitary length and time, respectively. The dimensions of a variable or rate constant Z are are written by surrounding the symbol with square brackets, thus: $[Z]$.

The variables A, B, F, and X of Model 2 are concentrations, and since concentration is the number of molecules of a chemical species per unit volume, we must have $[\mathrm{A}] = [\mathrm{B}] = [\mathrm{F}] = [\mathrm{X}] = L^{-3}$. Each term in a differential equation must have the same dimensions as the differential of the variable. Therefore, since $[d\mathrm{A}/dt] = L^{-3}T^{-1}$, both k_1 and $k_3\mathrm{AB}$ must also have units of $L^{-3}T^{-1}$. The dimensions of all of the rate constants and other parameters were calculated from this observation, and the results are collected in Table C.1. From these results we can choose a new time, τ, which is dimensionless, using the relationship

$$\tau = \frac{t}{1/k_{-2}},$$

Variable	Dimensions	Variable	Dimensions
A	L^{-3}	k_2	T^{-1}
B	L^{-3}	k_{-2}	T^{-1}
F	L^{-3}	k_3	L^3T^{-1}
X	L^{-3}	k_4	L^6T^{-1}
B_0	L^{-3}	k_5	L^3T^{-1}
E_0	L^{-3}	k_6	T^{-1}
k_1	$L^{-3}T^{-1}$	t	T

Table C.1: Dimensions of variables and parameters of Model 2.

and new dimensionless variables

$$a = \frac{\mathrm{A}}{\mathrm{B}_0}, b = \frac{\mathrm{B}}{\mathrm{B}_0}, f = \frac{\mathrm{F}}{\mathrm{E}_0}, x = \frac{\mathrm{X}}{\mathrm{B}_0} \tag{C.5}$$

Now, $\mathrm{A} = \mathrm{B}_0 a$, therefore

$$\begin{aligned} \frac{d\mathrm{A}}{dt} &= \frac{d(\mathrm{B}_0 a)}{dt} \\ &= \mathrm{B}_0 \frac{da}{dt} \\ &= \mathrm{B}_0 \frac{da}{d\tau}\frac{d\tau}{dt} \\ &= k_{-2}\mathrm{B}_0 \frac{da}{d\tau} \end{aligned}$$

Repeating as above for the other variables, we eventually arive at the dimensionless equations of Model 2:

$$\frac{da}{d\tau} = \alpha - \beta ab \tag{C.6}$$

$$\frac{db}{d\tau} = \gamma - b - \beta ab - \gamma bx(1-f) \tag{C.7}$$

$$\frac{df}{d\tau} = \epsilon bx(1-f) - \zeta xf \tag{C.8}$$

$$\frac{dx}{d\tau} = 2\beta ab - \delta bx(1-f) - \eta x \tag{C.9}$$

where the dimensionless constants bear the following relations to their dimensional counterparts:

$$\alpha = \frac{k_1}{k_2 B_0}, \beta = \frac{k_3 \mathrm{B}_0}{k_{-2}}, \gamma = k_2 \mathrm{B}_0, \delta = \frac{k_4 \mathrm{B}_0 \mathrm{E}_0}{k_{-2}}, \epsilon = \frac{k_4 \mathrm{B}_0^2}{k_{-2}}, \zeta = \frac{k_5 \mathrm{B}_0}{k_{-2}}, \eta = \frac{k_6}{k_{-2}}.$$

The differential system of Equations C.1 to C.4 has been reduced from nine to seven parameters, and transformed to a new set of dimensionless variables.

Steady-state expressions for each of the new variables were derived using the symbolic-algebra package Maple V (Maple V Release 5, Waterloo Maple Software, 1998). Setting the right-hand sides of Equations C.6 to C.9 to zero and solving for a, b, f and x, we get:

$$a = \frac{\alpha}{\beta\Delta} \tag{C.10}$$

$$b = \Delta \tag{C.11}$$

$$f = \frac{\eta\epsilon(\eta(\alpha + \Delta - \eta) + 2\Delta\alpha\gamma}{\Delta(\zeta\delta + \eta\epsilon)(2\alpha\gamma + \delta(\alpha + \Delta - \gamma))} \tag{C.12}$$

$$x = \frac{2\alpha\gamma - \delta\gamma + \delta\Delta + \delta\gamma}{\eta\gamma} \tag{C.13}$$

where

$$\Delta = \frac{-\theta \pm (\theta^2 - 4(\zeta\delta + \eta\epsilon)(\zeta\alpha\eta - \zeta\gamma\eta))^{\frac{1}{2}}}{2(\zeta\delta + \eta\epsilon)}$$

and

$$\theta = 2\zeta\alpha\gamma + \epsilon\alpha\eta - \epsilon\gamma\eta - \zeta\delta\gamma + \zeta\delta\alpha + \eta\zeta$$

Appendix D

Colour Plates

The following pages contain full-page colour reproductions of certain figures from earlier chapters.

Plate 1: Figure A.3, p.182
Plate 2: Figure A.4, p.183
Plate 3: Figure 4.9, p.55
Plate 4: Figure 4.8, p.54

Plate 1

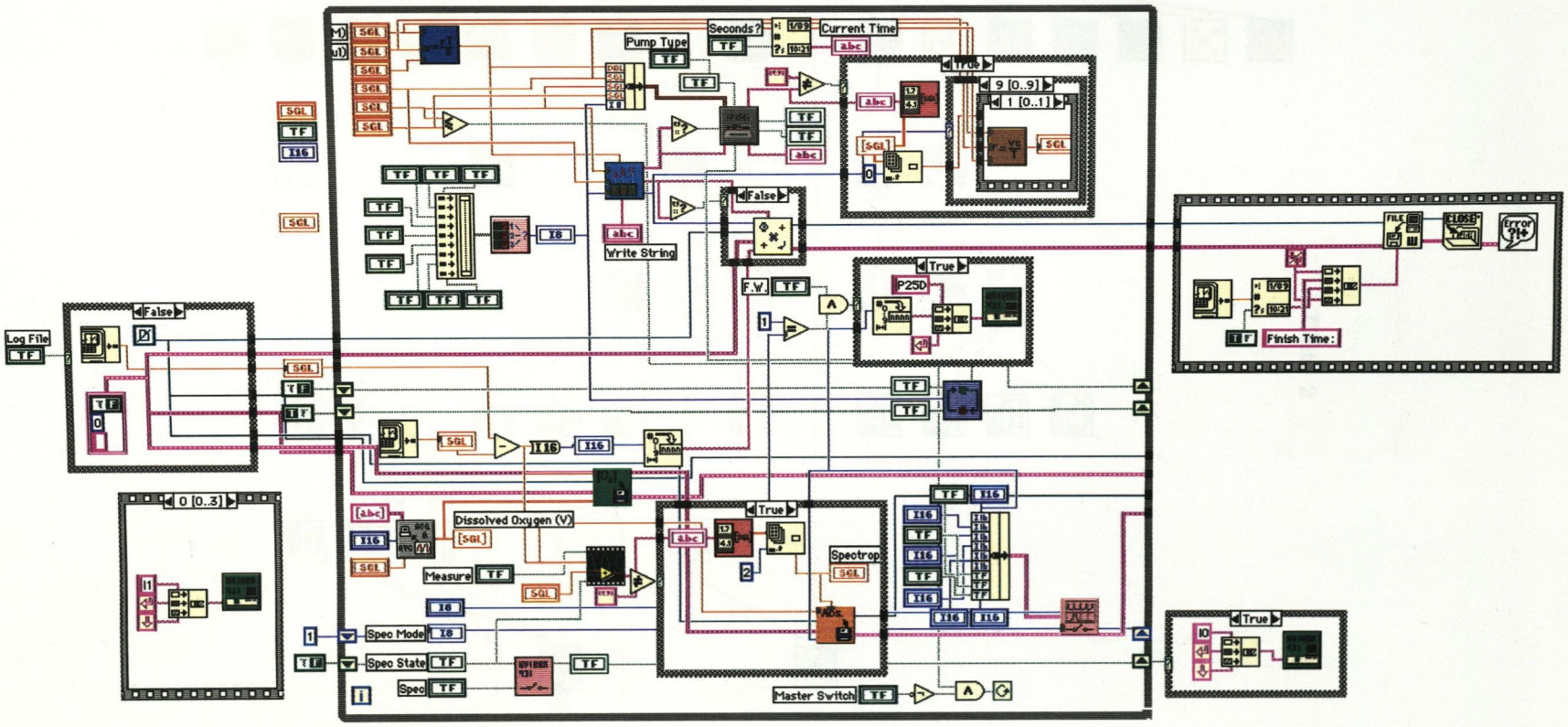
Pump Type
Seconds?
Current Time
True
9 [0..9]
1 [0..1]
False
Write String
F.W.
P25D
Log File
Finish Time:
0 [0..3]
Dissolved Oxygen (V)
Measure
Spec Mode
Spec State
Spec
Master Switch
Spectrop
ABS

Plate 2

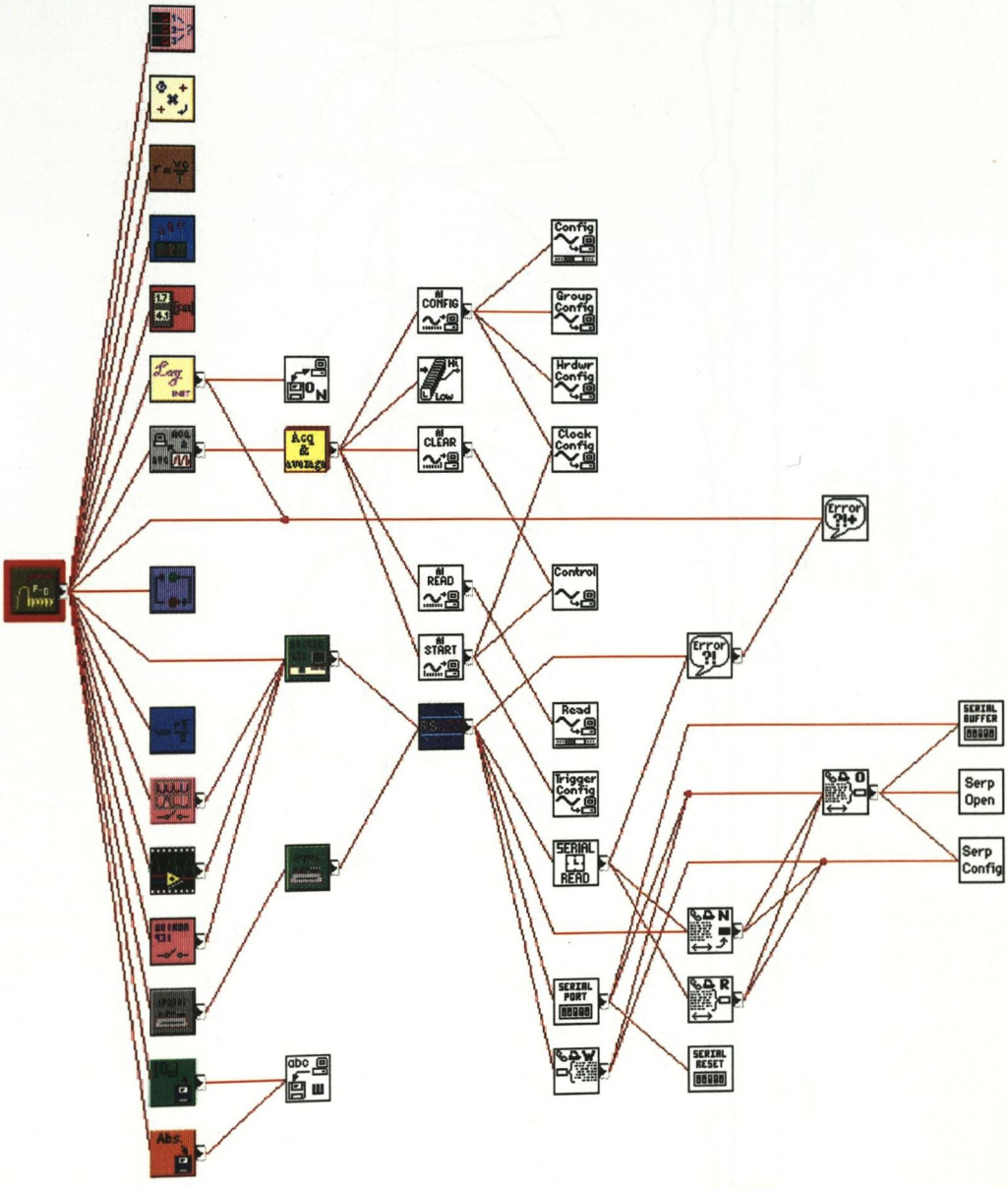
Config
Group Config
Hrdwr Config
Clock Config
Control
Read
Trigger Config
SERIAL READ
SERIAL PORT
SERIAL RESET
Error
SERIAL BUFFER
Serp Open
Serp Config
Acq & Average
abc
Abs

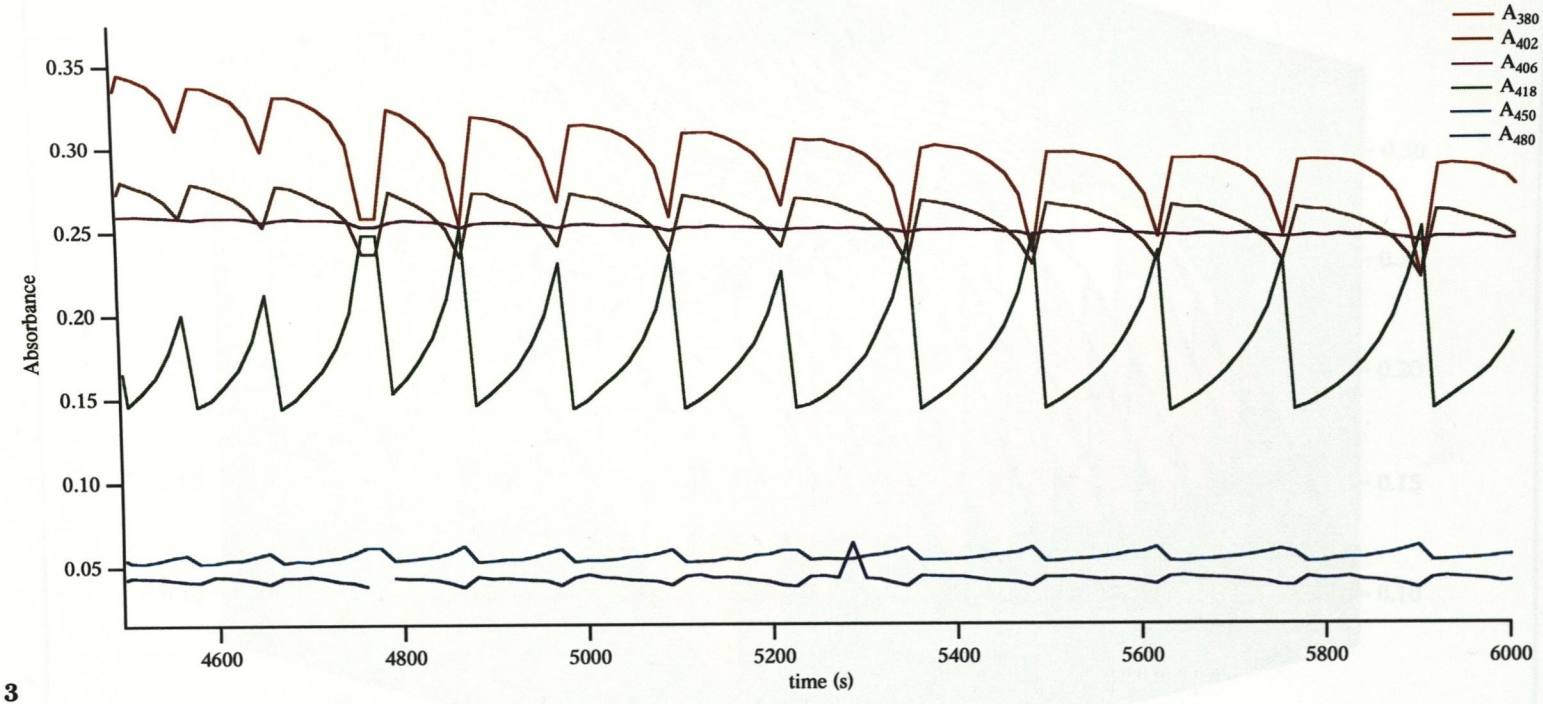
A380
A402
A406
A418
A450
A480
0.35
0.30
0.25
0.20
0.15
0.10
0.05
Absorbance
4600
4800
5000
5200
5400
5600
5800
6000
time (s)

Plate 3

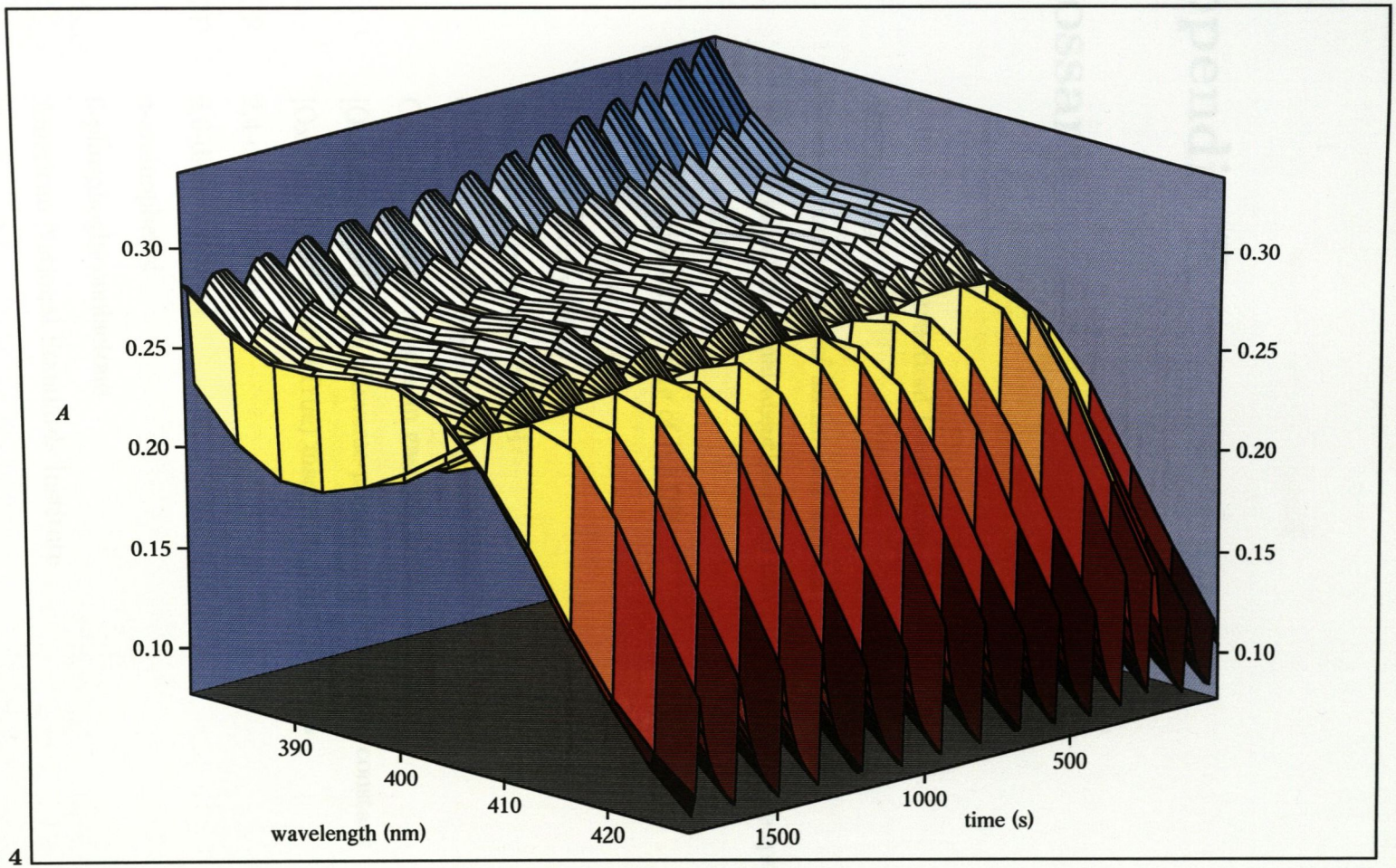
A
0.30
0.25
0.20
0.15
0.10
390
400
410
420
wavelength (nm)
1500
1000
500
time (s)

Plate 4

Appendix E

Glossary

T	[Attractor reconstruction] Delay time
τ	Mixing time
c_s	Stock concentration of an infused substance (u. NADH)
λ_{max}	Wavelength of maximal absorbance in the ultraviolet/visible spectrum
I	Ionic strength
r	Concentration-influx rate of NADH
U	unit of enzyme activity
V_T	Total solution volume
v_i	Volume-influx rate of NADH
$O_{2(aq)}$	Concentration of oxygen in aqueous phase
$O_{2(g)}$	Concentration of oxygen in gaseous phase
k_{-t}	[Oxygen equilibrium] (Reverse-phase) mass transport constant
k_t	[Oxygen equilibrium] (True) mass-transport constant
2,4-DCP	2,4-dichlorophenol
2,6-DCP	2,6-dichlorophenol
4-AP	4-aminophenol
6-PGL	6-phosphogluconolactone
ANSI	American National Standards Institute
CoI	Compound I
CoII	Compound II
CoIII	Compound III

CR	Chlorophenol red
DAQ	Data acquisition
EtOH	Ethanol
G6P	Glucose-6-phosphate
GPD	Glucose-6-phosphate dehydrogenase
HRP	Horseradish peroxidase
LP	Lactoperoxidase
MB	Methylene blue
MR	Methyl red
NaAc	Sodium acetate
NADH	Nicotinamide adenine dinucleotide (reduced form)
NADPH	Nicotinamide adenine dinucleotide phosphate (reduced form)
Per^{3+}	Ferriperoxidase (Fe^{3+})
PO	peroxidase-oxidase
RS232	[Computer] Serial communications protocol
SOD	Superoxide dismutase

Bibliography

[1] Hauser, M. J. and Olsen, L. F. The role of naturally occurring phenols in inducing oscillations in the peroxidase-oxidase reaction. *Biochemistry* **37**, 2458–2469 (1998).

[2] Prigogine, I. *Nonequilibrium statistical mechanics.* Wiley-Interscience, New York, (1962).

[3] Bray, W. C. A periodic reaction in homogeneous solution and its relation to catalysis. *J. Am. Chem. Soc.* **43**, 1262 (1921).

[4] Zhabotinsky, A. M. *Concentration oscillations.* Moscow, Nauka, (1974).

[5] Scott, S. K. *Oscillations, waves and chaos in chemical kinetics.* Oxford Science Publications, Oxford, (1994).

[6] Dateo, C. E., Orban, M., DeKepper, P., and Epstein, I. R. Bistability and oscillations in the autocatalytic chlorite-iodide reaction in a stirred-flow reactor. *J. Am. Chem. Soc.* **104**, 504–509 (1982).

[7] Duysens, L. N. M. and Amesz, J. Fluorescence spectrophotometry of reduced phosphopyridine nucleotide in intact cells in the near-ultraviolet and visible region. *Biochim. Biophys. Acta* **24**, 19–26 (1957).

[8] Ghosh, A. and Chance, B. Oscillations of glycolytic intermediates in yeast cells. *Biochem. Biophys. Res. Commun.* **16**, 174–181 (1964).

[9] Chance, B., Hess, B., and Betz, A. DPNH oscillations in a cell-free extract of *S. carlsbergensis. Biochem. Biophys. Res. Commun.* **16**, 182–187 (1964).

[10] Hess, B., Brand, K., and Pye, K. Continuous oscillations in a cell-free extract of *S. carlsbergensis. Biochem. Biophys. Res. Commun.* **23**, 102–108 (1966).

[11] Yuan, Z., Medina, M. A., Boiteux, A., Muller, S. C., and Hess, B. The role of fructose 2,6-bisphosphate in glycolytic oscillations in extracts and cells of *Saccharomyces cerevisiae*. *Eur. J. Biochem.* **192**, 791–795 (1990).

[12] Cuthbertson, K. S. R. and Cobbold, P. H. Phorbol ester and sperm activate mouse oocytes by inducing sustained oscillations in cell Ca^{2+}. *Nature* **316**, 541–542 (1985).

[13] Cuthbertson, K. S. R. and Cobbold, P. H. Oscillations in cell calcium. *Cell Calcium* **12**(2–3) (1990).

[14] Berridge, M. J. Calcium oscillations. *J. Biol. Chem.* **265**, 9583–9586 (1990).

[15] Berridge, M. J. Inositol triphosphate and calcium signalling. *Nature* **361**, 315–325 (1993).

[16] Seydel, R. *From equilibrium to chaos*, pp. 48–51. Elsevier, New York (1988).

[17] Lotka, A. J. Undamped oscillations derived from the law of mass action. *J. Am. Chem. Soc.* **42**, 1595–1599 (1920).

[18] Press, W. H., Flannery, B. P., Teukolsky, S. A., and Vettering, W. T. *Numerical recipes in C*, pp. 569–573. Cambridge University Press, Cambridge (1988).

[19] Olsen, L. F. and Degn, H. Oscillatory kinetics of the peroxidase-oxidase reaction in an open system: experimental and theoretical studies. *Biochim. Biophys. Acta* **523**, 321–334 (1978).

[20] Olson, D. L., Williksen, E. P., and Scheeline, A. An experimentally based model of the peroxidase-NADH biochemical oscillator: an enzyme-mediated chemical switch. *J. Am. Chem. Soc.* **117**, 2–15 (1995).

[21] Mader, M. and Amberg-Fisher, V. Role of peroxidase in lignification of tobacco cells. I. Oxidation of nicotinamide adenine dinucleotide and formation of hydrogen peroxide by cell wall peroxidases. *Plant Physiol.* **70**, 1128–1131 (1982).

[22] Yamazaki, I., Yokota, K., and Nakajima, R. Oscillatory oxidations of reduced pyridine nucleotide by peroxidase. *Biochem. Biophys. Res. Comm.* **21**, 582–586 (1965).

[23] Degn, H. Compound 3 kinetics and chemiluminescence in oscillatory oxidation reactions catalyzed by horseradish peroxidase. *Biochim. Biophys. Acta* **180**, 271–290 (1969).

[24] Yamazaki, I. and Yokota, K. Analysis of the conditions causing the oscillatory oxidation of reduced nicotinamide-adenine dinucleotide by horseradish peroxidase. *Biochim. Biophys. Acta* **132**, 310–320 (1967).

[25] Degn, H. Bistability caused by substrate inhibition of peroxidase in an open reaction system. *Nature* **217**, 1047–1050 (1968).

[26] Chance, B. The enzyme-substrate complexes of horseradish peroxidase and peroxidases. II. Kinetics of formation and decomposition of the primary and secondary complexes. *Arch. Biochem.* **22**, 224–252 (1949).

[27] Nakamura, S., Yokota, K., and Yamazaki, I. Sustained oscillations in a NADPH and O_2 system. *Nature* **222**, 794 (1969).

[28] Yokota, K. and Yamazaki, I. Analysis and computer simulation of aerobic oxidation of reduced nicotinamide adenine dinucleotide catalyzed by horseradish peroxidase. *Biochemistry* **16**, 1913–1920 (1977).

[29] Olsen, L. F. The oscillating peroxidase-oxidase reaction in an open system: analysis of the reaction mechanism. *Biochim. Biophys. Acta* **527**, 212–220 (1978).

[30] Lindblad, P. and Degn, H. A compiler for digital computation in chemical kinetics and its application to oscillatory reaction schemes. *Acta Chem. Scand.* **21**, 791 (1967).

[31] Olsen, L. F. and Degn, H. Chaos in an enzyme reaction. *Nature* **267**, 177–178 (1977).

[32] Li, T.-Y. and Yorke, J. A. Period three implies chaos. *Am. Math. Monthly* **82**, 985–992 (1975).

[33] Degn, H., Olsen, L. F., and Perram, J. W. Bistability, oscillations and chaos in an enzyme reaction. *Ann. N. Y. Acad. Sci.* **316**, 623–637 (1979).

[34] Ruelle, D. and Takens, F. On the nature of turbulence. *Comm. Math. Phys.* **20**, 167–192 (1971).

[35] Olsen, L. F. An enzyme reaction with a strange attractor. *Phys. Lett.* **94A**, 454–457 (1983).

[36] Lazar, J. G. and Ross, J. Changes in mean concentration, phase shifts, and dissipation in a forced oscillatory reaction. *Science* **247**, 189–192 (1990).

[37] Aguda, B. D., Frisch, L.-L. H., and Olsen, L. F. Experimental evidence for the coexistence of oscillatory and steady states in the peroxidase-oxidase reaction. *J. Am. Chem. Soc.* **112**, 2167–2174 (1990).

[38] Geest, T., Steinmetz, C. G., Larter, R., and Olsen, L. F. Period-doubling bifurcations and chaos in an enzyme reaction. *J. Phys. Chem.* **96**, 5678–5680 (1992).

[39] Rys, P. and Wang, J. Hydrogen/deuterium isotope effect in the oscillating peroxidase-oxidase reaction. *Biochem. Biophys. Res. Comm.* **186**, 612–616 (1992).

[40] Olson, D. L. *Experimental and theoretical studies of the peroxidase-NADH biochemical oscillator: an enzyme-mediated chemical switch.* PhD thesis, University of Illinois, Urbana, IL, USA, (1994).

[41] Hauck, T. and Schneider, F. W. Mixed-mode and quasiperiodic oscillations in the peroxidase-oxidase reaction. *J. Phys. Chem.* **97**, 391–397 (1993).

[42] Larter, R., Bush, C. L., Lonis, T. R., and Aguda, B. D. Multiple steady states, complex oscillations, and the devils staircase in the peroxidase-oxidase reaction. *J. Chem. Phys.* **87**, 5765–5771 (1987).

[43] Larter, R., Steinmetz, C. G., and Aguda, B. D. Fast-slow variable analysis of the transition to mixed-mode oscillations and chaos in the peroxidase reaction. *J. Chem. Phys.* **89**, 6506–6514 (1988).

[44] Watanabe, N. and Inaba, H. Oscillatory low-level chemiluminescence from a nonequilibrium β-nicotinamide adenine dinucleotide-peroxidase system: experimental observations and computer simulations. *Photochem. Photobiol.* **57**, 570–576 (1993).

[45] Y.-F. Hung, I. S. and Ross, J. New reaction mechanism for the oscillatory peroxidase-oxidase reaction and comparison with experiements. *J. Phys. Chem.* **99**, 1980–1987 (1995).

[46] Land, E. J. and Swallow, A. J. One-electron reactions in biochemical systems as studied by pulse radiolysis. iv. oxidation of dihydronicotinamide dinucleotide. *Biochim. Biophys. Acta* **234**, 34–42 (1971).

[47] Kummer, U., Valeur, K. R., Baier, G., Wegmann, K., and Olsen, L. F. Oscillations in the peroxidase-oxidase reaction: a comparison of different peroxidases. *Biochim. Biophys. Acta* **1289**, 397–403 (1996).

[48] Valeur, K. R. and Olsen, L. F. Kinetic studies of the oscillatory dynamics in the peroxidase-oxidase reaction catalysed by four different peroxidases. *Biochim. Biophys. Acta* **1289**, 377–384 (1996).

[49] Olson, D. L. and Scheeline, A. The peroxidase/NADH biochemical oscillator: experimental system, control variables, and oxygen mass transport. *Anal. Chim. Acta* **283**, 703–717 (1993).

[50] Lundsgaard, J. and Degn, H. Digital regulation of gas flow rates and composition of gas mixtures. *IEEE Trans. Biomed. Eng. BME* **20**, 384–387 (1974).

[51] Hung, Y.-F. and Ross, J. New experimental methods toward the deduction of the mechanism of the oscillatory peroxidase-oxidase reaction. *J. Phys. Chem.* **99**, 1974–1979 (1995).

[52] Treybal, R. E. *Mass-transfer operations.* McGraw-Hill, New York, third edition, (1980).

[53] Aguda, B. D. and Larter, R. Sustained oscillations and bistability in a detailed mechanism of the peroxidase-oxidase reaction. *J. Am. Chem. Soc.* **112**, 2167–2174 (1990).

[54] Dunford, H. Horseradish peroxidase: structure and kinetic properties. In *Peroxidases in Chemistry and Biology,* Everse, J., Everse, K., and Grisham, M., editors, volume 2, pp. 1–24. CRC Press, Ann Arbor (1991).

[55] Sigma-Aldrich Company Ltd, Poole, Dorset. *Sigma Catalogue,* (1997).

[56] Gray, P. and Scott, S. K. *Chemical Oscillations and Instabilities,* pp. 292–312. Clarendon Press, Oxford (1990).

[57] Argoul, F., Arneodo, A., Richetti, P., and Roux, J.-C. From quasiperiodicity to chaos in the Belousov-Zhabotinskii reaction. I. experiment. *J. Chem. Phys.* **86**, 3325–3338 (1987).

[58] Jeffrey, A. *Mathematics for engineers and scientists,* pp. 674–691. Van Nostrand Reinhold, London, fourth edition (1989).

[59] Takens, F. *Detecting strange attractors in turbulence,* pp. 366–381. Springer-Verlag, New York (1980).

[60] Packard, N. H., Crutchfield, J. P., Farmer, J. D., and Shaw, R. S. Geometry from a time series. *Phys. Rev. Lett.* **45**, 712–716 (1980).

[61] Eckmann, J.-P. Roads to turbulence in dissipative dynamical systems. *Rev. Mod. Phys.* **53**, 643–654 (1981).

[62] Olson, D. L. and Scheeline, A. The peroxidase-NADH biochemical oscillator. 1. examination of oxygen mass transport, the effect of light, and the role of methylene blue. *J. Phys. Chem.* **99**, 1204–1211 (1995).

[63] Price, N. C. and Dwek, R. A. *Principles and Problems in Physical Chemistry for Biochemists*, p. 57. Oxford University Press, second edition (1979).

[64] Dawson, R., Elliot, D., Elliot, W., and Jones, K. *Data for Biochemical Research.* Oxford University Press, third edition, (1986).

[65] Paul, K. G. Cytochrome *c* peroxidase. In *The Enzymes,* Boyer, P. D., editor, volume 12, pp. 227–274. Academic Press, New York (1963).

[66] Gross, A. J. and Sizer, I. W. The oxidation of tyramine, tyrosine and related compounds by peroxidase. *J. Biol. Chem.* **234**, 1611–1614 (1959).

[67] Valoti, M., Tipton, K. F., and Sgaragli, G. P. Oxidative ring-coupling of tyrosine and its derivatives by purified rat intestinal peroxidase. *Biochem. Pharmacol.* **43**, 945–951 (1992).

[68] Gerald, C. F. and Wheatley, P. O. *Applied numerical analysis*, pp. 384–387. Addison Wesley, fourth edition (1989).

[69] Press, W. H., Flannery, B. P., Teukolsky, S. A., and Vettering, W. T. *Numerical recipes in C*, pp. 592–597. Cambridge University Press, Cambridge (1988).

[70] Scott, S. K. *Chemical chaos*, pp. 103–109. Oxford University Press, New York (1991).

[71] Farey, J. On a curious property of vulgar fractions. *Philos. Mag. J. (London)* **47**, 385–386 (1816).

[72] Henon, M. On the numerical computation of Poincaré maps. *Physica* **5D**, 412–414 (1982).

[73] Lorenz, E. N. Deterministic nonperiodic flow. *J. Atmos. Sci.* **20**, 130–141 (1963).

[74] Jordan, D. W. and Smith, P. *Nonlinear ordinary differential equations*, p. 229. Clarendon Press, Oxford (1977).

[75] Shaw, R. Strange attractors, chaotic behaviour, and information flow. *Z. Naturforsch.* **36a**, 80–112 (1980).

[76] Wolf, A., Swift, J. B., Swinney, H. L., and Vastano, J. A. Determining lyapunov exponents from a time series. *Physica* **16D**, 285–317 (1985).

[77] Alexandre, S. and Dunford, H. B. A new model for oscillations in the peroxidase-oxidase reaction. *Biophys. Chem.* **40**, 189–195 (1991).

[78] Yamazaki, I., Yokota, K., and Tamura, M. Horse-radish peroxidase compound III. In *Hemes and Hemoproteins,* Chance, B., Estabrook, R., and Yonentani, T., editors, pp. 319–326. Academic Press, New York (1966).

[79] Wittenberg, J. B., Noble, R. W., Wittenberg, B. A., Antonini, E., Brunori, M., and Wyman, J. Studies on the equilibria and kinetics of the reactions of peroxidase with ligands. *J. Biol. Chem.* **242**, 626–634 (1967).

[80] Degn, H. and Mayer, D. Theory of oscillations in peroxidase catalyzed oxidation reactions in open system. *Biochim. Biophys. Acta* **180**, 291–301 (1969).

[81] Bray, R. C. Molybdenum iron-sulfur flavin hydroxylases and related enzymes. In *The Enzymes,* Boyer, P. D., editor, volume 12, pp. 299–419. Academic Press, New York (1975).

[82] Salaris, S. C., Babbs, C. F., and Voorhees, W. D. Methylene blue as an inhibitor of superoxide generation by xanthine oxidase. a potential new drug for the attenuation of ischemia/reperfusion injury. *Biochem. Pharmacol.* **42**, 499–506 (1991).

[83] Yotenati, T. Cytochrome *c* peroxidase. In *The Enzymes,* Boyer, P. D., editor, volume 12, pp. 345–361. Academic Press, New York (1975).

[84] Kaplan, N. O., Ciotti, M. M., v. Eys, J., and Burton, R. M. Effect of pyridine derivatives on animal tissue diphosphopyridine nucleotidases. *J. Biol. Chem.* **234**, 134–138 (1959).

[85] Zatman, L. J., Kaplan, N. O., and Colowick, S. P. Inhibition of spleen diphosphopyridine nucleotidase by nicotinamide, an exchange reaction. *J. Biol. Chem.* **200**, 197–212 (1953).

Index

From: Andrew G. McDonald, Ph.D.
To: The Library, Trinity College Dublin
Re: Permission for copying and lending Ph.D. thesis

To whom it may concern,
I hereby give permission to the Library of Trinity College Dublin to copy and lend my Ph.D. thesis.

Andrew G. McDonald